UNIVERSITY OF BIRMINGHAM

WIDEBAND RECONFIGURABLE ANTENNAS

by

MOHAMAD RIJAL HAMID

A Thesis submitted to
The University of Birmingham
For the degree of
Doctor of Philosophy (PhD)

School of Electronic, Electrical and
Computer Engineering
College of Engineering and Physical
Sciences
The University of Birmingham
May 2011

UNIVERSITY OF BIRMINGHAM

University of Birmingham Research Archive

e-theses repository

ABSTRACT

The work described in this thesis concerns the combining of wideband and reconfigurable narrow band functionality into a single antenna. This concept may be useful in reducing size and to give flexibility to a wireless terminal to operate in several different modes. The approach also offers additional pre-filtering to the front-end, which reduces the interference levels at the receiver, giving them a significant advantage over fixed non reconfigurable transceivers. Wideband-narrowband reconfiguration is potentially useful for future wireless communications such as software defined radio and cognitive radio, since they may employ wideband sensing and reconfigurable narrowband communications.

Five novel reconfigurable antennas are presented. One is a switchable log periodic patch array and four are Vivaldi antennas with various forms of reconfiguration. The log periodic is reconfigured by placing switches between the patches and the feed line whilst the Vivaldi antenna has switched resonators controlling the current in the edges of the tapered slots. Wideband to various narrowband functions, wideband with a tunable band rejection having a very wide tuning ratio, and combined three function wide, narrow and tunable band rejection in a single antenna are demonstrated. Prototypes are presented with PIN diode switches, varactors, fixed capacitor or hard wire switches. Measured and simulated results with a very good agreement are presented, thus verifying the proposed concepts.

ACKNOWLEDGMENTS

PUBLICATIONS

Journals

1. **Hamid M. R.**, Gardner P., Hall P. S., and Ghanem F., "Vivaldi Antenna with Integrated Switchable Pass Band Resonator," in press, *IEEE Transactions on Antennas and Propagation,* 2011.
2. **Hamid, M R**, Gardner, P, Hall, P S and Ghanem, F, "Switched Band Vivaldi Antenna", *IEEE Transactions on Antennas and Propagation,* Volume 53, No. 5, 2011
3. **Hamid, M R**, Gardner, P, Hall, P S and Ghanem, F, "Vivaldi with Tunable Narrow band Rejection", Microwave and Optical Technology Letters*, Volume 53, No 5, 2011
4. **Hamid, M R**, Hall, P S and Gardner, P, "Frequency Reconfigurable Log Periodic Patch Array", Electronics Letters Volume 46, Issue 25, Dec 2010
5. **Hamid, M R**, Gardner, P, Hall, P S and Ghanem, F, "Multi-Mode Vivaldi Antenna", Electronics Letters Volume 46, Issue 21, Oct 2010
6. **Hamid, M R**, Hall, P S, Gardner, P and Ghanem, F, "Switchable Filtering in Vivaldi Antenna", Electronics Letters Volume 46, Issue 7, April 2010
7. **Hamid, M R**, Gardner, P, Hall, P S and Ghanem, F, "Reconfigurable Vivaldi Antenna", Microwave and Optical Technology Letters, Volume 52, Issue 4, April 2010
8. **Hamid, M R**, Hall, P S, Gardner, P and Ghanem, F, "Switched WLAN-Wideband Tapered Slot Antenna", Electronics Letters Volume 46, Issue 1, Jan 2010

Conferences

1. **Hamid, M R**, Gardner, P, Hall, P S and Ghanem, F, "Reconfigurable Vivaldi Antenna with Tunable Band Stop", IEEE International Workshop on Antenna Technology 7-9 March, 2011, Hong Kong
2. **Hamid, M R**, Gardner, P, Hall, P S and Ghanem, F, "Review of Reconfigurable Vivaldi Antenna", IEEE International Symposium on Antennas and Propagation, APS 2010, Toronto, Canada, July 2010
3. **Hamid, M R**, Gardner, P, Hall, P S and Ghanem, F, "Reconfigurable Slot Line Filter", The IET seminar on Passive RF and Microwave Components, Birmingham, UK, April 2010
4. **Hamid, M R**, Hall, P S, Gardner, P and Ghanem, F, "Frequency Reconfigurable Vivaldi Antenna", European Conference on Antennas and Propagation, Eucap 2010 Barcelona, Spain, April 2010
5. **Hamid, M R**, Gardner, P and Hall, P S, Ghanem, F, "Switchable Wideband-Narrowband Tapered Slot Antenna", Loughborough Antenna and Propagation Conference, Loughborough, UK, 16-17 Nov 2009

6. **Hamid, M R**, Gardner, P and Hall, P S, "Reconfigurable Log Periodic Aperture Fed Microstrip Antenna", Loughborough Antenna and Propagation Conference, Loughborough, UK, 16-17 Nov 2009
7. Tariq A., **Hamid M.R.** and Shiraz H.G., "Reconfigurable Monopole Antenna", accepted in European Conference on Antennas and Propagation, Eucap 2011 Rome, Italy, 11-15 April 2011
8. Hall P S, **Hamid M R**, Ghanem F, Mirkamali A and Gardner P "RECONFIGURATION OF VIVALDI AND LOG PERIODIC ANTENNAS" in Proc. Allerton Antenna Symposium 09, USA, 22-23 Sept 2009,
9. Gardner P., **Hamid M. R**., Hall P. S., Kelly J., Ghanem F., and Ebrahimi E., "Reconfigurable antennas for cognitive radio: requirements and potential design approaches," in The IET seminar on Wideband, multiband antennas and arrays for defence or civil applications, London, UK, Mar. 2008.
10. P. Hall, Z. H. Hu, P. Song**, M. R. Hamid**, and Z. Wang, "Creating reconfigurable adaptive antennas for cognitive radio applications considering cost and portability", The IET Seminar on Cognitive Radio Communications, 4th Oct. 2010, London, U.K.
11. Hall P S, Gardner P., Hu Z., Song P., Kelly J., **Hamid M.R.,** 'Reconfigurable antennas for wideband wireless systems' Adaptable and Tunable Antenna Technology for Handsets and Mobile Computing Products Savoy Place, London, 22 Oct 2009,
12. Hall P. S., Gardner P., Kelly J., Ebrahimi E., **Hamid M. R**., Ghanem F., Herraiz-Martinez F. J. and Segovia-Vargas D., "Reconfigurable Antenna Challenges for Future Radio Systems," in Proc. EuCAP 09, Berlin, Germany, Mar. 2009.
13. Hall P. S., Gardner P., Kelly J., Ebrahimi E., **Hamid M. R**., and Ghanem F., "Antenna challenges in cognitive radio," (invited paper) in Proc. ISAP 08, Taiwan, Oct. 2008.

TABLE OF CONTENTS

LIST OF FIGURES

xiv

xv

LIST OF TABLES

LIST OF ABBREVIATIONS

CPW – Co-Planar Waveguide

CR – Cognitive Radio

dB - decibel

DC – Direct Current

EM – Electro Magnetic

GaAs FET – Gallium Arsenide Field Effect Transistor

GPS – Global Positioning System

GSM – Global Systems for Mobile Communications

ID – with the ring slots using ideal switches

IEEE – Institute of Electrical and Electronics Engineers

LPA – Log Periodic Array

MEMS – Micro Electro Mechanical system

PD – with the ring slots using PIN Diode switches

PIFA – Planar Inverted F Antenna

PIN DIODE – Positive Intrinsic Negative Diode

Q factor – Quality factor

RF – Radio Frequency

SMD – Surface Mount Device

TV - Television

UWB – Ultra Wideband

VSWR – Voltage Standing Wave Ratio

WLAN – Wireless Local Area Network

WR – without the ring slots

CHAPTER 1

INTRODUCTION

1.1 Introduction

Recent trends have seen the development of wideband antennas, multi-band antennas or reconfigurable antennas receiving much attention to fulfil different applications in just one single terminal. Single terminals or devices could have many applications such as, GPS, GSM, WLAN, Bluetooth, etc. To suit such applications wideband, multi-band or reconfigurable antennas have been developed [1]. The reconfigurable approach offers significant advantages of compactness and flexibility. Moreover, when considering the interference levels at the receiver, they are the best option since only one single band is used at a given time.

A significant number of reconfigurable antennas capable of switching between two particular narrow bands have been reported such as in [2-5]. Recently, wide to narrow band reconfigurable antennas have also received attention [6-8] as they offer multi-functionality. Wideband-narrowband reconfiguration is also essential for multi-mode applications that

include UWB or wideband system, and for future wireless communication concepts such as cognitive radio (CR), which employs wideband sensing and reconfigurable narrowband communications [9].

1.2 Motivation

Combining wide and narrowband functionality is useful to reduce size and to give flexibility to a terminal to operate in a multi-function mode, such as, wideband to reconfigured narrowband. The approach also offers additional pre-filtering, which reduces the interference levels at the receiver, giving them a significant advantage over fixed non reconfigurable transceivers. There are significant potential benefits in combining wideband and reconfigurable narrow band functionality into a single antenna. With a wideband antenna, multiple standards can be supported simultaneously but the receiver is vulnerable to out of band interference. To overcome this, more antennas that can be reconfigured from wideband to single narrow band or vice versa and can be operated with or without band rejection need to be studied and developed. The solutions including wideband to narrowband, and band notch reconfiguration are proposed here by the inclusion of diodes or by means of resonators that are switched in or out to interrupt the flow of currents in antenna structures.

1.3 Objective

The objectives of this thesis are:

i. To develop reconfigurable antennas to switch from wide to narrow bandwidth or vice versa, by reconfiguring an inherently wideband antenna i.e. a log periodic patch array and a Vivaldi antenna.

ii. To develop a high degree of flexibility in a reconfigurable antenna by combining wide, narrow and notch band functionality in one single antenna.

1.4 Thesis outline

A brief introduction to the systems that potentially require wide-narrow band reconfiguration and the principle motivation and objective of this thesis is presented here in chapter 1.

In chapter 2 the background of log periodic antenna and Vivaldi antenna is discussed. Previous works on reconfigurable antennas which includes narrowband to narrowband, wideband to narrowband, wideband with notch band and wideband to wideband reconfiguration are reported and summarised.

In chapter 3 a novel log periodic antenna with added switched band functionality to operate in a wideband or narrowband mode is presented. The antenna reconfiguration is realized by inserting switches into the slot aperture of the structure. A wide bandwidth mode is demonstrated from 7.0 – 10 GHz and three narrowband modes at 7.1, 8.2 and 9.4 GHz can be selected. A prototype with ideal switches is developed.

In chapter 4, a novel switched band Vivaldi antenna is proposed. It is relatively small, simple to manufacture and less complex in its biasing (fewer switches) compared to the reconfigurable log periodic patch array described in chapter 3. To demonstrate its functionality, the proposed antenna shows reconfiguration between a single wideband mode (1.0 - 3.2 GHz) and three narrowband modes. To achieve switched band properties,

eights ring slots which form filters were inserted in the antenna. The overall operating band can be switched by coupling each ring slot into the slot edges through the gaps controlled by means of PIN diode switches, which stop or pass the edge current to obtain frequency reconfiguration capability.

In chapter 5, a new design method of band switching in the Vivaldi antenna that allows a better control of the narrow operating bands is proposed. By incorporating only a single pair of slot resonators, six different narrow frequency bands can be switched within the wideband operation, double the number reported in the chapter 4. To achieve switched band properties, the proposed approach reconfigures the operating band by varying the electrical length of the slot resonators by means of PIN diode switches. This selectively stops, or passes, current at different frequencies.

In chapter 6, a Vivaldi antenna is presented with narrow band rejection characteristics within the 2 -7 GHz operating bandwidth. The band rejection is realised by incorporating a microstrip line resonator printed on the reverse side of the radiating element. The method, using a microstrip line resonator is proposed by Dr F. Ghanem [10], a Research Visitor at the University of Birmingham. A significant improvement from the original idea has been proposed. The original idea has a limited tuning range. A new idea has been developed to achieve a tuning capability within the whole band of operation, resulting in a very wide tuning range. To give a narrow tunable stop band action, the resonator is loaded with varactors. Three methods are presented. One with fixed band notching at 5.75 GHz, one with a single varactor to give a tunable band notch between 4.2 – 5.5 GHz and another with 3 varactors and a shorting post to the ground widening the stop band in the frequency range between 2 GHz and 7 GHz, giving a tuning ratio of 3.5:1. The proposed antennas have a capability of rejecting not only WLAN frequency but also any other band within the antenna operating bandwidth.

In chapter 7, a Vivaldi antenna with a high degree of multi-functionality is proposed. It can switch between wideband, notch band and narrowband mode by combining the concepts described in chapters 5 and 6. The antenna in a wideband mode is designed to have a bandwidth of 2 – 8 GHz. In the notch band mode, the antenna has tunable narrowband rejection between 5.2 GHz and 5.7 GHz. The Vivaldi can also operate in five narrow pass band modes centred on 3.6, 3.9, 4.8, 5.5 and 6.5 GHz.

Finally, chapter 8 concludes the thesis and suggests the future work.

CHAPTER 2

BACKGROUND AND LITERATURE REVIEW

2.1 Introduction

Frequency reconfigurable antennas are useful to support many wireless applications, where they can reduce the size of the front end circuitry and also allow some additional receiver pre-filtering. However they are limited to one service at one time and have additional loss resulting from the switches. Wideband antennas on the other hand can also support all the standards and have additional advantages operating simultaneous multiple services. This is good but since they have inherently poor out of band rejection, additional filtering is required, compromising the front end complexity. To overcome this, work on integration with interference rejection filters within the antennas, increasing the system versatility, has received attention and been published in the open literature.

Combining wideband and reconfigurable narrow band functionality is a new idea. The combination is important to achieve both benefits from wideband and frequency reconfigurable antennas. Wideband-narrowband reconfiguration is potentially useful for

military applications [11] where the primary use of wideband antennas is in Electronic Surveillance Measures (listening over very wide bandwidths) and Electronic Warfare (which may involve jamming or deception at any frequency which the enemy is using within a very wide bandwidths). The combination is also potentially useful for future wireless communications such as software defined or cognitive radio [9], since they may employ wideband sensing and reconfigurable narrowband antennas. A standard for fixed access using cognitive radio concepts has been established in IEEE 802.22 [12] which will operate in the TV bands. Two separate antennas are suggested with one directional for communications and the other omni-directional with gain of 0 dBi or higher for sensing. Single antenna cognitive radio platforms have also been proposed in [13], where the sensing and communications block is separated. The antenna used is a non-reconfigurable wideband one and is used both for sensing and communication. Frequency agile functionality is achieved using a tunable filter. The use of a single antenna in an integrated sensing and communication architecture has also been recently reported [14].

Instead of multiple antennas or a single wideband antenna, reconfigurable antennas are likely to be useful by combining wide and narrowband functionality and also allowing some additional pre-filtering, which is now considered to be potentially vital to successful cognitive radio operation [15]. In a fixed radio system, antennas with high gain can be used and their larger size can be handled in the big antenna assembly. A log periodic array and a Vivaldi antenna, both inherently wideband, are good prospects for this and also for achieving wide to narrow band reconfiguration.

Log-periodic antennas have multiple elements, which resonate in a log-periodic fashion. This thesis investigates the idea that a frequency reconfigurable log periodic antenna function can be achieved by switching off some of the elements. In the Vivaldi antenna, most of the current is flowing at the very edge of the tapered slot. Therefore

stopping the current can be done by perturbing the tapered slot edge. To provide the background for this study, in this chapter a brief review of log periodic arrays and Vivaldi antennas is given in section 2.2. Work on reconfigurable antennas which includes narrowband to narrowband, wideband to narrowband, wideband with notch band, and wideband to wideband reconfiguration is reported in section 2.3. Section 2.4 summarises the chapter.

2.2 Wideband Antenna

Wideband antennas like the Vivaldi, horn, log periodic arrays and wideband dipoles or monopoles are usually found in wideband systems. Vivaldis and horns are also widely used in positioning systems, imaging, through the walls radar, and cancer detection. These antennas are designed specifically for such systems and the possibilities for wide to narrow bandwidth reconfiguration are currently limited. This section describes a brief overview of log periodic arrays and Vivaldi antennas that have been chosen as candidates for wideband to narrowband reconfiguration.

2.2.1 Log Periodic Array

The log periodic is one of the earliest antennas proposed to achieve wideband performance. Generally, it is in a class of frequency independent antennas. A "frequency independent antenna", as explained in reference [16], is an antenna that is specified entirely by angles; hence when the dimensions in the radiating region are expressed in wavelengths, they are the same at every frequency. (See also section 2.2.2)

However log periodic arrays are not smoothly scaled but are discretised. The most well known type is the log periodic dipole array [17]. It has multiple elements that are scaled in a log periodic fashion. All the dimensions such as length, width (radius) and spacing are also scaled. If frequency element one, f_1, and frequency element two, f_2 are one period apart, the scale factor is defined as $\tau = \dfrac{f_2}{f_1}$. The log periodic antenna has an end fire beam where it is fed from the high frequency element end and has relatively high gain, of the order 10 dBi. Figure 2.1 shows a log periodic printed dipole [18] and monopole array [19]. They have multiple arms which are scaled log periodically, where each element operates at a different frequency but close to that of its neighbours, depending on the scale factor used. A typical value of τ is in between 1.05 and 1.43 [20]. As τ gets larger, a smaller number of elements will result. On the other hand, as τ gets smaller, more elements that are close together will result. A successful log periodic antenna however depends also on the individual element bandwidth. Smaller individual bandwidth will require smaller value of τ in order to maintain a smooth transition between elements. In contrast, larger individual bandwidth can afford to have appropriate larger value of τ and will result in more compact design.

(a)

(b)
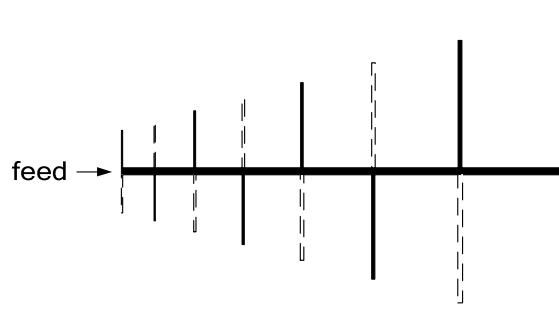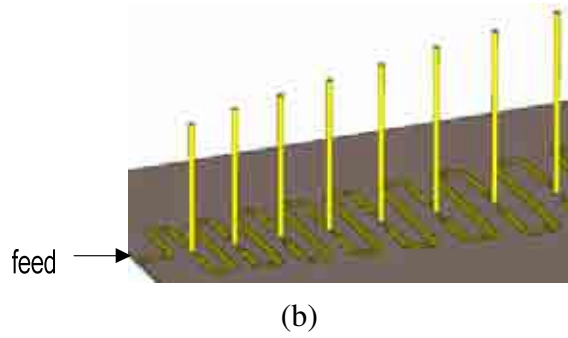
Figure 2.1 Log periodic arrays (a) printed dipole [18] (solid conductors on top of substrate, dotted on lower) (b) monopole array [19] (series feed on top of substrate, ground plane on lower)

A low profile log periodic array can be constructed from microstrip patch elements, as has been presented in [21-23]. Different feed techniques can be used such as an electromagnetic coupled feed [21], a series branch lines feed [22] and an aperture coupled feed [23]. Figure 2.2 shows the configurations.

(a)

(b)

(c)
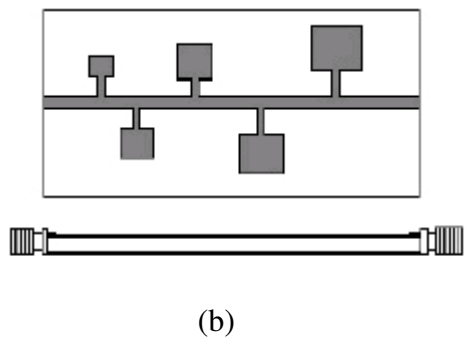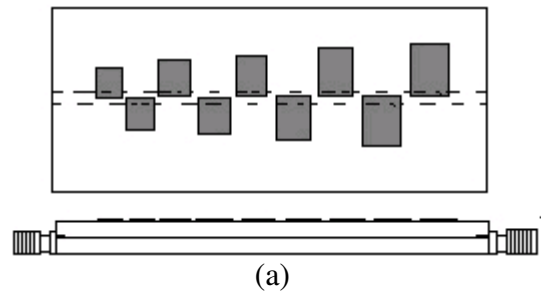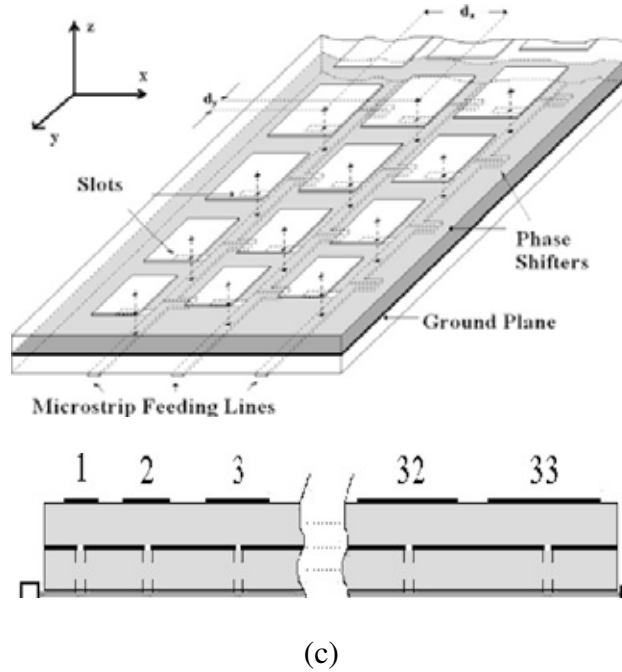
Figure 2.2 Log periodic patch array (a) electromagnetic coupled feed [21]- , (b) series branch lines feed -[22] , and (c) aperture coupled feed - [23] types

With multiple elements in log periodic array, wide to narrowband reconfiguration can be performed by switching off some of the elements. Recently, work on reconfigurable log periodic antennas has been reported, but in a dipole array type. The first idea proposing reconfigurable log periodic dipole array is presented in [24]. In the log periodic dipole array described in [18], ideal switches are used to control each pair of dipole arms of the antenna. This can switch from a wideband of 1 – 3 GHz, to several narrow bands. However, the proposed antenna needs to use two switches for each deactivated radiating element. Furthermore, application of dc bias is difficult and has not been demonstrated yet. Similar work on this has also been reported in [25, 26] as shown in Figure 2.3. As opposed to wideband to narrowband reconfiguration, work in [27-29] demonstrates a band notch method for log periodic antennas as shown in Figure 2.4.
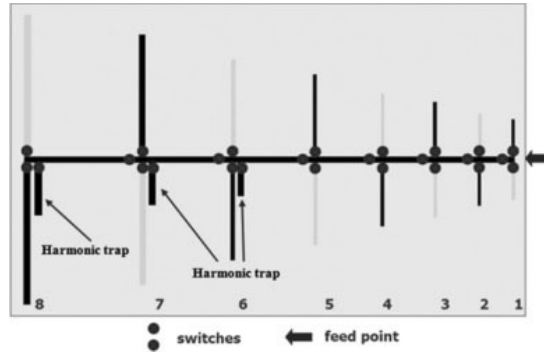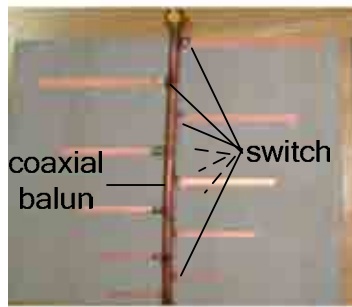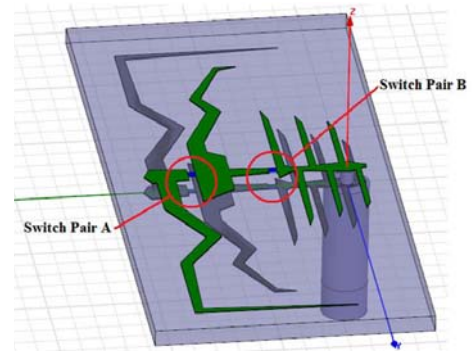
Figure 2.3 Reconfigurable log periodic antenna (a) [18] (only conductors on top of substrate shown), (b) [25] (only conductors on top of substrate shown), (c) [26] (grey-conductors on top of substrate, light grey - on lower)
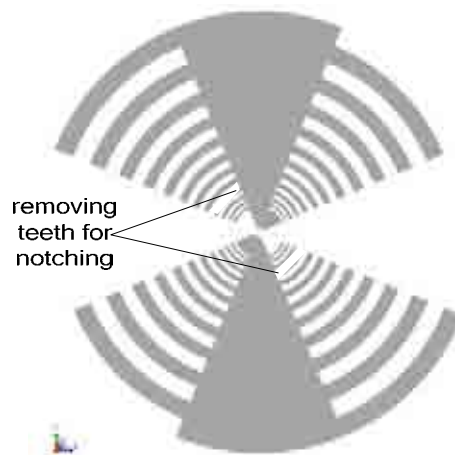
(a)
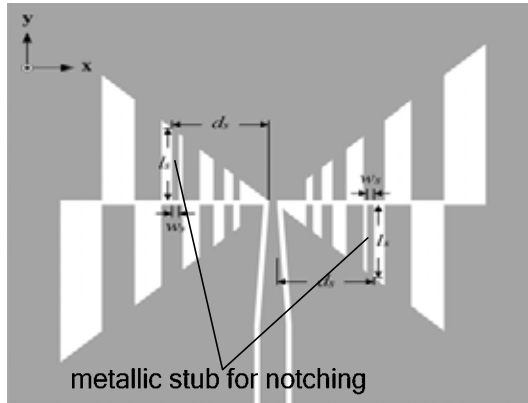
(b)
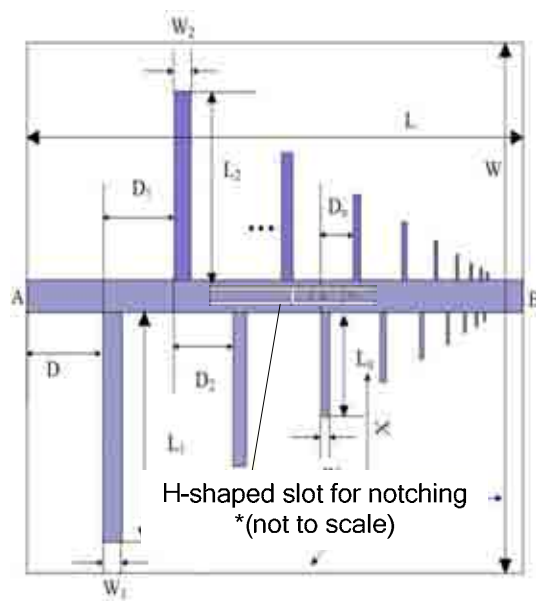
(c)

Figure 2.4 Band notch log periodic antennas, (a) [27], (b) [28] and (c) [29] (only conductors on top of substrate shown)

2.2.2 Vivaldi Antenna

The Vivaldi antenna is a well known structure that operates over a wide bandwidth. One form is shown in Figure 2.5. It achieves wideband performance by means of a gradual taper in a slot transmission line that forms a transition from a guided wave medium to free space radiation. In addition, it also has a well defined radiation mechanism in which it

radiates different frequencies from different parts. Radiation at high frequencies occurs closer to the narrower end and lower frequencies closer to the wider end of the slot. The radiating area size relative to the corresponding wavelength is constant and the structure expansion is smooth, and therefore the Vivaldi antenna is also classified as a frequency independent antenna. As such, the Vivaldi antenna can be divided into two regions i) transmission line region, and ii) radiating region. The transmission line region is the area where the slot line width $< \lambda_0/2$ and the radiating region is the area where the slot line width $> \lambda_0/2$.

The printed Vivaldi is formed by a tapered slot structure etched on substrate. It has been invented by Gibson [30]. Generally, it has a symmetrical end-fire beam, good gain, low side lobes and wide bandwidth [31]. These properties depend on flare geometry [32], dimensions (i.e. length, aperture size), and also the transition from the input to the slot line. In the Vivaldi antenna shown in Figure 2.5, the radiating element is etched on a single side of the substrate and fed by microstrip line. Other feeding techniques such as coaxial feed [33] and co-planar waveguide feed [34] are also used. The feed line to radiating slot transition has a significant effect on the bandwidth. There is also another type called the antipodal Vivaldi. In this type, the radiating element or slot line is etched symmetrically, half on each side of the substrate [35-37] as shown in Figure 2.6. This configuration removes the feed line transition to slot line and improves further the wide bandwidth of the Vivaldi.
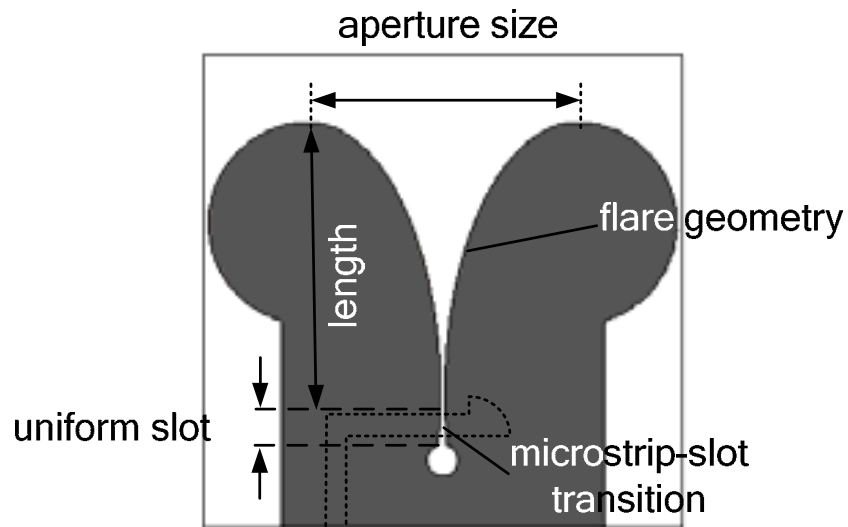
Figure 2.5 Vivaldi antenna showing microstrip feed (dash line) on the reverse side
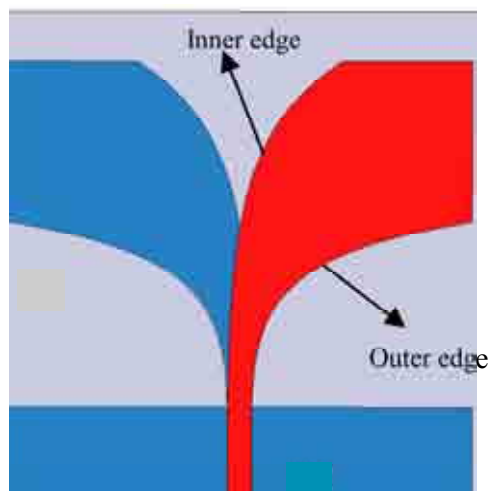
Figure 2.6 Antipodal Vivaldi [37] (black conductor on front of substrate, grey on back)

During Vivaldi operation, most of the current is flowing at the very edge of the tapered profile as shown in Figure 2.7. These characteristics help in designing a wideband-

narrowband reconfiguration. By knowing this, stopping the current can easily be done by perturbing the tapered slot edge. An example is shown in [38] where a quarter wavelength short stub was inserted into a radiating region as shown in Figure 2.8a, to cut-off the 5.05-5.93 GHz band. Other work on band notching of a Vivaldi antenna has also been reported in [39] where a U-shaped slot was employed to notch out the 5.1 – 5.8 GHz WLAN band. Figure 2.8b shows this.
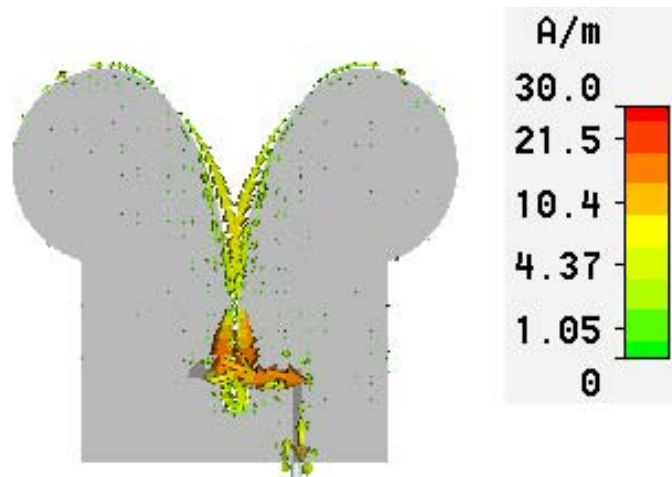
Figure 2.7 Typical simulated surface current distributions in Vivaldi excited at 3 GHz (current $I^2 = I_x^2 + I_y^2$ shown)
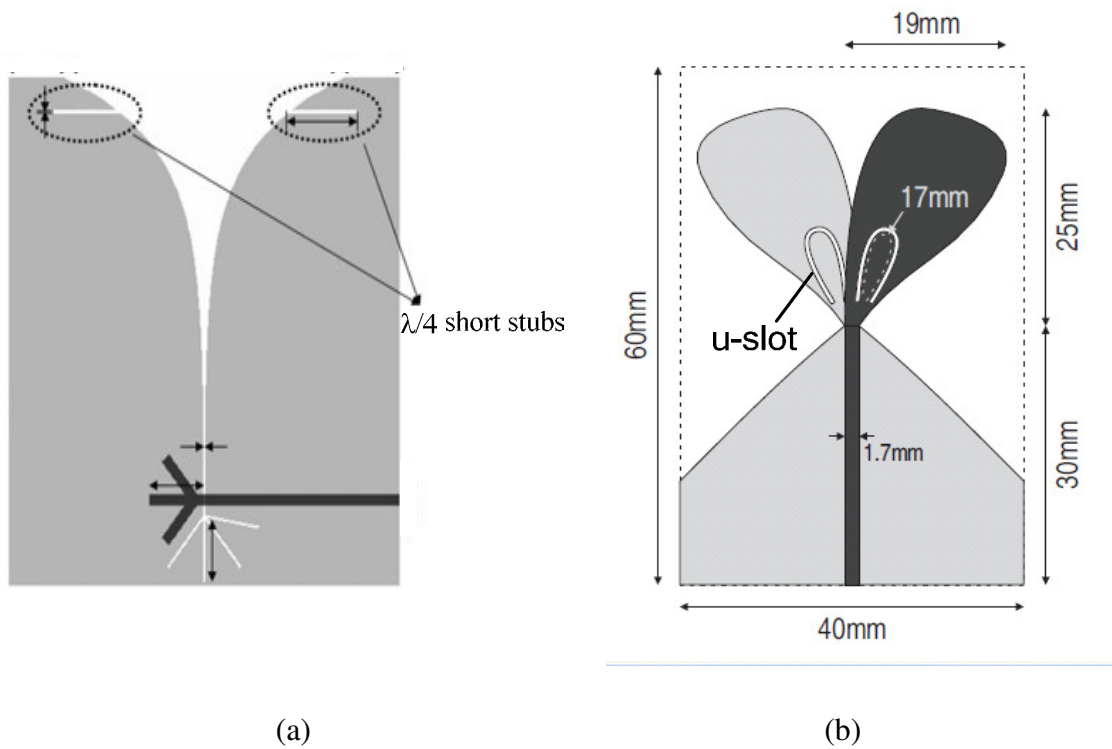
Figure 2.8 Band notch Vivaldi antennas (a) slot stubs in edge [38], (b) u shaped slot in conductors [39]

2.3 Reconfigurable Antennas

Reconfigurable antennas exhibit many advantages over their traditional counterparts. The antenna can be used to support multiple functions at multiple frequency bands. This will significantly reduce the hardware size and cost. Antenna reconfiguration is normally achieved in one of three ways: (a) switching parts of the antenna structure in or out using electronic switches (b) adjusting the loading or matching of the antenna externally and (c) changing the antenna geometry by mechanical movement. Switching or tuning within an antenna or in an external circuit can be achieved by means of PIN diodes, GaAs FETs, MEMs devices or varactors[40, 41]. MEMS devices have the advantage of very low loss, but the disadvantages are high operating voltage, high cost and lower

17

reliability than semiconductor devices [42]. GaAs FETs used in switching mode, with zero drain to source bias current, have low power consumption but poorer linearity and higher loss. PIN diodes can achieve low loss at low cost, but the disadvantage is that in the on state there is a forward bias dc current, which degrades the overall power efficiency. Varactor diodes have the advantage of providing continuous reactive tuning rather than switching, but suffer from poor linearity. These devices have been used and deployed in many antennas in a number of ways as reported in many publications [43-46]. There are four types of reconfigurable antennas reviewed here. One is capable of switching between two particular narrow bands or a multiband and the other one is capable of switching between wide and narrow bands. Also reviewed is a wideband antenna with band rejection and wideband to wideband capability.

2.3.1 Narrowband to narrowband reconfiguration
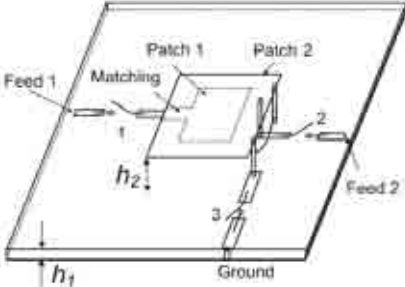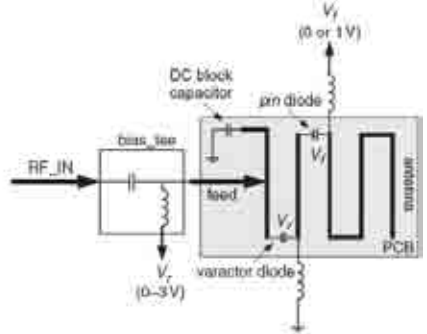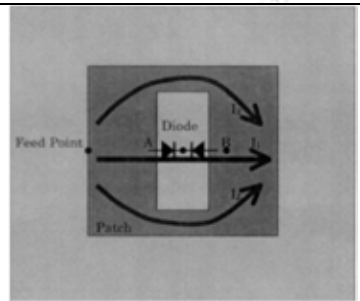
A significant number of reconfigurable antennas have been reported which are capable either of switching between two particular narrow bands or of multiband operation. Examples reviewed in this section are just a few selected from an extensive literature. Recently, a reconfigurable monopolar patch antenna was presented in [3]. Using four open stubs attached to a rectangular patch through four PIN diodes, eight different patch sizes are achieved and consequently configure eight operating frequencies. PIN diodes also can be used to change the antenna structure, as in the E shaped patch, [47], which can switch from a band covering 9.2 – 15.0 GHz to 7.5 – 10.7 GHz with 15 switches, by varying the width of the E-shape. Switching from a patch to a PIFA configuration, [48], with 3 switches, changed the frequency from 0.688 to 1.75 GHz. A monopole with switched length, using 2 switches, tuned from 2 to 5 GHz, [49]. Use of 2
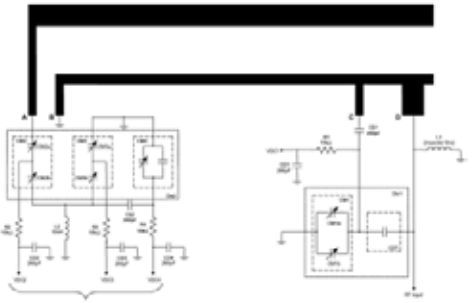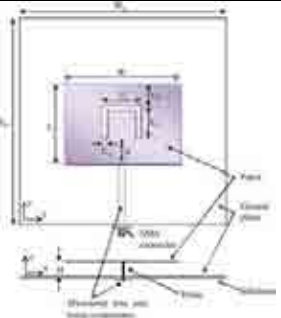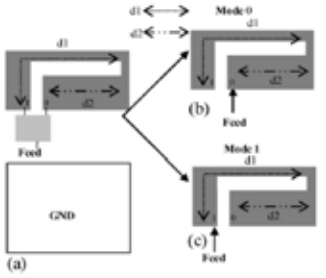
switches in a slot in a patch shifted the operating frequency from 3.11 to 3.43 GHz, [50]. External control can take the form of switching or matching. An external re-matching circuit, [51], was used to switch a 0.748 to 0.912 GHz antenna to operate over a 1.84 to 2.185 GHz band. In [4], a matching circuit is used in the 50 Ω feed line near to the microstrip patch input to tune operation from 2.6 to 3.35 GHz. Switching between ports in a PIFA, [52], giving coverage in either the 0.85, 0.9 and 1.8 GHz bands or the 0.9, 1.9 and 2.05 bands has been demonstrated. Similarly, switching from open to short circuit, [52], allowed operation in the 0.85, 0.9, 1.8 and 1.9 GHz bands or 1.8, 1.9, 2.05 and 2.45 bands. A two port combination of a PIFA and a monopole [2] switches frequency from 0.75 to 0.92 GHz in the PIFA, and 1.92 and 3.6 GHz to 3.6 and 5.25 GHz in the monopole when a switch is used in the PIFA, to change the effective electrical length of both antennas. These antennas are summarised in Table 2.1.

There are a number of ways, as described above, to reconfigure the antenna frequency. However examples shown in this section are only capable of switching between two particular narrow bands or multiband operation. These antennas are specifically designed for such systems and possibilities for narrow to wide bandwidth reconfiguration are limited. Wide to narrow band reconfiguration are potentially important for systems that combine UWB and multi-radio applications. A number of reconfigurable antennas have been demonstrated that combine wideband and narrowband functionality, recently. This is reviewed in the next section.
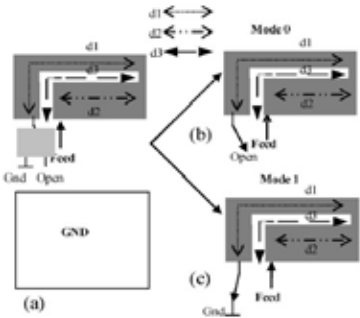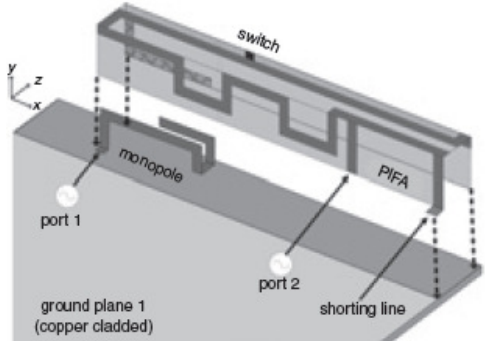
Table 2.1 Narrowband-Narrowband Reconfiguration

Ref.	Antenna Figure	Antenna structure	Switching band (GHz)	Frequency switching technique	Switch type	Number of switch
[3]		Rectangular patch	Mode 1 to Mode 8 (1.82-2.48)	Varying the patch size	PIN diode	4
[47]		E-shaped structure	Mode1: 9.2-15 Mode2: 7.5-10.7	Varying the width of E-shape.	PIN diode	15

Ref.	Antenna Figure	Antenna structure	Switching band (GHz)	Frequency switching technique	Switch type	Number of switch
[48]		Stacked square microstrip patch	Mode1: 1.75 Mode2: 0.688	Switching from stacked square to PIFA type antenna	PIN diode	3
[49]		Microstrip monopole antenna	Mode1: 2.0 Mode2: 5.0	Reconfigure the geometric structure (antenna length)	PIN and Varactor diode	2
[50]		Microstrip planar antenna with a rectangular slot	Mode1: 3.43 (SC) Mode2: 3.11 (OC)	Controlling the effective path length	PIN diode	2

Ref.	Antenna Figure	Antenna structure	Switching band (GHz)	Frequency switching technique	Switch type	Number of switch
[51]		PIFA	Mode1: 0.748-0.912 Mode2: 1.84-2.151,1.849-2.156,1.9-2.185	Re-matching antenna externally	MEMS	2
[4]		Rectangular patch	Tunable: 2.6 – 3.35	Controlling the impedance matching	Varactor	1
[52]		PIFA	Mode 1: 0.85,0.9,1.8 Mode 2: 0.9,1.9,2.05	i) Switched feed	PIN diode	2

Ref.	Antenna Figure	Antenna structure	Switching band (GHz)	Frequency switching technique	Switch type	Number of switch
[52]	Switched ground design.	PIFA	Mode 1: 0.85,0.9,1.8,1.9 Mode 2: 1.8,1.9,2.05,2.45	ii) Switched ground	PIN diode,	1
[2]		PIFA and monopole	Mode 1: 0.75-0.92 Mode 2: 1.92 &3.6 – 3.6 &5.25	Two port and switched length	PIN diode	1

2.3.2 Wideband to narrowband reconfiguration

In general, there are two ways to achieve wideband to narrowband reconfiguration. One approach is to integrate a wideband with a narrowband antenna using separate excitation ports. A second approach is to reconfigure an inherently wideband antenna either by switching parts of the antenna structure in or out or altering the loading of the antenna internally or externally.

There are six published works [7, 8, 53-57] at the time this thesis was written that integrate a wideband with a narrowband antenna using separate excitation ports. In [7], a switched sub-band antenna was integrated with a wideband antenna onto the same substrate as shown in Figure 2.9. The central part of the antenna is rotated through 180^0 by means of an electrical motor to transform between two antenna structure causing two different sub-band. The idea is good but the number of the sub-bands achieved is limited to the number of radiating patches printed on the rotating circular part. Furthermore, a rotational motor will increase the complexity of the antenna structure and also the cost. Switching time is also usually slower compared to electronic switches.
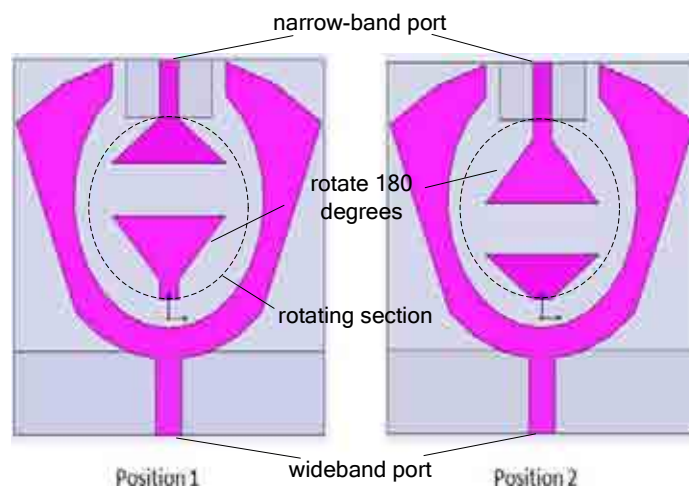
Figure 2.9 Rotation controlled antenna (dark grey-conductor on top of substrate, light grey-conductor on back) [7]

In [8], a single disc monopole, excited from two ports at opposite sides, is proposed and shown in Figure 2.10. One side was fed with coplanar waveguide (CPW) and the other with microstrip line. The CPW port is kept wideband. The second port is operated in a narrow band mode and can be reconfigured by varying the meandered rectangular slot length inserted in the ground plane. However, since the slot is within the ground plane of the monopole, one could argue that the filtering function, is being carried out by a separate filter and hence not integrated with the antenna.
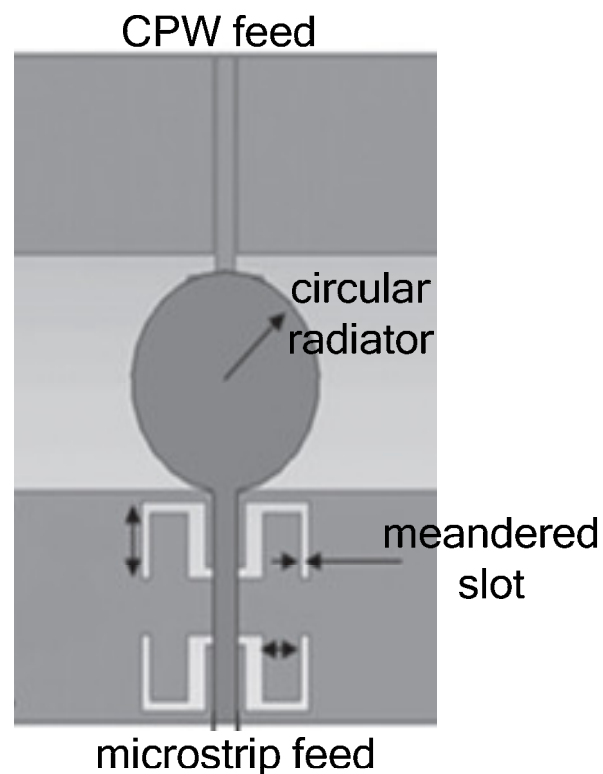
Figure 2.10 Two ports wideband monopole (microstrip feed on top of substrate, CPW feed and meandered slot on back [8]

In [53] a wideband monopole has been integrated with a planar inverted F antenna (PIFA) as shown in Figure 2.11. The PIFA used the monopole radiator as part of its ground plane and it can be reconfigured to various frequencies by external matching circuits. The

PIFA is designed to operate at 5.2 GHz. Owing to the external matching circuits, the efficiency decreased when the PIFA is tuned to other frequencies.
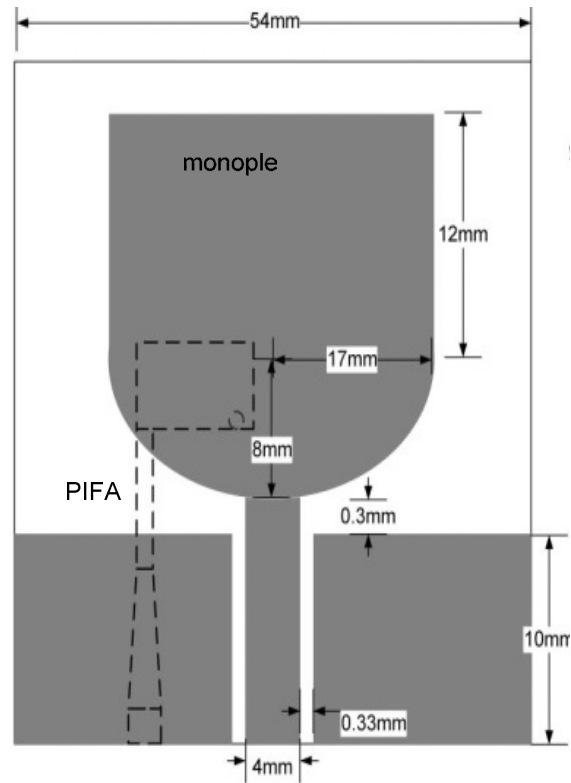
Figure 2.11 Integrated PIFA and wideband monopole (grey – conductor on top of substrate, dash- conductor on back) [53]

In [54], an ultrawide band disk monopole antenna is integrated with a narrowband slot antenna as shown in Figure 2.12. A microstrip resonator is also employed in order to produce a notch band at 5.2 GHz in the UWB frequency response. The slot antenna is designed to operate at 9.3 GHz. An external matching circuit could be used to alter the operating frequency of the antenna.
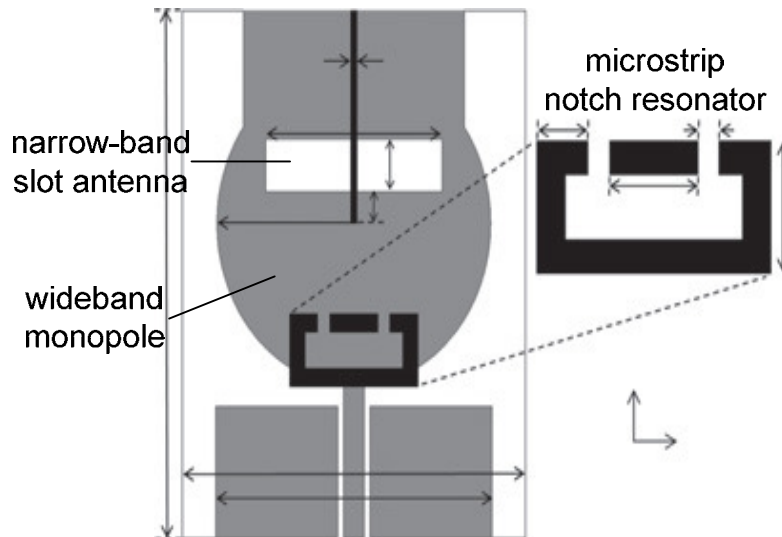
Figure 2.12 Integrated slot antenna and wideband monopole (black-conductor on top of substrate, grey-conductor on back [54]

The best configuration so far in terms of narrow-band tunability is described in [55] where a combination of a narrow band left-handed loop antenna and a printed wideband monopole is demonstrated. The left-handed loop is made tunable between 1.5 and 3 GHz using variable capacitances. Figure 2.13 shows the proposed structure.
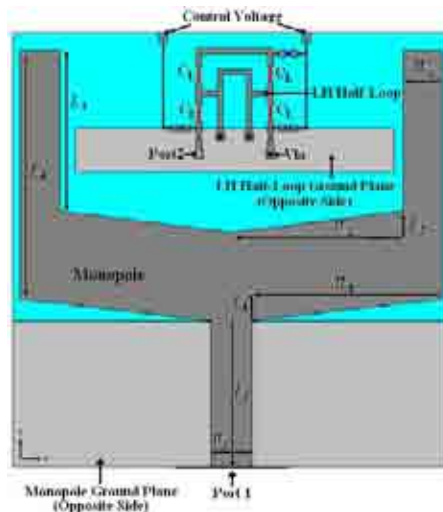
Figure 2.13 Integrated left hand loop and wideband monopole (dark grey-conductor on top of substrate, light grey-conductor on back) [55]

Other methods are described in [56] and [57], where two monopoles are fabricated on the same substrate and spaced apart side by side as shown in Figure 2.14. The monopole on the left provides wideband performance whilst the second monopole gave tunable narrow multi-band operation. The multi-band is due to harmonics. The antenna integration method suggested here may not be considered as a truly integrated, unlike the antennas presented in [7, 8, 53-55] as they do not occupy the same area.

(a)   (b)
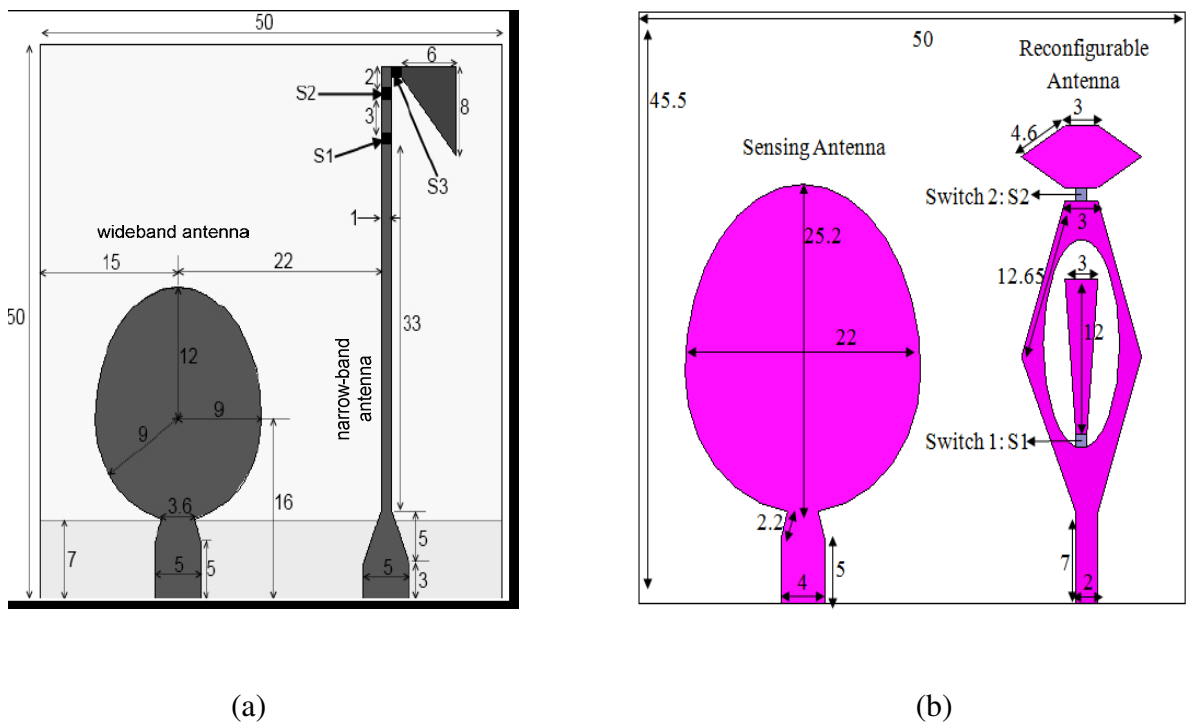
Figure 2.14 Integrated narrow and wideband monopole (a) [56] and (b) [57]

The above antennas use two separate excitation ports. In the following paragraphs, a second approach using a single excitation port, is reviewed.

In [58] a reconfigurable planar monopole to microstrip patch antenna is proposed as shown in Figure 2.15. The transformation from wide to fixed narrowband operation is rather straight forward and demonstrated by switching "in" and "out" the ground plane beneath the patch. However switching to a different narrowband operation was found to be

28

more difficult and the structure may need to be altered to reconfigure the frequency of the fixed narrowband mode.
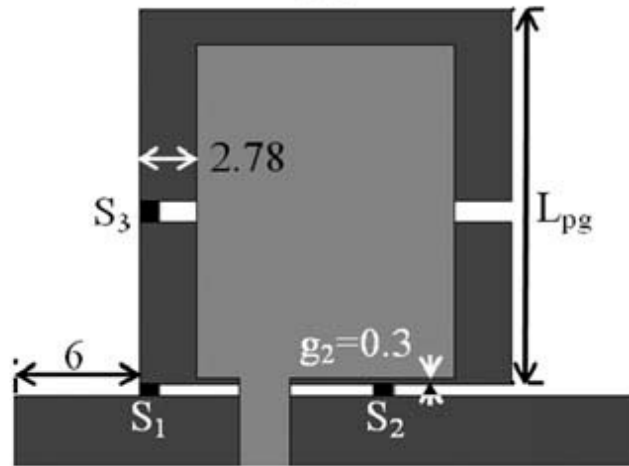
Figure 2.15 Switched ground plane patch antenna (grey- conductor on top of substrate, black-conductor on back, S_1, S_2, S_3 – switches) [58]

In [59], the same author proposed a circular slot antenna nested with two circular annuli shown in Figure 2.16. By connecting the annuli to the feed line at specific locations, it is possible to reconfigure the antenna between two wideband modes and one single narrowband mode.
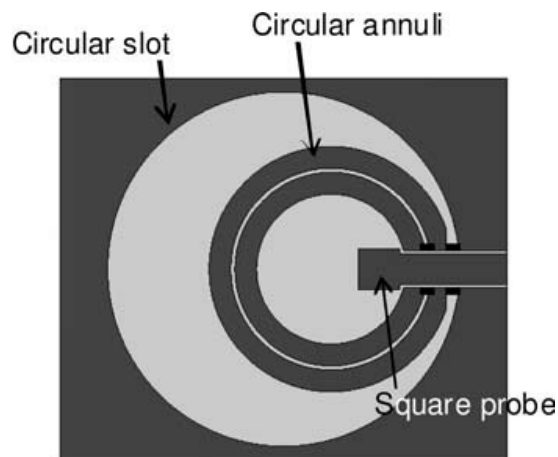
Figure 2.16 Switched annuli wideband slot antenna (black-conductor, grey-non conductor) [59]

29

A circular disk monopole that can be connected directly to the port or coupled through a halfwave resonator was presented in [60] and shown in Figure 2.17. This configuration has a resonator which is coupled to the feed line of a circular disk monopole to reconfigure an inherently wideband monopole to three narrowband modes. Ten ideal switches are used to demonstrate this. Although the paper is interesting, one could argue that the concept is merely the same as connecting a tunable filter to an UWB antenna. An example of such method is presented in [61], where an external tuning with a four stub tuner using varactor diodes (Figure 2.18) has been shown to allow wideband antenna tuning over a 30% bandwidth.
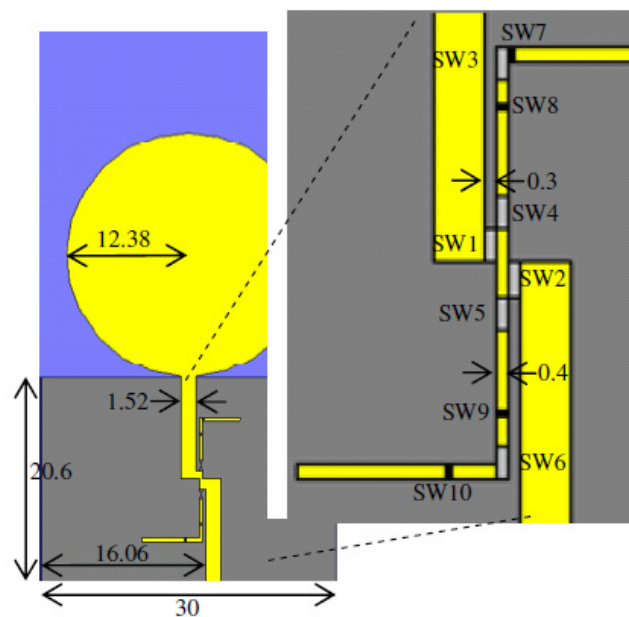
Figure 2.17 Wideband monopole with coupled resonator in the feed line (light grey-conductor on top of substrate, grey-conductor on back, dimensions in mm) [60]
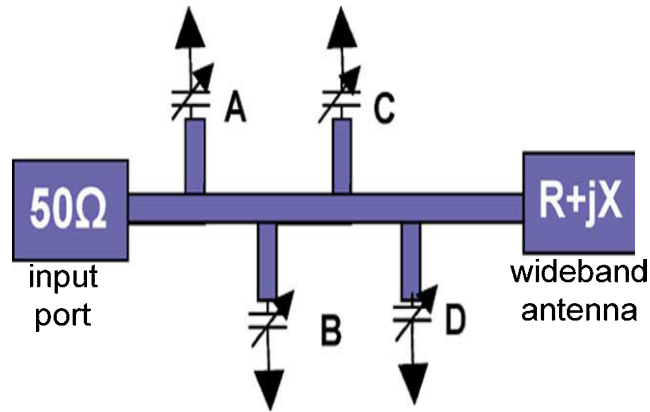
Figure 2.18 RF impedance tuner [61]

Other antennas that have been proposed for cognitive radio systems include an L-shaped slot antenna [62] where wideband-narrowband reconfiguration has been achieved by using microelectromechanical switches. The switchable quad-band antenna described in [6] used four ports to achieve four different bands and in [63] a switched wideband-dual band antenna has been described.

2.3.3 Wideband to notch band reconfiguration

A combined wideband and narrowband antenna using separate excitation ports has an advantage for systems that need two modes (wideband and narrowband) to communicate simultaneously. In this type, the challenge is to provide good isolation between ports. For a system that just requires one mode at one time, single port wide to narrowband reconfiguration can be used. Multiple communications can also be supported in the wideband mode, however it may suffer from adjacent channel interference. In this condition, alternatively, a wideband mode with a notch band capability could be useful. Work on this will now be reviewed in this section.

Work on the integration of wideband antennas with integrated fixed band interference rejection filters hence, increasing the system versatility, has appeared in the literature [64-67]. Work on fixed band notching of a Vivaldi antenna has also been reported in [39] and [38]. In [39] a U-shaped slot was employed to notch out the 5.1 – 5.8 GHz WLAN band while in [38] a quarter wavelength short stub was inserted into a radiating region to cut-off the 5.05-5.93 GHz band. The structure is shown in Figure 2.8. Considering the future wireless applications, such as cognitive radio, achieving a reconfigurable band notch operation could make an important contribution to the reduction in the level of interference reaching the RF front end [9]. Reconfiguring the notch band is useful for systems where the possibility of interference between users has been recognized as an expected issue causing degradation of the performance. Some work on reconfigurable band notch operation has been reported recently. Switched band notch operation can be obtained using switches such as PIN diode or MEMS switches as described in [68-70]. In [68], a CPW-fed wideband slot bow-tie, etched with a rectangular slot, is proposed and is shown in Figure 2.19. The antenna provides wide band rejection and is switched using PIN diode switches. Creating a slot within the radiator element will usually change or disturb the current properties either in a pass band region or in a stop band. Therefore, changing the electrical length of the slot will change the pass band performance accordingly. The method proposed here creates a reasonably wide band-notch that covers more than 1 GHz. Because the band rejection is wide, the three states can cover approximately 2 – 4.5 GHz. The band notches were switched off by shifting them out of band.
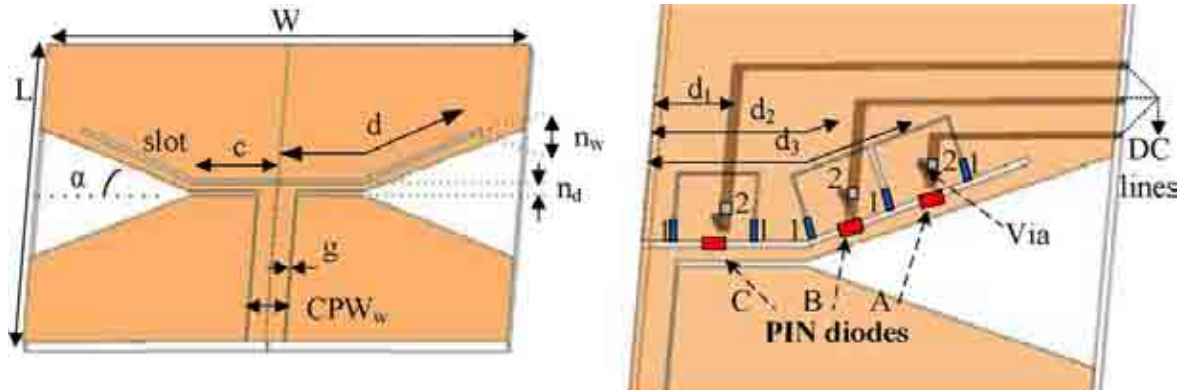
Figure 2.19 Integrated rectangular slot and wideband slot bow-tie [68]

In [69], the proposed antenna also has an on and off narrow band rejection functionality, using MEMS switches to connect and disconnect the stub into the radiator as shown in Figure 2.20a. However the band notch is fixed at one particular frequency. The switching on and off of the band rejection has also been proposed in [70] where a parasitic patch is added in the back of the rectangular monopole to obtain the band notch, as shown in Figure 2.20b.
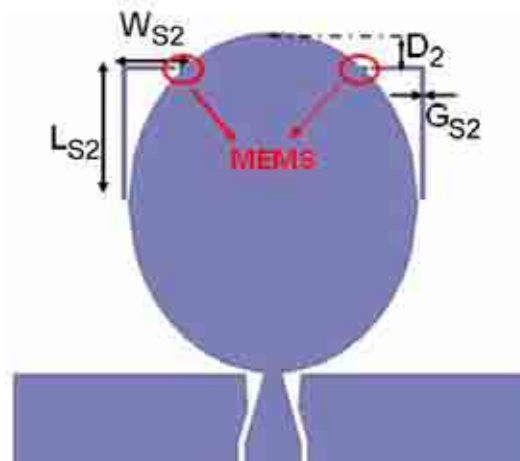
(a)
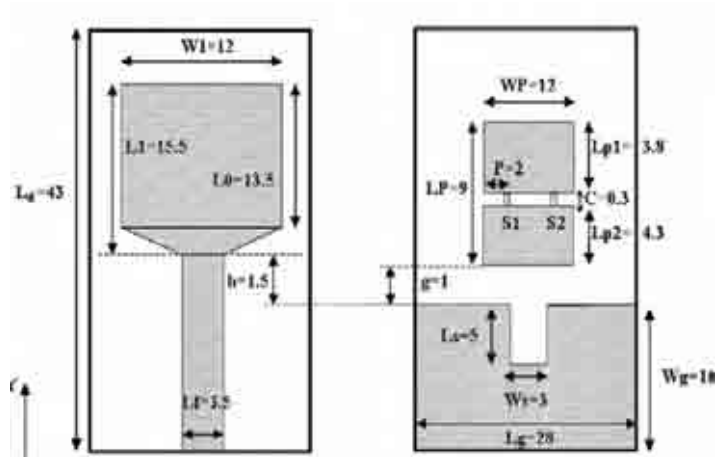
(b)

Figure 2.20 (a) Circular monopole with switchable stubs [69] and (b) Rectangular monopole with parasitic patch at the back (left-front view, right- rear view) [70]

A tunable band notch is usually achieved by using varactors as in [71-74]. In [71] a square ring slot is etched in a planar monopole to create band rejections. The monopole is perpendicular to the ground plane as shown in Figure 2.21. A varactor diode is used to obtain a tunable band rejection capability from 5.2 – 5.8 GHz.
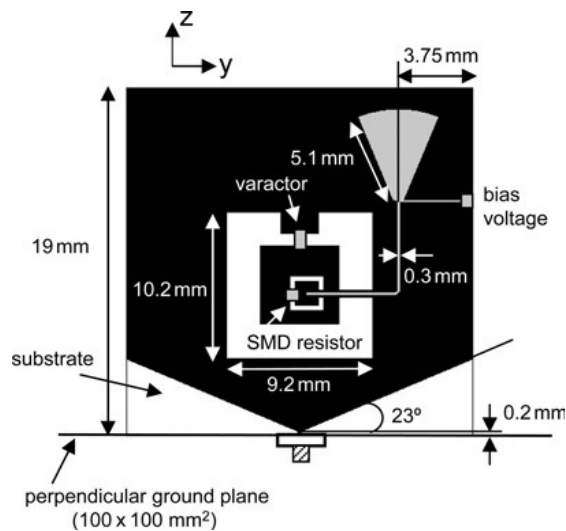
Figure 2.21 Planar wideband monopole perpendicular to ground plane (black-conductor, white-non conductor, light grey-bias line at the back) [71]

In [72], a short circuited quarter wavelength stub with a varactor is applied to a wideband planar monopole as shown in Figure 2.22. A tuning range from 4.6 – 6.5 GHz was achieved using two varactors.
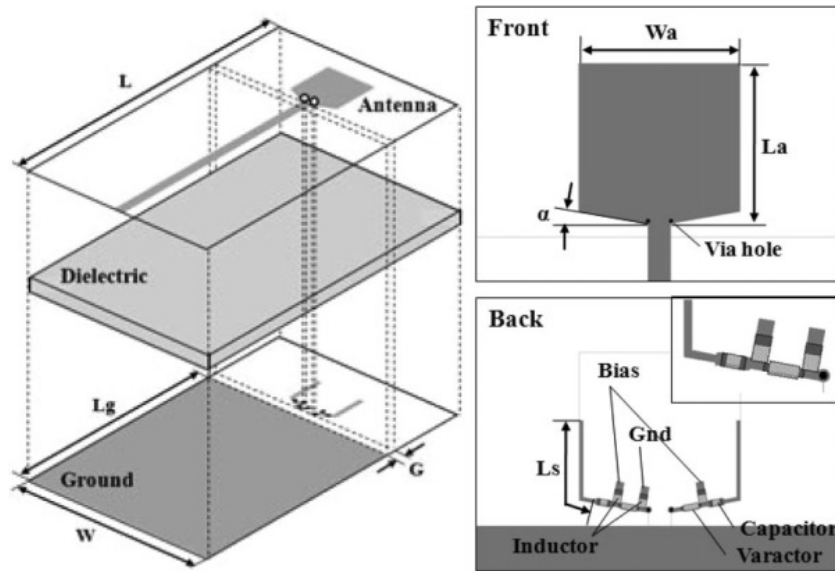
Figure 2.22 Planar monopole with short circuited microstrip stub [72]

In [73], a pyramidal monopole with slots in each face, as shown in Figure 2.23a, provides 4.8 – 7.47 GHz tunable band rejection with four varactors. In [74] a planar monopole as shown in Figure 2.23b used two slots, to demonstrate dual band notches. One capacitor is used in each slot to tune the corresponding band notch.
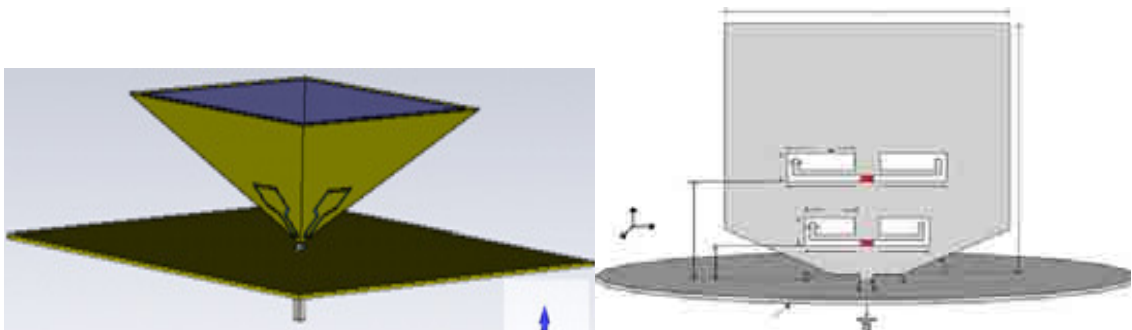
Figure 2.23 (a) Pyramidal monopole with four slots [73], (b) Planar monopole with two slot [74]

These antennas are only capable to tune the notch band over a limited range and the possibilities for a very wide tuning range are limited. In this thesis, an antenna with a notch capable of a 3.5:1 tuning ratio, or 2 – 7 GHz tuning range is proposed [75]. Table 2.2 compares the performance of the tunable notch antennas reviewed in this section [71-74] with that of the new configuration proposed in this thesis [75].

Table 2.2 Tunable band notch antenna

Antenna	Band notch technique	Number of Varactor	Rejection tuning ratio	Gain suppresion, dB
[71]	1-slot ring	1	1.11:1	7.5 (with varactors)
[72]	λ/4 short circuit microstrip line	2	1.41:1	-
[73]	4 – oval slot ring	4	1.56:1	10 (with fixed capacitors)
[74]	2- U slot shaped	2	1.26:1 (approx)	8 (with fixed capacitors)
[75]	λ/2 open circuit microstrip line	3 (in series)	3.5:1	7 – 14 (with fixed capacitors)

2.3.4 Wideband to wideband reconfiguration

Other concepts show wideband to wideband reconfiguration as presented in [76], where a wideband reconfigurable rolled planar monopole antenna demonstrated a shift in the resonant frequency by adjusting the degree of spiral tightness. The reconfiguration shows different and multiple 10-dB return loss bandwidth as opposed to a single narrowband operation. Figure 2.24 shows the antenna structure.
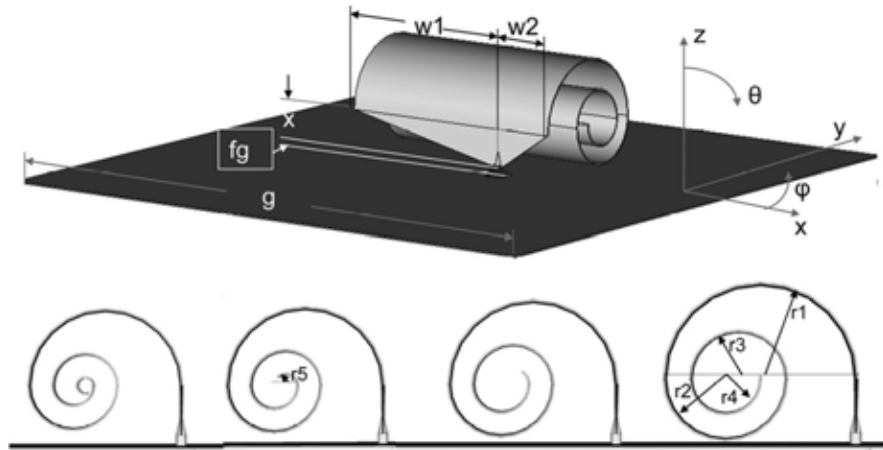
Figure 2.24 Wideband reconfigurable rolled planar monopole antenna (top – 3D view, bottom – Side view with different spiral tightness) [76]

2.4 Summary

Evolution in the world of antennas is very rapid. They have been designed to suit one or more systems. Some of them are fixed in frequency but some are not. Some of them are narrow bandwidth and some are wide in bandwidth. Most reconfigurable antennas have moderate performance due to additional loss arising from switches. With future advances in switch technology, a low loss and low cost switch may make the performance comparable with the non-switched antennas. Also, most reconfigurable antennas only allow communication in one band at a time. With narrowband to wideband reconfiguration, multiple standards can be supported at one time, however at a cost of poor out of band rejection. To overcome this, more antennas that can be reconfigured from wideband to single narrow band and can be operated with or without band rejection, need to be studied and developed. A range of possible solutions including wideband to narrowband and wideband to narrow and band notch are proposed here by the inclusion of diodes or by means of resonators that are switched in or out to interrupt the flow of currents in antenna structures. The antenna could be a suitable solution for a multi-mode

application requiring wideband and frequency reconfigurable antennas, such as in cognitive radio and military applications. Two types of antennas are chosen, namely a log periodic patch array and a Vivaldi antenna, as candidates to demonstrate wide to reconfigured narrowband operation which are potentially useful for fixed CR radio systems where a reasonably high gain antenna is needed for sensing purposes. From the literature shown in this chapter, no attempt yet has been reported to reconfigure wide to narrowband using a log periodic patch array. Also no attempt has been reported to reconfigure wide to narrowband or tunable band rejection using a Vivaldi antenna. This will now be described in the five following chapters.

CHAPTER 3

RECONFIGURABLE LOG PERIODIC APERTURE COUPLED PATCH ARRAY

3.1 Introduction

Log-periodic antennas have multiple elements, which are scaled in a log-periodic fashion. Using this property, and by inserting switches, a frequency reconfigurable log periodic antenna is proposed. Recently, work on reconfigurable log periodic antennas has been reported. In the log periodic dipole array described in [18], ideal switches are used to control each pair of dipole arms of the antenna. This can switch from a wideband of 1 – 3 GHz, to several narrow bands. Similar work on this has also been reported in [25, 26]. As opposed to wideband to narrowband reconfiguration, work in [27-29] demonstrates band notch method for log periodic antennas. In this chapter a novel log periodic antenna with added switched band functionality to operate in a wideband or narrowband mode is presented. The antenna is based on the log periodic monopole array [19], but the monopole is replaced by a patch with an aperture coupled feed which makes the proposed antenna very low profile yet has the added functionality to reconfigure into a narrow band mode.

The patch arrangement is similar to that of the uniform series feed aperture coupled leaky wave antenna presented in [77]. The antenna reconfiguration is realized by inserting switches into the slot aperture of the structure. A wide bandwidth mode demonstrated from 7.0 – 10 GHz and three narrowband modes at 7.1, 8.2 and 9.4 GHz can be selected. A prototype with ideal switches has been developed. Measured results show good performance of the proposed designs. Section 3.2 discusses the advantages in choosing an aperture coupled log periodic patch array as a candidate for reconfiguration. Section 3.3 and 3.4 discuss the problem of the structural stop band and the procedure for eliminating it. The effect of the scaling factor and element bandwidth are explained in section 3.5. The fabricated antenna is discussed in section 3.6. Finally the results are presented in section 3.7 and 3.8, followed by summary in section 3.9.

3.2 Motivation

The criteria defining the best reconfigurable design, such as the number of switches used to reconfigure the structure and the design simplicity, are investigated here. For that purpose, the structure of the log periodic printed dipole, an electromagnetic coupled patch array and an aperture coupled patch array are compared. Potentially, the aperture coupled log periodic patch array (LPA) is a good candidate. The configuration allows each radiating element to be controlled using one switch, thus, offering fewer switches compared to a log periodic printed dipole [18]. This thus reduces the problems of biasing many switches. In addition, because each patch is coupled to the feed line through a slot aperture in a ground plane, switching on or off the radiating element can be achieved relatively easyly by allowing a single switch to be placed at the centre of the aperture. On the other hand, an electromagnetic coupled structure such as that reported by [21] will be

very hard to switch because there is no specific coupling mediator between the patch and the feed line, like the slot aperture as proposed here. Furthermore, biasing for the switches can be located within the ground plane and therefore coupling to radiation will be small. In this chapter the design of a wideband log periodic aperture coupled microstrip antenna and its reconfigurable version is proposed. Because of the structure size, the proposed antenna is designed to operate from 7 – 10 GHz. A wider bandwidth can be obtained but with more elements and bigger in size. A nearly omnidirectional pattern could be achievable by placing a set of LPA's around a tapered shape cylinder where each of the LPA's has a beam in forward fire direction. To feed a circular array in order to get a nearly omnidirectional pattern, one can use a '1 to N' power splitter, where N is the number of power splitter output ports, each output port being connected to an LPA. The number of LPA's will determine how smooth or rippled the omni pattern will be. The tapered cylindrical shape is shown in Figure 3.1. It can be seen that the patches are log periodically distributed around the cylinder, where $D_{n-1} = \tau(D_n)$, and τ is the expansion factor. This arrangement may not be possible if made on a straight shaped cylinder. Figure 3.2 explains this.
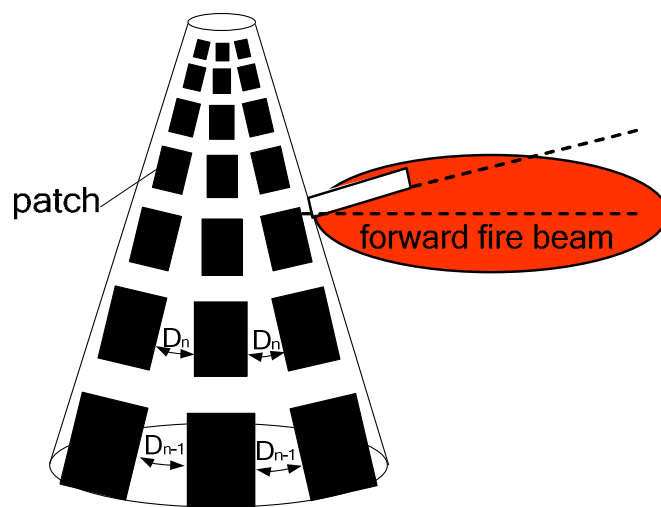
Figure 3.1 LPA arrangement on the taper shaped cylinder

41
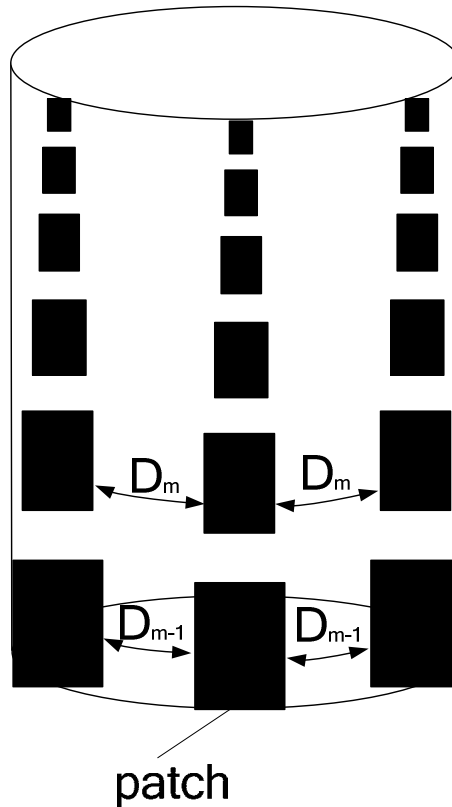
Figure 3.2 LPA arrangement on the straight shaped cylinder

3.3 Structural Stop Band

To achieve a broadside direction, the feeding phase should be either set to 0^0 or 360^0. The physical spacing between adjacent elements can be of any value but should be less than one wavelength to avoid grating lobes [20]. The simulation results however show that high VSWR occurs when the phasing is one wavelength between elements in the log periodic aperture coupled patch array. This can be explained as in Figure 3.3, showing a transmission line loaded with patches. Generally, each patch creates a small mismatch in the line. Therefore if phasing of 0^0 or 360^0 between each element is employed, the reflections will add up in phase and thus poor input return loss will result.
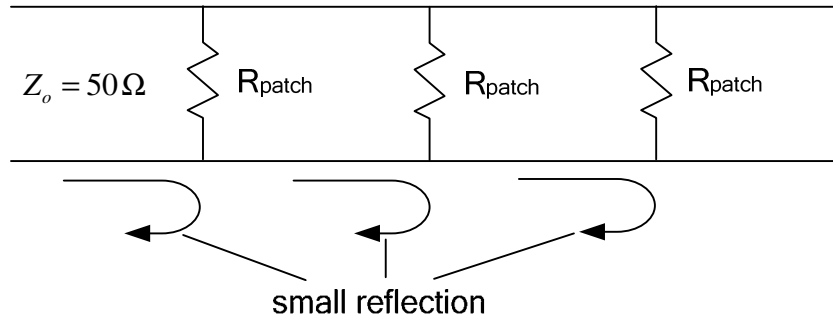
Figure 3.3 Simplified equivalent circuit of series patch in the transmission line

The condition of minimal VSWR is only met when the phase is set less or more than 360^0, which then diverts the beam angle to a forward or end fire direction. The forward fire direction is chosen when the structure is fed from the high frequency end in order to obtain nearly an omni-directional pattern when placing around a tapered shape cylinder as shown in Figure 3.1. Furthermore, feeding at this end should stop excitation of higher order mode resonances in the low frequency elements beyond the active region [21]. In general, the condition for forward fire at $\theta = 0^0$ can be met when the phasing between elements, β, is 270^0 if the distance between array elements in free space, σ is 0.25λ. This is obtained from equation 3-1 given by [20].

$$\beta = -k\sigma\cos\theta \qquad\qquad \textbf{3-1}$$

and $k = 2\pi/\lambda$. Figure 3.4 shows the configuration of the log periodic aperture coupled patch array. The excess length, d, between adjacent elements is determined by β. For $\beta = 270^0$, $d = 0.75\lambda_g$.
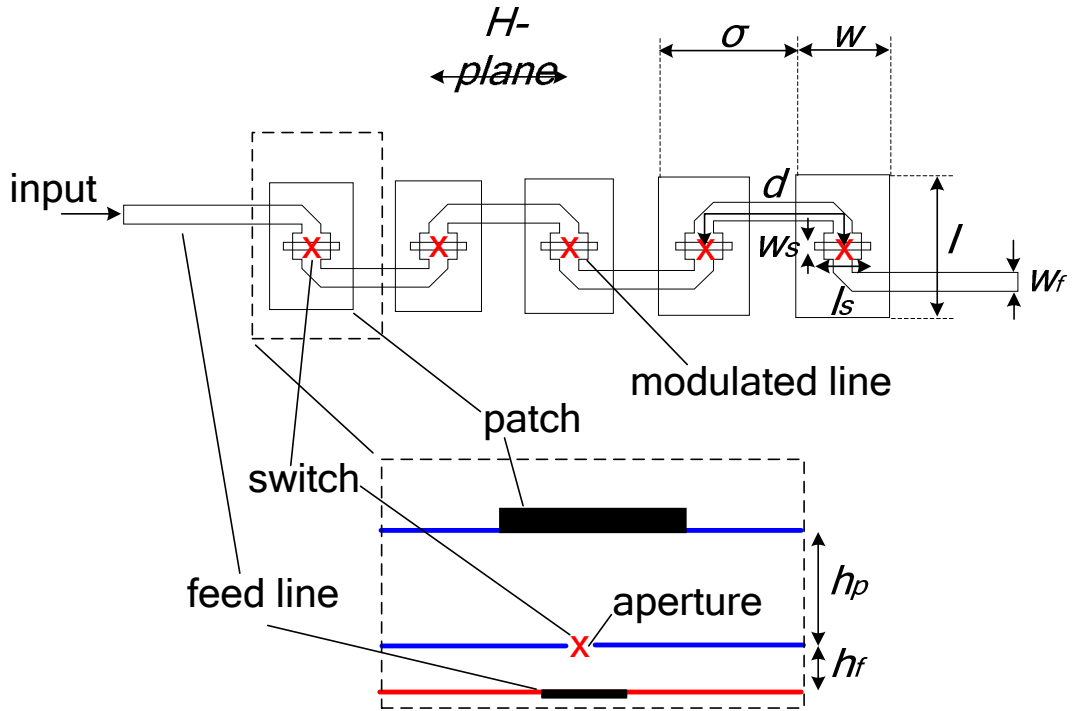
Figure 3.4 Log periodic aperture coupled patch array, w_f - feed line width, h_f - feed line substrate thickness, h_p - patch substrate thickness, d – excess length, σ - free space spacing, w - patch width, l - patch length, w_s - aperture width, l_s - aperture length

If d is greater then half a wavelength, attenuation below the resonant frequency will occur [78]. This attenuation is called a structural stop band. The structural stop band will reflect a portion of energy and cause high VSWR to the input. To understand the structural stop band completely one can examine the dispersion data and the image impedance of each of the cells of the log periodic structure. Figure 3.5 shows a single cell of the periodic structure with a shunt load whose characteristic impedance is, Z_s. R_s represents loss in the load whilst L is the length of the load. Z_o is a characteristic impedance of the line. For the periodic structure, the characteristic equation is given by [79]

$$\cosh \gamma d = \frac{A + D}{2} \qquad \text{3-2}$$

where $\gamma d = (a + jb)d$ and A and D are parameters of the ABCD matrix for the cell.

Strong attenuation, ad, occurs when $bd = 0^0$ or 180^0 where $ad = \cosh^{-1} \mid \dfrac{A+D}{2} \mid$. For a

symmetric cell, the image impedance is given by [79]

$$Z_i = \sqrt{\dfrac{B}{C}} \hspace{8cm} \text{3-3}$$
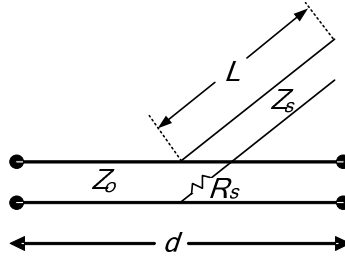
Figure 3.5 Single cell with a shunt load of periodic structure

The shunt load Y_s is given by [78]

$$Y_s = \dfrac{1}{R_s - jZ_s \cot kL} \hspace{6cm} \text{3-4}$$

and

$$A = \cos kd + j\dfrac{Y_s Z_o}{2}\sin kd \hspace{6cm} \text{3-5}$$

$$B = jZ_o \left[\sin kd + j\dfrac{Y_s Z_o}{2}(1-\cos kd) \right] \hspace{4cm} \text{3-6}$$

$$C = jY_o \left[\sin kd - j\dfrac{Y_s Z_o}{2}(1+\cos kd) \right] \hspace{4cm} \text{3-7}$$

$$D = \cos kd + j\dfrac{Y_s Z_o}{2}\sin kd \hspace{6cm} \text{3-8}$$

For a case (case 1) where d is a quarter of the guided wavelength, it is observed that the image impedance calculated from equation 3.3, 3.6 and 3.7 does not vary much from 50 Ω below the resonant frequency (see Figure 3.6a). The concept of "image impedance" is

explained in reference [79]. It is the impedance that occurs when the section is embedded in an infinite line of similar sections. In other word it can also be defined as the terminating impedance on the output port which leads to an input impedance that has the same value.

An attenuation owing to radiation, copper and dielectric loss can be seen in Figure 3.6b. This attenuation occurs when bd reaches 180^0 (see Figure 3.6c). However for a case (case 2) where excess length is used (i.e $d \geq$ half of the guided wavelength) the image impedance varies from 50 Ω and the structural stop band exists because bd reaches 180^0 before resonance (see Figure 3.7). When feeding from the high frequency end, energy goes to the resonant region and is mostly radiated. Beyond that there is not much energy left and therefore the stop band at high frequency will not affect the antenna operation too much. However the stop band below the resonant frequency is really the problem.

(a)

46
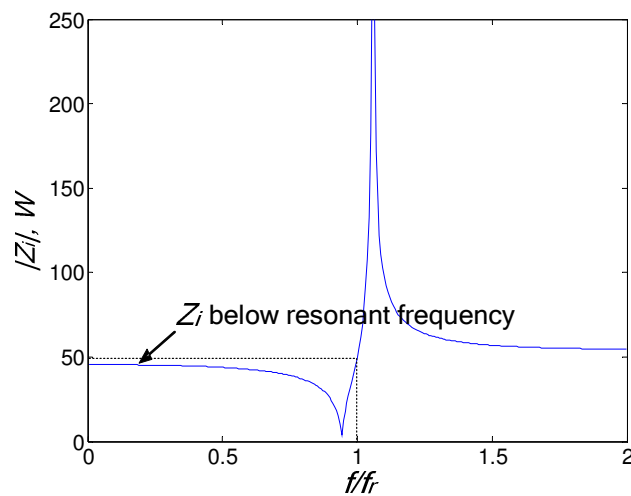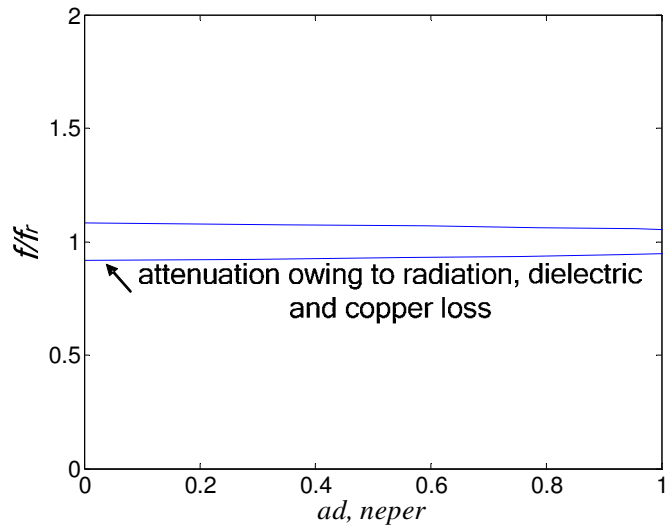
(b)
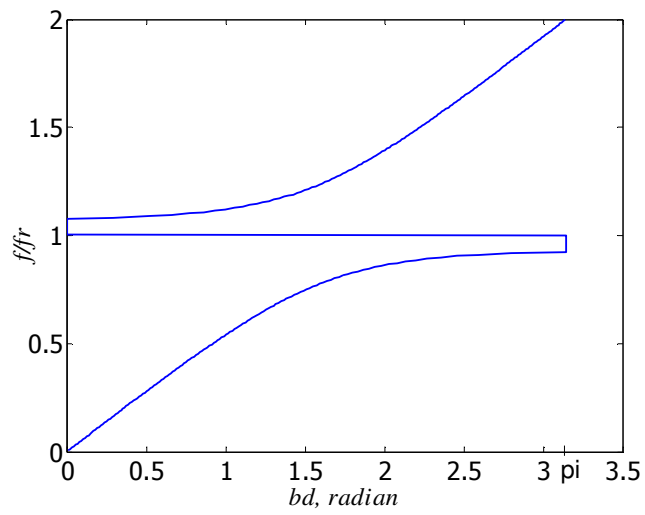
(c)

Figure 3.6 (a) Image impedance, Z_i, (b) Attenuation, αd , (c) Phase, *bd*,

Case1, $d = 0.25\lambda_g$
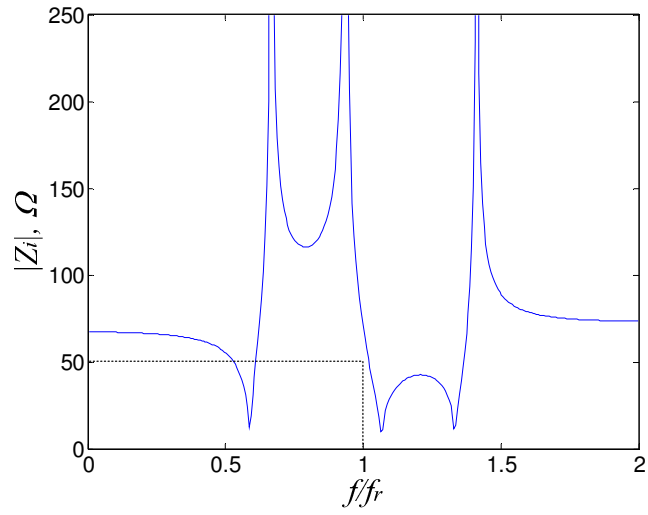
(a)
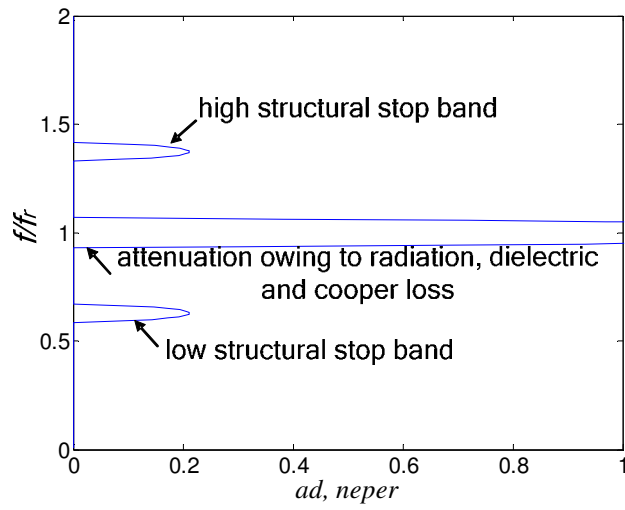
(b)
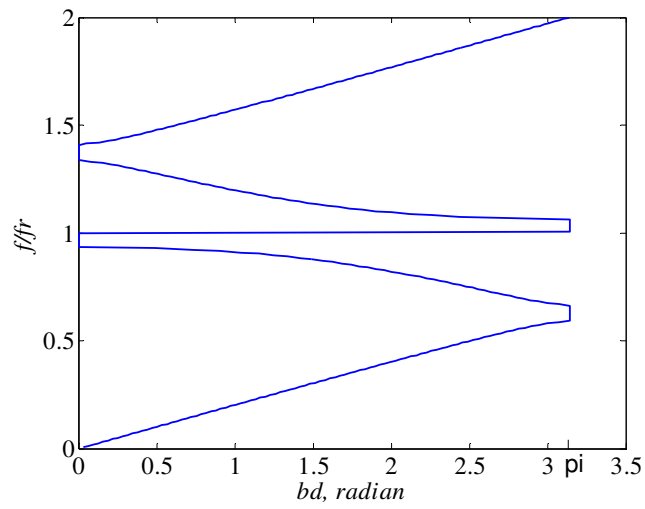
Figure 3.7 (a) Image impedance, $|Z_i|$ (b) Attenuation, αd (c) Phase, bd,

Case2, $d = 0.75\lambda_g$

A cascade of single cells forming a log periodic structure loading by shunt loads with an expansion factor, τ, is shown in Figure 3.8. If each cell has at least one structural stop band as shown in Figure 3.7b, a limited bandwidth (<2:1) log periodic array will result. To overcome this, the variation of image impedance must be minimal as in case 1 to eliminate the structural stop band.
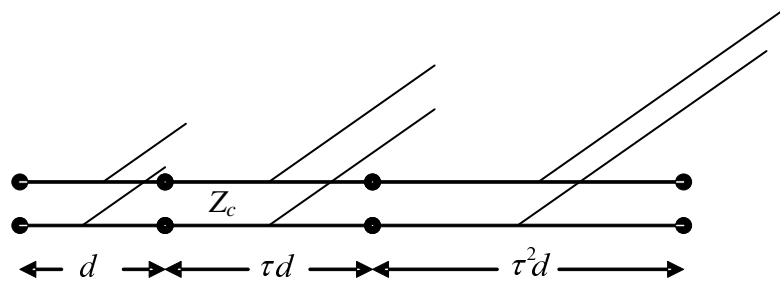
Figure 3.8 A cascaded single cells forming a log periodic structure

3.4 Eliminating Structural Stop Band

A method suggested by [78] for minimizing the variation of image impedance is applied here. The minimization is achieved when the impedance of the line is modulated. Figure 3.9 shows how the line is modulated by changing the characteristic impedance on a small part of the line. $d = 0.5d_2 + d_1 + 0.5d_2$ as in Figure 3.9.

.
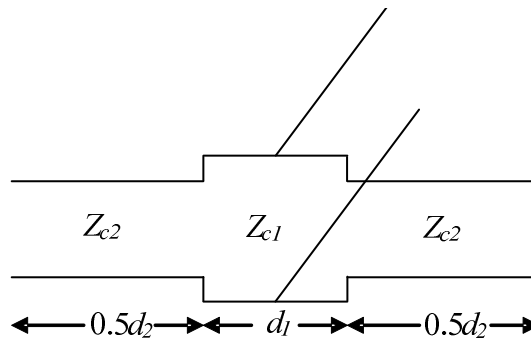
Figure 3.9 Transmission line with impedance modulation

An example of eliminating the structural stop band is now described. A two-port section representing a single element of the structure is shown in Figure 3.10a. d is $0.75\lambda_g$. The structure resonates at 9.583 GHz as shown in Figure 3.10b. Figure 3.10c shows the calculated image impedance. It shows the image impedance is very different from 50 Ω between 6.65 and 7.84 GHz. This causes a stop band between those frequencies, as shown in Figure 3.10d. It occurs below the resonant frequency of 9.583 GHz. The magnitude of the image impedance at this frequency is 31 Ω.

port 1

d

port 2

(a)

9.583 GHz
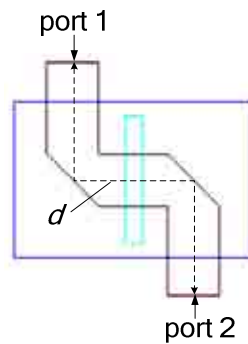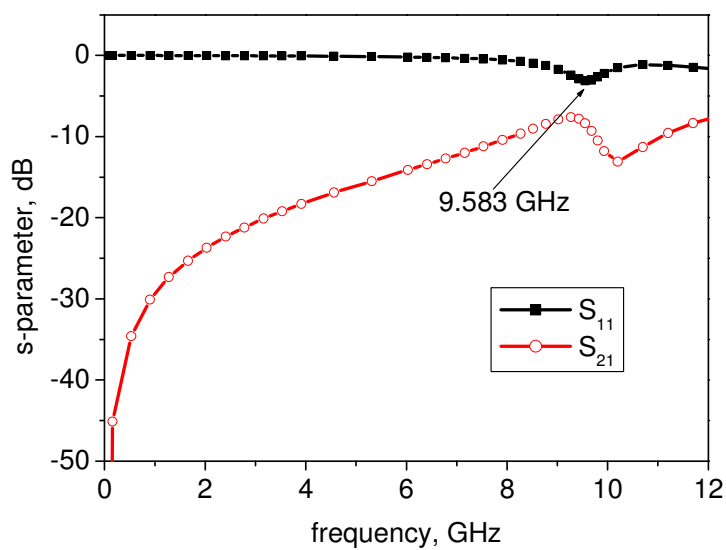
(b)
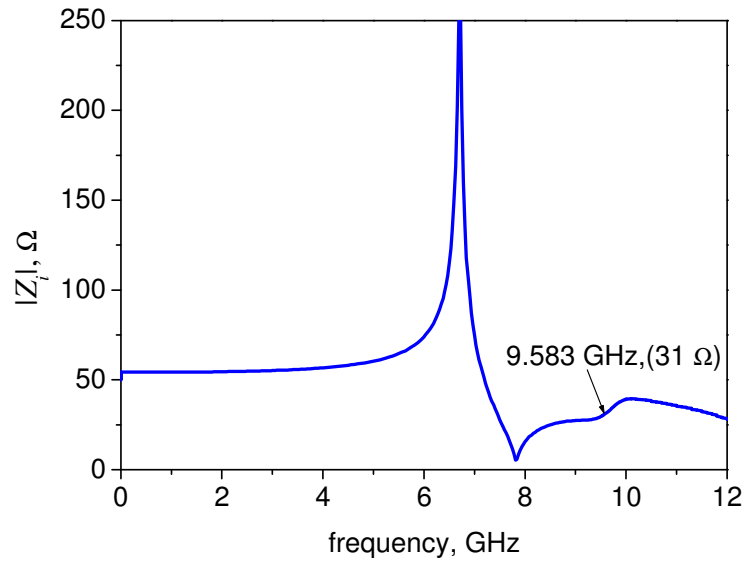
(c)
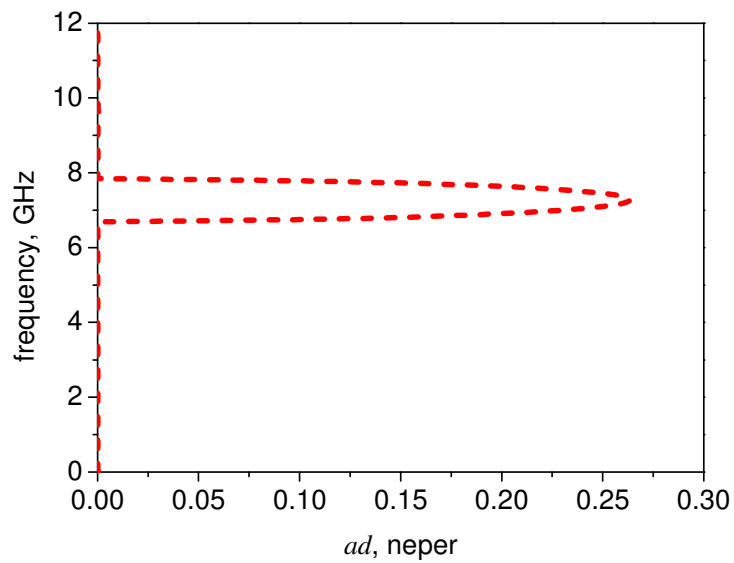
(d)

Figure 3.10 (a) Single cell of aperture coupled fed structure without impedance modulation, (b) simulated S_{11} and S_{21}, (c) Image impedance, $|Z_i|$, (d) Attenuation, ad

To eliminate the stop band, the variation of image impedance has to be minimized. This is done by modulating the impedance of the line. Figure 3.11a shows the line, where the modulated part has a width, w and a length d_1. In this example the line width, w, is set

according to the value of image impedance at 9.583 GHz, when the feeder is unmodulated. d_1 is then optimised until the variation of the image impedance is minimised. Figure 3.11b shows the image impedance and Figure 3.11c shows the stop band response after the modulation. The variation of image impedance below the resonant frequency is now small and it is now 44.28 Ω at the resonant frequency. The attenuation plot shows $ad = 0$, from 0 to 12 GHz, demonstrating that no stop band occurs. This method is applied for each element that produces a stop band within the operating frequency of 7 – 10 GHz.
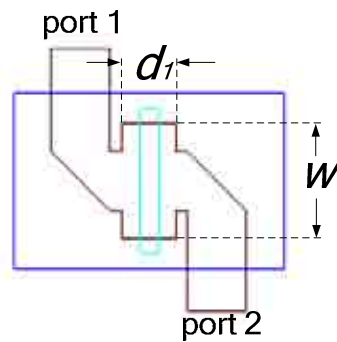
(a)
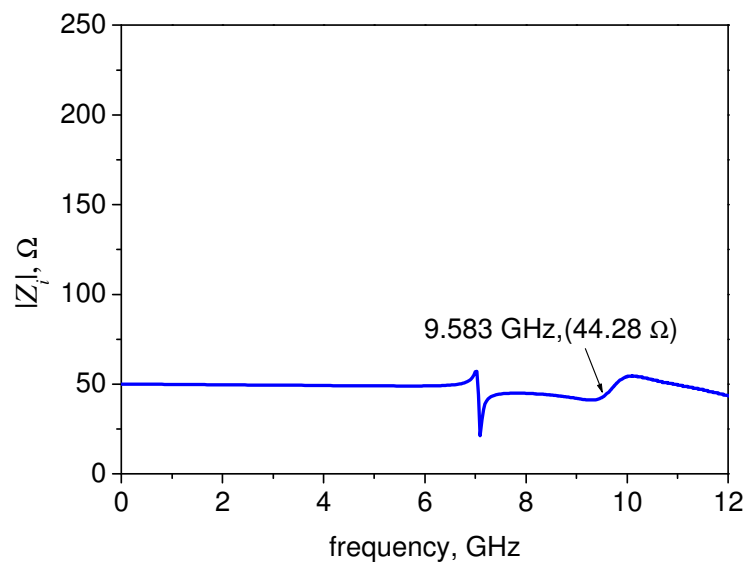
(b)
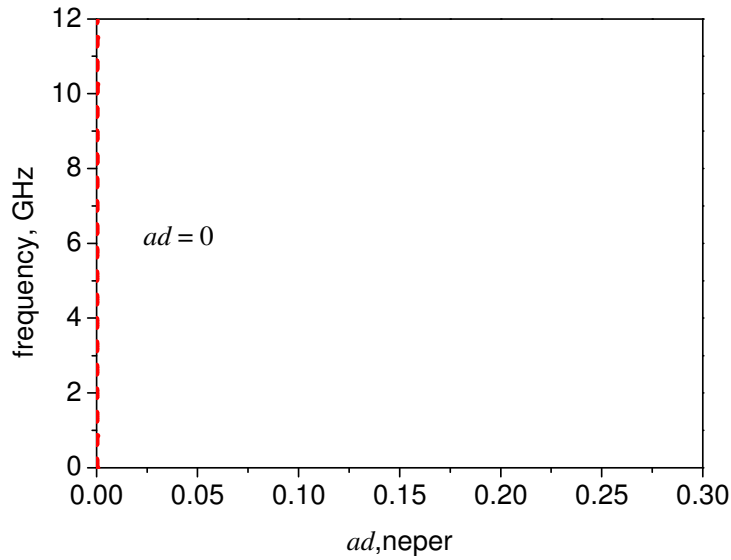
(c)

Figure 3.11 (a) Single cell of aperture coupled fed structure with impedance modulation, (b) Image impedance, |Z_i|, (c) Attenuation, *ad*

3.5 Scaling Factor and Element Bandwidth

The first two criteria needed to design a very wideband log periodic aperture coupled fed array have been described. A good match can only be achieved if the radiation pattern is set to forward or backward fire, whilst a very wideband response is achieved by employing a modulated impedance feeder, eliminating the structure stop bands. In this section, two other criteria are further discussed.

The relation between element bandwidth and scaling factor is studied. The scaling factor must suit the bandwidths of individual elements in order to obtain a reasonable efficiency. Figure 3.12 shows the calculated efficiency of a ten element array with 1.03 and 1.015 expansion factors simulated on Duroid substrate.

53
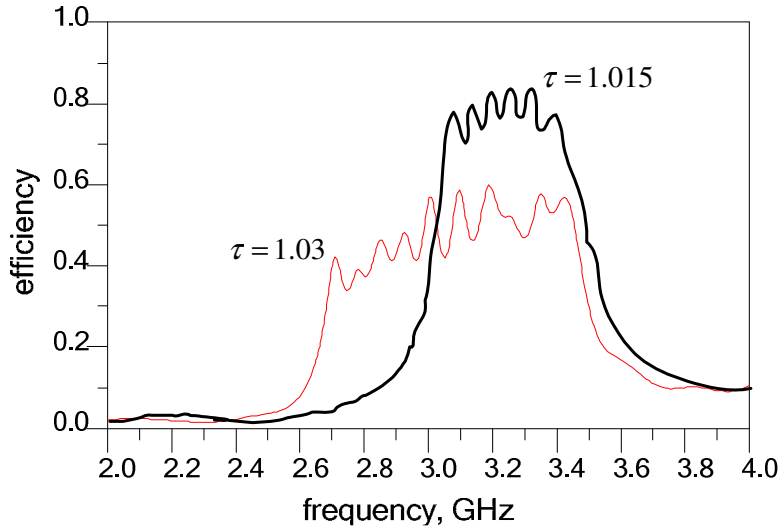
Figure 3.12 Efficiency of 10 elements array, $\varepsilon_r = 2.2$ **,** $w_f = 2.38$ **mm,** $h_f = 0.787$ **mm,**
$h_p = 1.575$ **mm, (**$d_1 = 53.31$ **mm,** $\sigma = 35.14$ **mm for** $\tau = 1.015$ **), (**$d_1 = 53.7$ **mm,** $\sigma = 35.54$ **mm**
for $\tau = 1.03$ **),** $w_1 = 20.25$ **mm,** $l_1 = 27$ **mm, see Figure 2.4 for definition of the**
dimensional parameters

The efficiency can be approximated as follows:.

$$P = 1 - |S_{11}|^2 - |S_{21}|^2 \qquad\qquad \textbf{3-9}$$

where losses are ignored.

The efficiency is low and varies between 40 to 60% within the frequency band for the array using $\tau = 1.03$. This suggests the scaling factor is far too high. The efficiency increased about 30% for the array using $\tau = 1.015$. The overall bandwidth however reduced to 50%. Alternatively the efficiency can be increased by using a wider individual element bandwidth. Generally this can be done by reducing the dielectric constant and increasing the substrate thickness. A 2 mm thick rohacell substrate with dielectric constant 1.09 is chosen for the optimum coupling and bandwidth. The coupling factor is proportional to the substrate thickness. A thin Duroid substrate (height = 0.245 mm, ε_r = 2.2) is used to provide radiating elements. Figure 3.13 shows the antenna in Figure 3.4 after it has been sandwiched with the Rohacell.
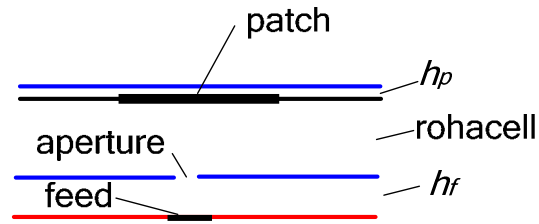
Figure 3.13 Cross section of microstrip patch log periodic array with rohacell in the middle to increase individual bandwidth

Figure 3.14 shows the efficiency of a five element LPA using rohacell substrate with an expansion factor of 1.02. The efficiency is observed to be much higher and varies from 76 to 98% between the operating bands. Based on this, a wideband LPA is designed.
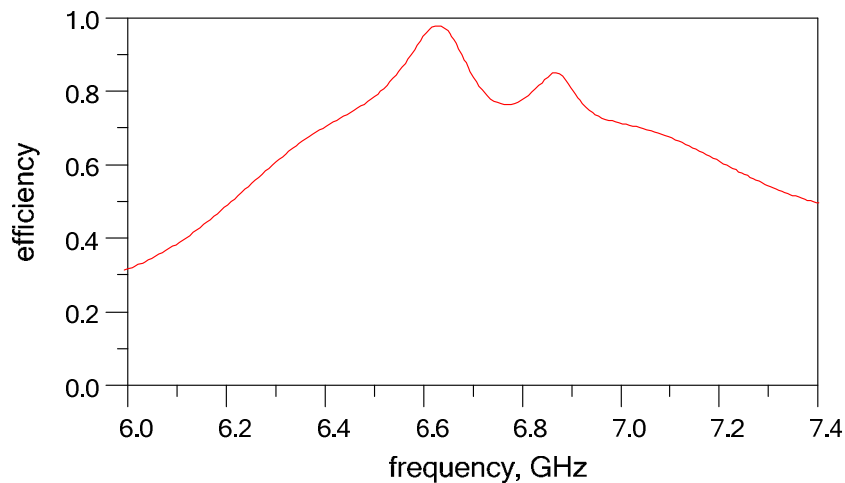
Figure 3.14 Efficiency of 5 element array, $\tau = 1.02$, $\varepsilon_r = 2.2$ (for h_f and h_p), $\varepsilon_r = 1.09$ (for rohacell), w_f = 2.38 mm, h_f = 0.787 mm, h_p = 0.254 mm, rohacell = 2 mm, d_1 = 23.72 mm, $\sigma = 15.86$ mm, w_1 = 10.4 mm, l_1 = 16 mm,

3.6 Reconfigurable Log Periodic Aperture Coupled Patch Array Design

In this section the design of the antenna is described. Figure 3.15 shows the proposed antenna structure with 20 radiating elements. The smallest element (patch 1) size

55

is $w_1 = 7$ mm and $l_1 = 10.77$ mm. The expansion factor of 1.02 is used. The patches are printed on a 0.254 mm thick Duroid 5880 substrate with the dielectric constant of 2.2. The meandered $50\,\Omega$ feed line and slot apertures are etched on a similar 0.787 mm thick substrate. The array is terminated with a matched load at the end of the line to prevent reflections. Each aperture is spaced a quarter wavelength apart and fed with 270^0 phasing thus giving a forward fire radiation pattern. A single switch, denoted as 'x' in Figure 3.15b and Figure 3.15c, is placed at the centre of each aperture. Rohacell foam with a dielectric constant of 1.09 and thickness of 2 mm is sandwiched between the patch and feed substrates. The patch configuration is arranged in the H-plane axis. The feed line is enclosed with a screening box size of h_b x l_b. This is important to reduce back radiation. The box size (h_b is 4.18 mm and l_b is 12.7 mm) is designed so that the cut off frequency is at 11.8 GHz which is above the top end operating band of 10 GHz. In the simulation, metal pads, of size 1 mm x 1 mm, have been used to approximate switching devices. The presence of the metal pad represents the switch on state and their absence represents the off state. This is believed acceptable and suitable to demonstrate the basic switching concept. For a twenty element LPA, twenty switches are employed. Wideband operation is achieved when all the switches are in off states thus making the antenna act as a normal log periodic antenna. To provide narrow band operation, such as high band mode, the four most high frequency slots were kept open. The rest of the slots are closed by bridging them with the switches. The other sub bands are achieved by bridging a group of slots of the antenna as shown in Table 3.1. The design has been simulated by CST simulation software. The boundary has been set to open add space and the port used in the model is a waveguide port. All details of the box, excluding the screw as seen in the photograph of Figure 3.15 for clamping the box, were included in the simulation. Details of box dimensions are presented in Appendix E.
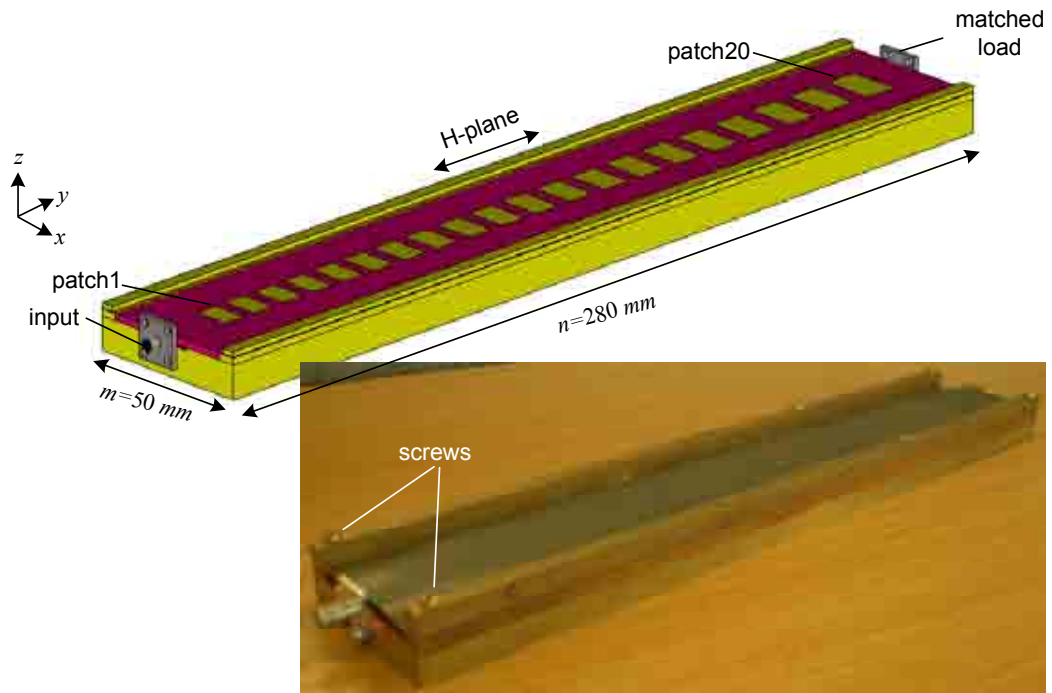
(a)
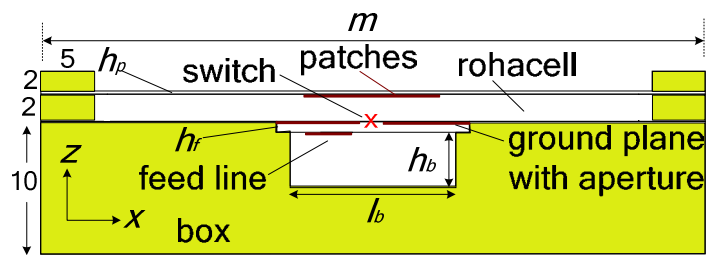
(b)
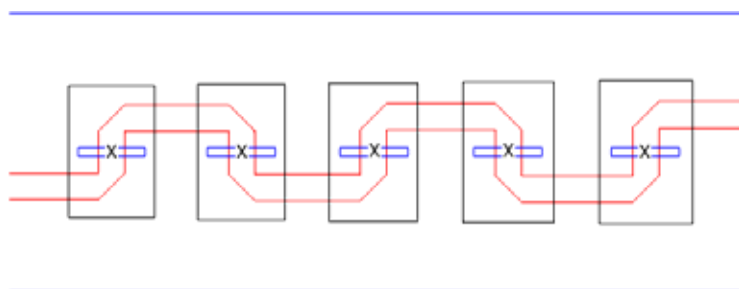
(c)

Figure 3.15 Proposed antenna structure (a) Perspective view (b) Side view (c) Top view, $\tau = 1.02$, $\varepsilon_r = 2.2$ **(for** h_f **and** h_p**),** $\varepsilon_r = 1.09$ **(for rohacell),** w_f **= 2.38 mm,** h_f **= 0.787 mm,** h_p **= 0.254 mm, rohacell = 2 mm,** d_1 **= 16.1 mm,** $\sigma = 15.86$ **mm,** w_1 **= 7 mm,** l_1 **= 10.77 mm,**

Table 3.1 Switches location

No of Slot	Wide band	High band	Mid band	Low band
1	o	o	X	X
2	o	o	X	X
3	o	o	X	X
4	o	o	X	X
5	o	X	X	X
6	o	X	X	X
7	o	X	X	X
8	o	X	o	X
9	o	X	o	X
10	o	X	o	X
11	o	X	o	X
12	o	X	o	X
13	o	X	o	X
14	o	X	X	X
15	o	X	X	X
16	o	X	X	o
17	o	X	X	o
18	o	X	X	o
19	o	X	X	o
20	o	X	X	o

o-, OFF states (open); x-, ON states (closed)

3.7 Simulation Results

In this section, simulation results are first presented to demonstrate the concepts. The simulated wideband mode scattering parameters and the simulated efficiency are shown in Figure 3.16a and Figure 3.16b. The antenna operates over a frequency range of 7 to 10 GHz with efficiency ranging from 70 to 95%. Figure 3.17 shows the effects on the radiation patterns with and without the screening box. There is strong back radiation from the feed line in Figure 3.17a when the screening box is absent. The back radiation is effectively reduced as in Figure 3.17b after the screening box is in place. Figure 3.18

shows the simulated radiation pattern in wideband mode. The pattern is forward fire of 60^0 at 7.1GHz, 55^0 at 8.2 GHz and 50^0 at 9.4 GHz.
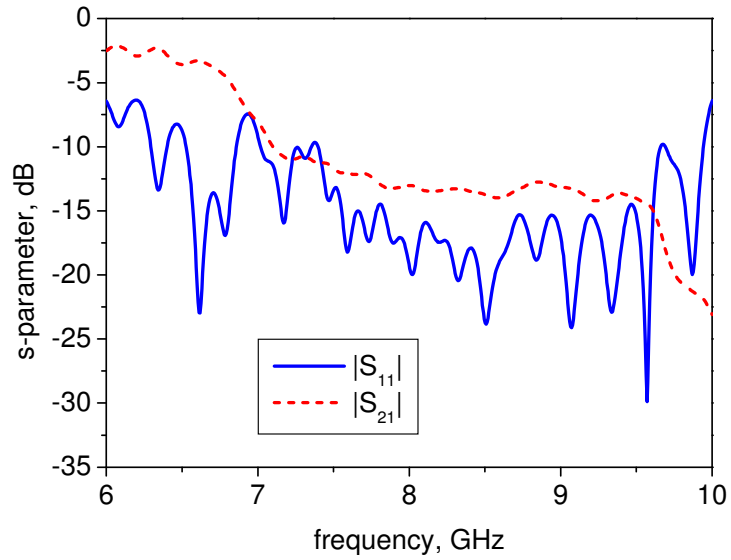
(a)
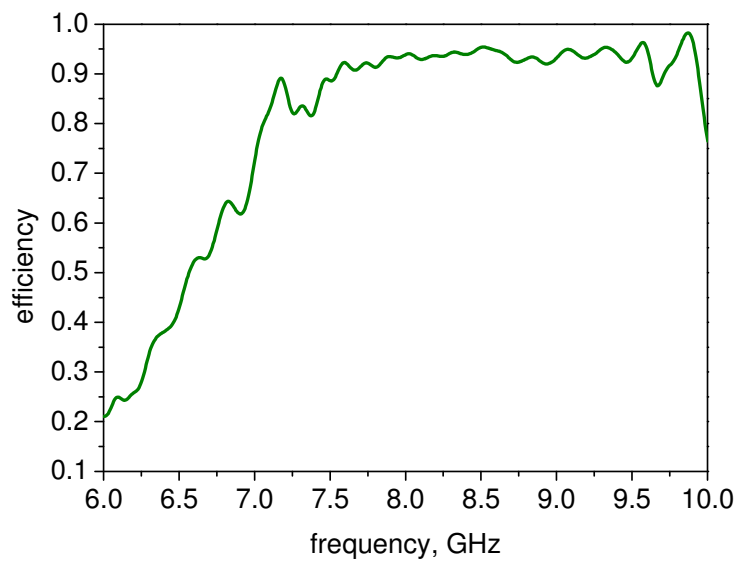
(b)

Figure 3.16 Simulated wideband mode, (a) scattering parameters (b) efficiency
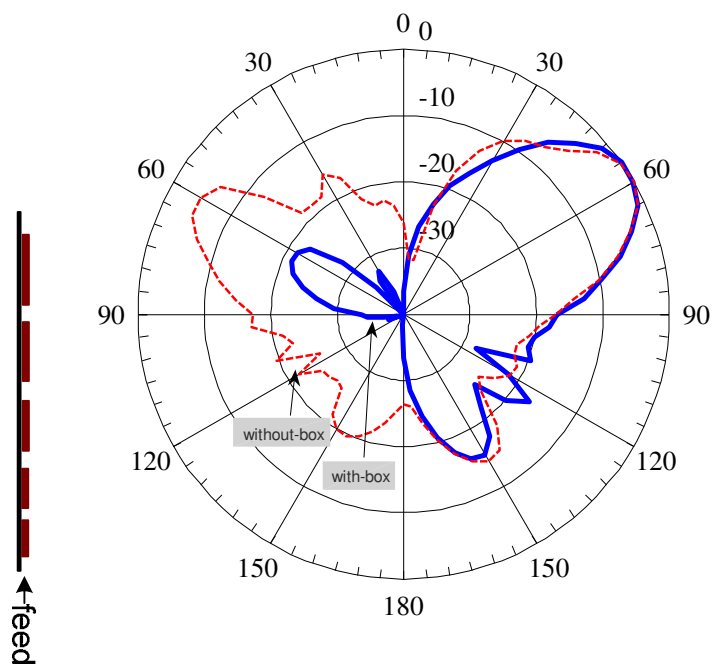
(a)   (b)

Figure 3.17 Simulated effects of screening box on radiation pattern (H-plane) excited at 8.2 GHz, (a) without-, (b) with screening box
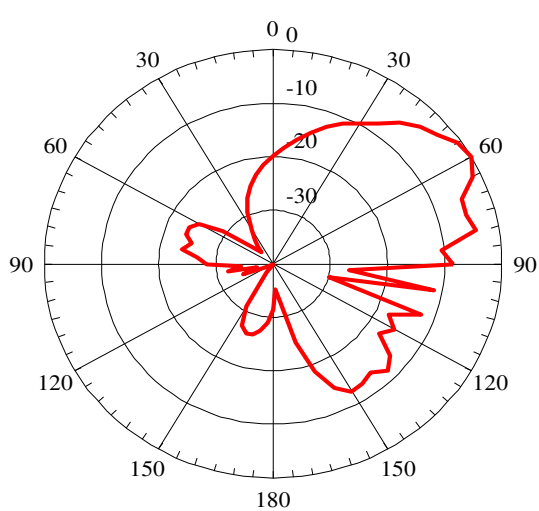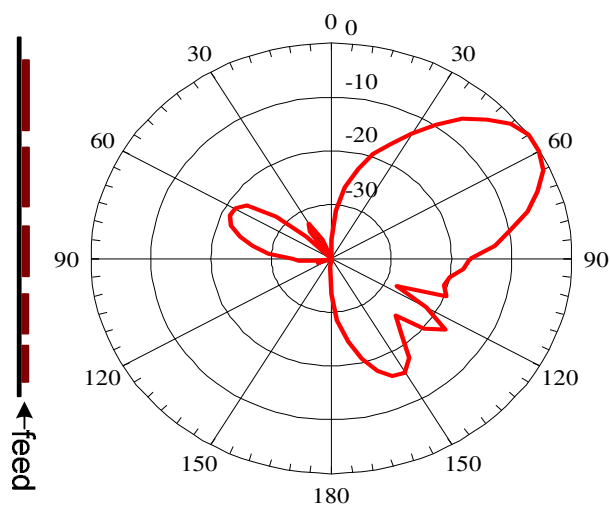
(a)   (b)
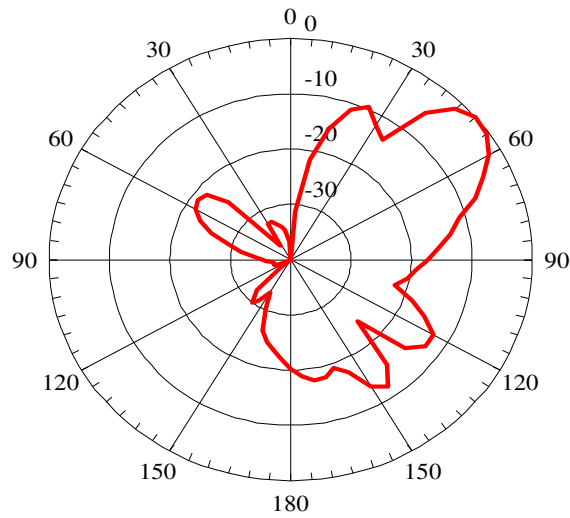
(c)

Figure 3.18 Simulated wideband radiation pattern (H-plane) excited at (a) 7.1-, (b) 8.2-, (c) 9.4 GHz

Figure 3.19 shows the simulated efficiency of the reconfigurable LPA in the three frequency bands. It shows that some degree of frequency reconfiguration can be achieved, with high, mid and low bands clearly seen, corresponding to the switched on patch groups. There are, however, ripples in the various bands which are very pronounced at low frequencies. There are some features of the design that might account for these issues. There is a change in the impedance seen by the feed line when the switch is short circuited. This may reintroduce the structural stop band within the low end band and this might be responsible for some of the strong ripples and high reflection seen in the low band mode. Also, higher order modes in the patches are believed to give rise to patch excitation outside the desired band [10]. A slight drop in efficiency in the narrow band mode is expected because fewer patches are excited. The radiation pattern for each band is shown in Figure 3.20. The patterns are taken at 9.4 GHz, 8.2 GHz and 7.5 GHz for high, mid and low band respectively. The maximum beam angle for the three bands is approximately 55^0.

61

Simulated radiation patterns are, on the whole, well formed and show reasonable similarity with those at the same frequency from the non-switched array.
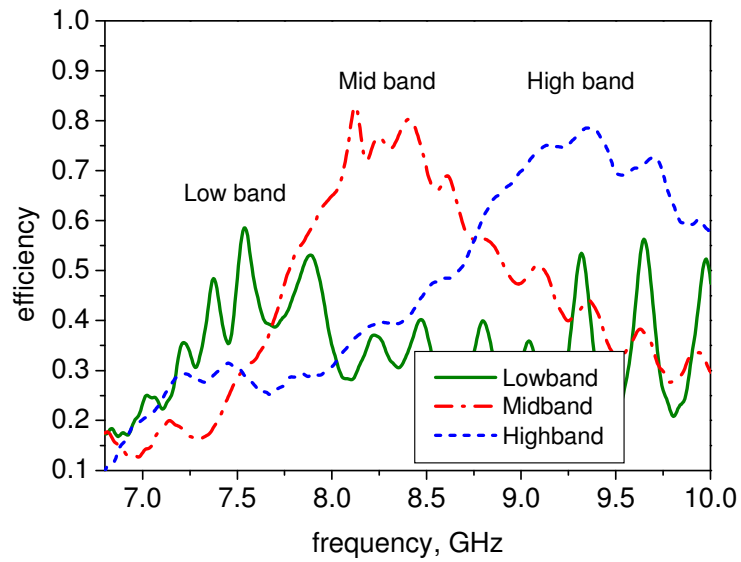
Figure 3.19 Simulated efficiency for selected three frequency bands

(a)   (b)

(c)
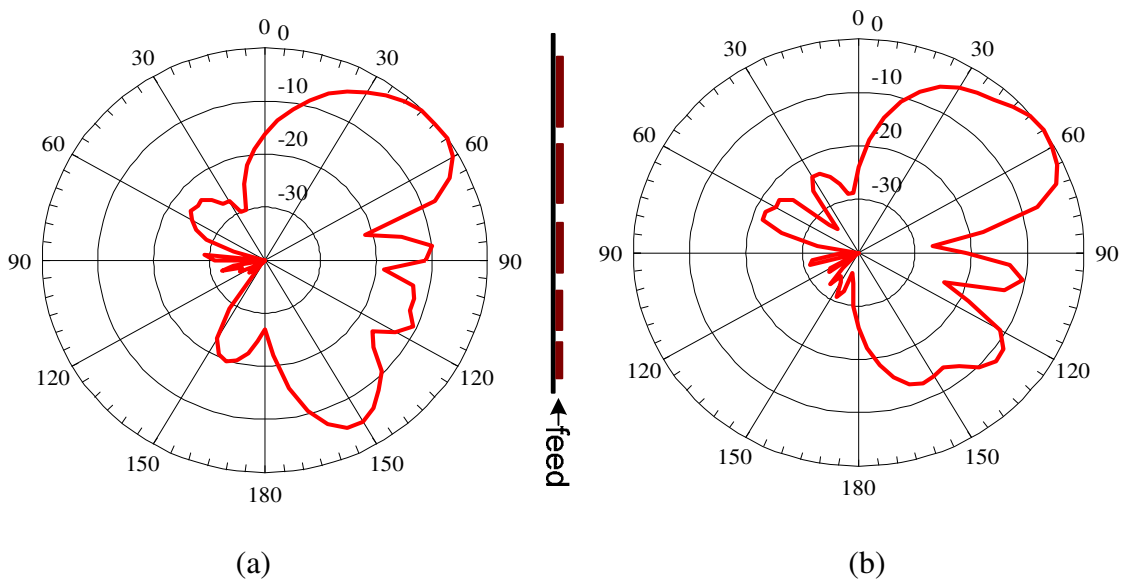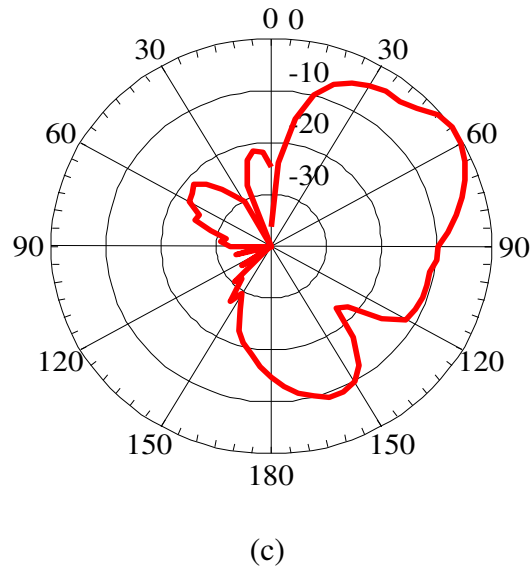
Figure 3.20 Simulated radiation pattern (H-plane) for selected three frequency bands (a) Low -, (b) Mid- and (c) High band

3.7.1 Improving Low Band Performances

When the high frequency slot is short circuited, there will be a change in the impedance seen by the feed line. This will upset the image impedance and will again introduce the structural stop band and resulting high reflection in low band mode. To compensate for the change, the impedance of the modulated line is modified. Figure 3.21 shows the modulated impedance line and its *pi* equivalent circuit. Figure 3.22a shows the structure when the slot is short circuited with S_a switch. As a convenient first approximation, the inductor in the equivalent circuit can be assumed zero as shown in Figure 3.22b. This can be explained as the current path, *i* is shorten when the slot is bridged. This has changed the image impedance and produces a structural stop band.

feed line

slot

patch

ref-plane

(a)

L

C

C
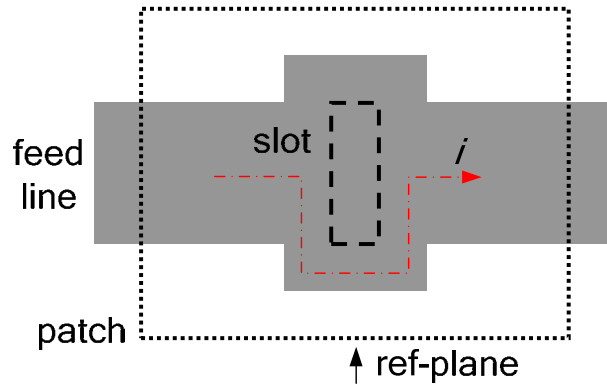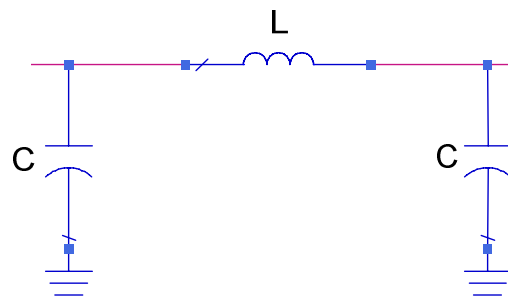
(b)

Figure 3.21 Modulated impedance feeder and the equivalent circuits

S_a

(a)

C

C

(b)
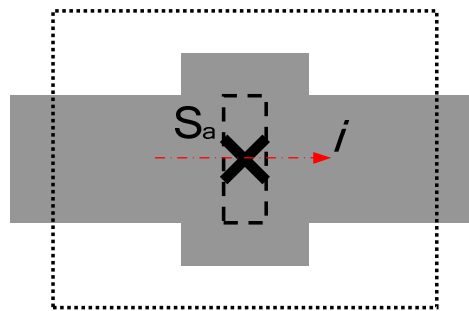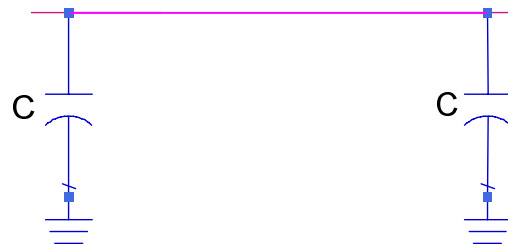
Figure 3.22 *Pi* equivalent circuits after slot is bridged, S_a – switch on slot

Elimination of the structural stop band of the second cell of the 20 element array is now described. Figure 3.23a shows the structural stop band and Figure 3.23b shows the image impedance of the second cell after the slot is bridged as shown in Figure 3.22. To eliminate the stop band, the modulated line is modified somewhat as shown in Figure 3.24a. Figure 3.24b shows its equivalent circuit. This modification makes the equivalent circuit similar to that Figure 3.21b. To simplify the design process, L_m is set equal to the aperture width and therefore by choosing the W_m appropriately, the variation of image impedance can be minimised and the structural stop band will be eliminated. In this example, the structural stop band is zero when L_m is 0.8 mm and W_m is 1 mm. Figure 3.25 shows an image impedance and a structural stop band of the cell when the slot is bridged for the modified lines as in Figure 3.24. It is observed that the structural stop band is eliminated.

(a)

(b)
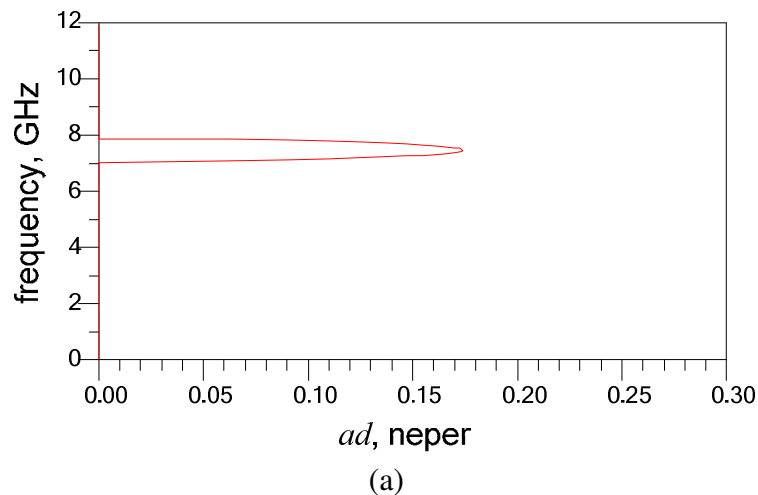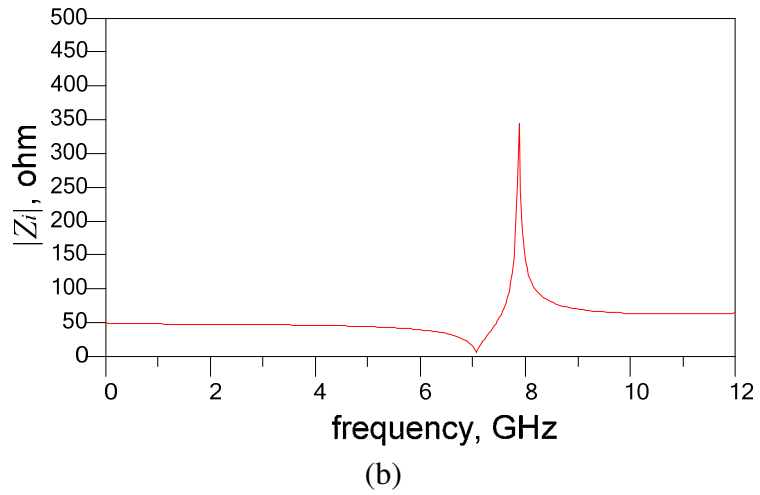
Figure 3.23 (a) A structural stop band and (b) an image impedance of a cell when slot is closed

(a)

(b)
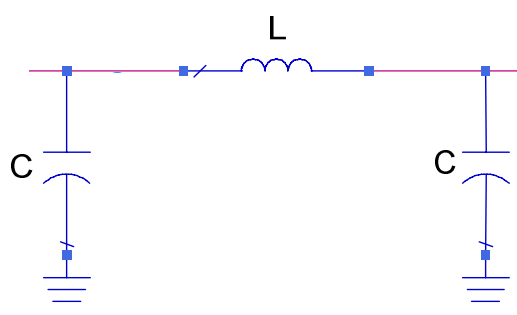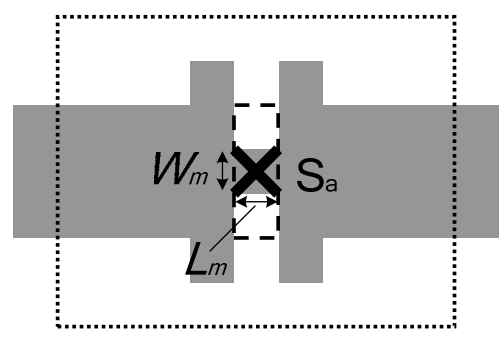
Figure 3.24 Modified line and its equivalent circuit, S_a – switch on slot
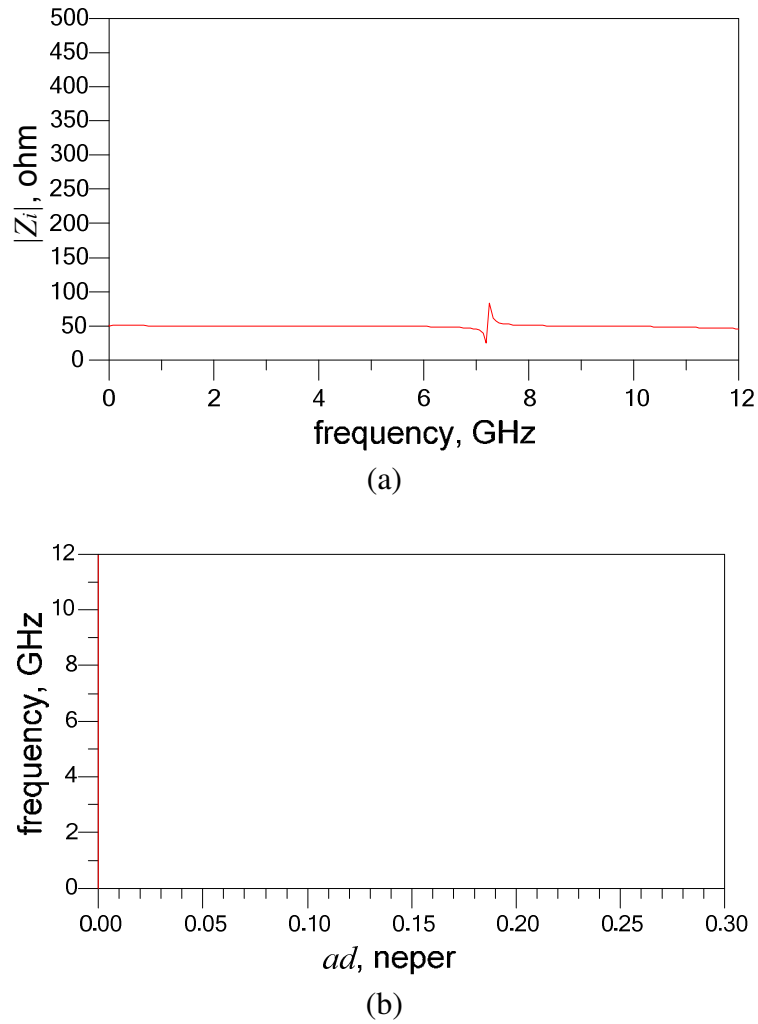
Figure 3.25 (a) An image impedance and, (b) a structural stop band for the modified lines of cell 19th after slot is closed

The improvement of low band mode efficiency is shown in Figure 3.26. To maintain the performance of the other band, two S_f switches are added to the line as shown in Figure 3.27. The S_f switches are open when the S_a switch is closed to improve low band mode efficiency. On the other hand, the S_f switches are closed when the S_a switch is open, to keep reasonably similar performances in the other mode. Simulated wideband efficiency with the S_f and S_a switches present is shown in Figure 3.28. The wideband performance is approximately similar in both cases. The selected three narrow band modes shown in

Figure 3.29 verify that the proposed concepts of reconfigurable log periodic patch array can be achieved.
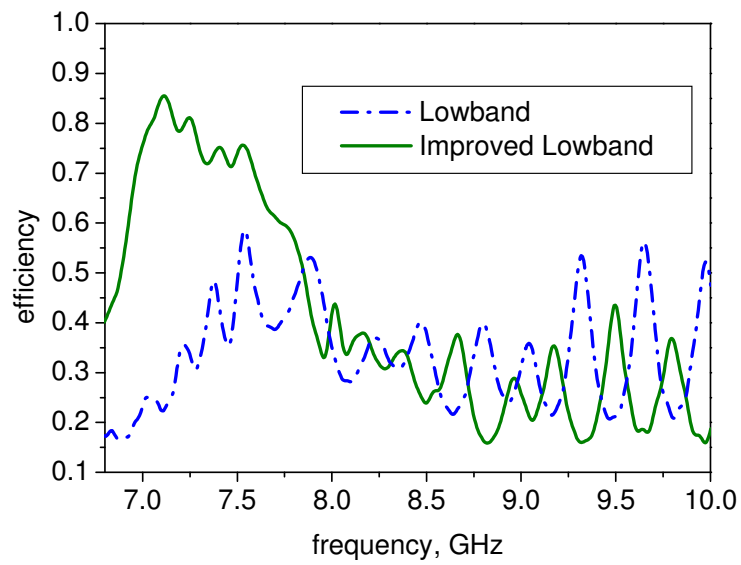
Figure 3.26 Simulated low band mode efficiency before and after improvement
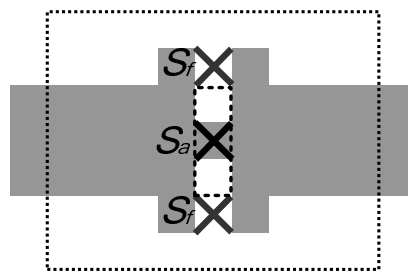
Figure 3.27 Switch position, S_f – switch on feed, S_a – switch on slot
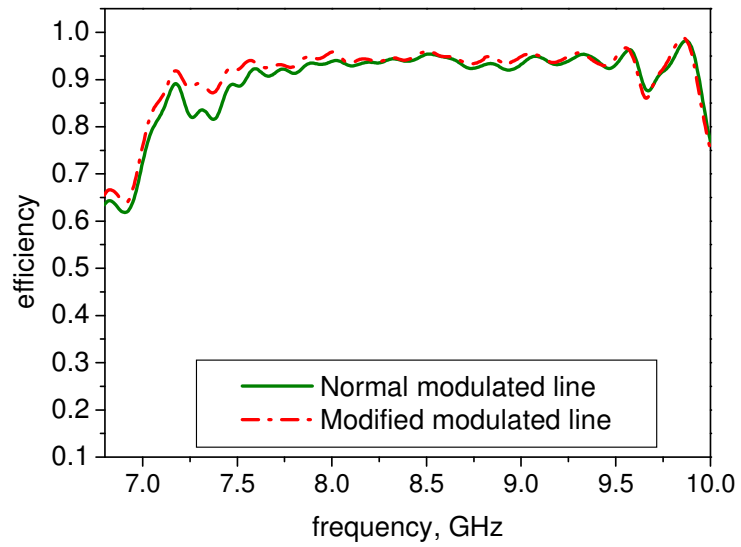
Figure 3.28 Simulated wideband efficiency before and after improvement of low band mode
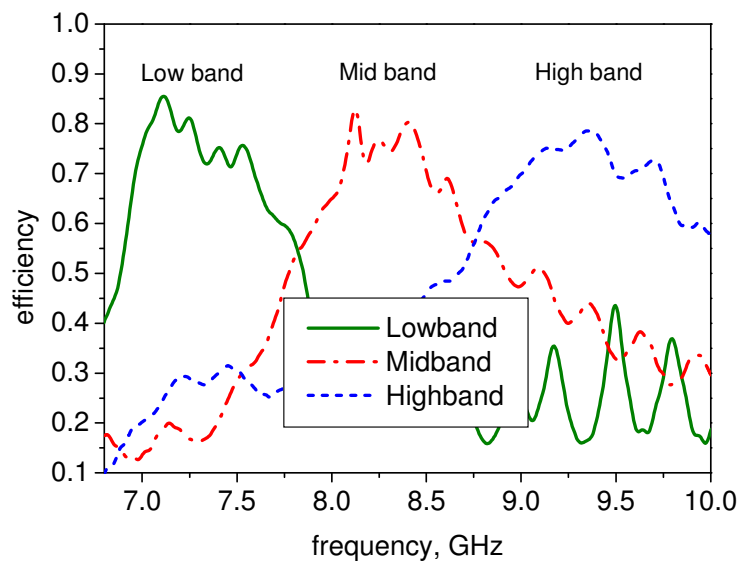
Figure 3.29 Three selected narrow band of the proposed reconfigurable log periodic patch array

3.8 Measurement result

The measured wideband mode scattering parameters are shown in Figure 3.30. The measured and simulated efficiency is presented in Figure 3.31. The antenna operates over a frequency range of 7 to 10 GHz with efficiency ranging from 80-95%. Good agreement is achieved although there are small differences. At some frequencies the measured efficiency is higher than simulated. This may be accounted for by improper shielding between h_f substrate and the box. Leakage from the gap between the ground plane and the box was found to be a significant problem which was solved by improving the electrical connection between the two. In the simulation, no leakage occurs.
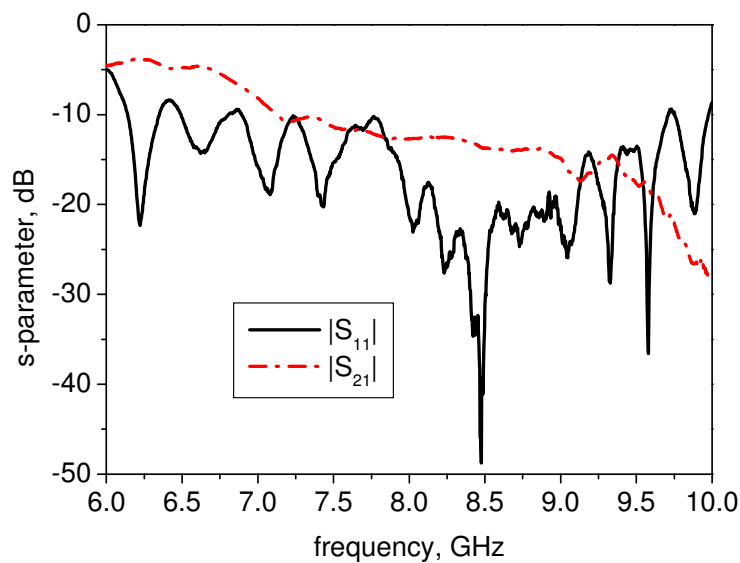
Figure 3.30 Measured wideband mode scattering parameters
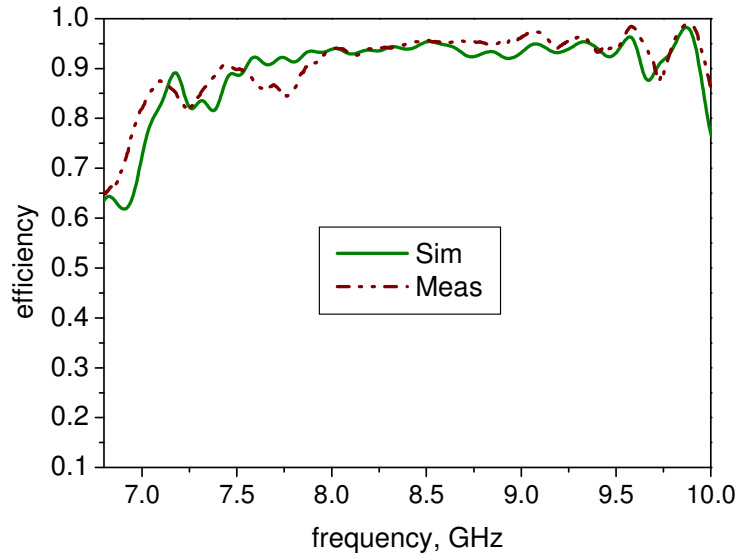
Figure 3.31 Wideband mode efficiency

Figure 3.32 shows the measured and simulated efficiency of the reconfigurable LPA for each selected three frequency bands. It shows that a good agreement is achieved, with the three bands clearly seen, corresponding to the switched on patch groups. In Figure 3.32b (mid band mode) the measured efficiency in the high band is higher than the simulated efficiency, suggesting that less rejection is being achieved. Similarly, in Figure 3.32c (low band mode), the measured efficiency in mid and high bands is higher than in the simulation, again suggesting reduced rejection. This may be accounted for by improper shielding between h_f substrate and the box. Leakage from the gap between the ground plane and the box was found to be a significant problem which was solved by improving the electrical connection between the two. Figure 3.33 shows a better rejection out of band is achieved if the copper tape is soldered to the substrate and the box as shown in Figure 3.34. Figure 3.35 shows the measured efficiency of the three narrowband modes of the proposed reconfigurable log periodic patch array.

(a)

(b)

72
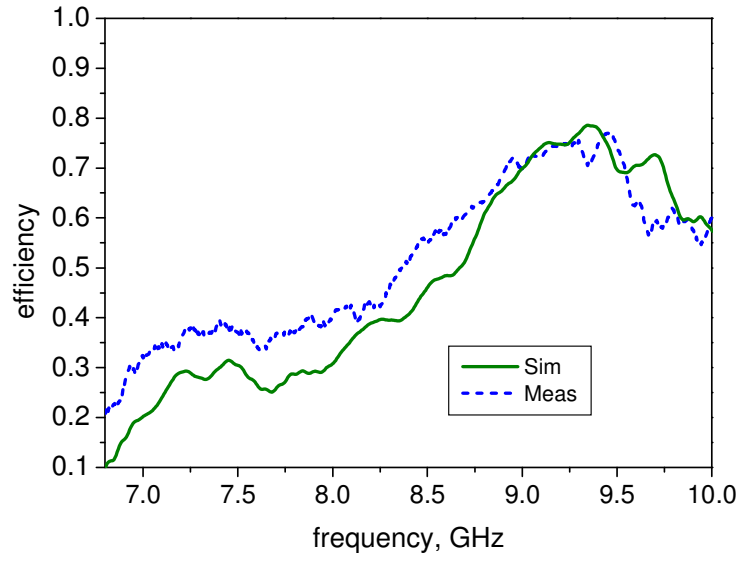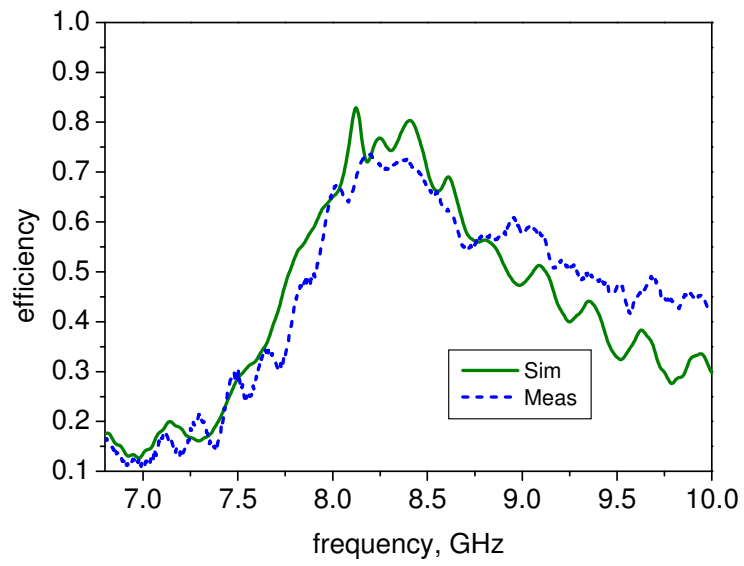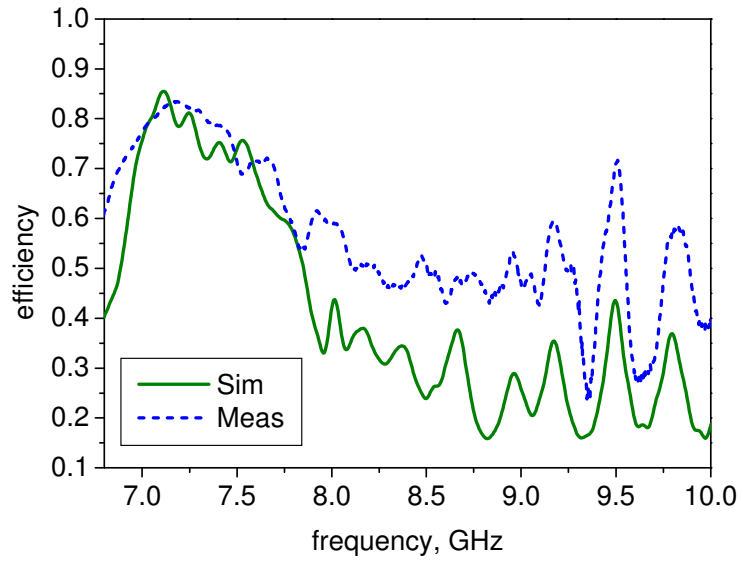
(c)

Figure 3.32 The selected three narrowband mode, (a) High band, (b) Mid band, and (c) Low band
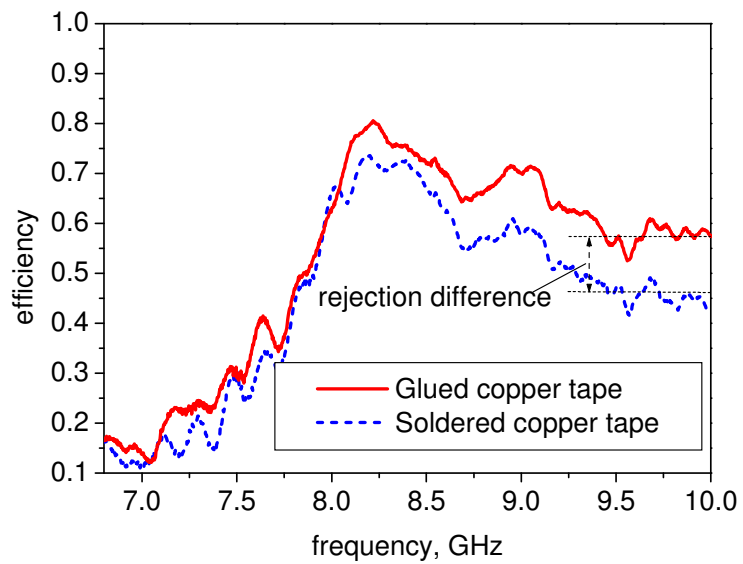
Figure 3.33 Out of band rejection in mid band mode
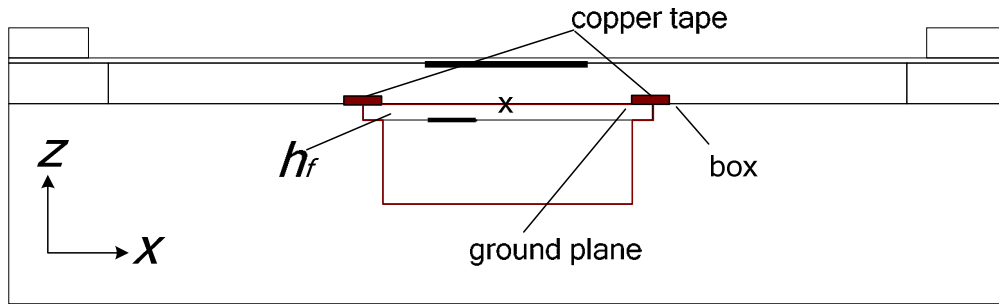
Figure 3.34 Proposed screening box where a copper tape is used to reasonably enclose the lower substrate, h_f into the shielding box
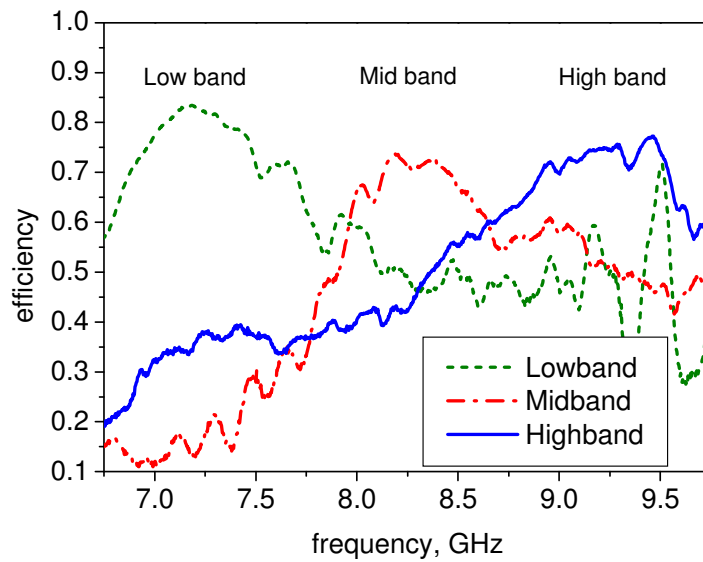
Figure 3.35 Measured efficiency of the reconfigurable log periodic patch array

The modification of the line to improve low band performance shows minimal effect on the other bands. An example of wideband performance with and without line modification is shown in Figure 3.36.
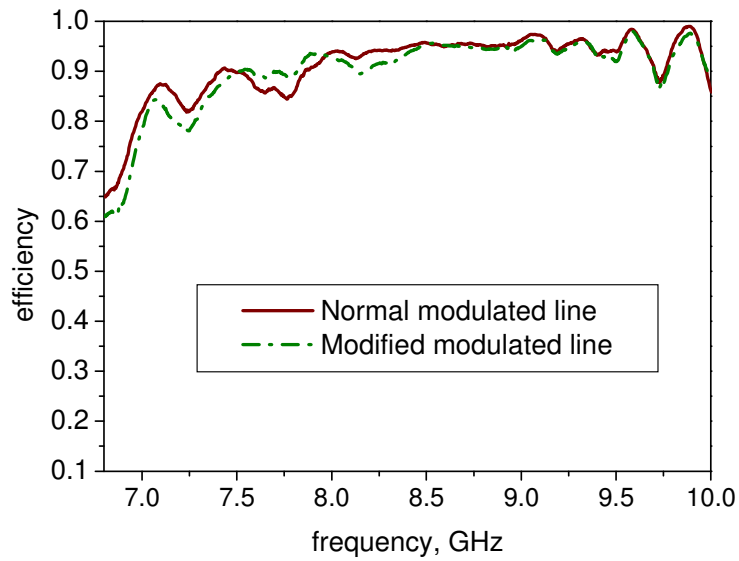
Figure 3.36 Measured wideband efficiency on modified and unmodified line

The measured and simulated H-plane radiation patterns for the wideband mode excited at 7.1 GHz, 8.2 GHz and 9.4 GHz are shown in Figure 3.37. A good agreement and well behaved radiation patterns are obtained. The measured and simulated H-plane radiation patterns for the narrowband modes are presented in Figure 3.38. Also a good agreement and well behaved radiation patterns are obtained. It is observed that the beam is tilted even closer to forward fire as the frequency increases, which is presumably due to the increasing length of the active region at higher frequency. Finally, the measured and simulated gains are compared, wideband mode in Table 3.2 and narrowband mode in Table 3.3. At some frequencies the measured gain is higher than simulated. This may be accounted for by improper shielding between h_f substrate and the box as mentioned previously.

(a)

(b)

(c)
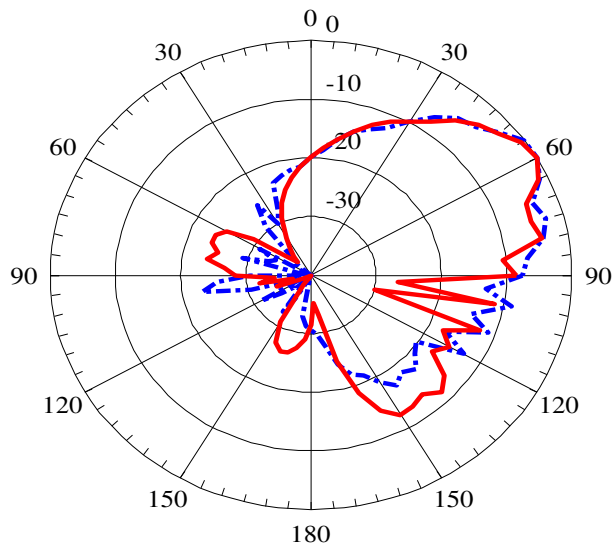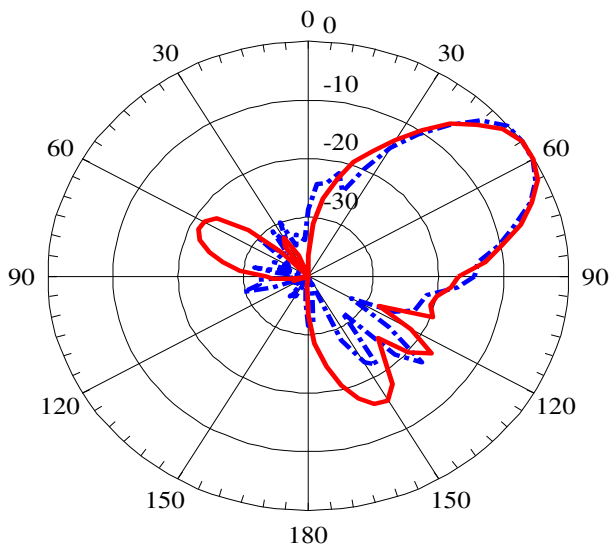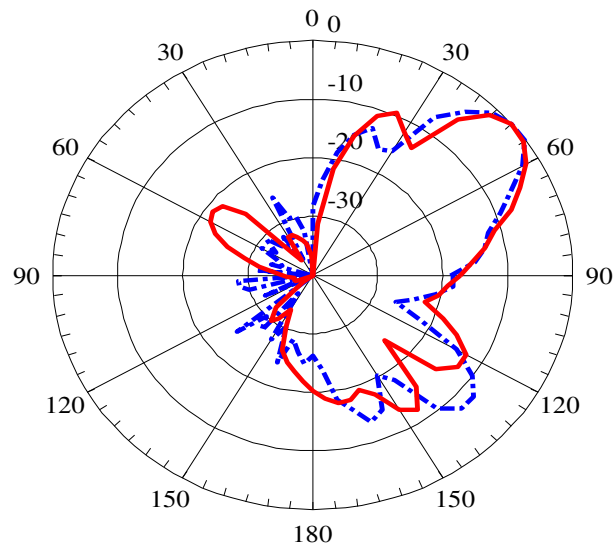
——— simulated, — - — measured

Figure 3.37 Wideband mode radiation pattern excited at (a) 7.1 GHz, (b) 8.2 GHz and (c) 9.4 GHz

(a)

(b)

(c)
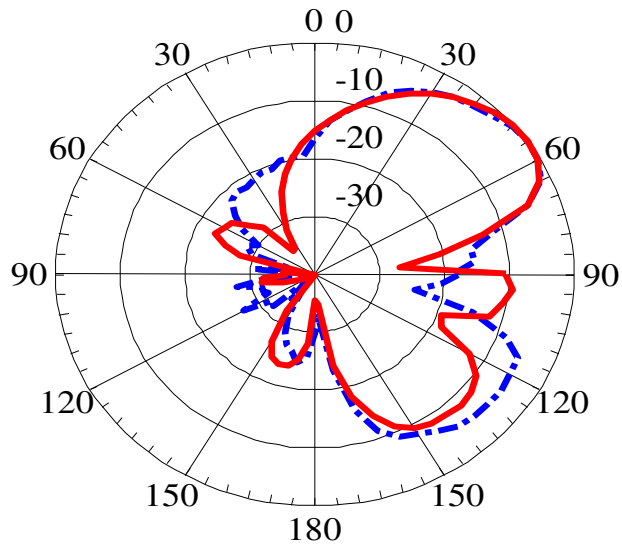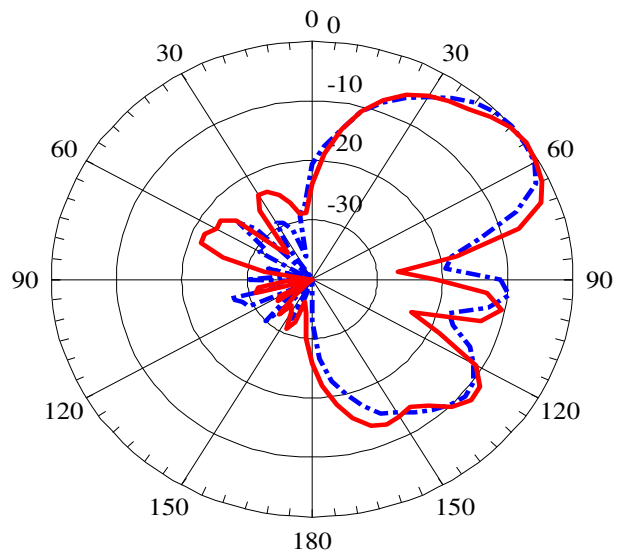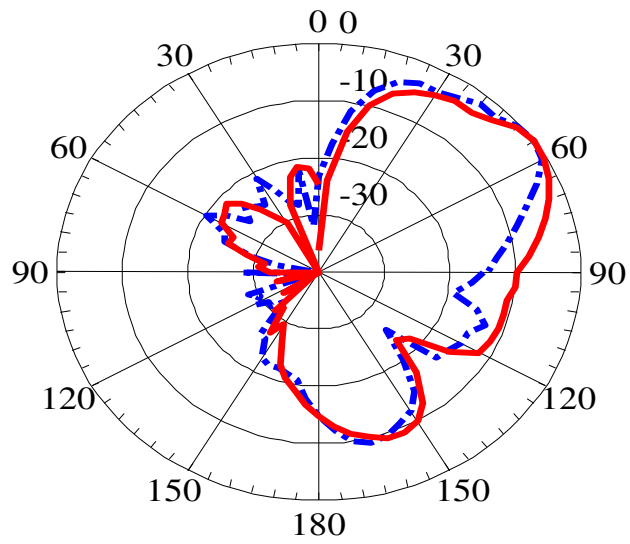
——— simulated, — - — measured

Figure 3.38 Narrow band mode radiation pattern (a) Low band mode excited at 7.1 GHz, (b) Mid band mode excited at 8.2 GHz and (c) High band mode excited at 9.4 GHz

Table 3.2 Gain of the proposed antenna in wideband mode

Gain, dBi	7.1 GHz	8.2 GHz	9.4 GHz
Simulated	11.64	13.60	13.08
Measured	9.83	16.42	14.54

Table 3.3 Gain of the proposed antenna in narrow band mode

Gain, dBi	Low band	Mid band	High band
Simulated	10.91	10.74	10.61
Measured	8.08	13.69	11.56

3.9 Summary

A novel reconfigurable log periodic patch array has been proposed by inserting the switch within the aperture slots. Three modes of reconfiguration are shown, when three groups of patches were selected within the array. The design guideline has been derived to allow some optimizing of the low band performances. More sub-bands could be achieved with different patches group selection. Nevertheless, in the relatively simple example shown, good efficiency has been obtained for each of the sub bands. The antenna is low profile and can be easily mounted to any structure such as in the body of an aircraft. Furthermore the bias circuit can be implemented easily in the ground plane which will help to reduce coupling to radiation. The proposed antenna could be a suitable solution for applications requiring wideband sensing and dynamic band switching, such as in military applications or cognitive radio. The work described here has been published in [80, 81]. However there are some drawbacks. Ideally there should be only one single switch needed to switch off one element, however because of the reintroduction of the stopband in the low band mode, two extra switches are needed to improve the performance. The need for a screening box also makes the structure more complex. Furthermore, because individual

elements have narrow bandwidth, a smaller scale factor is used which results in more elements. This then will increase the complexity of the bias circuits.

Now it has been shown that for a frequency independent antenna, where radiation occurs at different parts at different frequencies, a frequency reconfigurable antenna can be achieved by switching off some of the radiating elements. In the next chapter, the same general idea is applied but in a Vivaldi antenna, since they also radiate from different parts at different frequencies.

CHAPTER 4

WIDE-NARROW RECONFIGURABLE BAND MULTIPLE RING VIVALDI ANTENNA

4.1 Introduction

In this chapter, a novel switched band Vivaldi antenna is proposed. It is relatively small, simple to manufacture (no shielding box) and less complex in biasing circuit (fewer switches) compared to the reconfigurable log periodic patch array described in the previous chapter. To demonstrate its functionality, the proposed antenna shows reconfiguration between a single wideband mode (1.0 - 3.2 GHz) and three narrowband modes. Potentially, it can be designed to cover a very wide bandwidth and can have a wide range of frequency reconfiguration. To achieve switched band properties, eight ring slots which form filters were inserted to the antenna. The overall operating band can be switched by coupling each ring slot into the slot edges through the gaps controlled by means of PIN diode switches, which stop or pass the edge current to obtain frequency reconfiguration capability. Details

of the proposed design are described. Wideband antenna design and narrowband reconfiguration design is explained in section 4.2 and 4.3. In section 4.4, the effect of switch controlled ring slots is discussed through pass band-stop band analysis. The prototype antenna is discussed in section 4.5. Finally the results are presented in section 4.6 followed by a summary in section 4.7.

4.2 Wideband Antenna Design

A Vivaldi antenna has been chosen as a basic structure due to the fact that it can operate over wide bandwidth. In addition, it also has a well defined radiation mechanism where most of the current flow is at the edge of the tapered slot. These characteristics help in designing a wideband-narrowband reconfiguration. The Vivaldi used was based on [82], and has been scaled to operate over a bandwidth of $1.0 - 3.2$ GHz. The bandwidth of $1.0 - 3.2$ GHz was chosen to demonstrate the concepts because the PIN diode parasitic is less significant at low frequency. It is shown in Figure 4.1. The antenna is simulated and fabricated on FR4 substrate which has $\varepsilon_r = 4.9$. The height of the substrate is 1.6 mm. The slot consists of a 4.6 mm radius circular hole and an elliptical tapered slot with 40 mm horizontal and 80 mm vertical radius respectively. The tapered slot is fed with a $W = 2.75$ mm wide feed line terminated in a $R = 5.1$ mm radius quarter circle. The substrate size is $m = 144$ mm x $n = 140$ mm. The aperture size $a = 81.2$ mm and the antenna length $b = 120$ mm. Figure 4.2 shows the simulated response of non reconfigurable Vivaldi antenna.
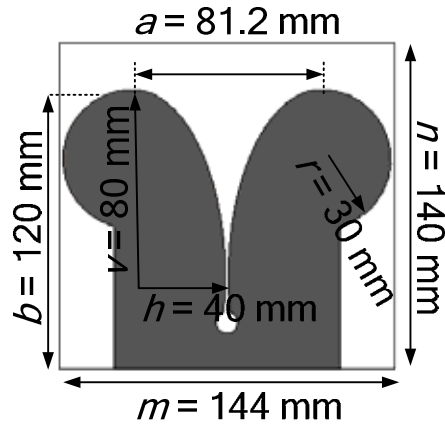
(a)
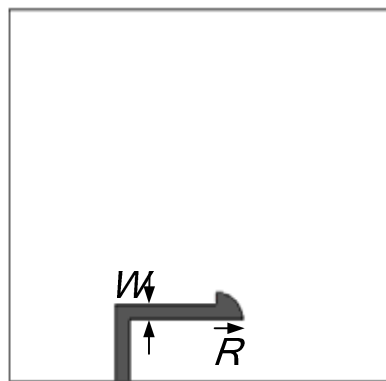
(b)

Figure 4.1 Non reconfigurable Vivaldi antenna, (a) front view, (b) rear view showing microstrip feed
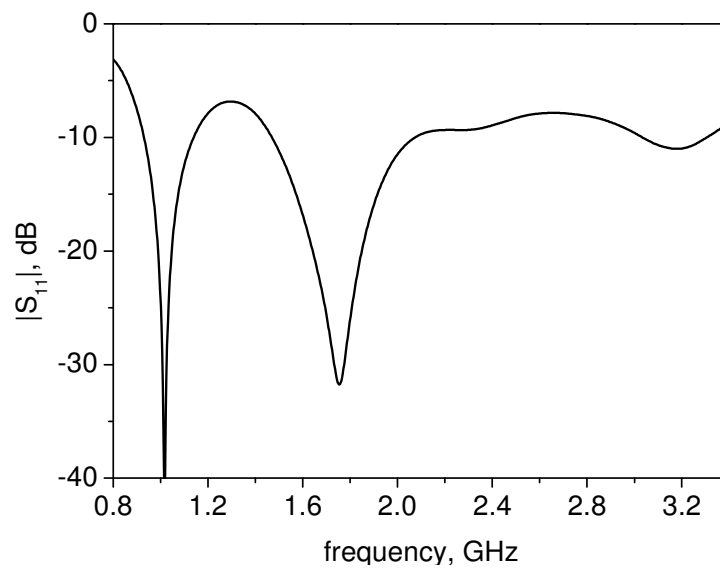
Figure 4.2 Simulated wideband non reconfigurable Vivaldi antenna

4.3 Narrowband Frequency Agile Antenna Design

The Vivaldi can be reconfigured by perturbing the edge of the tapered slot, distorting the current flow. Figure 4.3 shows the surface current before, and Figure 4.4 after, the insertion of a ring slot into the antenna. It is clear that the current along the radiating edges is significantly reduced.
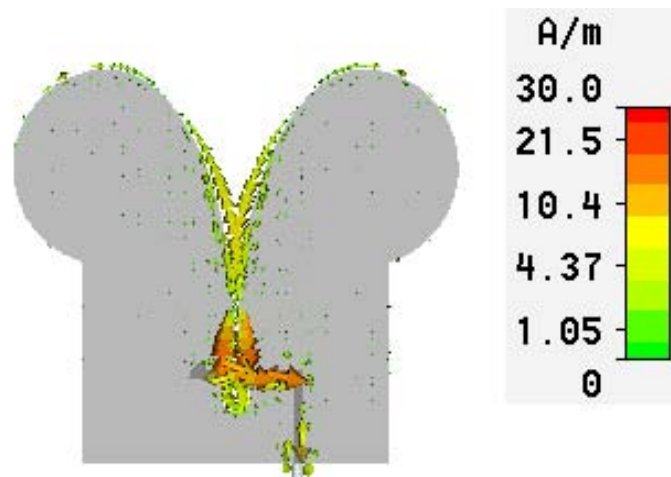
Figure 4.3 Simulated surface current distributions excited at 3GHz
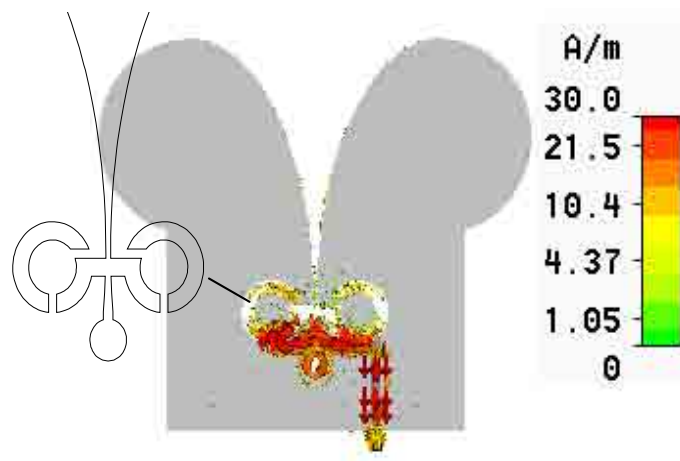
Figure 4.4 Simulated surface current distributions after perturbation excited at 3GHz

There are a number of candidate shapes for the insertion, like ring, triangle, rectangle and thin rectangle, as shown in Figure 4.5a, 4.5b, 4.5c and 4.5d respectively. In terms of frequency band, losses and size, the slot resonator has to be low stop band Q in

order to have wide stop band ranges, have low pass band loss and high stop band loss and be small in size. Figure 4.6 shows the simulated admittance showing that the Q factor is almost similar for ring, triangle and rectangle shape but slightly higher in the thin rectangle. A similar behaviour is also observed in the insertion loss plot shown in Figure 4.7. The loss is almost similar for ring, triangle and rectangle shape but slightly lower in the thin rectangle. In term of Q factor, ring, triangle or rectangle shapes are good candidates. Nevertheless, the ring shape slot, Figure 4.5a, has been chosen because it's relatively easy to design. The Q factor of the ring slot is 1.16.
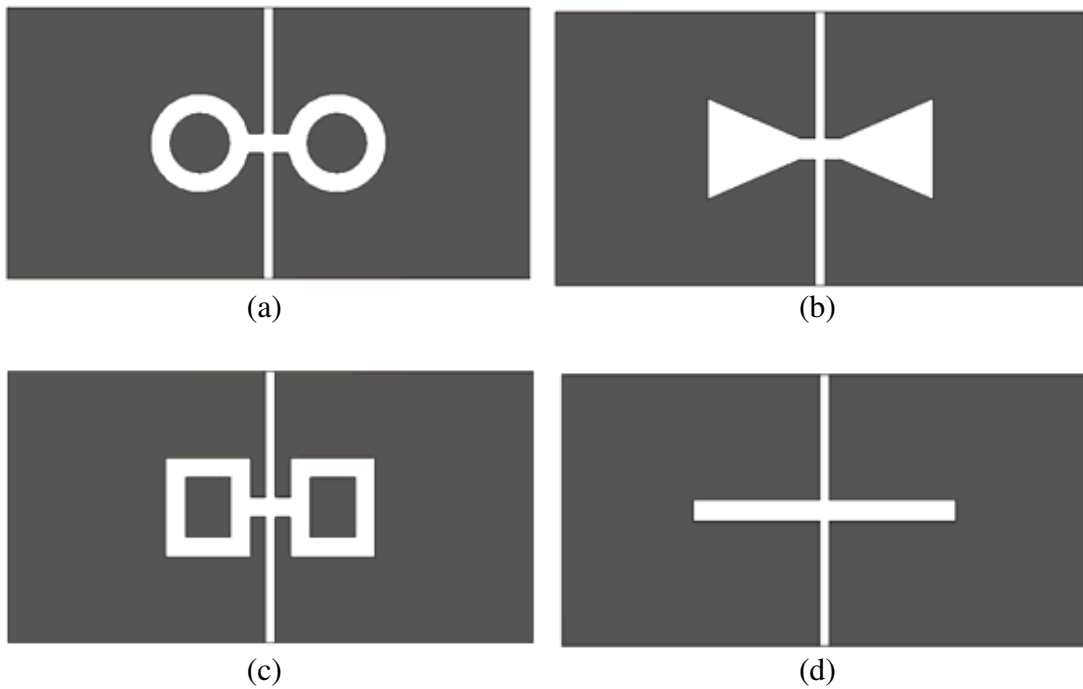
Figure 4.5 Slot shapes (a) ring-, (b) triangle-, (c) rectangle-, (d) thin rectangle shape
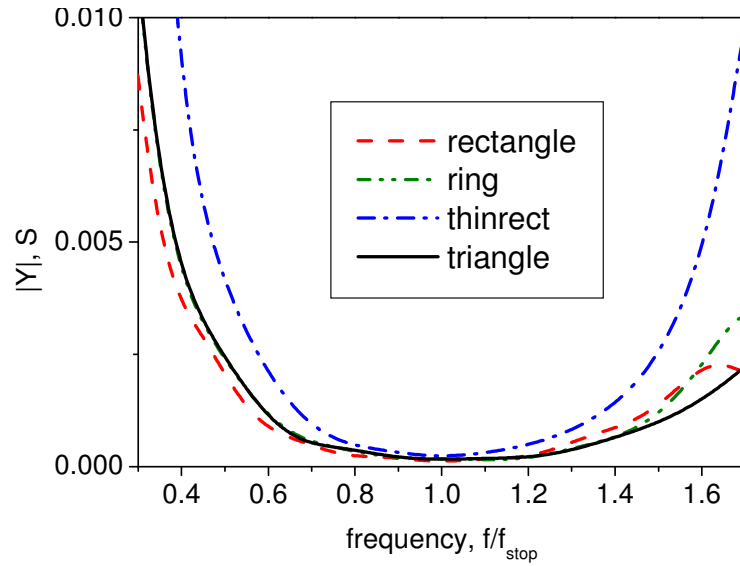
Figure 4.6 Simulated admittance, |Y| of various slot shapes
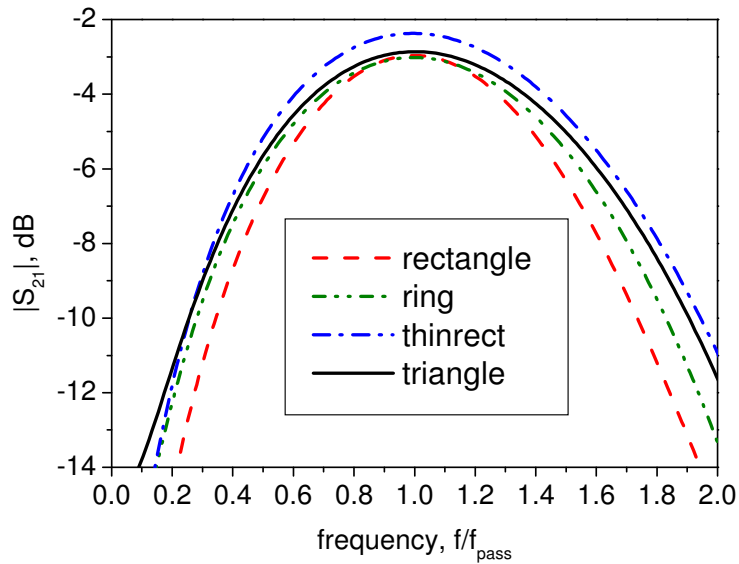
Figure 4.7 Simulated |S₂₁| of various slot shapes

The Vivaldi can be divided into two regions, namely the propagation and active regions. The propagation region is the area which acts like a transmission line and the active region is the area where the signals start to radiate. The radiation occurs when the slot width is approximately half of the wavelength, which makes each part of the Vivaldi radiate at different frequencies. The radiation at lower frequencies occurs closer to the wider end of the slot whilst higher frequencies occur at the narrower end. This suggests

that the ring slots should be placed at various positions along the tapered slot to control the frequency performance. The way this is done is now described.

Wideband to narrowband reconfiguration can be made by integrating a switched ring slot in the Vivaldi. For simplification purposes three narrowband modes were selected, namely low band, mid band and high band. Ideally the frequency response of each ring slot should be chosen depending on which narrowband configurations it is designed for. For example a low pass filter response is used in selecting low band mode while a band pass response can be used to select mid band mode. Figure 4.8 shows the geometry and simulated response of the ring slots on a uniform slot line. A single ring slot produced a stop band response while cascaded ring slots produced a pass band response. In addition, adding bridges as shown in Figure 4.8c transformed the band stop to low pass response.

The equivalent transmission line models of the ring slot resonator are now described. The average circumference of the single ring slot in Figure 4.9a is 52.3 mm which is approximately a half wavelength at 2.3 GHz. The differential operation of the slot line creates a virtual short circuit, denoted as *sc,* at the middle point of the structure as shown in the figure. The short circuit transforms over a quarter wavelength to an open circuit at the excitation point which produces a stop band at 2.3 GHz. On the other hand, the cascaded ring slots in Figure 4.9b make the length approximately half wavelength long at 2.2 GHz. This thus makes a short circuit at the excitation point, which produces a pass band around 2.2 GHz. Finally, with added bridges, the ring slot shown in Figure 4.9c becomes a very short slot, an eighth wavelength long. This transforms to a stop band at 4.6 GHz or to an inductance at a low band 1.2 GHz at the excitation point.
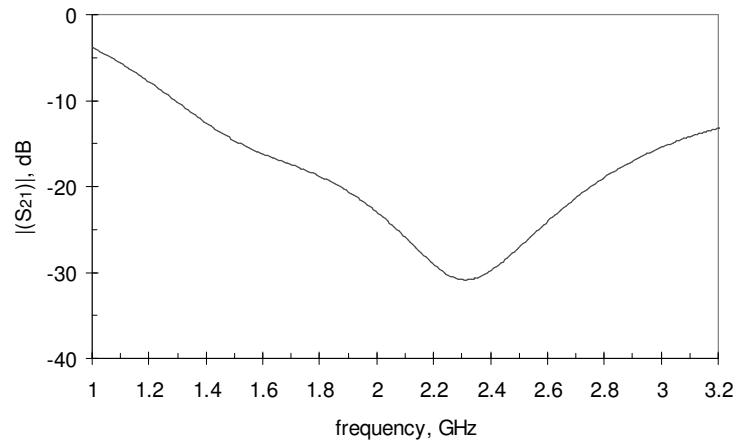
(a)
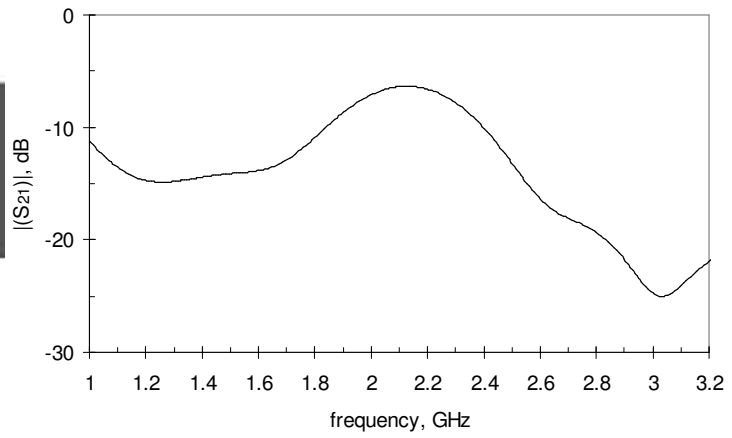
(b)
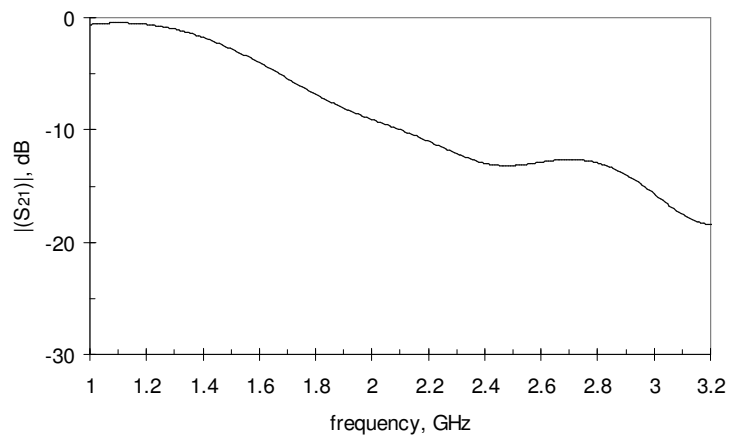
(c)

Figure 4.8 Simulated S$_{21}$ of ring slot resonator (a) band stop (b) band pass (c) low pass; (slot line width = 2 mm, ring outer radius = 10 mm, ring inner radius = 6 mm, small connecting gap = 4 mm x 3.48 mm, small bridge[case (c) only] = 4 mm x 2 mm)

88
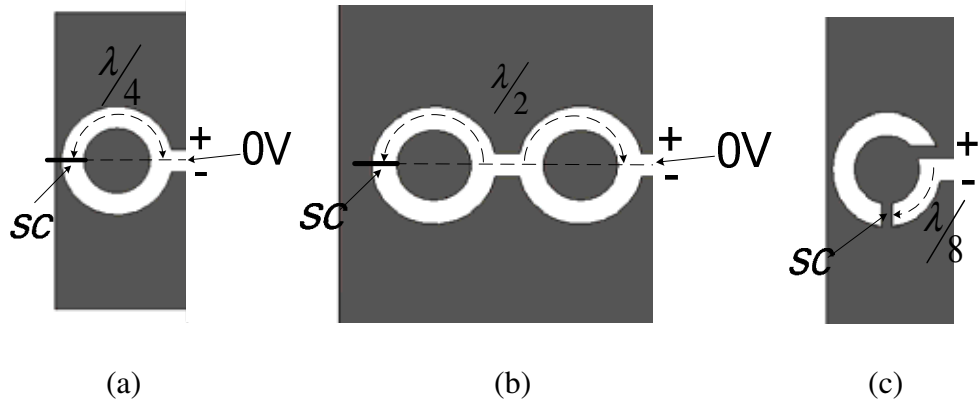
Figure 4.9 Ring slot resonator (a) band stop (b) band pass (c) low pass

Since the Vivaldi radiates from different parts of the structure at different frequencies, the narrower end area will become the radiating region for high frequency signals. It is thus appropriate to locate the ring slot there, in order to get the low band mode. Figure 4.10 shows a pair of low pass ring slots at the lower end. From the S_{11} it is clear that this produces a low band response. In order to stop the low band, the top end of the antenna has the band stop ring slot. Figure 4.11 shows the effect of ring slot radius on the Vivaldi S_{11}. With $r = 15$ mm good return loss of top end band is achieved. This is because the larger the value of r, the lower is stop-band, resulting in less perturbation of the pass-band thus giving better S_{11}.
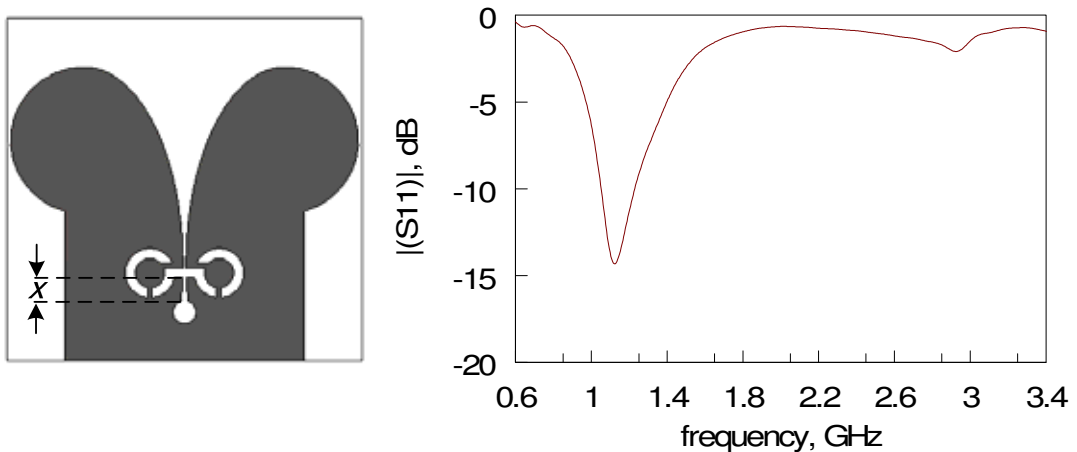
Figure 4.10 Simulated S_{11} of low band configurations ($x = 9.55$ mm)
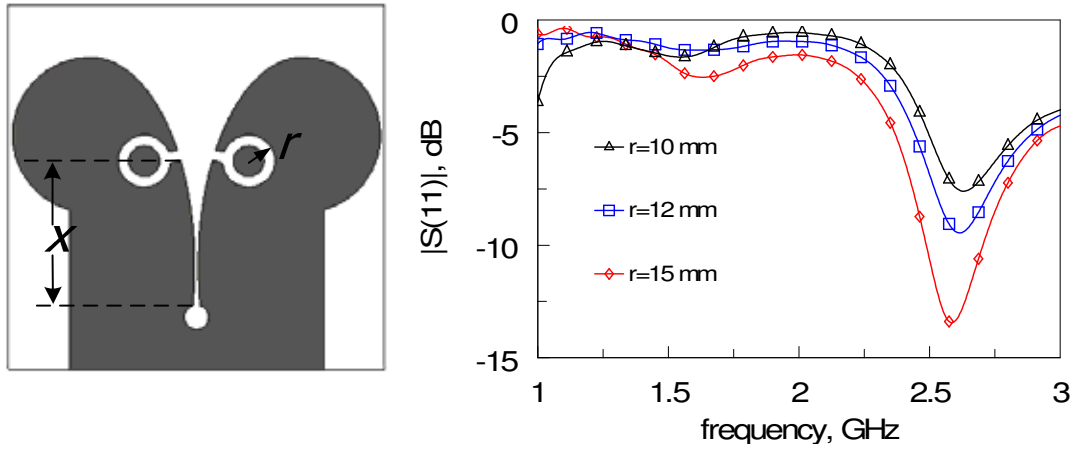
Figure 4.11 Simulated S₁₁ of high band configurations (*x* = 56.2 mm)

Mid band operation is selected by using a band pass ring slot configuration. The position of the ring slot section has an effect on the frequency response. Figure 4.12 compares the performance for optimally and non optimally positioned 2.2 GHz ring slot resonators. Theoretically, to minimize the perturbation of the travelling wave on the tapered slot at the pass band frequency, the ring slot section should be positioned at a point on the line where its image impedance, Z_{RS}, is equal to the characteristic impedance of the line, Z_{SLOT}. The image impedance of a short section of line containing the ring slot resonator (Figure 4.13) is defined as the terminating impedance on the output port (*AA'*) which leads to an input impedance (at *BB'*) that has the same value. In Figure 4.14, resonators causing four different pass bands have all been optimally positioned to achieve good pass band match.

The frequency of the pass band can be selected by designing the ring slot as shown in Figure 4.14a. If reconfiguration from a wideband to a single narrow band is required the narrowband frequency can be chosen in this way. However there are size constraints if, as

in the demonstration described in this chapter, wideband and low, middle and high pass modes are integrated together.
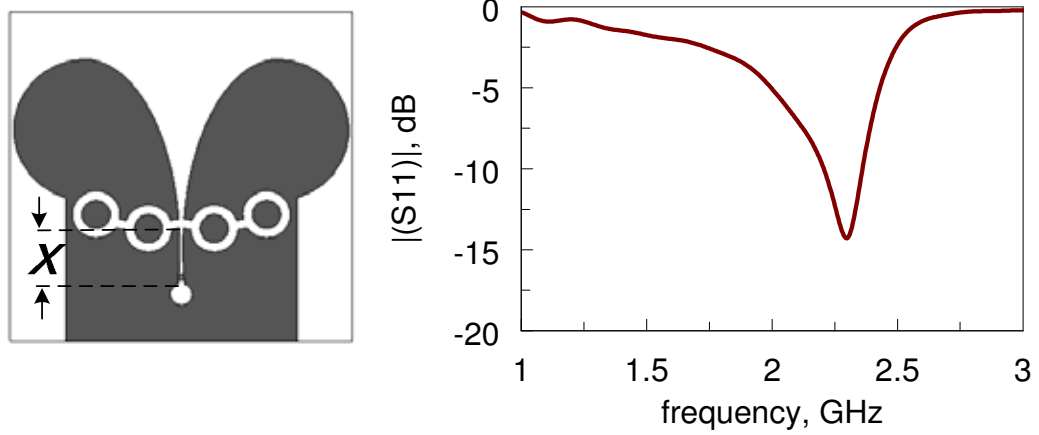
(a)
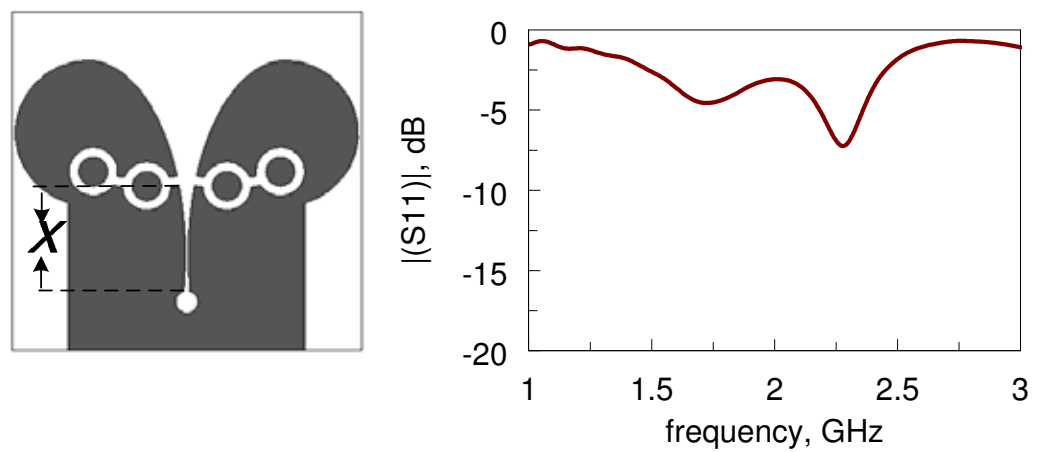
(b)

Figure 4.12 (a) Simulated antenna S$_{11}$ when resonators at matched position, $x = 23.69$ (b) resonators at $x = 43.77$ mm
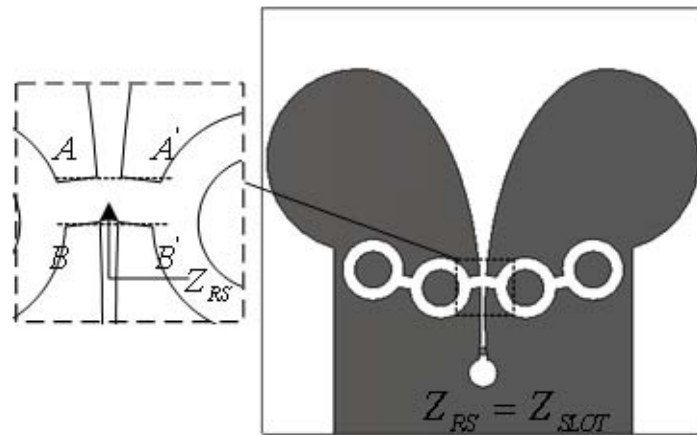
Figure 4.13 Impedances associated in finding optimum ring slot position, ideal condition when $Z_{RS} = Z_{SLOT}$

(a)

(b)
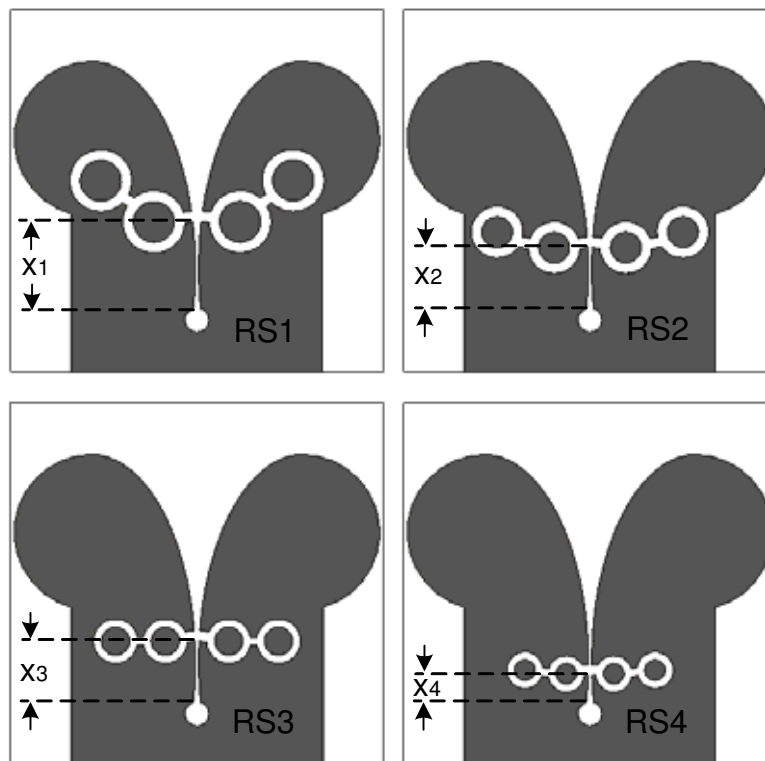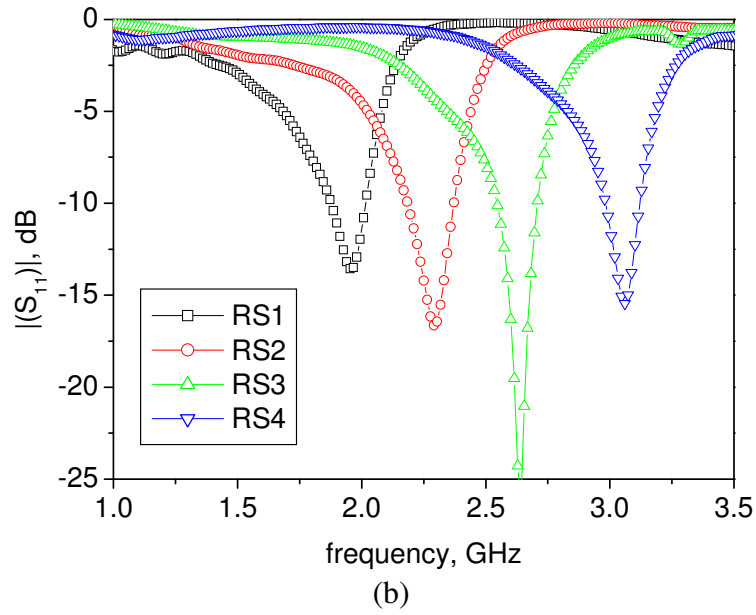
Figure 4.14 (a) Vivaldi with different band pass ring slots; RS1 (ring outer radius = 12 mm, ring inner radius = 8 mm, small connecting gap = 4 mm x 2.5 mm, x_1 = 33.68 mm), RS2 (ring outer radius = 10 mm, ring inner radius = 6 mm, small connecting gap = 4 mm x 2.88 mm, x_2 = 23.69 mm), RS3 (ring outer radius = 8.5 mm, ring inner radius = 5.5 mm, small connecting gap = 3 mm x 2.5 mm, x_3 = 18.59 mm), and RS4 (ring outer radius = 7 mm, ring inner radius = 4 mm, small connecting gap = 3 mm x 2.32 mm, x_4 = 10.37 mm), (b) Simulated S_{11} of four band pass configurations at matched position

4.4 Four Mode Reconfigurable Configuration

A wideband to 3 narrowband modes reconfigurable antenna is demonstrated here by inserting all three sets of ring slots into the antenna as shown in Figure 4.15. To fit all in, the position of the middle ring slots is shifted up by 10.04 mm from the matched position. The outer radius of the uppermost ring slots have also been reduced to 10 mm to allow integration. This makes all ring slots have an inner radius of 6 mm and an outer radius of 10 mm. The positions of the switches necessary for reconfiguration are also shown in the figure.
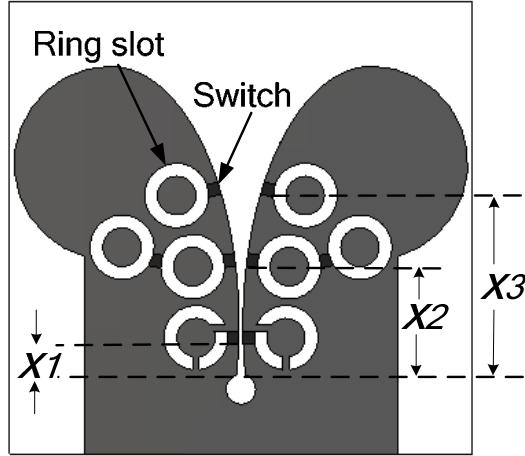
Figure 4.15 Four band reconfigurable antenna, (ring outer radius = 10 mm, ring inner radius = 6 mm, small connecting gap = 4 mm x 3.5 mm, x_1 = 9.55 mm, x_2 = 33.73 mm, x_3 = 56.2 mm, small bridge [the lowest slot only] = 4 mm x 2 mm)

Whilst CST Microwave Studio® is used to simulate the scattering parameters of the proposed antenna for comparison with the prototype, an alternative analysis is now described which gives insight into the performance of each set of ring slots in the presence of others. Figure 4.16 shows the antenna of Figure 4.15 in its three narrowband states. On each figure two right pointing arrows indicate the points at which the voltage across the tapered slot is extracted from the simulation. Figure 4.17 shows an expanded view of the line in the vicinity of one of the resonators, indicating more precisely where V_o and V_d are measured in each case. Taking the ratio of the complex voltages V_o and V_d gives the

propagation constant $\gamma d = (a + jb)d = \left[-\ln\left(\dfrac{V_d \sqrt{Z_{o1}}}{V_o \sqrt{Z_{02}}} \right) \right]$ where ad is neper and bd is

radians, which can thus be extracted. These are now examined for each of the three cases.
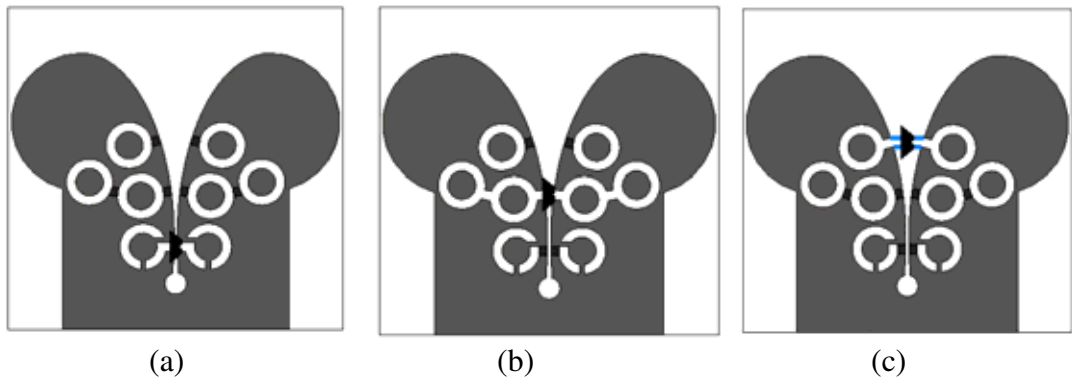
Figure 4.16 (a) Low band- (b) Mid band- (c) High band configuration
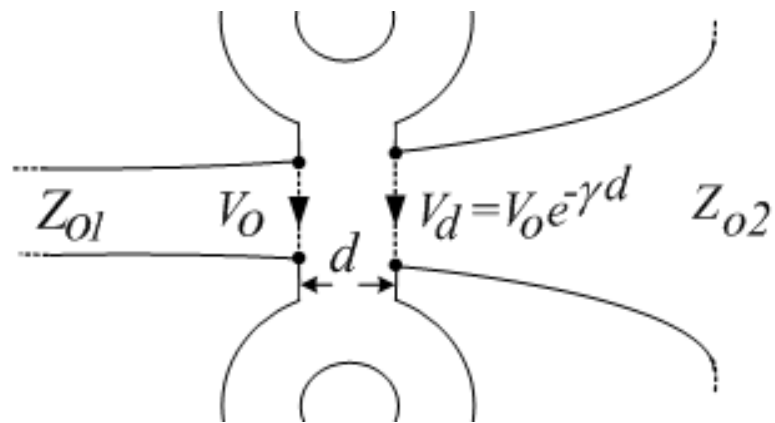
Figure 4.17 Tapered slot line voltages

4.4.1 Narrow low band mode

The low band mode characteristic is shown in Figure 4.18. It can be seen that a very high attenuation occurs from 1.25 to 3.2 GHz, and thus the structure prevents any signals beyond 1.25 GHz propagating up the tapered slot. The minimum attenuation occurs at 1.15 GHz. The positive value of *ad*, neper (*ad* > 0) means loss and/or standing waves

and a minima in *ad* or *ad* = 0, means a pass band or low loss travelling wave. Small

negative values of *ad* are due to small inaccuracies in the Z_{o1}/Z_{o2} calculation, due to the slot

line impedance expressions having width limits below the slot width in the antenna. The

maximum attenuation in the rejection band depends on how lossy is the structure. Higher

loss in the structure reduces the attenuation in the stop band [78]. One way to increase the

rejection is by using a very low loss material such as superconductor.
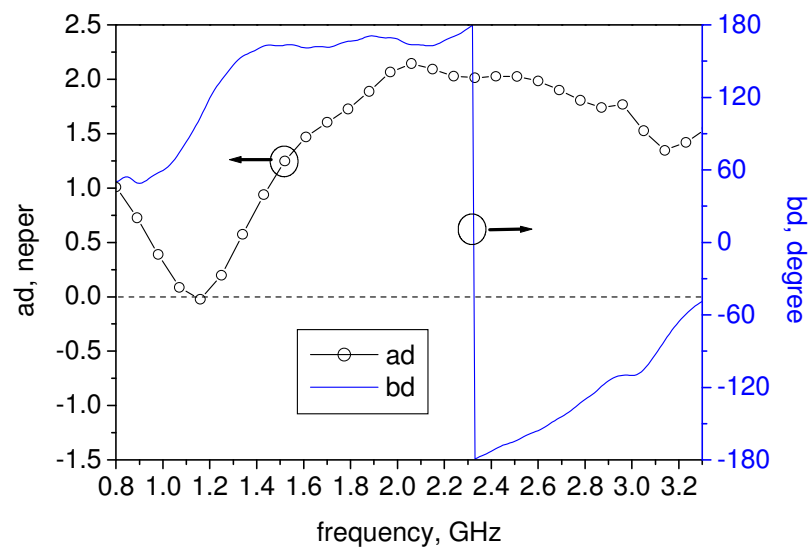
Figure 4.18 Low band dispersions curve, (attenuation and phase)

4.4.2 Narrow mid band mode

Figure 4.19 shows the characteristic of the mid band mode structure. Its shows that

minimum attenuation occurs from 2.05 to 2.22. A high value of *ad* in the pass band region

reflects the low gain noticed in the Table 4.1. There is evidence of a pass band above

3.2 GHz, which is also noticed in the S_{11} plots shown in Figure 4.31b.
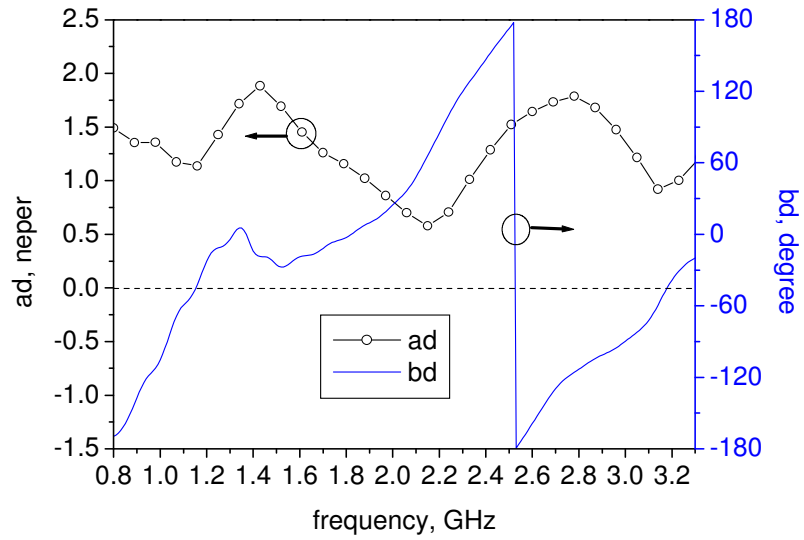
Figure 4.19 Mid band dispersions curve, (attenuation and phase)

4.4.3 Narrow high band mode

Figure 4.20 shows the characteristic of the high band mode structure. Its shows a stop band, from 1.0 to 2.9 GHz. The pass band around 0.8 GHz is also seen in S_{11} in Figure 4.31c. The minimum attenuation occurs around 3.2 GHz.
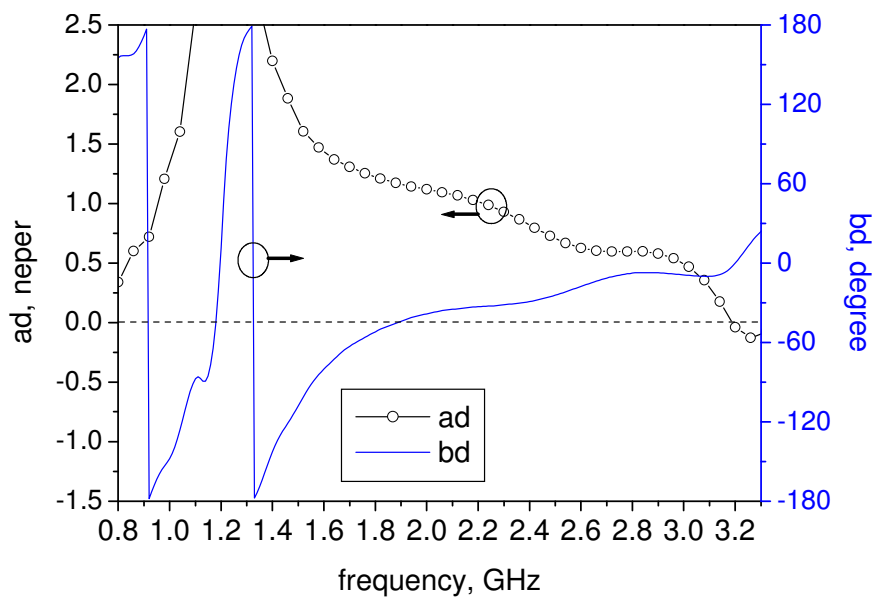
Figure 4.20 High band dispersions curve, (attenuation and phase)

The effects of the ring slots on the gain of the antenna can be analyzed by comparing three antenna configurations, one without the ring slots (*WR*), as indicated in Figure 4.1, one with the ring slots using ideal switches (*ID*), as shown in Figure 4.15, and one with the ring slots using PIN diode switches (*PD*), as shown in Figure 4.27. Even though the ring slots occupy a substantial part of the antenna surface, it is observed that the difference in the gain between *WR* and *ID* antennas is small except from 2.6 to 3.2 GHz as shown in Figure 4.21. On the other hand, Figure 4.22 compares the measured gain of the *ID* and *PD* antennas in wideband mode. It is observed that the PIN diode switches have effects on the gain degradation.
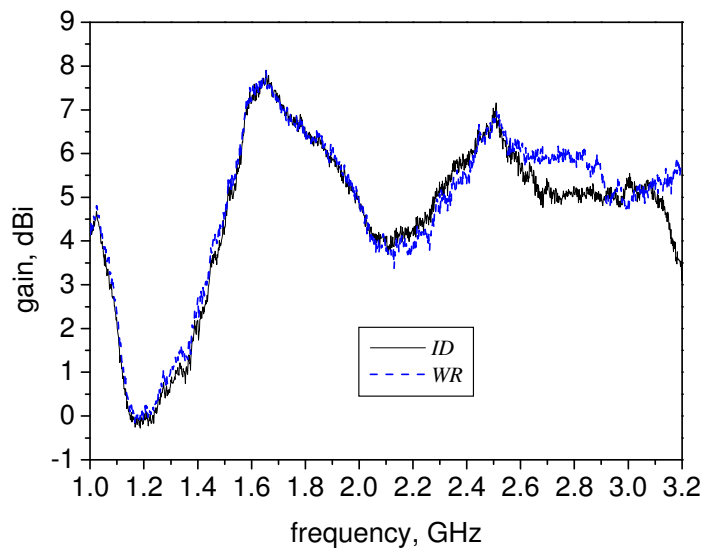
Figure 4.21 Gain comparison between *WR* and *ID* antennas
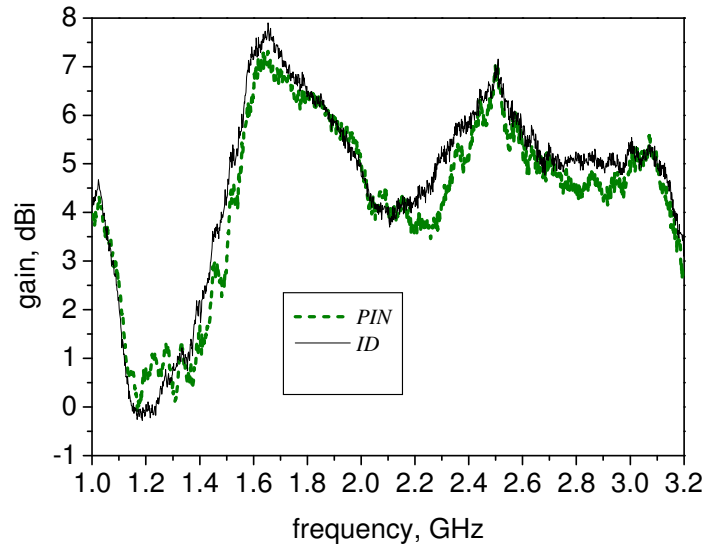
Figure 4.22 Gain comparison between *PIN* and *ID* antennas

Further insight may be gained by examining the current distributions in the various modes. The comparison between the simulated surface current distributions in the three narrowband operative states and the wideband mode are shown in Figure 4.23. In general a similar current distribution is observed between the low band and wideband configurations when excited at the same frequency. The same behaviour is also observed between the mid- and high band configuration. The current distributions excited beyond the operating frequencies for low band configurations are also shown in Figure 4.24. It is clearly observed that the current at the resonant frequency, 1.1 GHz, propagates through the upper part of the antenna, as shown in Figure 4.23b. However most of the current at 2 and 3 GHz is cut off by the lower ring slots, therefore stopping high frequency band operation. Figure 4.25 shows the current distributions for the mid band configuration excited at 1.1GHz and 3 GHz, and Figure 4.26 shows the current distributions for the high band configuration

excited at 1.1GHz and 2 GHz. It can clearly be seen that there is less current in the stop band.

(a)   (b)

(c)   (d)

(e)   (f)
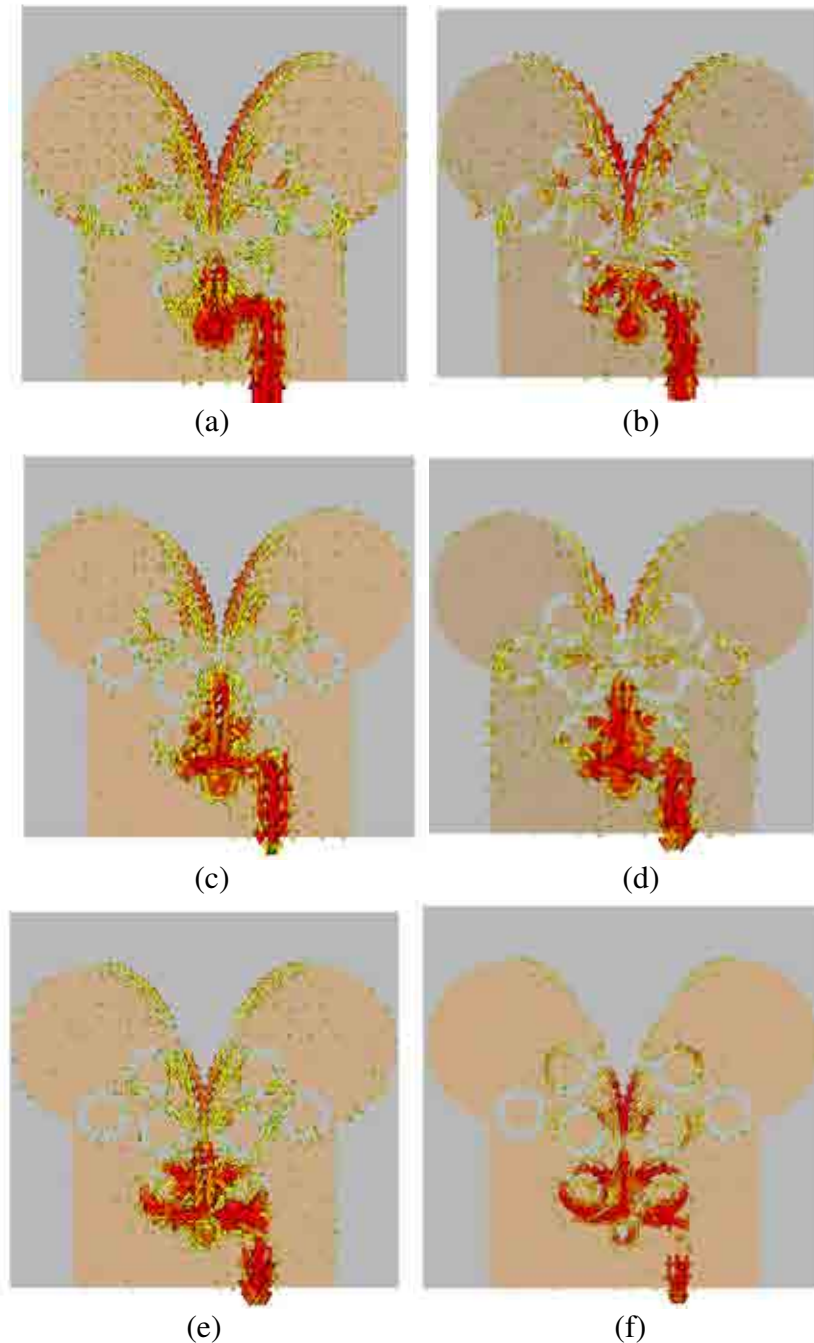
Figure 4.23 Simulated surface current distributions for (a) Wideband configuration excited at 1.1GHz, (b) Low band configuration excited at 1.1GHz, (c) Wideband configuration excited at 2.2GHz, (d) Mid band configuration excited at 2.2GHz, (e) Wideband configuration excited at 3.1GHz, (d) High band configuration excited at 3.1GHz
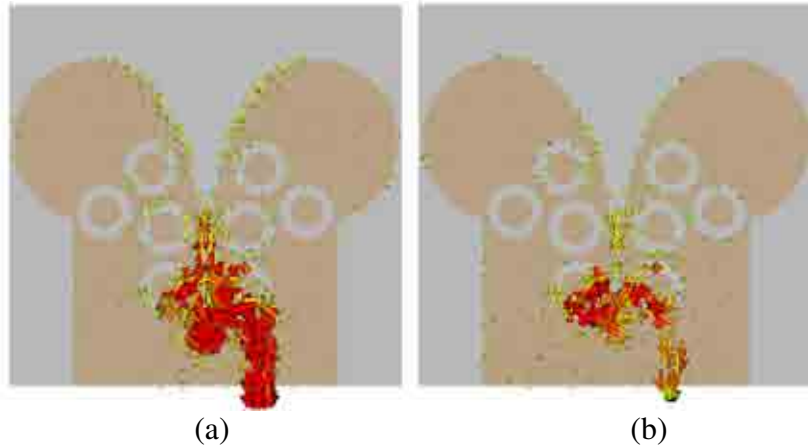
Figure 4.24 Simulated current distributions for the low band configuration excited at (a) 2 GHz and (b) 3 GHz
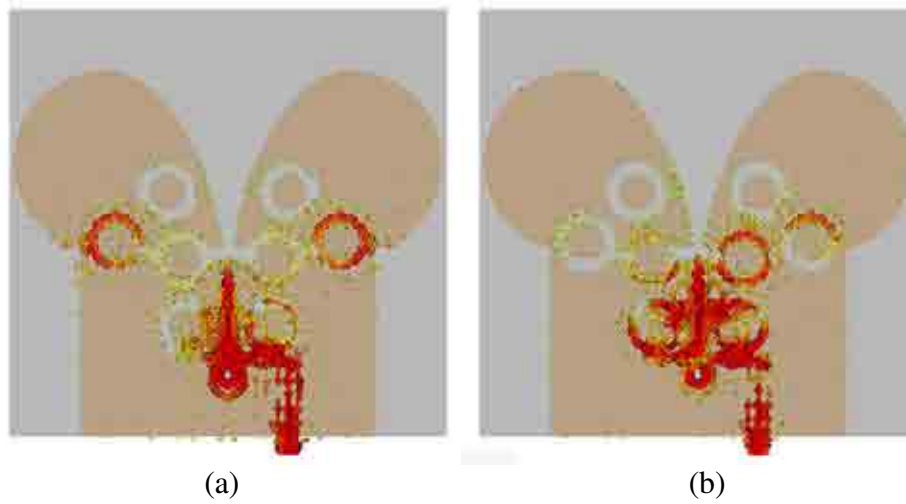
Figure 4.25 Simulated current distributions for the mid band configuration excited at (a) 1.1 GHz and (b) 3 GHz
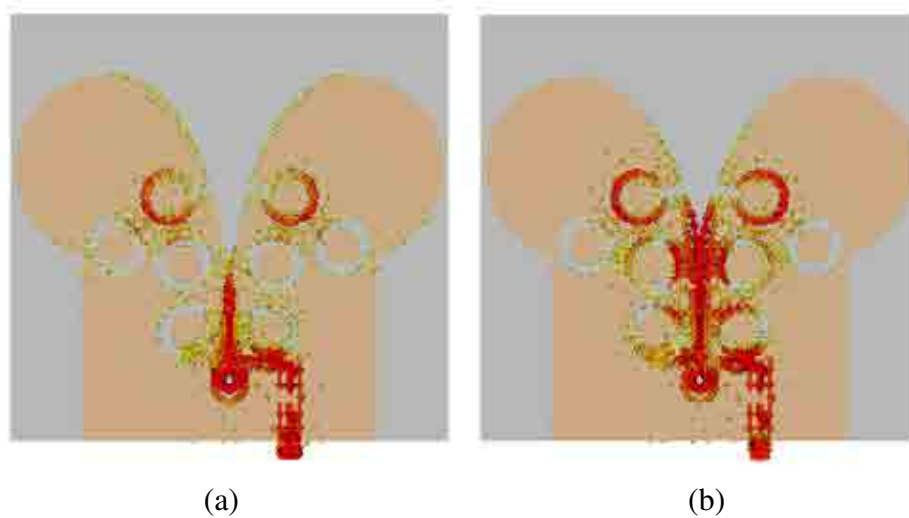
Figure 4.26 Simulated current distributions for the high band configuration excited at (a) 1.1 GHz and (b) 2 GHz

4.5 Prototype Antenna

In the CST simulation, the PIN diode was modeled in its on state as a 2 Ω resistance and in its off state using an S-parameter file supplied by the diode manufacturer. The dc lines and dc decoupling components are included in the simulation. The practical antenna is shown in Figure 4.27. To give a minimal effect on the radiation pattern, four very thin dc lines were printed parallel to the beam direction on either side of the antenna. Therefore if there are any RF leakages through the dc line, the effect will be negligible. The dc line was isolated from the RF signal by using 27 nH SMD inductors. The tapered slot is dc isolated into four sections with 0.3 mm width slots. To preserve RF continuity, 22 pF SMD capacitors bridged the slots every 10 mm. Each switch in Figure 4.15 consists of two in-series Infineon PIN diodes, BAR50-02V. Two diodes are used in series because a single diode having 1.2 mm length is unable to bridge the 4 mm gaps. Gaps of 4 mm are used to reduce spurious resonances at higher frequency due to parasitic capacitance across the gap sides. Figure 4.28 shows the simulated S_{11} with different sized gaps used for low band operation. There is very small spurious when 4 mm gaps are used. Nevertheless, further work might reveal alternative ways to design the gap that could be bridged by a single diode having 1.2 mm length while avoiding spurious resonance problems. The diodes were forward biased appropriately with dc voltage to obtain 100 mA on state bias current. To obtain the off state, the diodes were left unbiased.

Figure 4.27 Prototype

1. Gap= 1mm

2. Gap= 1mm and tapered

3. Gap= 1mmx1mm

4. Gap= 4mm (no spurious)

(a)
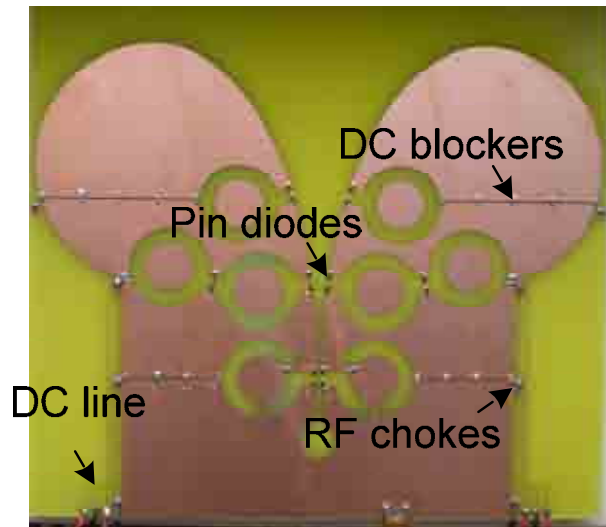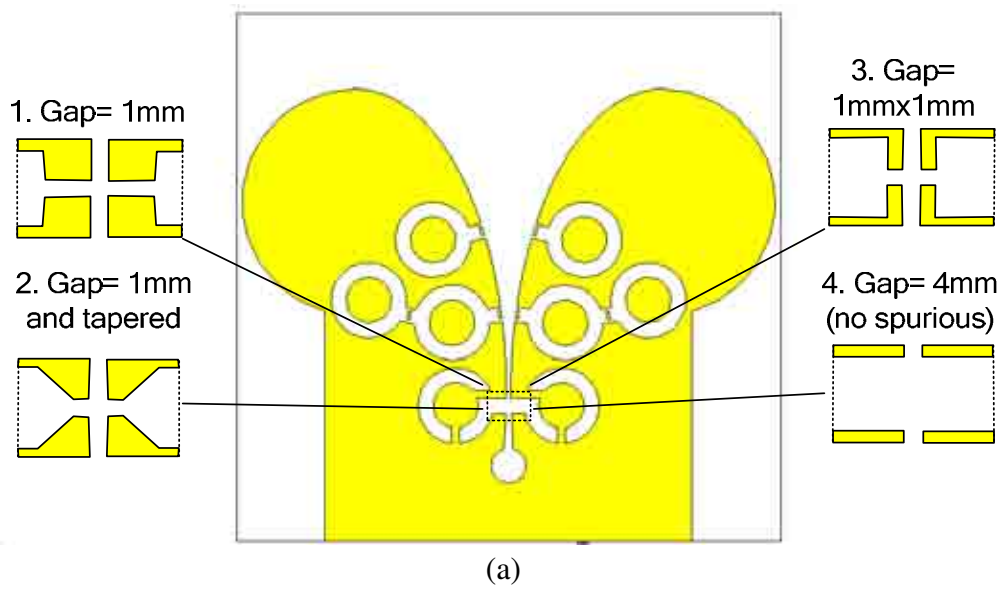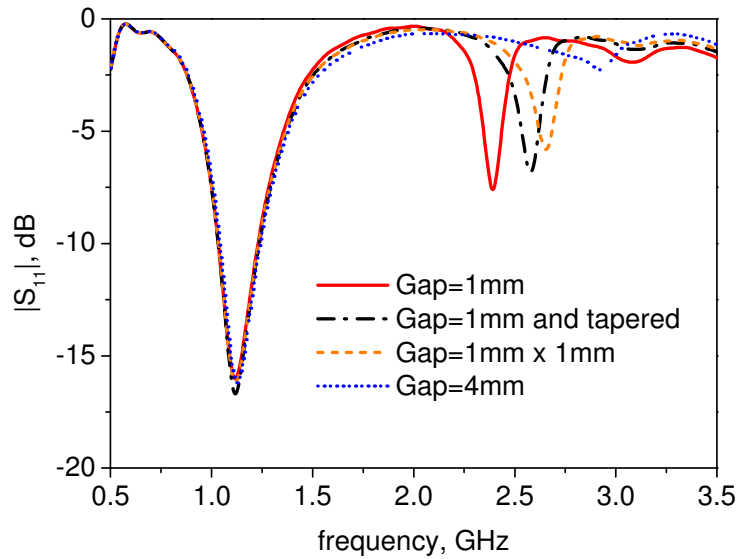
(b)

Figure 4.28 Spurious in S_{11} responses as a function of gap sizes.

4.6 Results

Figure 4.29 compares the simulated return loss for wideband operation with and without the ring slots. It is noticed that the S_{11} between 1.8 and 3.0 GHz has been improved by the ring slots. The simulated and the measured wideband responses with ring slots are shown in Figure 4.30. Good agreement can be seen between them. The results show that a good matching for wideband operation is achieved over a 1.0 – 3.2 GHz bandwidth. The return loss for the other three states, low band 1.1 GHz, mid band 2.25 GHz and high band 3.1 GHz are shown in Figure 4.31. A small frequency shift between the measurement and simulation is presumably due to the effect of parasitics in the PIN diodes, fabrication tolerances and biasing components. However, in general, a good agreement has been achieved.
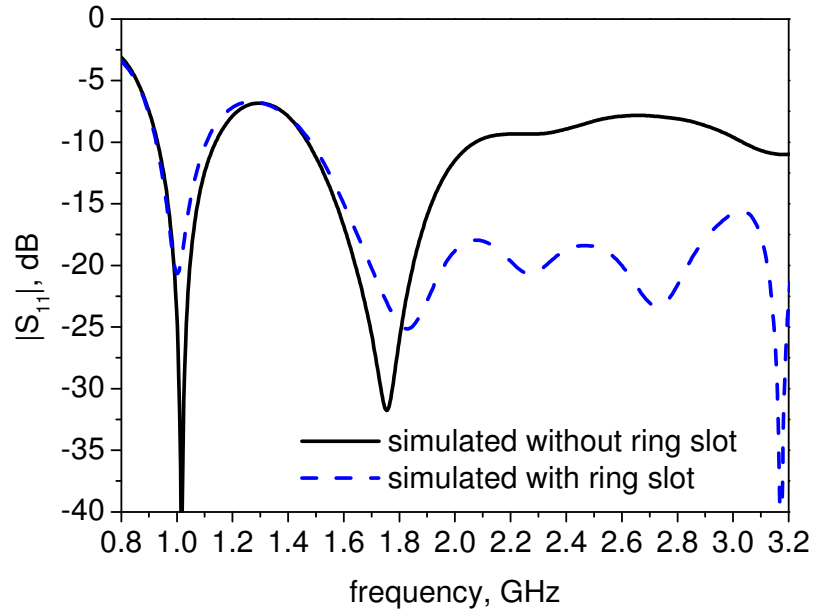
Figure 4.29 Simulated wideband mode S$_{11}$ response of antenna with and without ring slots
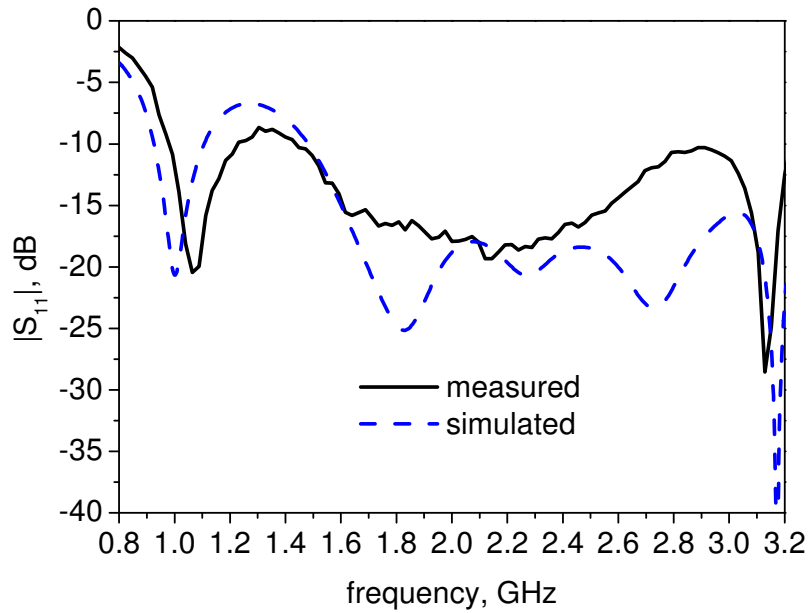
Figure 4.30 Simulated and measured wideband mode S$_{11}$
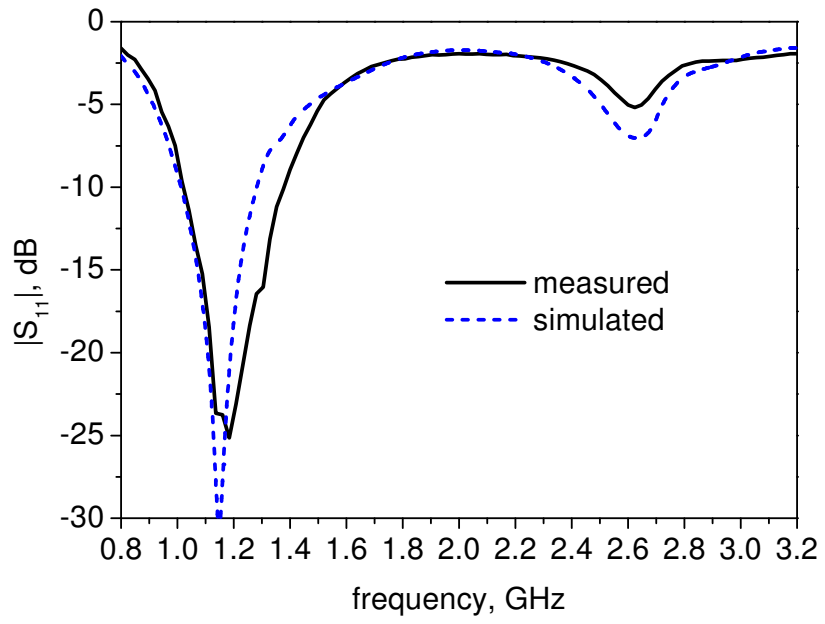
(a)
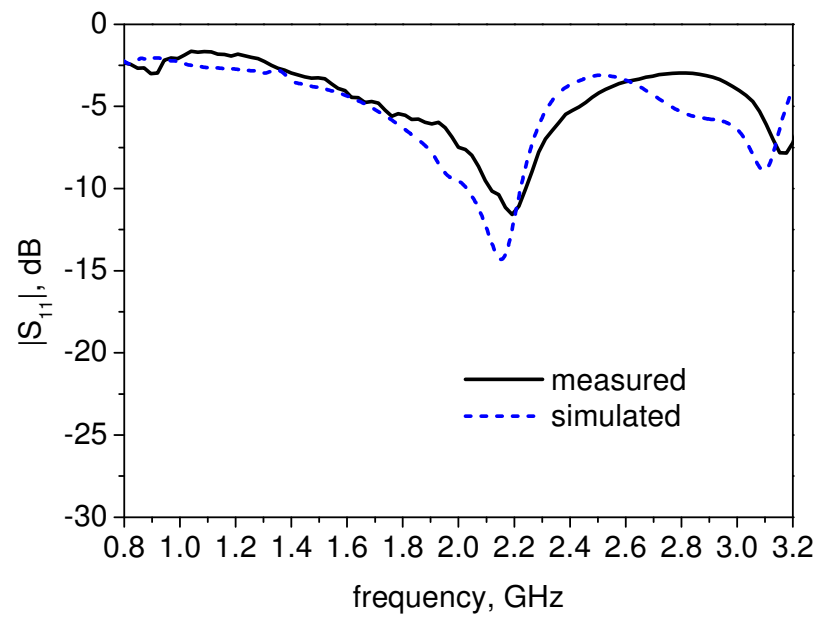
(b)
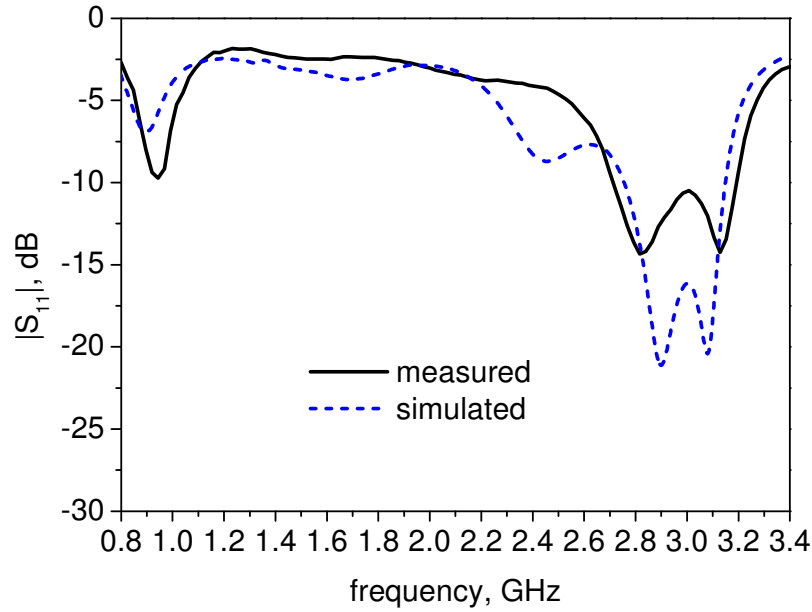
(c)

Figure 4.31 Simulated and measured S_{11} of antenna in narrowband modes (a) Low band state (b) Mid band state (c) High band state.

The out of band rejection is relatively poor. This can only be expected as the filtering or reconfiguration is achieved with single resonator which has relatively low Q due to being mounted in an antenna, as well as the switch losses. However the main factor of that relatively poor rejection in S_{11} mainly comes from the dielectric losses of the FR4 substrate. Figure 4.32 shows this, where the simulated S_{11} of lossy FR4 substrate of low band mode is compared with the lossless case. The effect of the ideal and real switches on the S_{11} is also compared as shown in Figure 4.33. It is seen that the loss that contributed to poor rejection is small from the switch but very pronounced from the FR4 substrate.
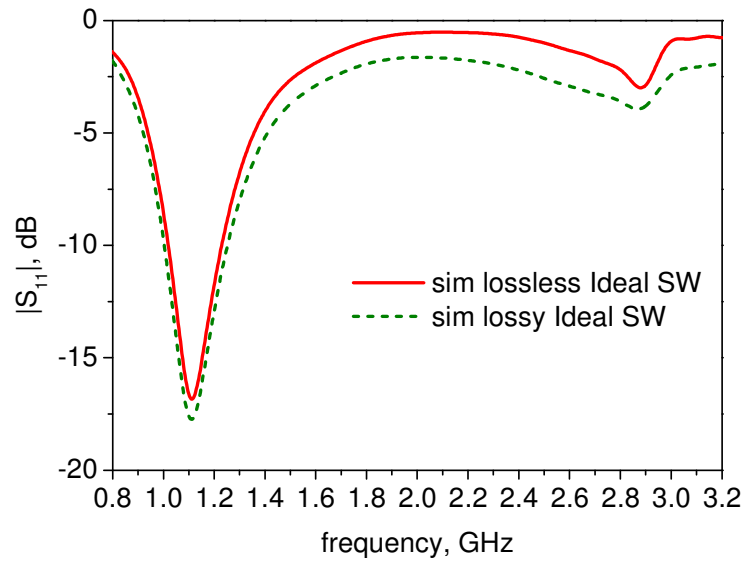
Figure 4.32 Rejection in S_{11} as a function of substrate loss
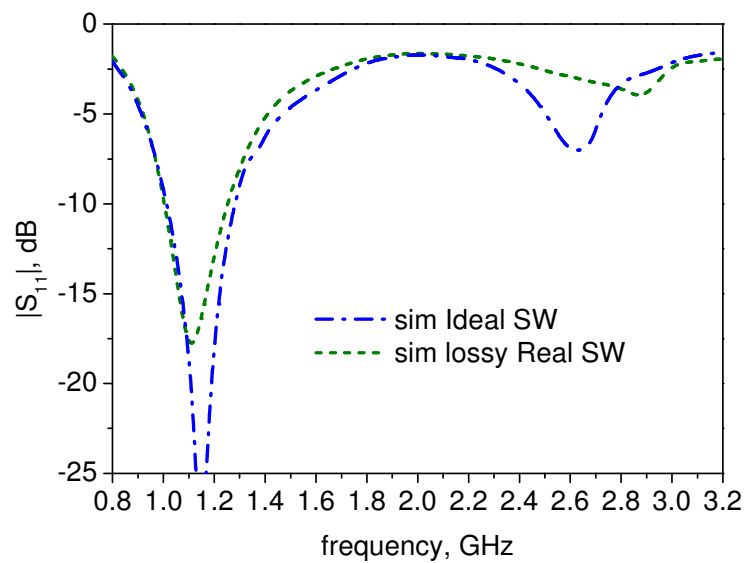
Figure 4.33 Rejection in S_{11} as a function of switch loss

To give a better measure of out of band rejection, the measured return loss and gain vs frequency for each narrow band mode and the wideband mode is presented. The low band mode achieved a comparable gain with the wideband mode at the pass band region

but decreased about 14 dB at out off band region as shown in Figure 4.34. A very sharp gain reduction is seen at 2.55 GHz caused by the spurious occurring in this mode.
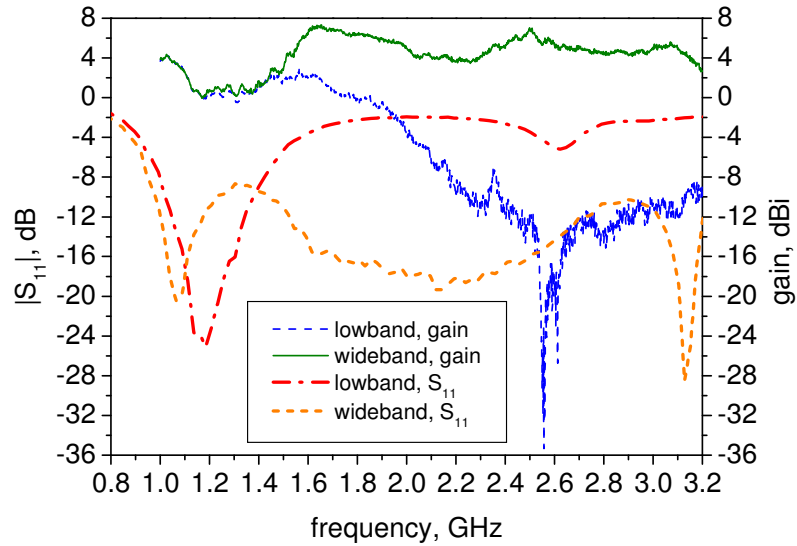
Figure 4.34 Measured low band gain of the proposed antenna

In the mid band mode, the pass band gain is approximately 4 dB lower than in the wideband mode as shown in Figure 4.35. This is presumably due to the filter action where the match condition is low as the mid band ring slots are not at the optimum position as described previously. A wider pass band occurs and can be explained by low reflection as seen in the S_{11}. Also, the gain reduction is higher at the high frequency band than at the low frequency band even though the reflection at high frequency is low. This can be understood because the loss is higher as the frequency is increased. Also seen is the spurious at 3.2 GHz in the S_{11} plot. However the gain at the direction taken is low.
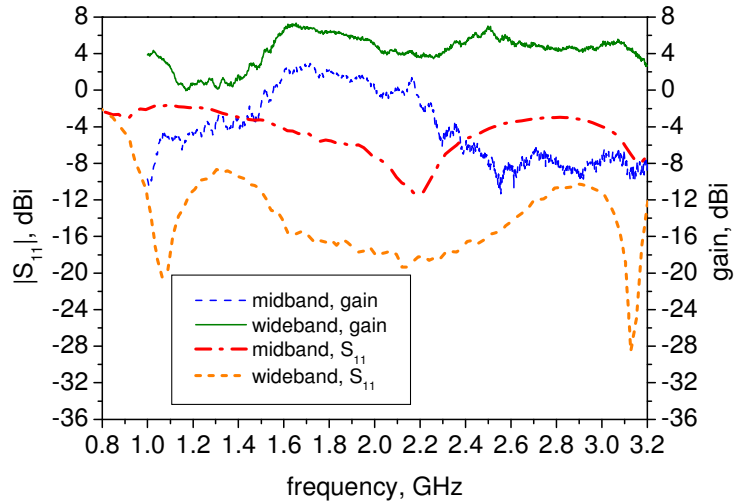
Figure 4.35 Measured mid band gain of the proposed antenna

The pass band gain in the high band mode shown in Figure 4.36 is nearly comparable with the wideband gain as the matching is good. The gain is gradually dropped as the reflection is slowly increased in the rejection band. Also the gain is seen to increase below 1.0 GHz where the pass band occurs at 0.9 GHz. Table 4.1 compares the measured and simulated gains for each state. In the narrowband state, the roll off at the edge of the pass bands is not fast. This is presumably related to the fact that the antenna itself is inherently wideband and also as expected since the antenna is a low Q radiator.
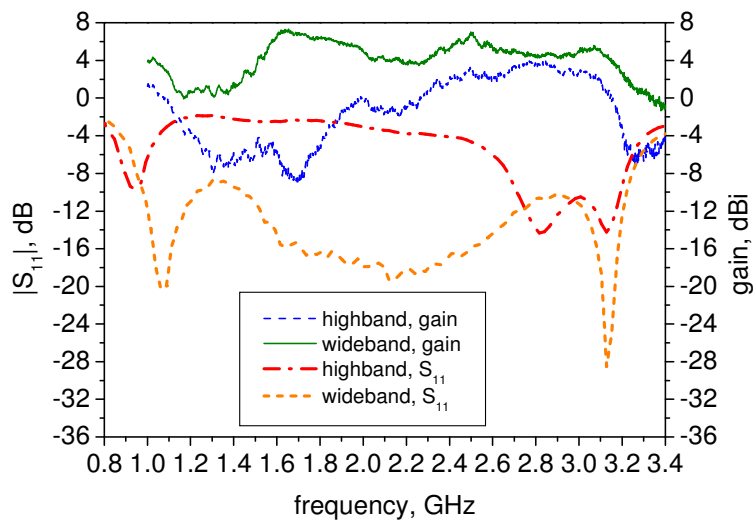
Figure 4.36 Measured high band gain of the proposed antenna

The E- and H-plane simulated and measured radiation patterns are presented in Figure 4.37. Good agreement between simulation and measurement has been achieved. It can be concluded that the biasing circuit has a small effect on the antenna performance. It is also observed that the 3 dB beam width becomes narrower as the frequency increases, which is usual for the Vivaldi antenna. The cross-polar radiation pattern in particular the main direction is lower than -10 dB. It is suggested that the ring slot resonators have some effect on cross polar radiation performance.

(a)

(b)
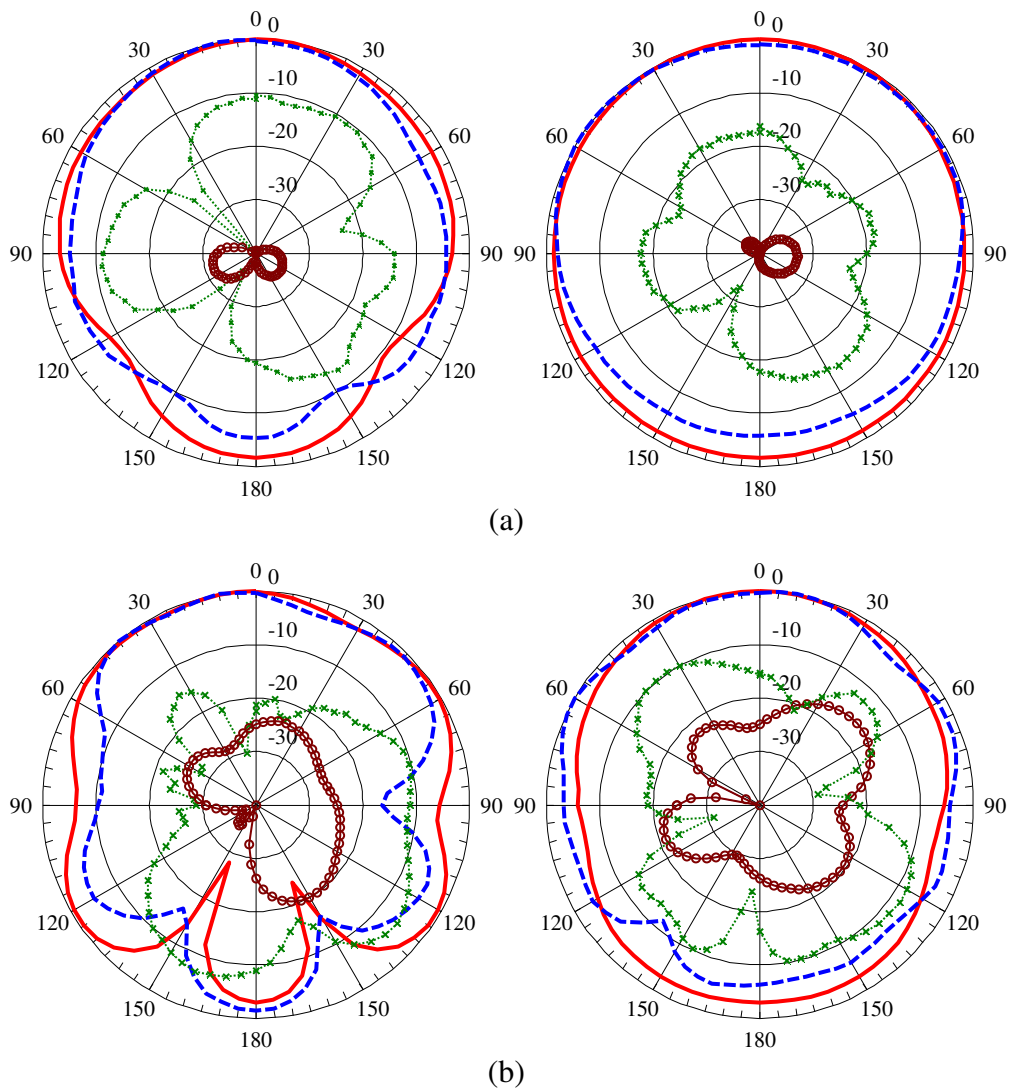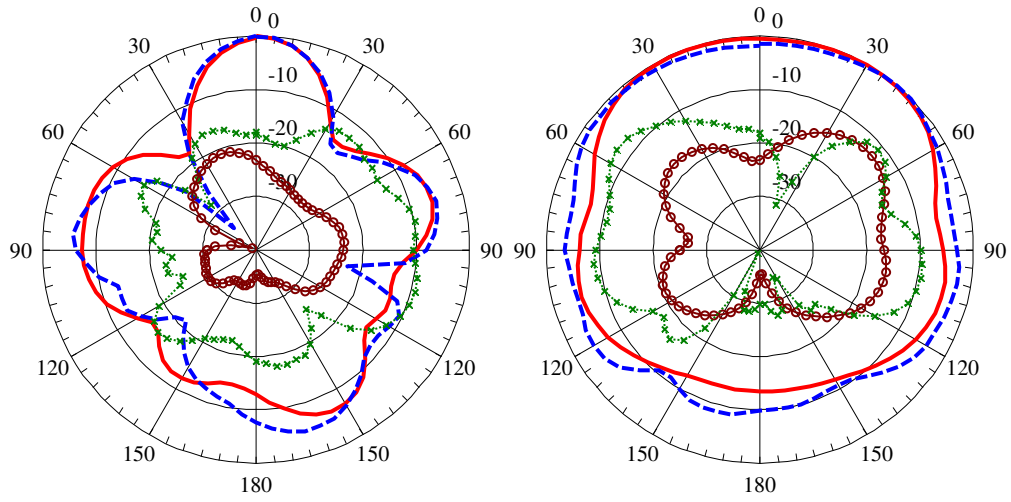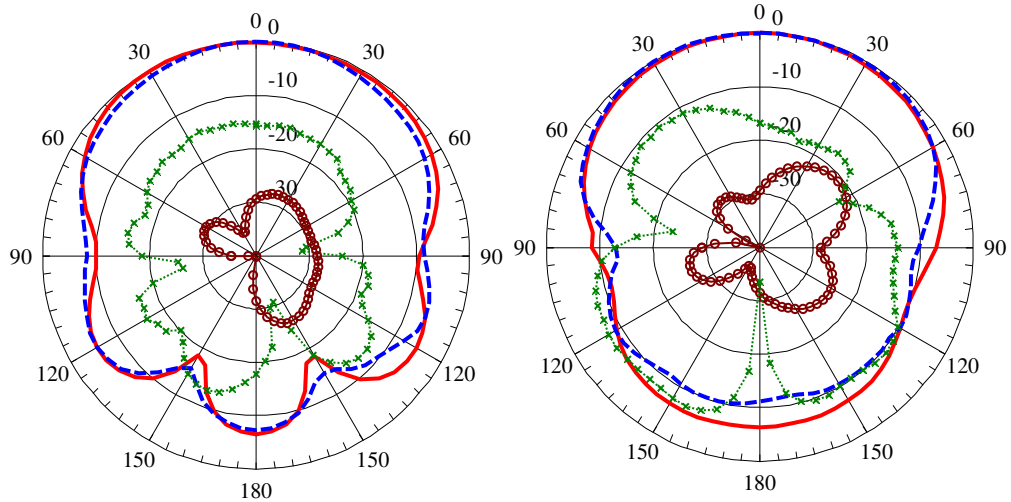
— co-polar simulated   ----- co-polar measured

-o-o- cross-polar simulated   -x-x- cross-polar measured

Figure 4.37 Radiation pattern. (a) Low band mode excited at 1.1 GHz, E-plane (left), H-plane (right). (b) Mid band mode exited at 2.2 GHz, E-plane (left) , H-plane (right). (c) High band mode excited at 3.1 GHz E-plane (left) , H-plane (right). (d) Wideband mode excited at 2.0 GHz, E-plane (left) , H-plane (right).

Table 4.1 Gain of the proposed antenna

Gain, dBi	Wide band (at 2 GHz)	High band	Mid band	Low band
Simulated	3.61	3.31	0.57	1.75
Measured	3.27	1.56	0.28	1.47

4.7 Summary

A novel switched band Vivaldi antenna has been proposed by introducing the ring slots. Three modes of reconfiguration are shown, when three pairs of ring slots were employed in three different positions within the Vivaldi. The design guideline has been derived and allows some optimizing of the band positions. More sub-bands could be achieved with additional resonators, in a longer version of the antenna. Nevertheless, in the relatively simple example shown, good return loss has been obtained for each of the sub bands. The proposed antenna could be a suitable solution for applications requiring wideband sensing and dynamic band switching, such as in military application or cognitive radio. The work described here has been published in [83-86].

CHAPTER 5

VIVALDI WITH SINGLE RING RESONATOR

5.1 Introduction

In the previous chapter, a Vivaldi antenna incorporating multiple rings has been demonstrated. The antenna shows band switching between a wideband mode (1.0 - 3.2 GHz) and three narrowband modes. In that configuration, the number of frequency bands controlled depends on the number of resonators incorporated. This means that if more bands were desired, the antenna has to be much longer to incorporate more resonators. In this chapter a new design method of band switching in the Vivaldi antenna, that allows a better control of the narrow operating bands, is proposed. By incorporating only a single pair of slot resonators, six different narrow frequency bands can be switched within the wideband operation, double the number reported in the previous chapter. To achieve the switched band properties, the proposed approach reconfigures the operating band by varying the electrical length of the slot resonators by means of PIN diode switches. This effectively stops, or passes, current at different frequencies. The design principles of the

proposed antenna are described. Section 5.2 and 5.3 discuss the initial design of the Vivaldi antenna and the switchable slot line resonator. In section 5.4, the switchable narrowband antenna configuration is explained. The fabricated antenna is discussed in section 5.5. Finally the results are presented in section 5.6 and followed by conclusions in section 5.7.

5.2 Wideband Antenna Design

The reconfigurable antenna is based on the same wideband Vivaldi antenna operating from 1 to 3 GHz as described in previous chapter. The Vivaldi is illustrated in Figure 5.1. The simulated $S_{11,}$ in Figure 5.2, shows that $1 - 3$ GHz wideband operation is achieved.

(a)

(b)
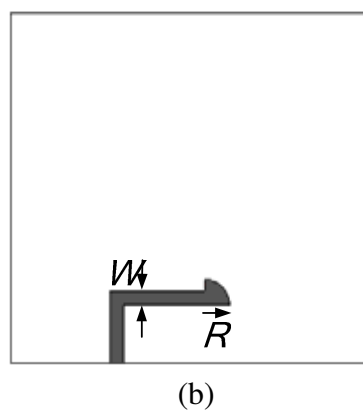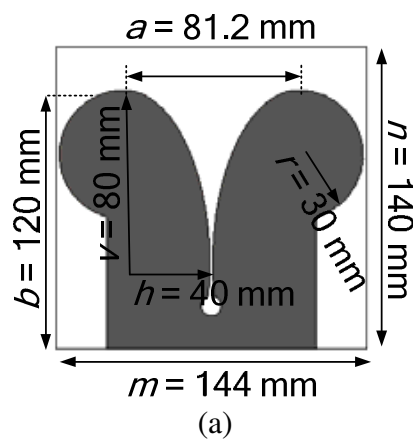
Figure 5.1 Vivaldi antenna, (a) front view, (b) rear view showing microstrip feed.
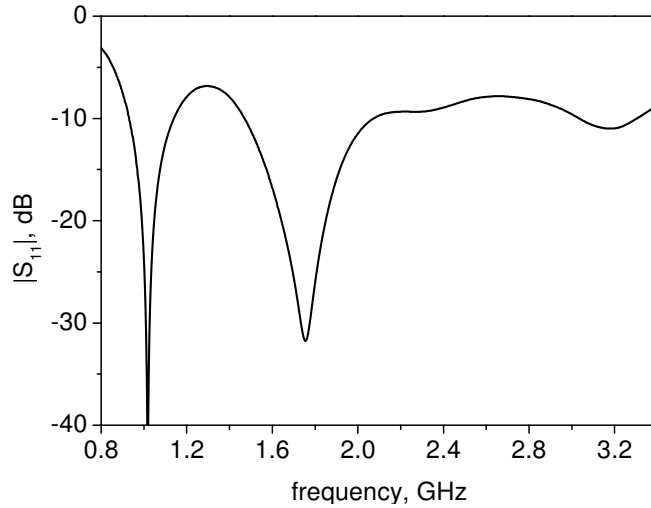
Figure 5.2 S_{11} of Vivaldi antenna in Figure 5.1

5.3 Slot Line Resonator Design

In principle, distorting the current distributions along the antennas current path will change the radiation properties. The Vivaldi has currents that propagate near the edge of the tapered slot, as shown in Figure 5.3. The narrower end is acting as a transmission region whilst the wider end is acting as a radiation region. It is thus appropriate to locate the filter in the narrower end. A slot ring resonator with a perimeter, P_s as shown in Figure 5.4 is chosen for this. The basic principle of the reconfigurable ring slot band pass resonator is described below.
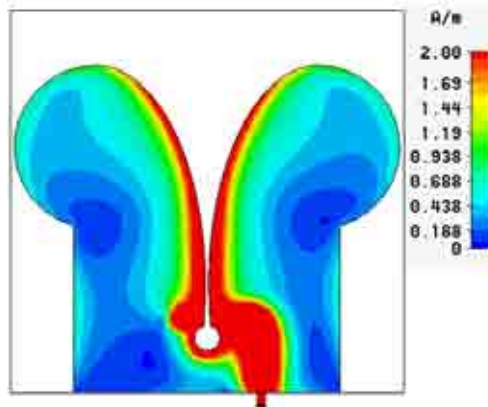
Figure 5.3 Simulated surface current distribution at 2 GHz
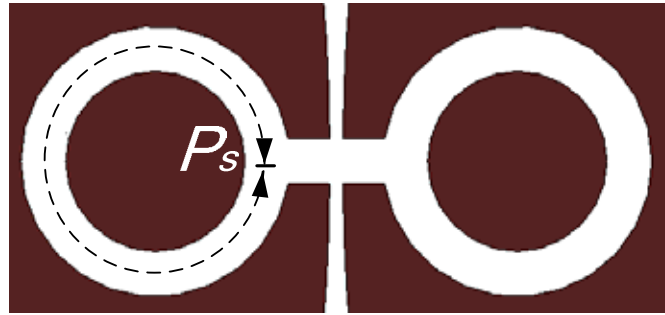
Figure 5.4 Slot ring resonator

A pass band response can be obtained either by cascading two different quarter wavelength short circuit stubs in series to form two different stop band filters or by having a single half wavelength short circuit stub. A possible equivalent circuit of two different stop band filters in series is shown in Figure 5.5. Two parallel RLC circuits are arranged in series, where each parallel RLC circuit represents a stop band filter. Figure 5.6 shows the response simulated using Microwave Office AWR software when L_1, C_1, R_1 and L_2, C_2, R_2 are set to (45 nH, 0.41 pF, 82.9 kΩ) and (24.61 nH, 0.154 pF, 21.15 kΩ) respectively. It is clearly seen that two stop bands occur at 1.17 GHz and 2.59 GHz which correspond to the resonances of circuit one and two respectively. Together, the circuits form a band pass filter at 1.68 GHz. Therefore, the slot ring resonator is designed in such a way to form two stop band filters in series. The slot ring design is now described.
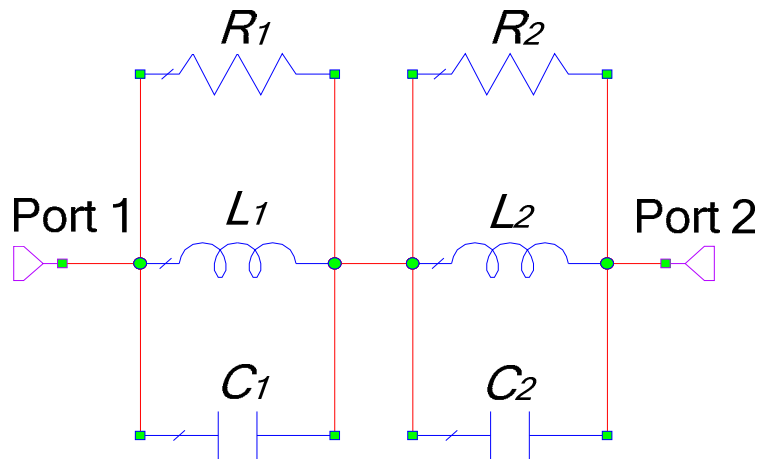
Figure 5.5 RLC shunt circuits in series
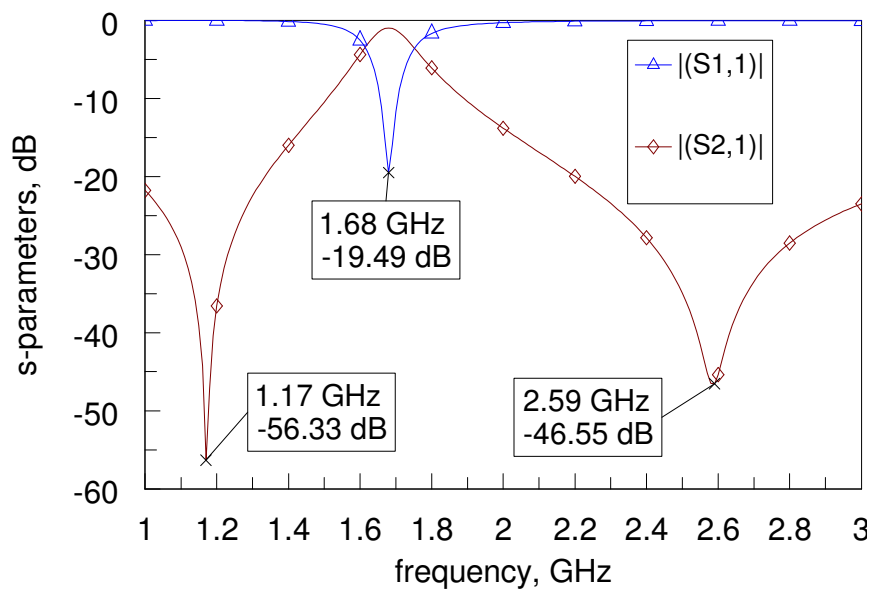
Figure 5.6 Simulated s-parameters of RLC shunt circuits in series

The shape of the ring slots is chosen so that two tunable stop band filter in series can be easily designed. They have an inner radius of 8 mm and an outer radius of 12 mm. Small gaps, of size 3.67 mm x 4 mm are used to couple the resonator to the slot line. Figure 5.7a shows a single stop band filter configuration, stopping at 1.69 GHz. The ring slot is acting

118

as an open circuit stub, where its average perimeter P_s = 72 mm is approximately a half wavelength at 1.69 GHz. Since the slot length determines the stop band frequency, it is now possible to form two stop band filters by bridging the slot at an appropriate location. Figure 5.8 shows the configuration required to obtain a band pass response at 1.68 GHz. Instead of acting as a single open circuit stub, the slot now has two short circuit stubs in series which have different length P_1 and P_2, giving two stop band responses. P_1 = 18 mm represents a quarter wavelength at 3.2 GHz while P_2 = 54 mm represents a quarter wavelength at 1.13 GHz.
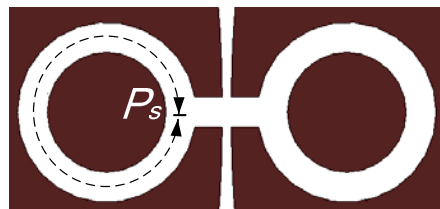
(a)
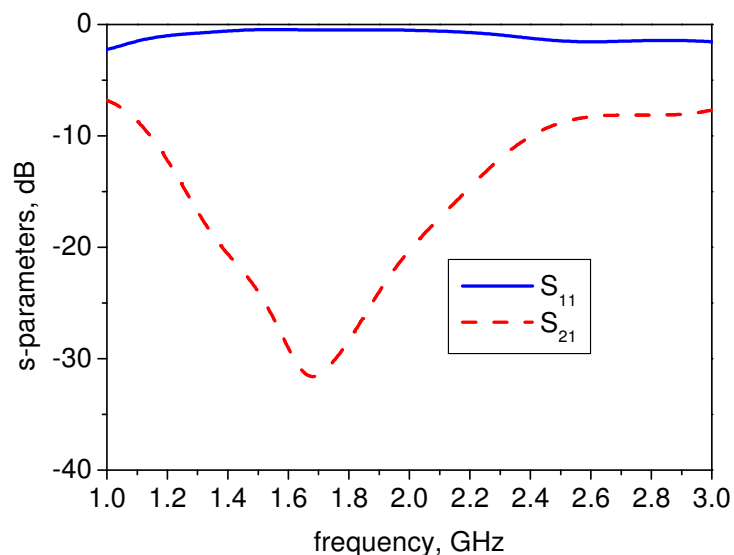
(b)

Figure 5.7 Single stop band filter, (a) the configuration, (b) the responses
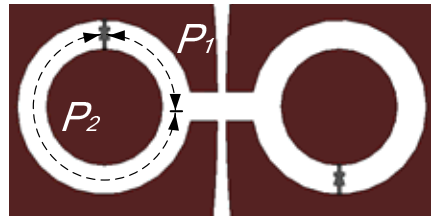
(a)
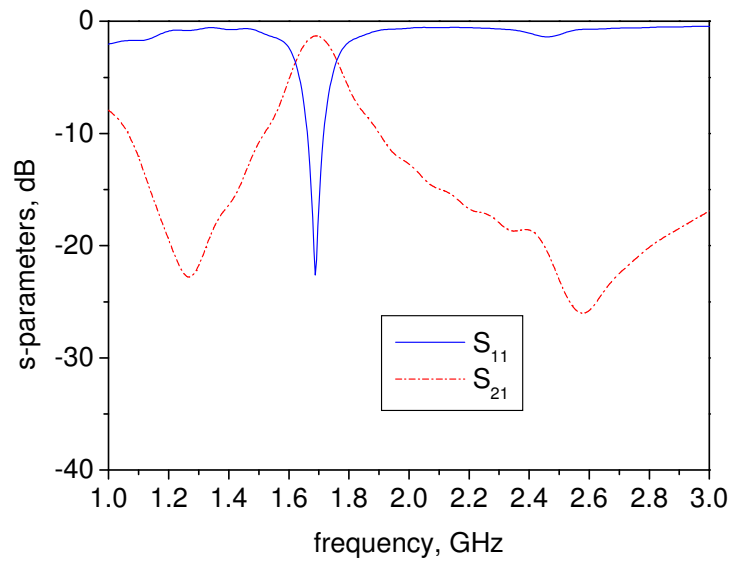
(b)

Figure 5.8 Band pass filter, (a) the configuration, (b) the responses

To switch to a different pass band, the bridges are moved to other specific positions, changing the electrical length of P_1 and P_2. Alternatively an extra bridge can be added. For example, Figure 5.9 shows how a new band pass configuration at 2.3 GHz is achieved after an extra bridge is added in the ring slot. P_2 is reduced to 36 mm representing a quarter wavelength at 1.68 GHz, whilst P_1 is kept to 18 mm.
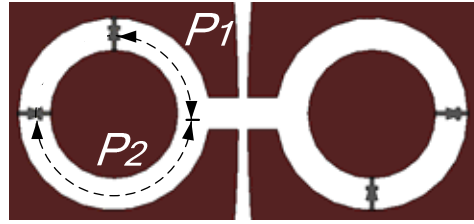
(a)
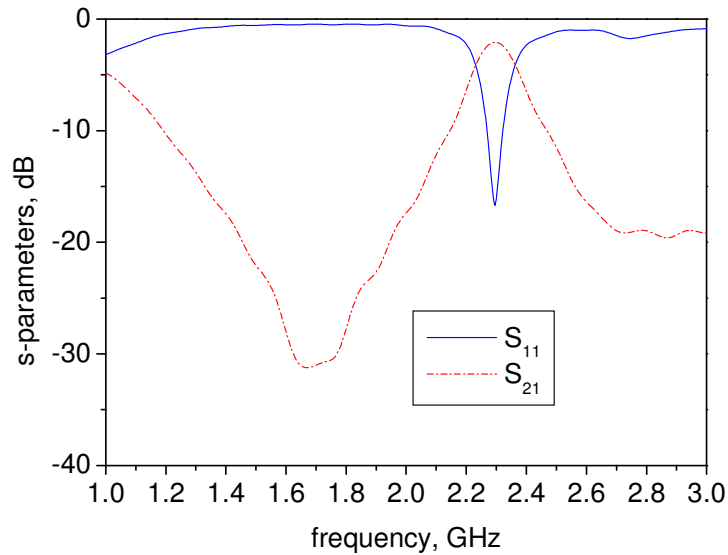
(b)

Figure 5.9 Band pass filter, (a) the configuration, (b) the responses

Alternatively, the pass band response can also be obtained by transforming the slot ring in Figure 5.4 to a half wavelength short circuit stub by bridging the slot at the position shown in Figure 5.10. The total length, *P* from the edge of the small gaps is approximately a half wavelength (78 mm) at 1.52 GHz. To switch the frequency, an extra bridge is added to shorten the length. The different pass band configurations as a function of bridge position are summarized in Figure 5.11.

121
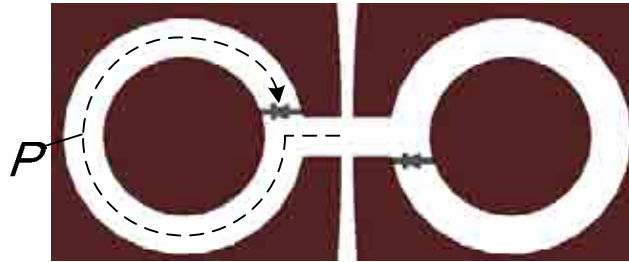
Figure 5.10 Pass band configuration using a half wavelength short circuited stub
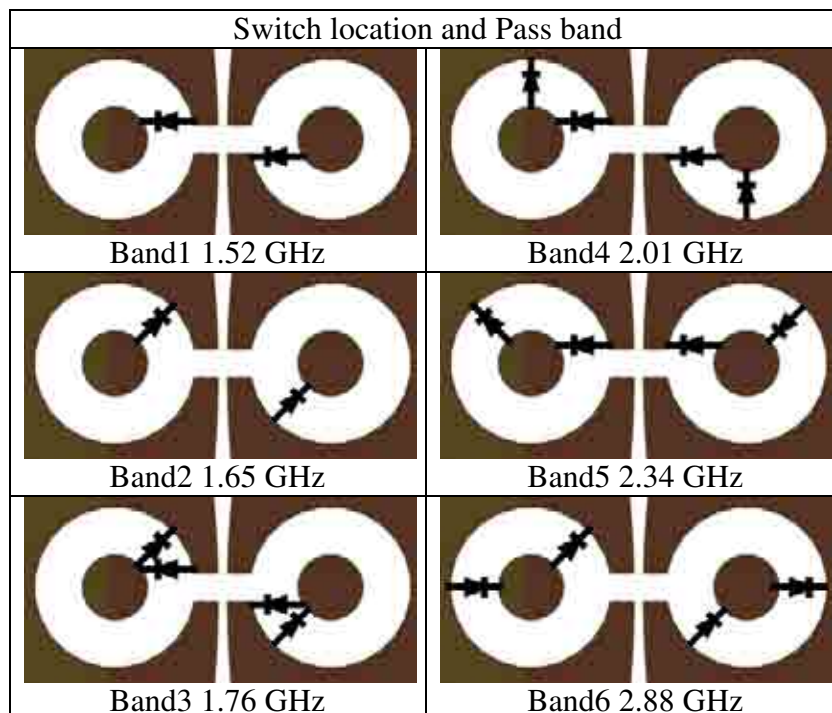
Asymmetric position: Band 1, Band 2, Band 3, Band 4 and Band 6
Symmetric position: Band 5

Figure 5.11 Bridge position for various pass band centre frequencies

The use of different forms of pass band circuit is useful to reduce number of switches. For example, the same switch used in Band 1 and Band 2 is also being used in Band 3. Band 2 is using two stop bands in series to operate at 1.65 GHz, whilst Band 1 and Band 3 is operated using a half wavelength short circuit stub method. As also can be seen in Figure 5.11, most of the relative switch positions are asymmetric rather than symmetric.

This arrangement provides good and equal match in both ports (S_{11} and S_{22}). Figure 5.12 shows a 2 port slot ring configuration (Band 2) in an asymmetric and a symmetric position. For the symmetric position (Figure 5.12b), the impedance seen from different ports is different, because the symmetry is only with respect to the vertical plane but not in the horizontal plane. A better match is only obtained in the symmetric arrangement when excited from port 2 which is near to the switches. However, when the ring slot is embedded in the antenna, the overall matching will be perturbed as the ring slot will be positioned near to the lower throat of the antenna in order to obtain a reasonably good Q, as will described in section 5.4 and shown in Figure 5.23. This is presumably because the current on the feed line of the antenna has perturbed the current flow through the switch in the ring slot (because the switch position is near to the feed line) and this, is believed to have disturbed the standing wave at the resonant frequency which then disturbed the overall match. To reduce this effect, asymmetric switch positions are used. The simulated S_{11} shows that good match is obtained in an asymmetric arrangement as will described in Figure 5.18, Figure 5.19 and Figure 5.20. The final switch arrangement in Band 5 configuration however, is decided to be symmetrical since good responses are achieved after the ring slot is embedded in the antenna. This result will be shown in section 5.4.

(a)   (b)
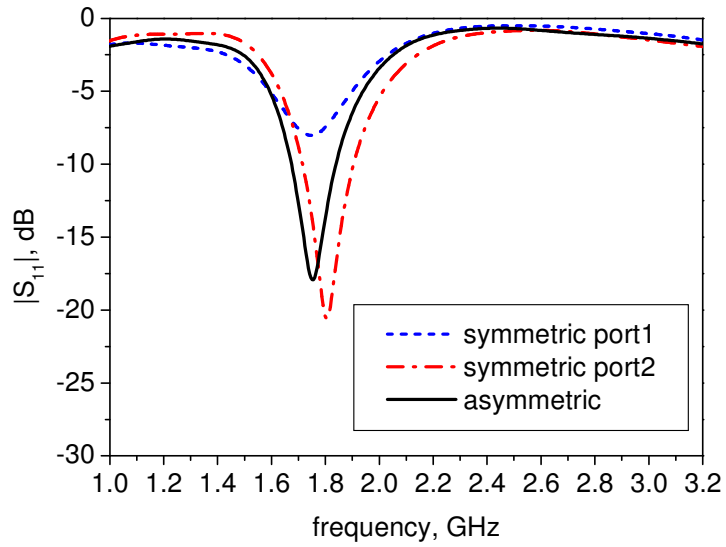
(c)

Figure 5.12 2 port (a) Asymmetric, and (b) Symmetric position on (c) S_{11} responses

The effect of ring radius on the pass band frequency is studied. Figure 5.13 shows this. As resonant frequency is inversely proportional to the length of the ring slot in guided wavelengths, reducing the outer radius, r_o, from 12 mm to 8 mm and inner radius r_i, from 8 mm to 4 mm respectively, shifts the pass band response from 1.68 GHz to 2.72 GHz. If a smaller ring slot as in the configuration shown in Figure 5.13a is chosen, narrowband operation lower than 2 GHz, will be impossible to obtain.

(a)
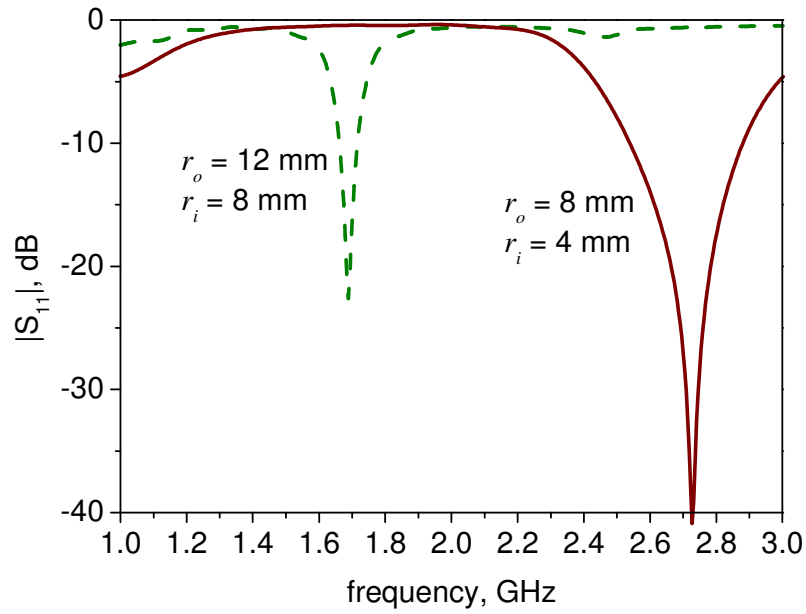
(b)

**Figure 5.13 Effect of slot ring radius (a) configuration, (b) responses for outer radius,
r = 12mm and 8 mm, with inner radius = 8mm and 4 mm respectively**

The width of the slot ring is important to determine the quality factor, Q. Figure 5.14 shows the Q at the pass band is decreased when the slot gap, G, reduced from 4 to 1 mm. Therefore the Q of a 4 mm was chosen to demonstrate the action and final choice may depend on application.
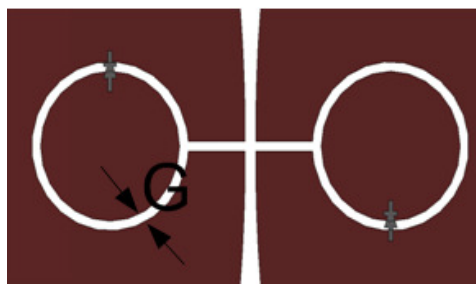
(a)
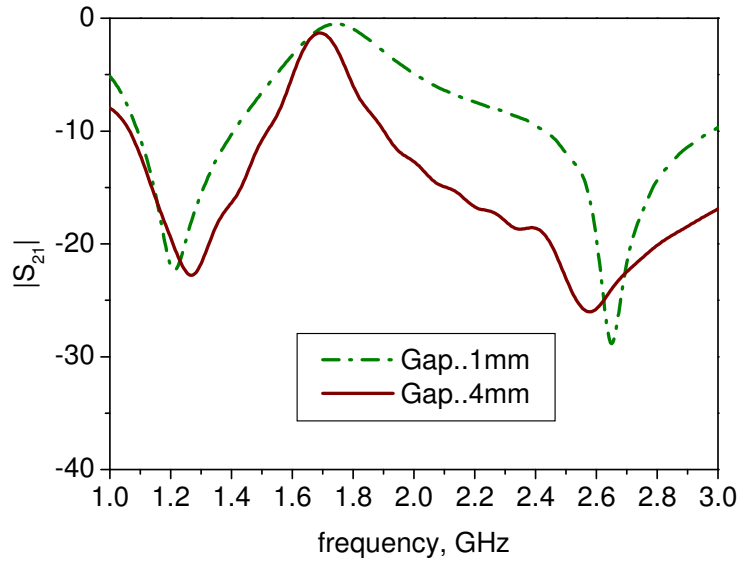
(b)

Figure 5.14 Effect of slot ring width (a) configuration, inner radius, = 8 mm, (b) responses for gap, G = 4 mm and 1 mm, with outer radius = 12 mm and 9 mm respectively

.

5.4 Seven Mode Reconfigurable Configuration

The design and simulation of a Vivaldi antenna with seven modes is now described. To reconfigure the antenna electronically, the CST simulation uses on state s2p-data of Infineon PIN diode switches, model BAR50-02V to represent the on state. To simplify the simulation process, the off state is represented by a gap. Also to reduce computation time, there are neither dc lines nor dc decoupling components included in the simulation. An example of Band 2 (Figure 5.11) configuration is shown in Figure 5.15. The ring slot is placed x = 21.26 mm above the circular slot stub to reduce strong coupling from the feed line located on the reverse side of the substrate. When using ideal switches, consisting of metal pads of size 1 mm x 4 mm, the simulated resonance of Band 2 configuration occurs at 1.7 GHz. However with Infineon PIN diode switch models, the simulated resonance is

shifted down around 14.7% to 1.45 GHz. This can be explained by the package parasitic effects. The simulated S_{11} results are shown in Figure 5.16.
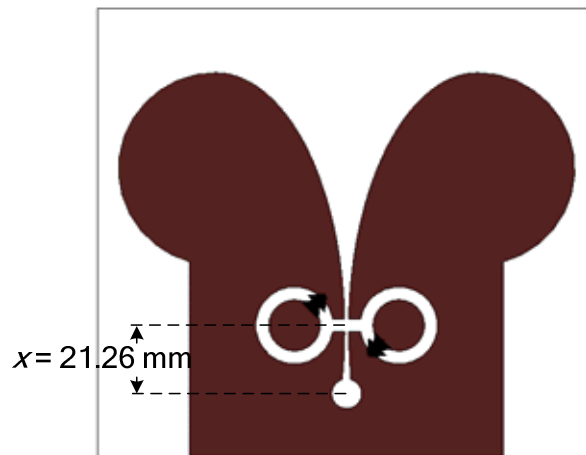
Figure 5.15 Band 2 configuration, x = 21.26 mm
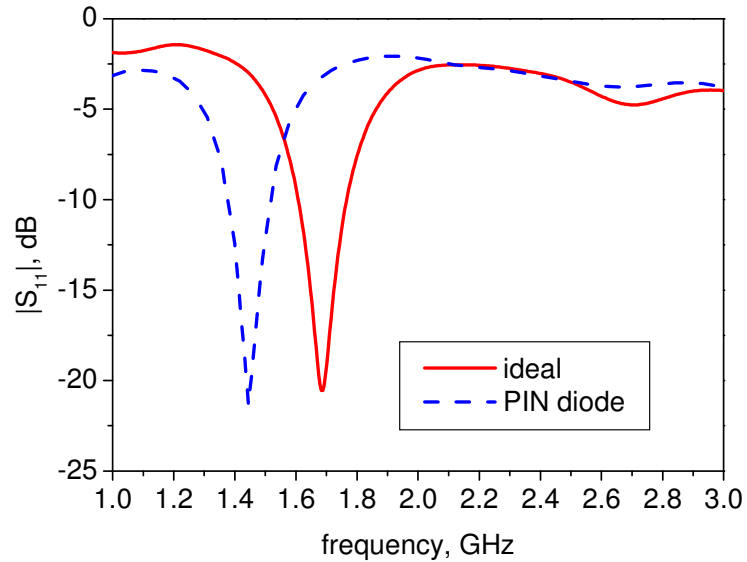
Figure 5.16 Simulated S_{11} of band 2 configuration

Figure 5.17 shows the current distributions of Band 2 configuration using ideal switches when excited at the resonance frequency, 1.7 GHz (Figure 5.17a) and at out of

band frequencies 1 GHz (Figure 5.17b) and 3 GHz (Figure 5.17c). It is observed that the ring slot, passes the current at 1.7 GHz but significantly reduces the current on the upper part of the antenna at 1 and 3 GHz.

(a)

(b)   (c)
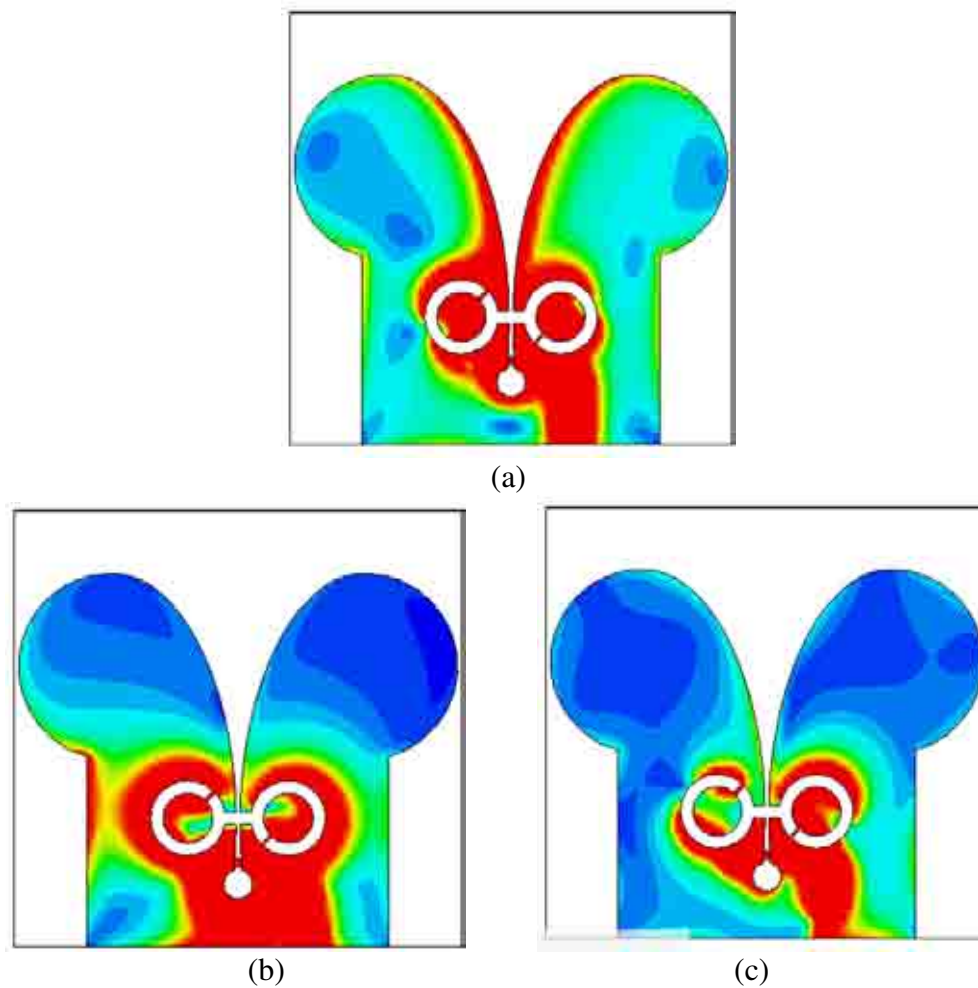
Figure 5.17 Current distributions (a) excited at 1.7 GHz, (b) excited at 1.0 GHz, (c) excited at 3.0 GHz.

The effects of the switch arrangement style (asymmetric or symmetric) for Band 2 are shown in Figure 5.18 and Figure 5.19. It is observed symmetric arrangements gave poor impedance match and good match is only obtained when asymmetric arrangement is used. Figure 5.20 shows the effect of asymmetric and symmetric arrangements for the

other bands. Generally, an asymmetric arrangement give a good match hence a good return loss in all bands, however at some frequencies i.e. in Band 5 and Band 6, it is observed that a symmetric arrangement also give a good match.

(a)
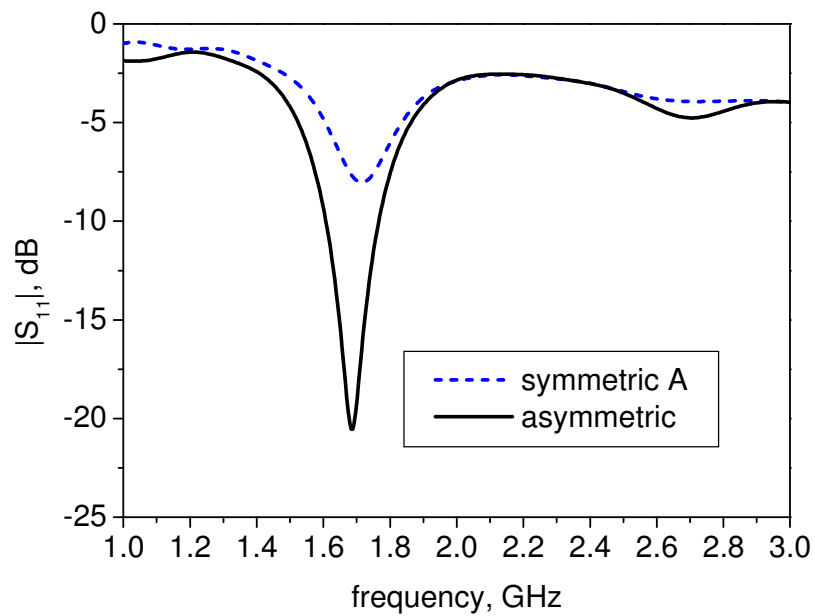
(b)

Figure 5.18 Asymmetric vs symmetric type A, (a) symmetric type A arrangement and (b) the S₁₁

(a)
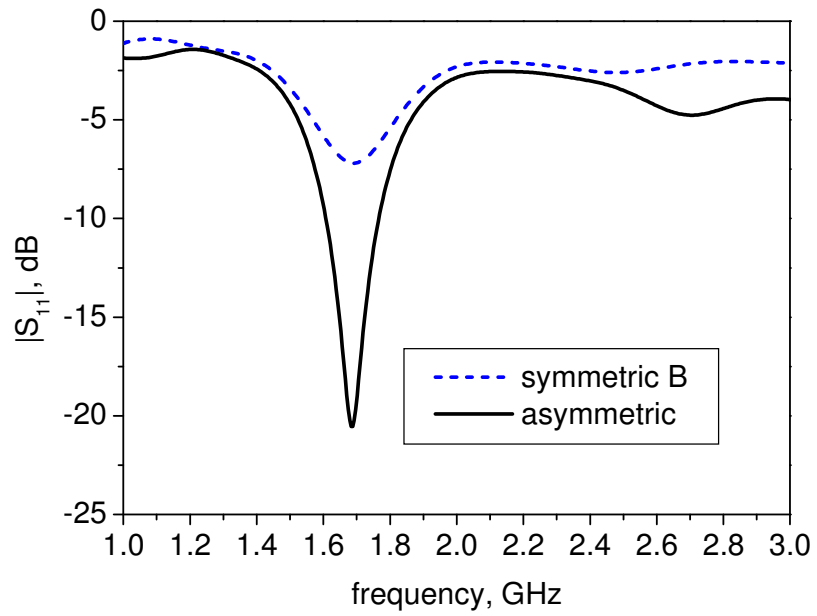
(b)

Figure 5.19 Asymmetric vs symmetric type B, (a) symmetric type B arrangement and (b) the S_{11}
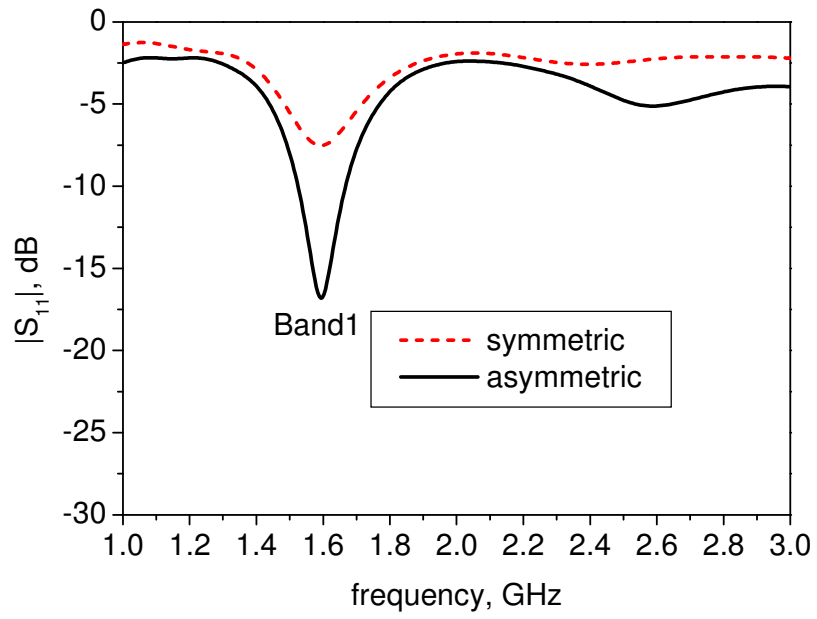
(a)
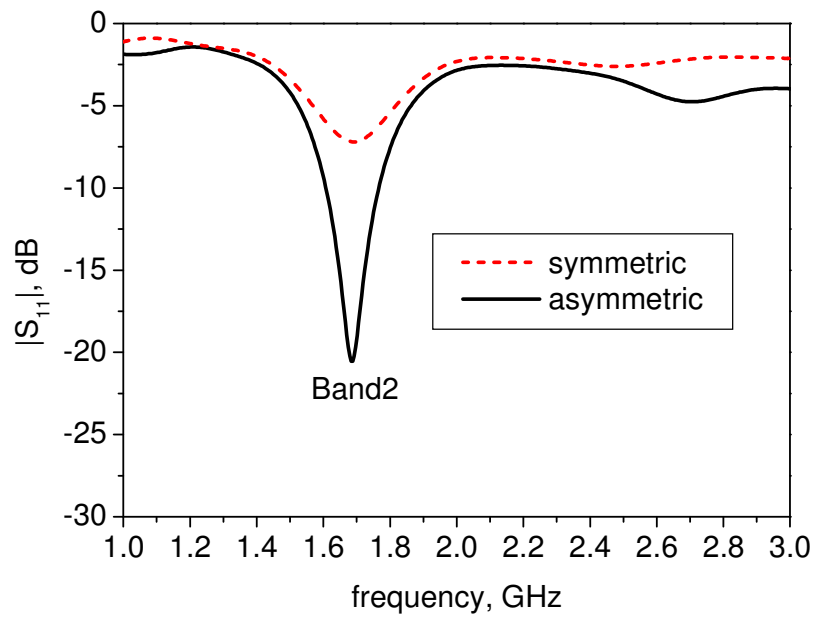
(b)
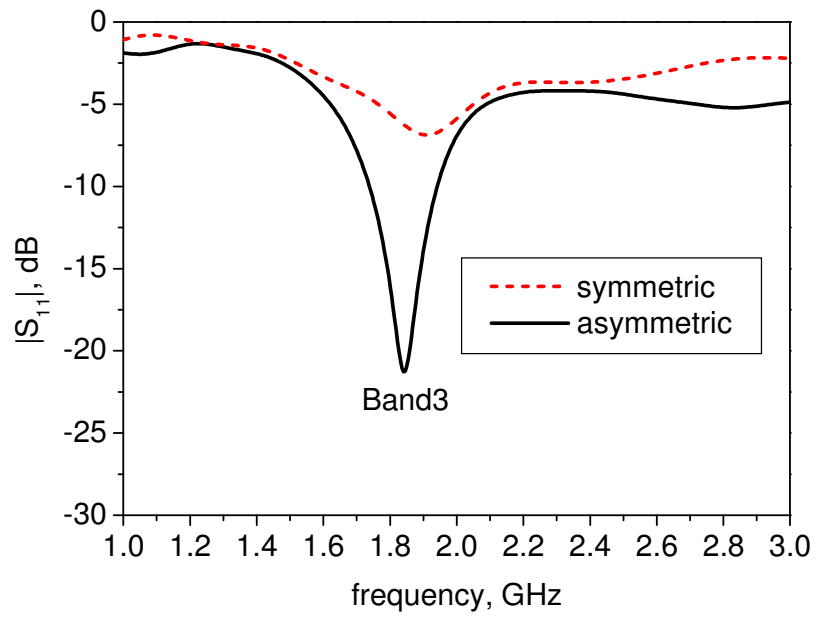
(c)
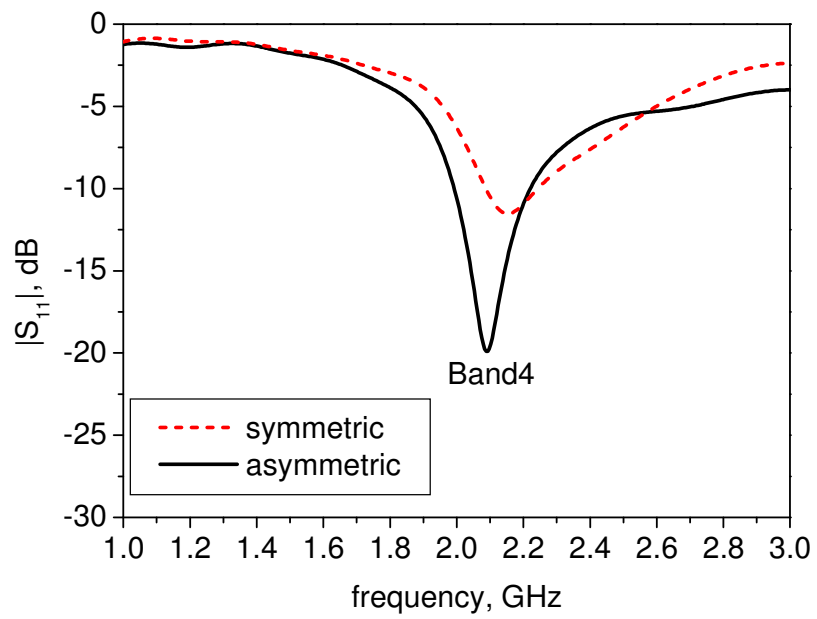
(d)
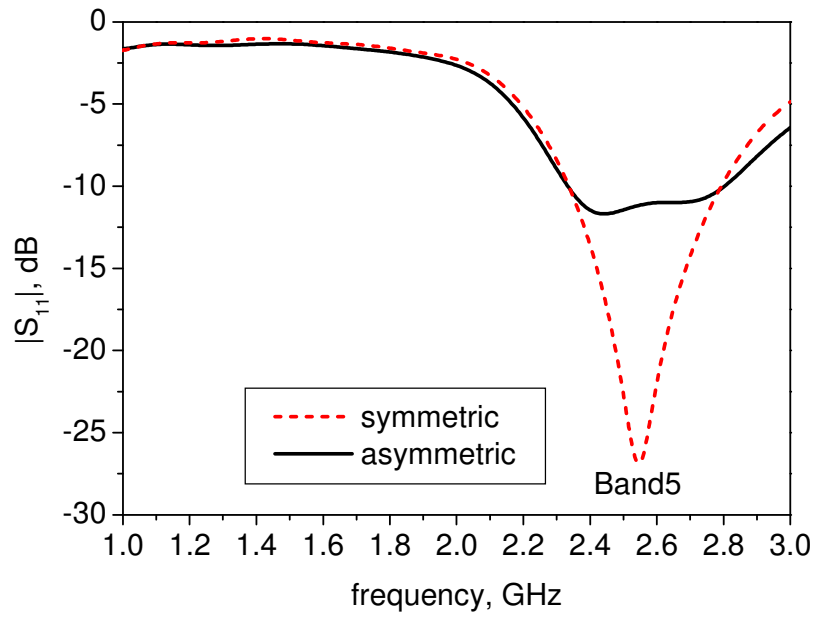
(e)
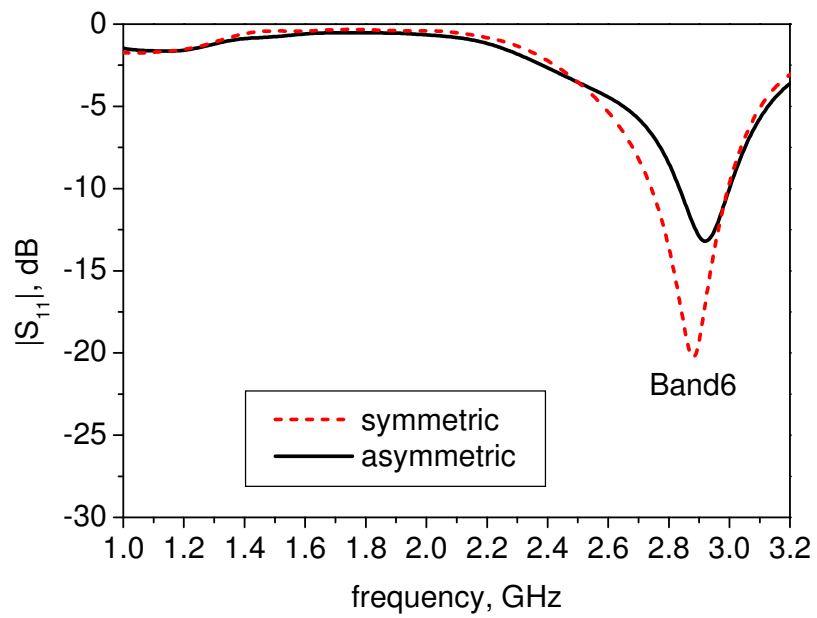
(f)

Figure 5.20 Effects of symmetric and asymmetric slot configuration on the matching

An asymmetric arrangement has an effect on the radiation pattern as shown in Figure 5.21. The symmetry of the radiation pattern is slightly perturbed but on the whole the radiation pattern is well behaved and the perturbation is hardly noticeable in the E-plane and H-plane polar plot as shown in Figure 5.22. A symmetric radiation pattern is good, but in that configuration a low match or high reflection will result. Further work might reveal better return loss in a symmetric arrangement by positioning the ring slot section at the right position. As described in chapter 4 and reported in [85], the right position of the ring slot section may improve the frequency response.

(a)   (b)
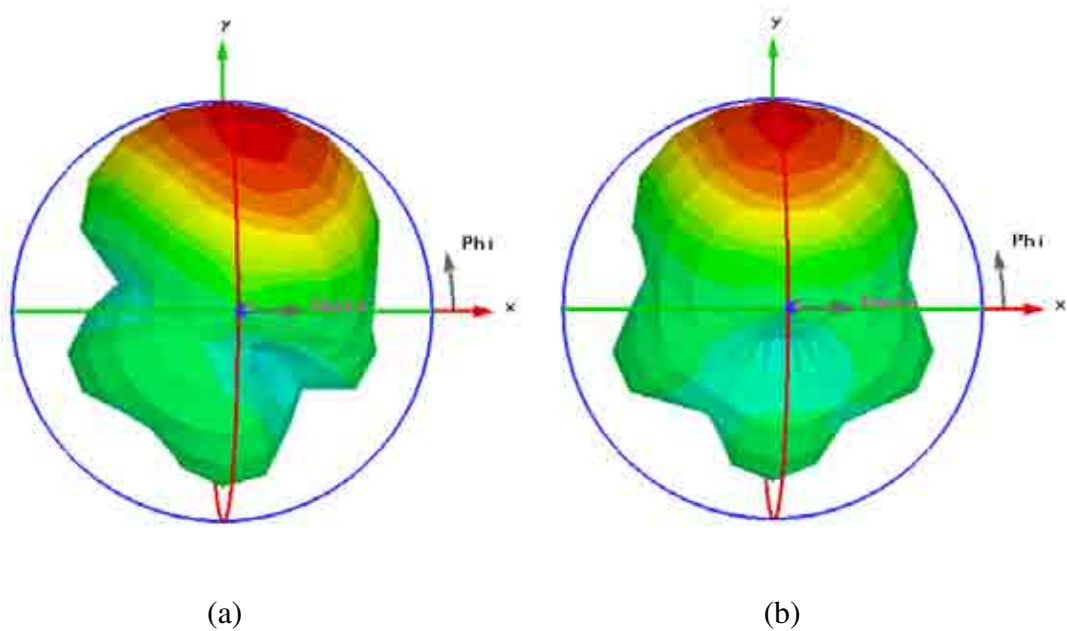
Figure 5.21 3-D pattern for Band 2 excited at 1.65 GHz, (a) asymmetric-, (b) symmetric arrangement

——— asymmetric, – – – – – symmetric

(a)   (b)
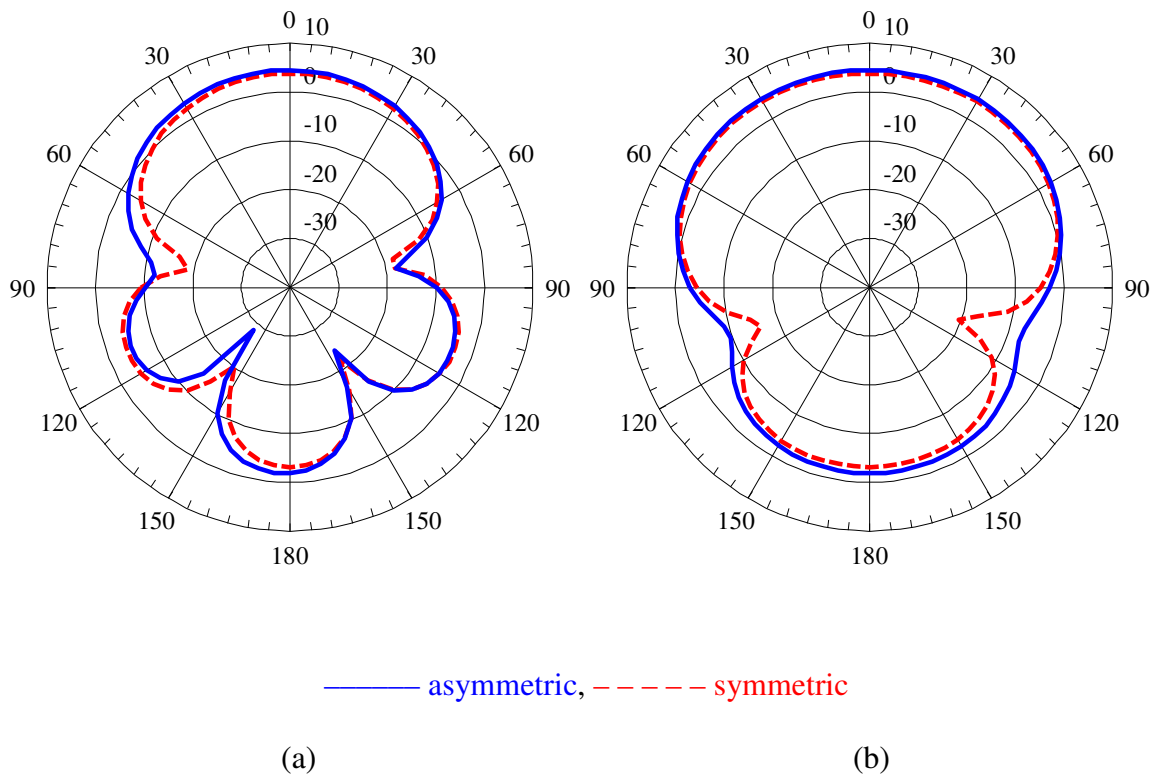
Figure 5.22 Polar plot for Band 2 excited at 1.65 GHz, (a) E-plane, (b) H-plane

The effect of the positions of the ring slot is examined by moving it up toward the wider end ($x = 36.26$ mm) of the tapered slot as shown in Figure 5.23a. The pass band become wider at the upper end band, as can be seen in Figure 5.23b. It is presumed that the ring slot has little current interception at high frequencies, thus reducing the quality factor. Similar behaviour is also noticed for Band 1, Band 3, and Band 4 after the ring slot is positioned at $x = 36.26$ mm. Bands 5 and 6, however, show poor match. Figure 5.24 shows this. Therefore the x_1 position is chosen for a relatively high Q and good impedance matching.
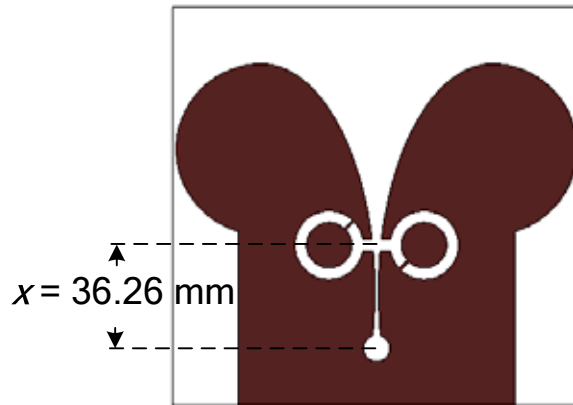
(a)
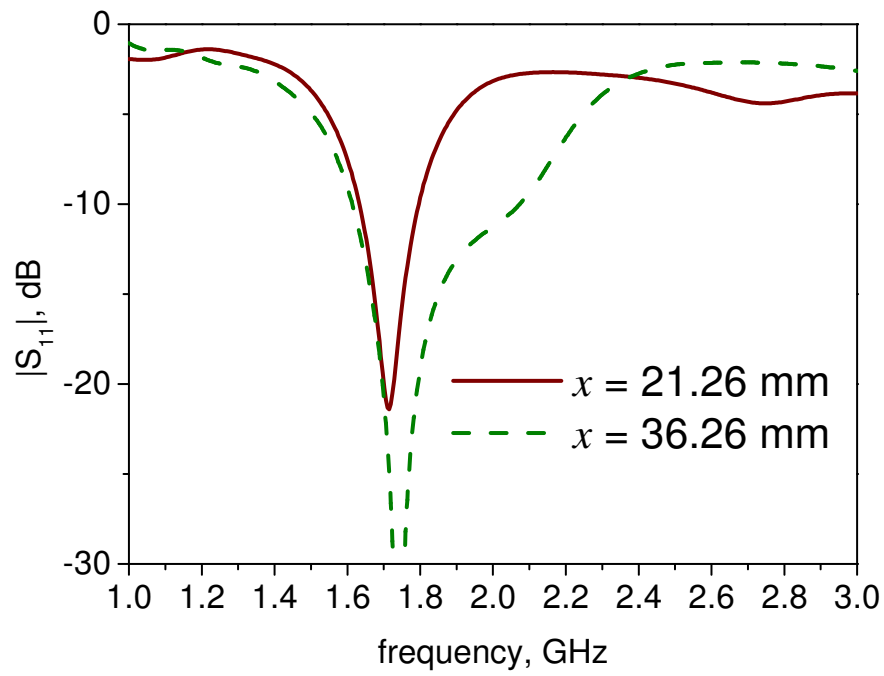
(b)

Figure 5.23 (a) Band 2 configurations, *x* = 36.26 mm (b) simulated S₁₁ when ring slot at *x* = 21.26 mm and *x* = 36.26 mm.

(a)

(b)

(c)

(d)

138
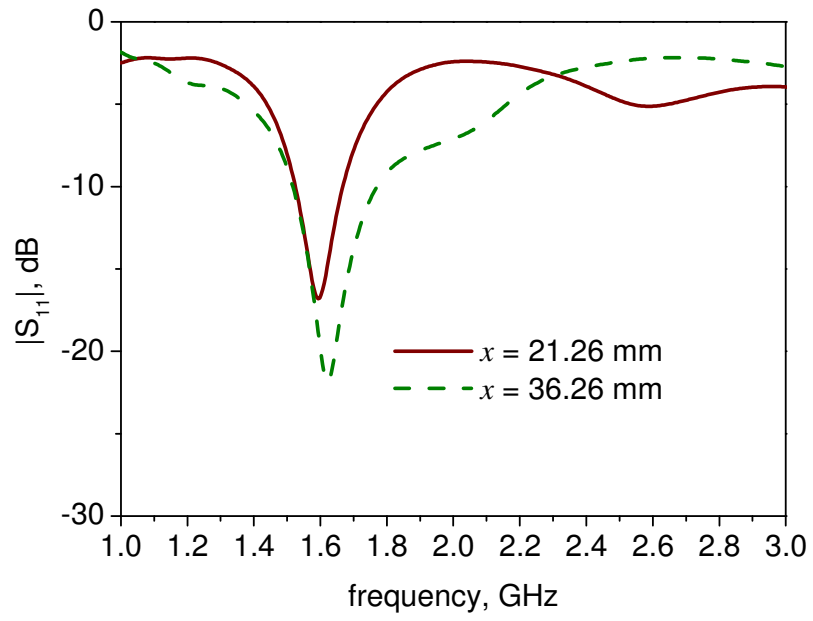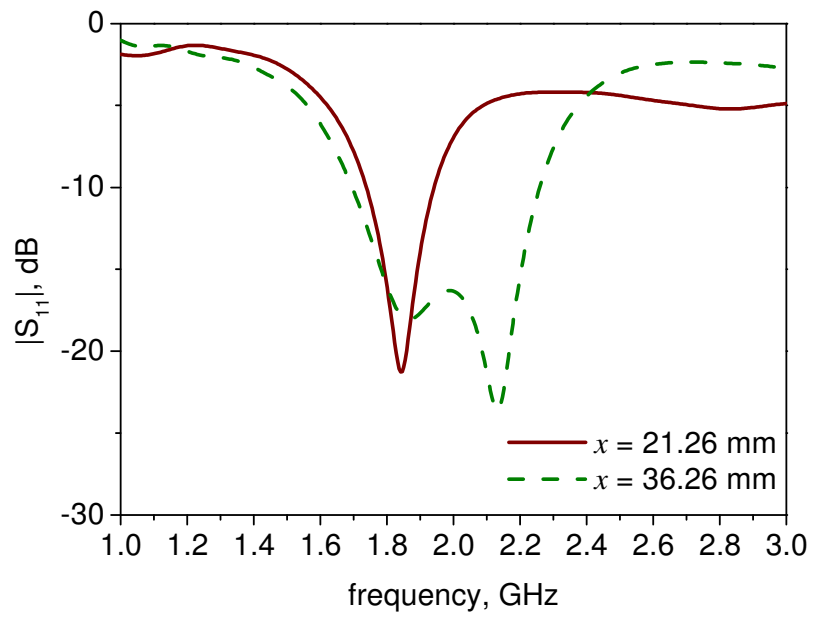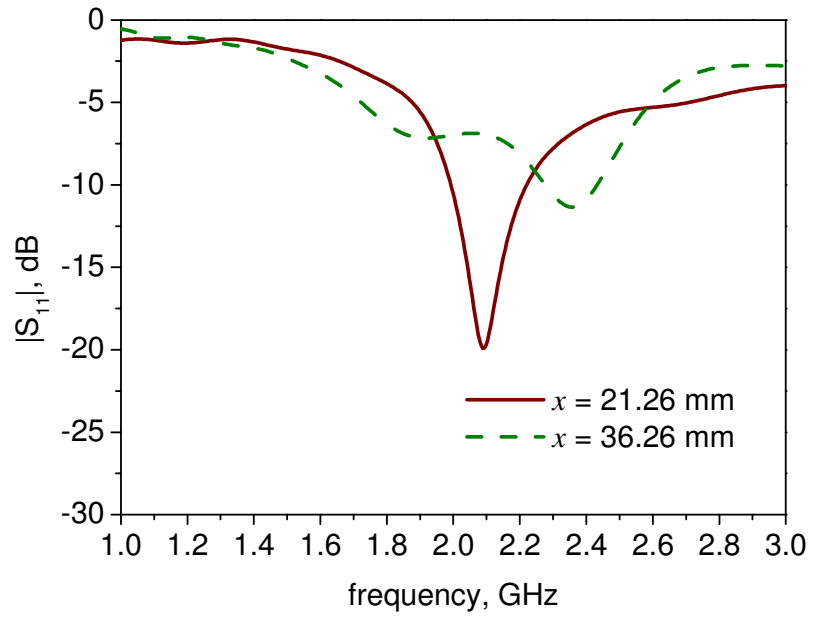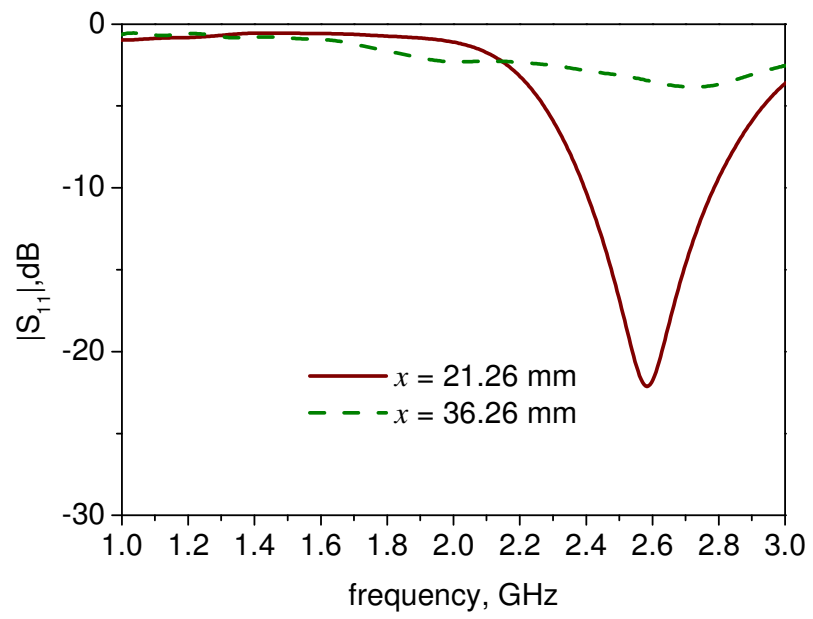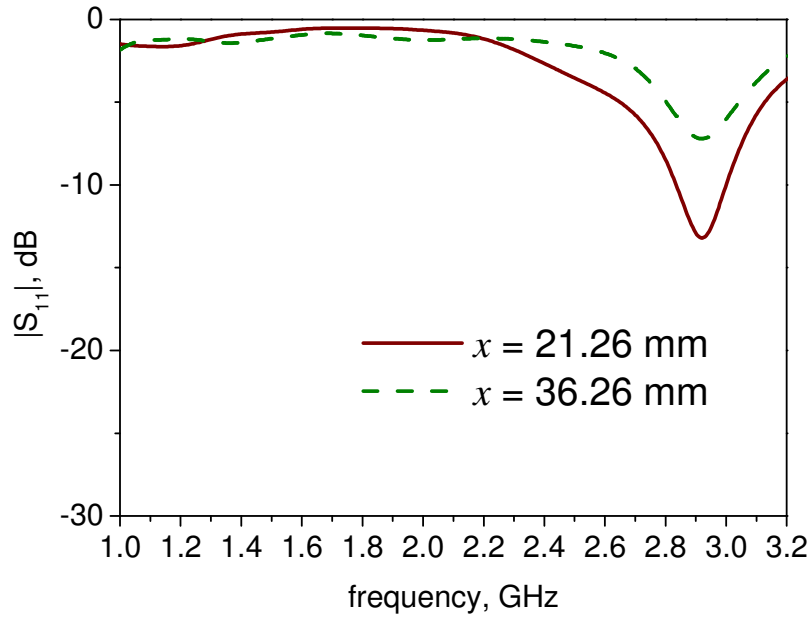
(e)

Figure 5.24 Simulated S_{11} (a) Band 1, (b) Band 3, (c) Band 4, (d) Band 5, (e) Band 6 when ring slot at x = 21.26 mm and x = 36.26 mm position.

The switch on state resistance has an effect on the impedance match and antenna efficiency. Figure 5.25 shows the simulated S_{11} as a function of the on state resistance between 0 and 8 Ω. The return loss degrades as the resistance is increased. Table 5.1 compares the simulated antenna efficiency and gain for different on state resistances. The PIN diodes noted previously and MEMs switch model RMSW100 from Radant Mems, including package parasitics, have also been compared in simulation. The simulated S_{11} of Band 2 and Band 5 are shown in Figure 5.26. The MEMS switch has lower on state resistances than PIN diode switches, thus giving the higher efficiency and gain as noted in Table 5.2.
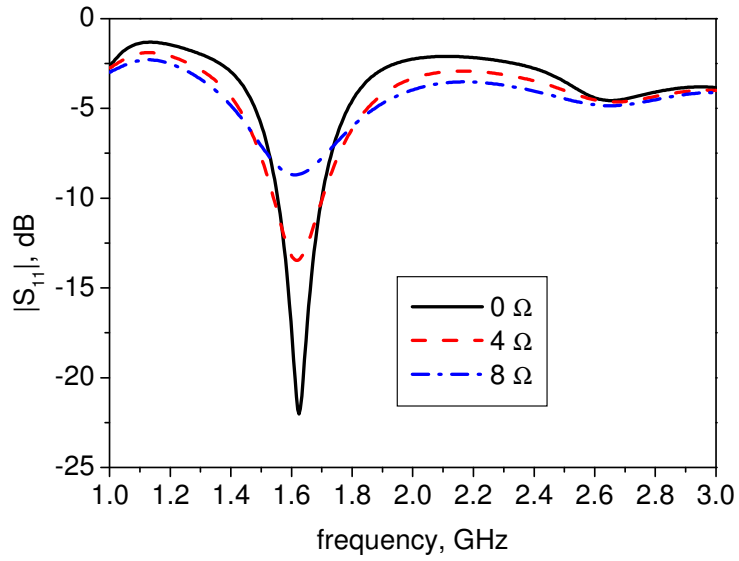
Figure 5.25 Effects of On state resistance on S_{11}

Table 5.1 Simulated Antenna Efficiency and Gain for Band 2 Configuration with Different ON State Resistance Values

Rs	0 Ω	4 Ω	8 Ω
Efficiency, %	80.2	41.88	27.48
Gain, dBi	4.94	2.34	0.56
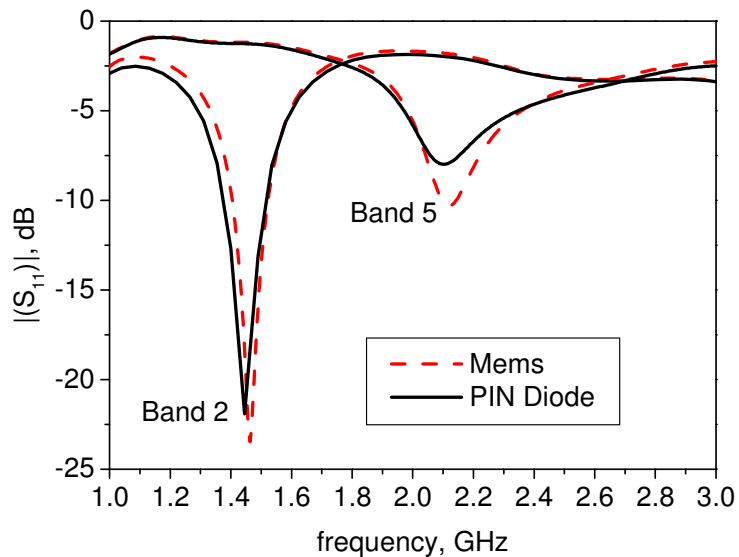
Figure 5.26 Effects of PIN diode and MEMs switches on S_{11} responses

Table 5.2 Simulated Efficiency and Gain for Band 2 and Band 5 Configuration for Different Type of Switches

Switch	PIN diode		MEMs	
	Band 2	Band 5	Band 2	Band 5
Efficiency, %	51.92	47.92	69.51	61.1
Gain, dBi	3.23	1.69	4.43	2.71

5.5 Antenna Construction and Measurements

The configuration of the reconfigurable Vivaldi antenna including switch bias is presented in Figure 5.27. Switches are placed at specific locations along the ring resonators in order to achieve specific frequency bands as summarized in Figure 5.11.
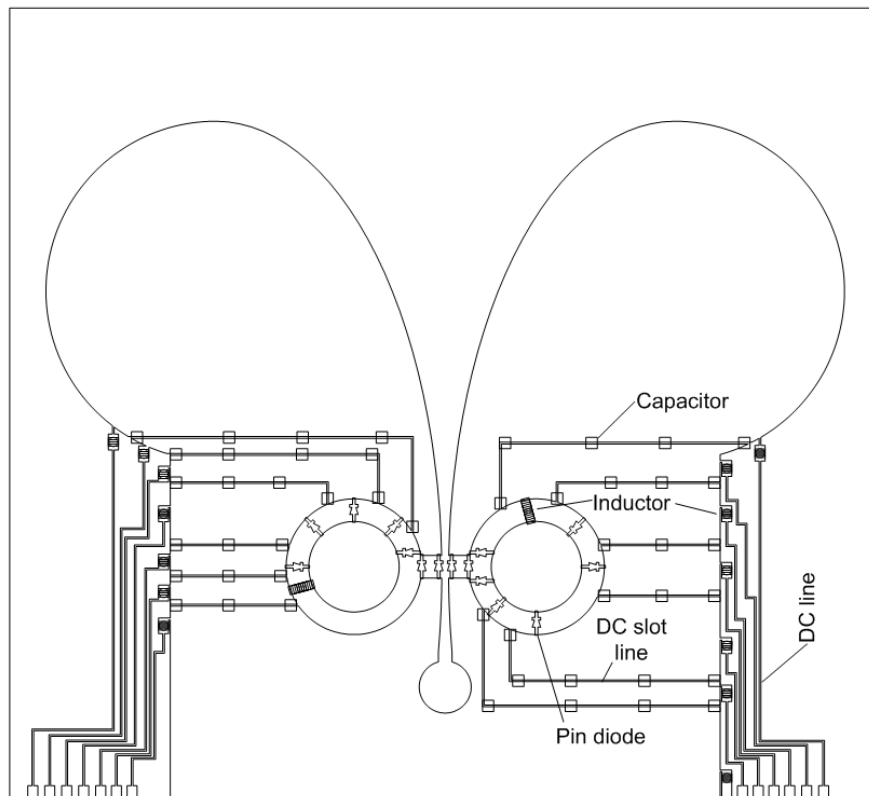
Figure 5.27 The proposed antenna diagram

There are seven switches used on the left ring and eight switches used on the right. Two switches in the small gaps at each side are used to decouple the resonator from the tapered slot, whilst the rest of the switches are used to vary the effective electrical lengths of the ring resonator by using different combinations of the on and off states. Infineon PIN diodes switches, model BAR50-02V, are used. The diodes were forward biased appropriately with dc voltage to obtain 100 mA on state bias current. To obtain the off state, the diodes were left unbiased. In order to bias the switches appropriately, several 0.3 mm dc lines were printed parallel to the beam direction on either side of the antenna. The dc line is isolated from the RF signal by using 27 nH SMD inductors. On the antenna radiating part itself, 0.3 mm width slots are created for dc isolation. The RF continuity is preserved by bridging the slots every 10 mm with 22 pF SMD capacitors. Two switches each having 1.2 mm length, are needed to bridge the slot gaps of 4 mm on each side.

5.6 Results

Figure 5.28 compares the simulated return loss for wideband operation with and without the ring slots. It is noticed that the S_{11} at 1.3 GHz and between 2.0 and 3.0 GHz has been improved by the ring slots. The simulated and measured wideband responses of the proposed antenna with ring slots are shown in Figure 5.29. To select the wideband mode, the slot resonators are decoupled from the tapered slot edges. Wideband operation is obtained over a 1 – 3 GHz bandwidth with a very good agreement between them. To select the narrowband mode, the slot resonators are coupled through the gaps. By short circuiting a specific set of diodes as indicated in Figure 5.11, the narrowband modes are achieved. The measured return loss for the six narrow band states are shown in Figure 5.30. The simulated and measured S_{11} for each of the narrow band states (1.45 GHz, 1.53 GHz, 1.66

GHz, 1.93 GHz, 2.11 GHz and 2.23 GHz) are compared in Figure 5.31. In general, a good agreement has been achieved. Small frequency shifts can be accounted for by the fabrication tolerance, the diode package parasitics and bias components. The rejection band S_{11} levels are relatively poor. These are presumably due to switch losses as well as the filter action. A better measure of the rejection would be a plot of gain vs frequency as shown in Figure 5.32. Overall, good rejection is obtained in each narrow band mode as seen in the gain plot. The gain is decreased around 4 – 6 dB (in Band 1 to Band 4) at 3.0 GHz even though the S_{11} levels shown are about -5 to -7 dB. The practical measurement standard equipment setup for gain and radiation pattern is described in Appendix B. The antenna is mounted using L bend SMA feed as shown in Figure B4.
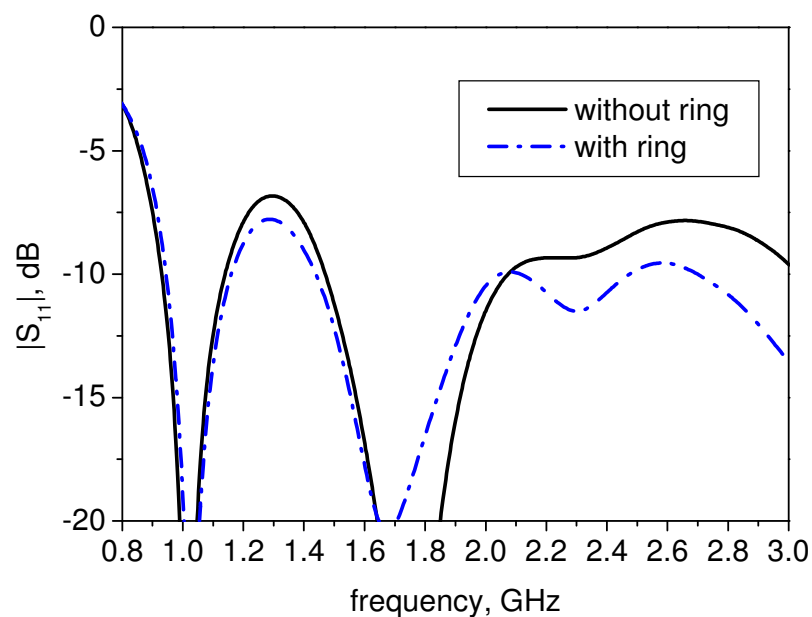
Figure 5.28 Simulated wideband mode S_{11} response with and without ring slots
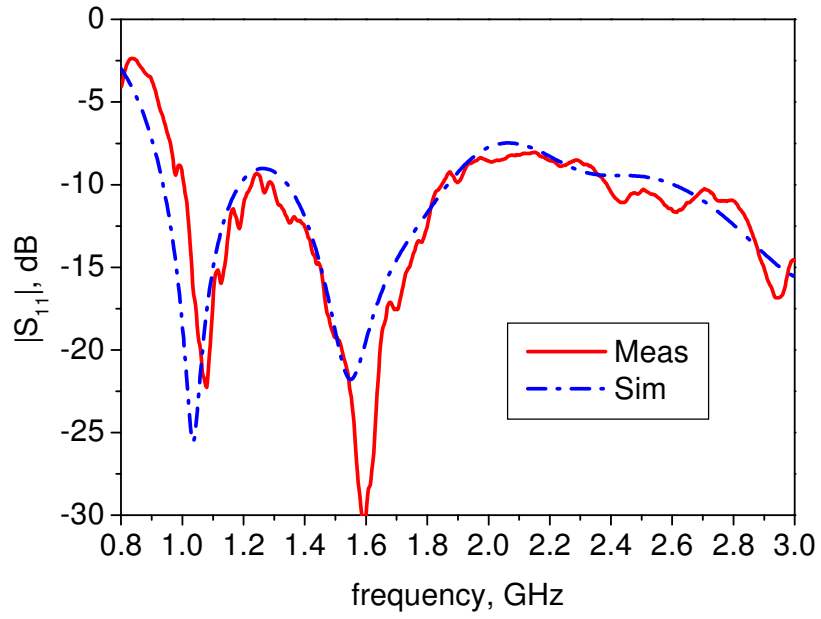
Figure 5.29 Wideband mode S$_{11}$ response of the proposed antenna
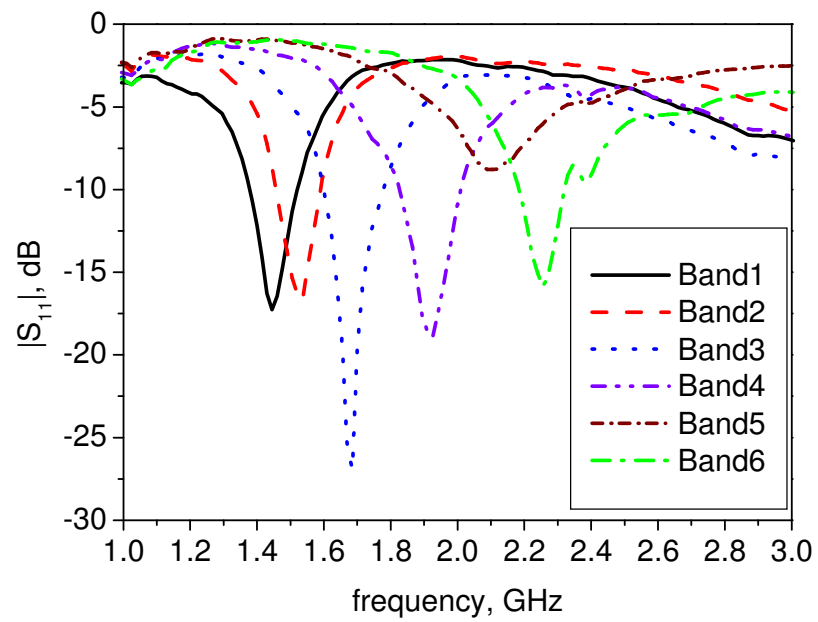
Figure 5.30 Measured narrow band mode S$_{11}$ of the proposed antenna

(a)

(b)

(c)

(d)

146
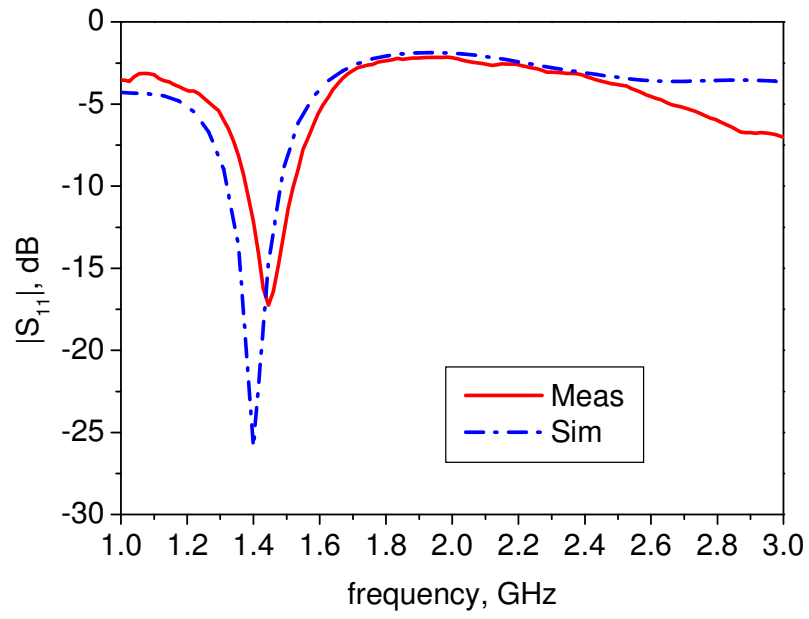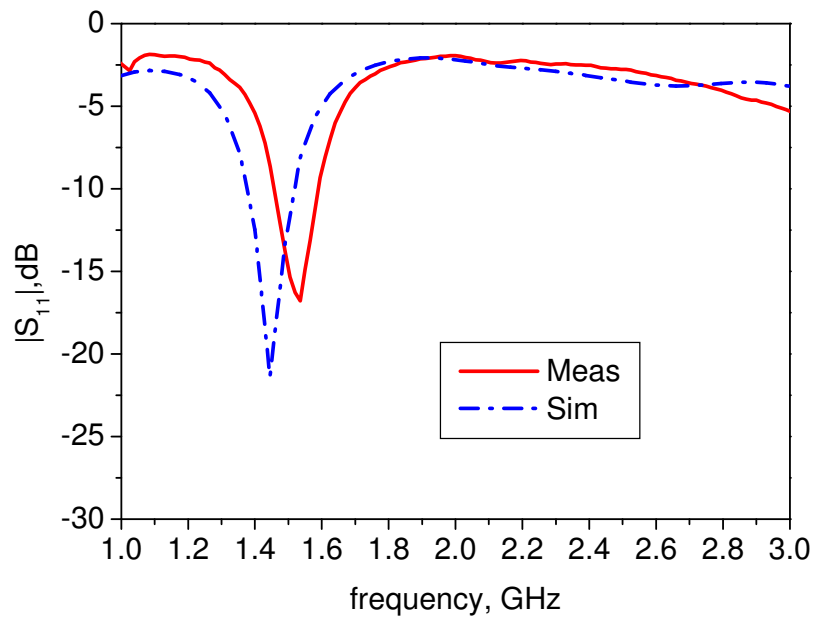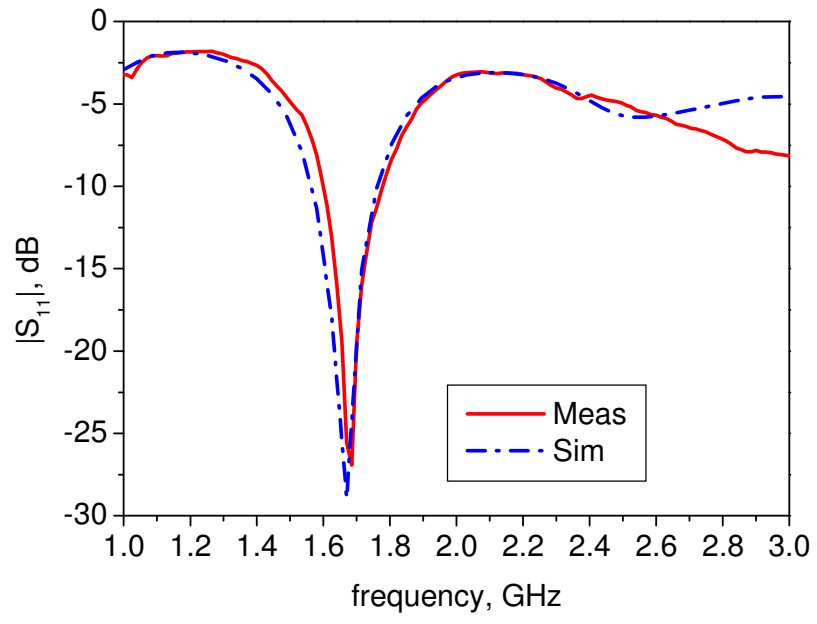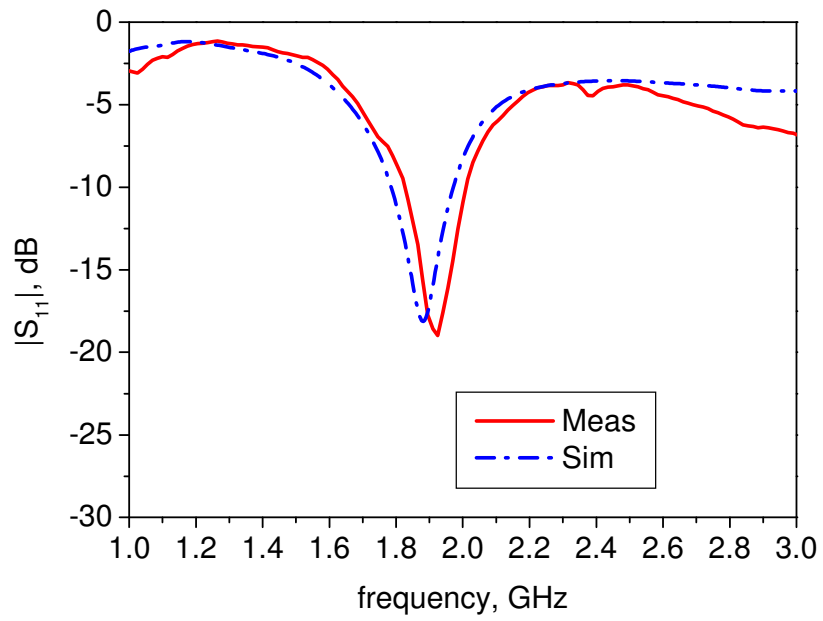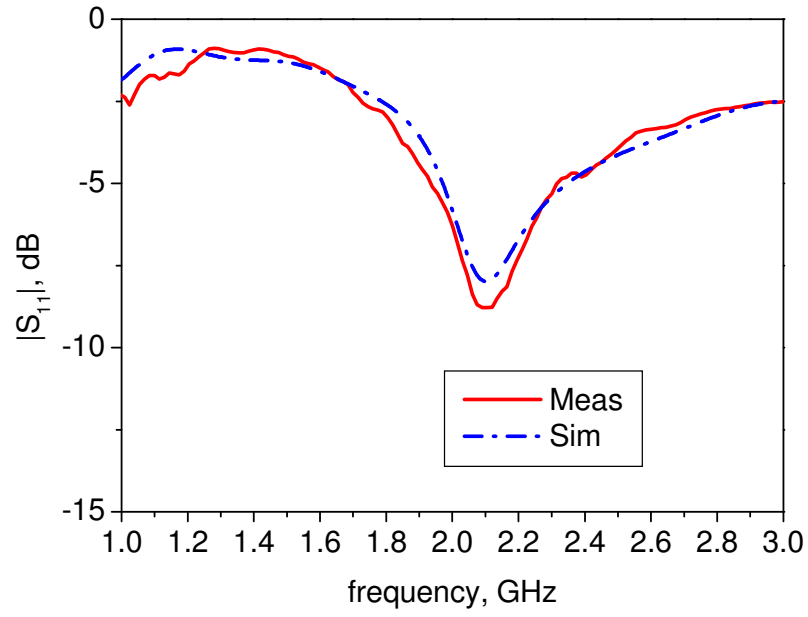
(e)
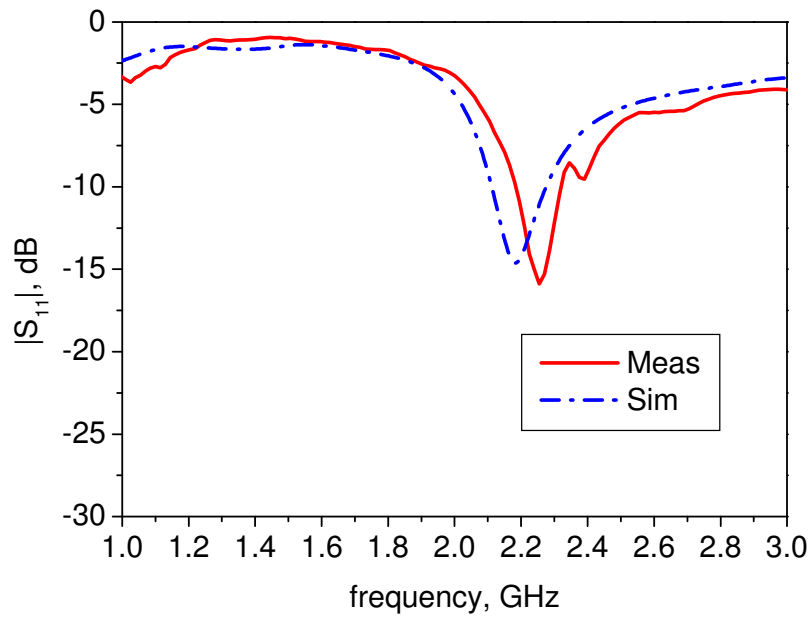
(f)

Figure 5.31 Measured and simulated narrow band mode S₁₁ (a) Band 1-, (b) Band 2-, (c) Band 3-, (d) Band 4-, (e) Band 5-, (f) Band 6 of the proposed antenna

(a)

(b)

(c)

(d)

149
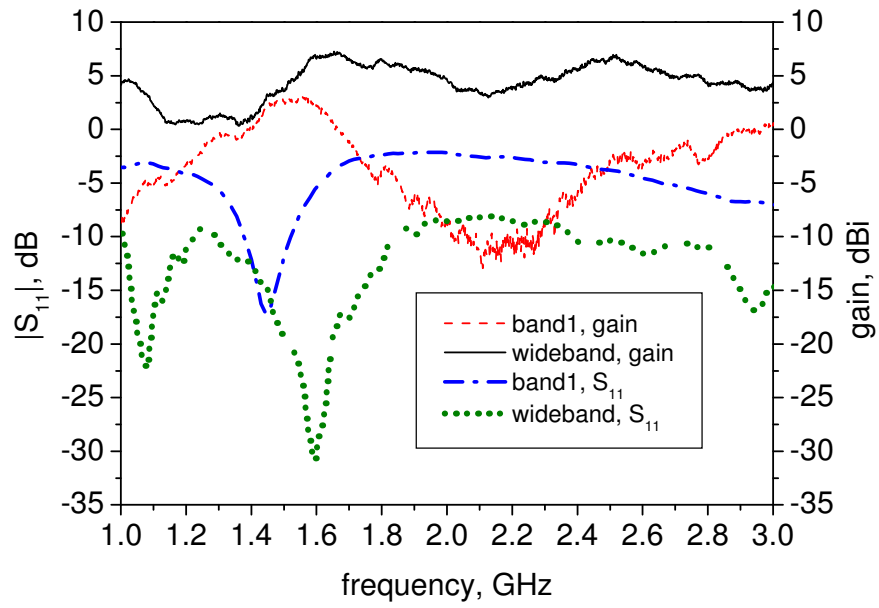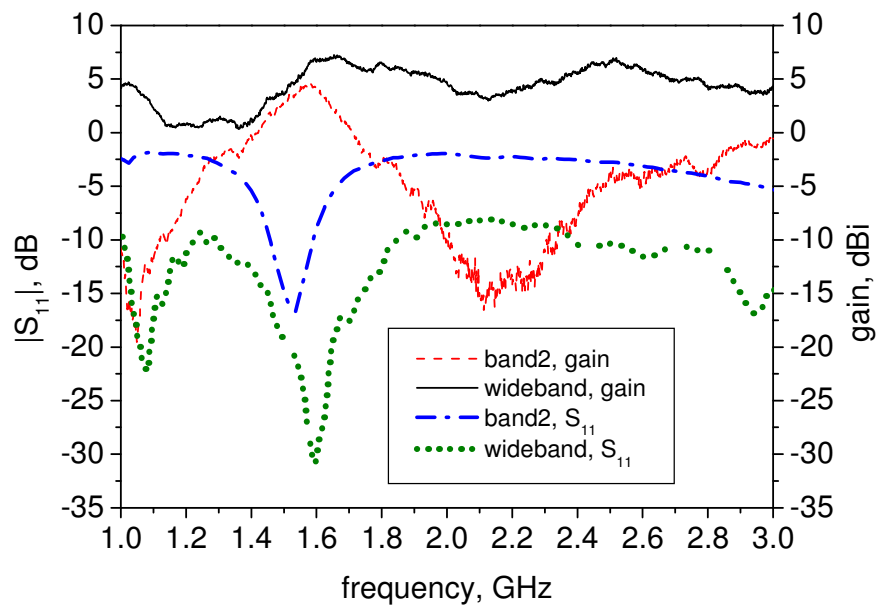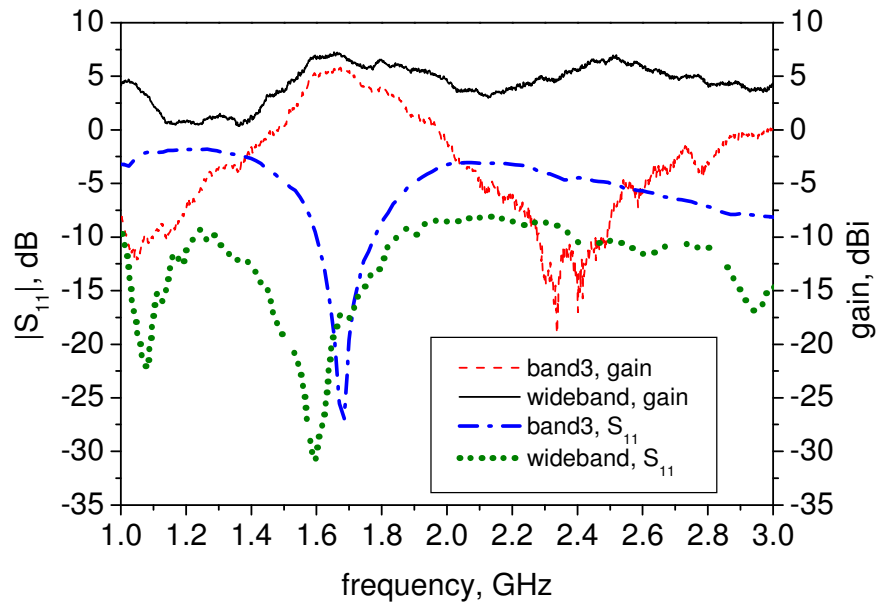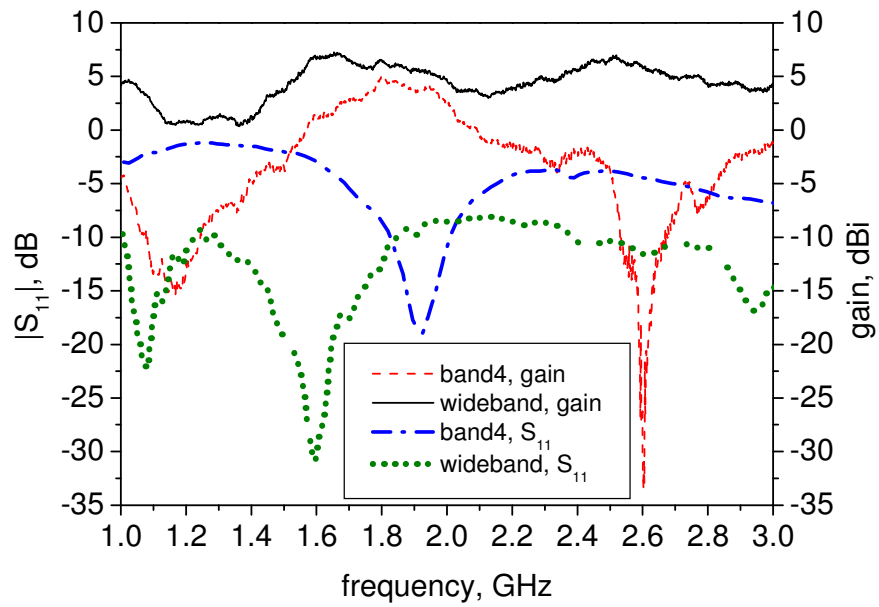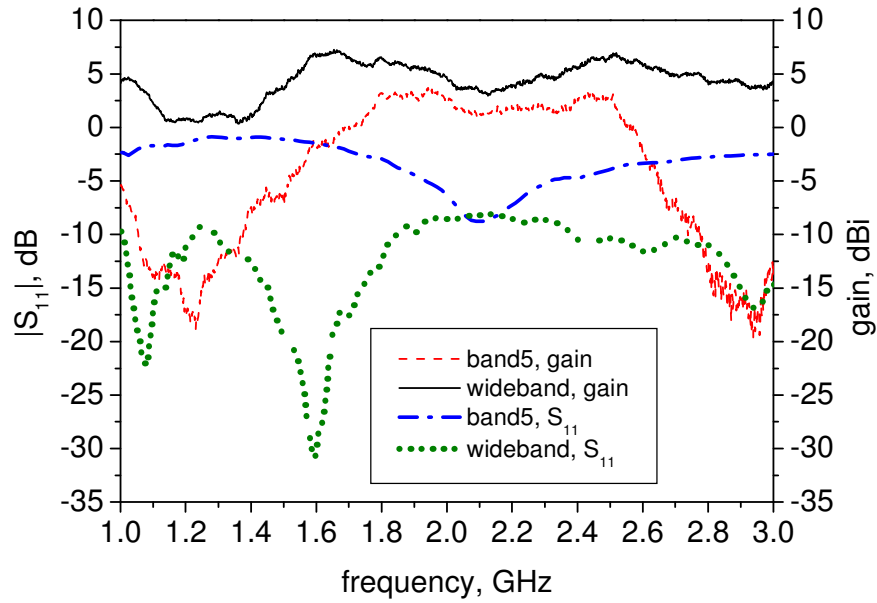
(e)
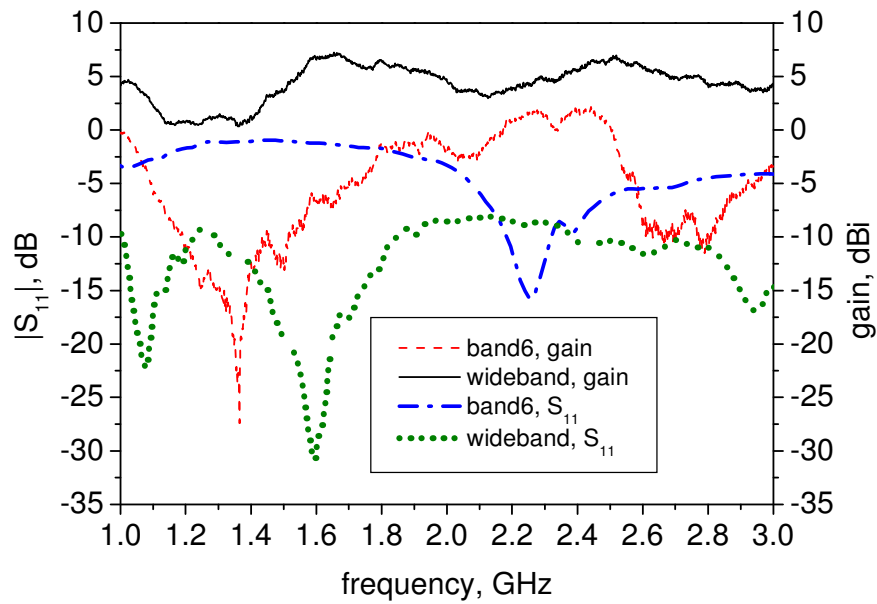
(f)

Figure 5.32 Measured gain and S$_{11}$ for wideband and (a) Band 1, (b) Band 2, (c) Band 3, (d) Band 4, (e) Band 5, and (f) Band 6

The simulated and measured E- and H-plane radiation patterns for the wideband

mode excited at 1.45 GHz and 1.925 GHz are shown in Figure 5.33 and the narrowband

modes are presented in Figure 5.34. A good agreement and well behaved radiation patterns are obtained. The cross-polarisation is less than -20 dB at the peak direction for most of the bands. Finally, the measured and simulated gains are compared, wideband mode in Table 5.3 and narrowband mode in Table 5.4.

(a)

(b)
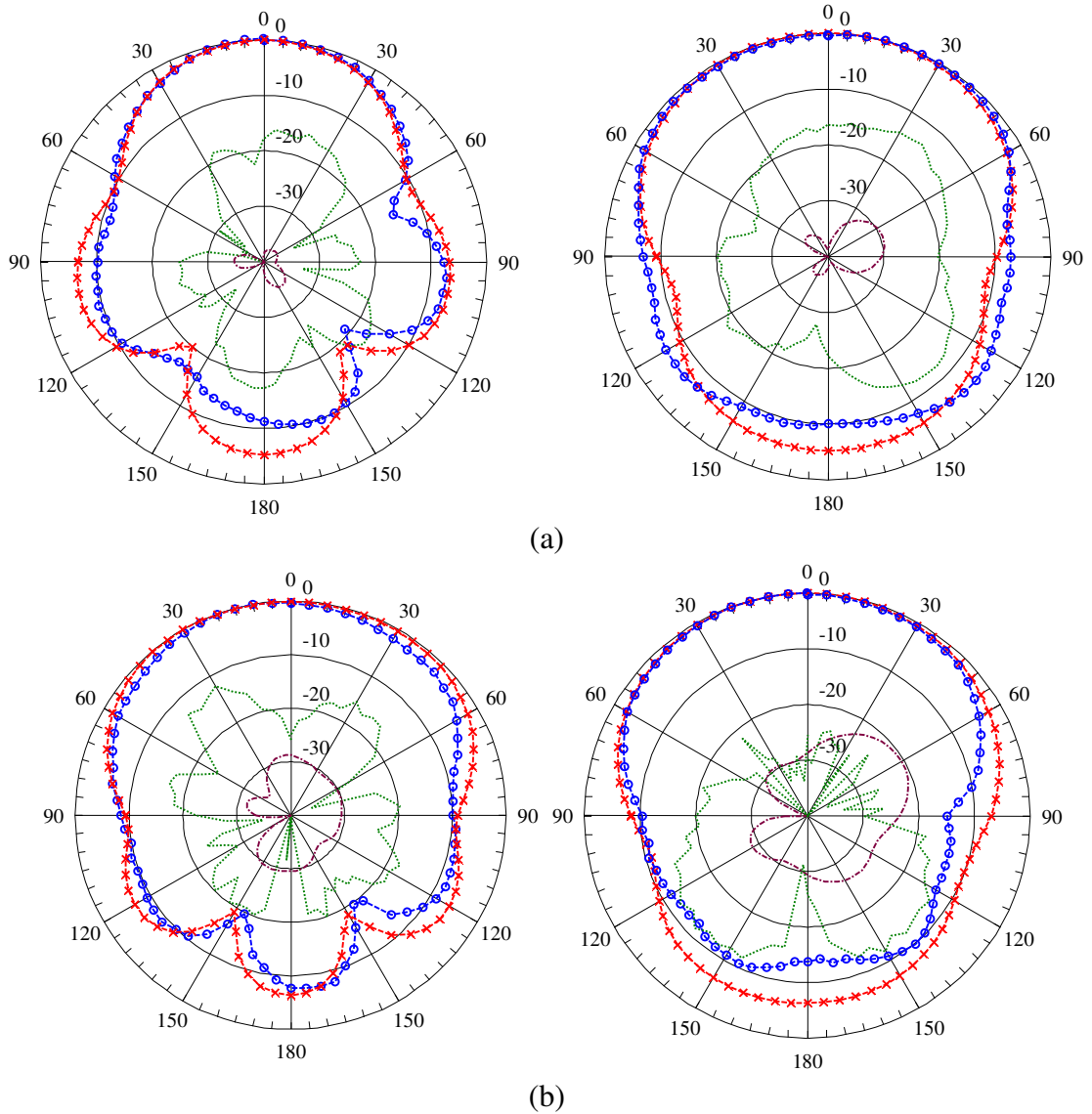
--o-- Measured Co-, ---- Measured Cross-, --x-- Simulated Co, –.– Simulated Cross

Figure 5.33 Wideband radiation pattern. (a) excited at 1.45 GHz, E-plane (left), H-plane (right), (b) exited at 1.92 GHz, E-plane (left) , H-plane (right)

151

Gain in the narrowband mode is lower than in the wideband state. There are two factors to account for the reduction in gain. One is switch loss. The other one is the change in current distribution in the narrowband mode, which might reduce the effective aperture. From a gain-beamwidth relationship, wider beamwidth will result in low gain. For example, it is observed that the simulated beamwidth in the Band 6 is wider than in the wideband mode when excited at the same frequency, 2.2 GHz. Table 5.5 shows this.

(a)

(b)

(c)

(d)

(e)

153
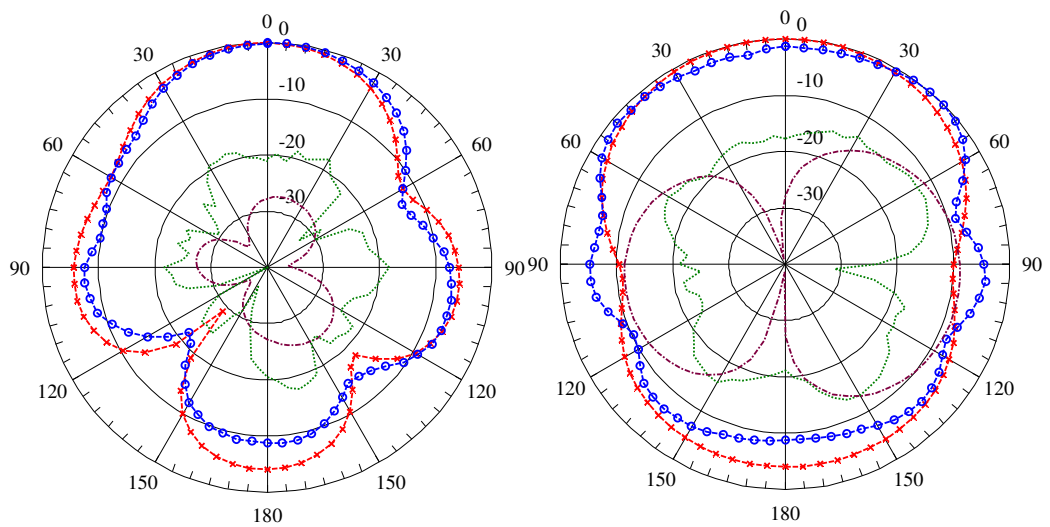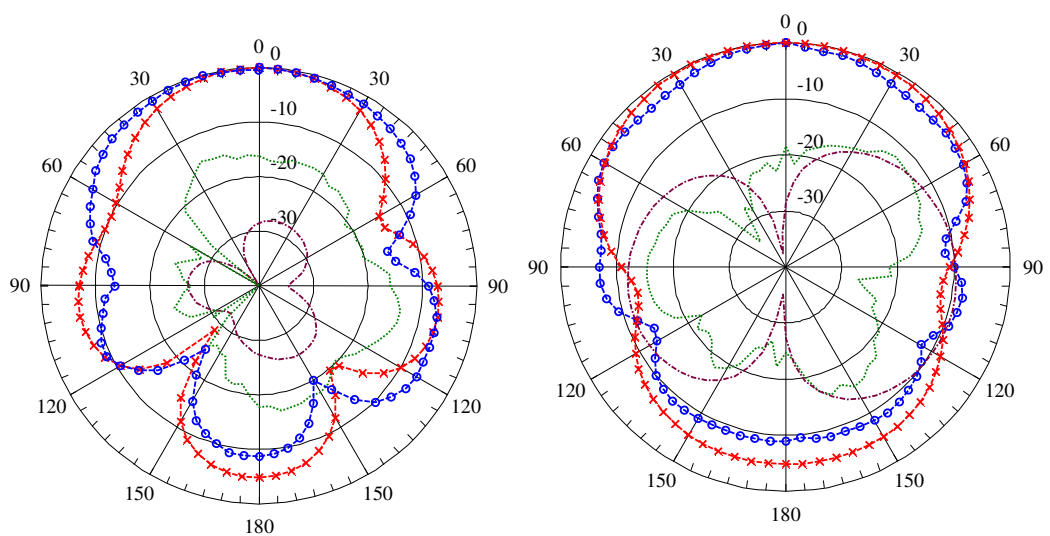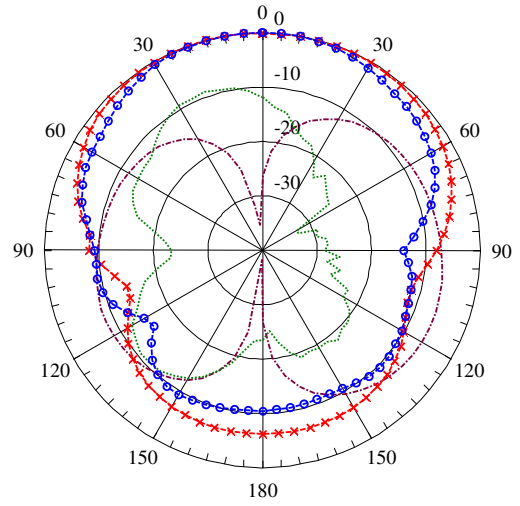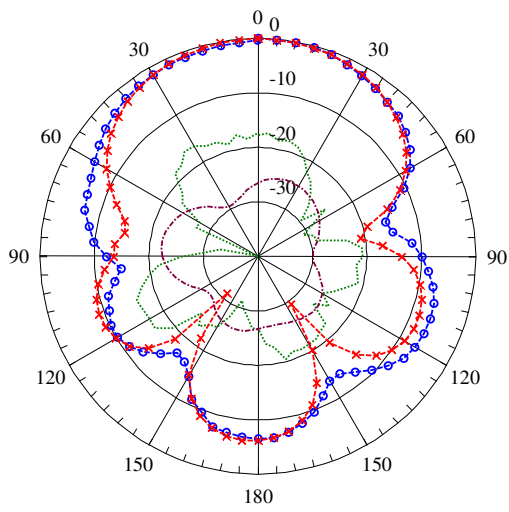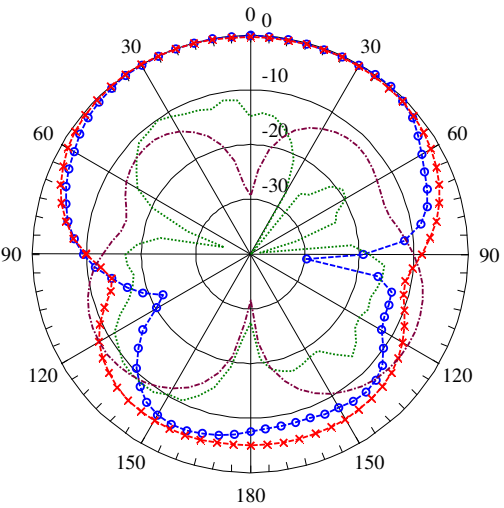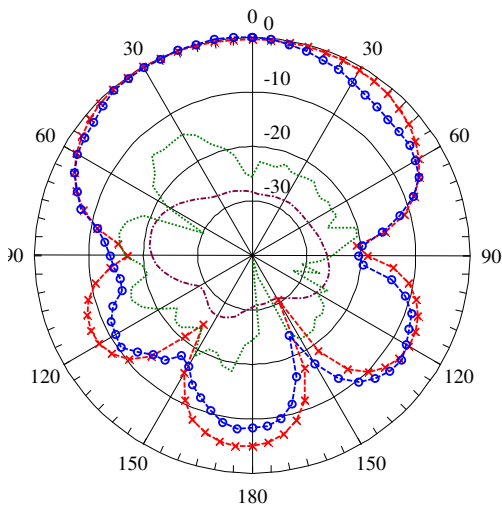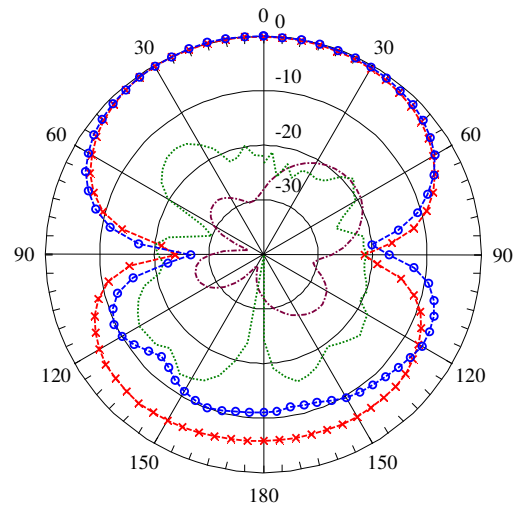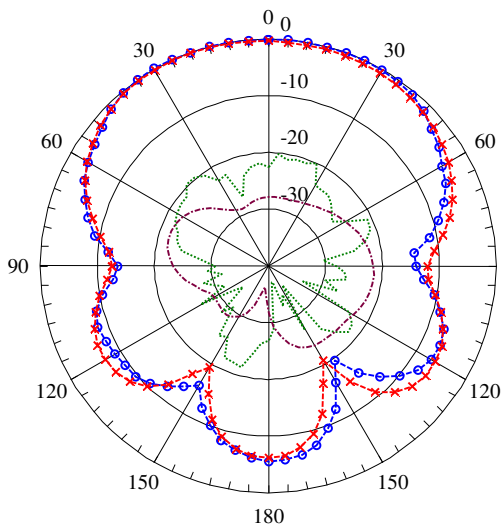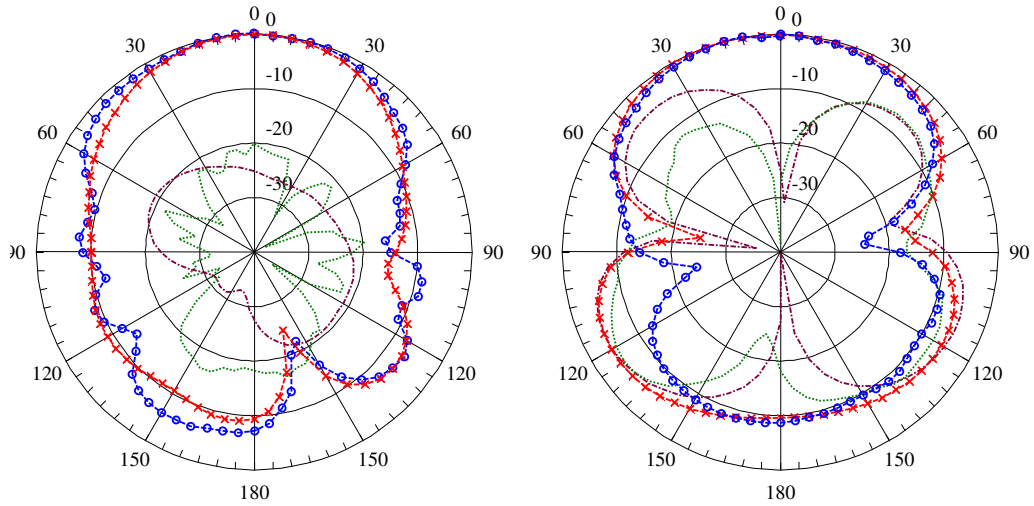
(f)

--o-- Measured Co-, ---- Measured Cross-, --x-- Simulated Co, –.– Simulated Cross

Figure 5.34 Narrow band radiation patterns. (a) Band 1 excited at 1.45 GHz, E-plane (left), H-plane (right), (b) Band 2 exited at 1.53 GHz, E-plane (left) , H-plane (right), (c) Band 3 excited at 1.68 GHz E-plane (left) , H-plane (right), (d) Band 4 excited at 1.92 GHz, E-plane (left) , H-plane (right), (e) Band 5 excited at 2.1 GHz, E-plane (left) , H-plane (right) and (f) Band 6 excited at 2.2 GHz, E-plane (left) , H-plane (right).

Table 5.3 Gain in wideband mode

Gain, dBi	1.445 GHz	1.535 GHz	1.685 GHz	1.925 GHz	2.100 GHz	2.225 GHz
Simulated	4.95	5.39	4.92	2.96	3.26	4.83
Measured	2.90	4.66	6.91	5.56	3.42	3.93

Table 5.4 Gain in narrow band mode

Gain, dBi	Band1	Band2	Band3	Band4	Band5	Band6
Simulated	3.23	2.65	3.97	2.70	1.69	2.06
Measured	2.03	3.48	5.51	3.56	1.22	1.07

Table 5.5 Beamwidth in narrow and wideband mode at 2.2 GHz

Beamwidth, degree	Band 6	Wideband
E-plane	75.4	55.7
H-plane	103.2	89.5

5.7 Summary

A new concept of switchable filtering in a Vivaldi antenna has been demonstrated. Instead of switching between different resonator positions, the approach described here alters the operating frequency band by varying the electrical length of the resonators inserted into the tapered slot. This allows a better control of the operating bands but using only two slot resonators. The narrowband operation can be switched between six different frequency bands, which is double of what has been proposed in the multiple position ring resonators. The example shown has good return loss for each mode and well controlled patterns. The work described here has been published in [87]

Now it is shown that wide-narrow frequency reconfigurable Vivaldi antennas are possible to achieve by using two methods described previously. Switching from wide to narrowband mode provides better out of band rejection. During wideband operation, this is not available. Therefore, it is important to provide band notch capability in order to reject the interferer, improving the antenna versatility. In the next chapter, this will be described.

CHAPTER 6

VIVALDI WITH TUNABLE NARROW BAND REJECTION

6.1 Introduction

Frequency reconfigurable antennas are useful to support many wireless applications, where they can reduce the size of the front end circuitry and also allow some additional receiver pre-filtering. However they are limited to one service at one time. Wideband antennas on the other hand can support all the standards and also can operate multiple services at a time. This is good but since they have inherently poor out of band rejection, additional filtering is required, compromising the front end complexity. Work on integration with fixed [38, 39, 64-67] and reconfigurable [68, 71, 72, 74] band interference rejection filters, increasing the system versatility, have appeared in the literature. Considering future wireless applications, for example cognitive radio, achieving a reconfigurable band notch operation could make an important contribution to the reduction

in the level of interference reaching the RF front end. Reconfiguring the notch band is useful for future cognitive radio systems where the possibility of interference between cognitive radio users and primary users has been recognized as an expected issue causing degradation of performance. In this chapter, a Vivaldi antenna is presented with narrow band rejection characteristics within the 2 -7 GHz of the antenna operating bandwidth. The tuning range is wider than that reported in [68, 71, 72, 74]. Instead of using a slot resonator as in [39] and [38], the proposed antenna used a microstrip resonator printed on the reverse side of the radiating element. The method, using a microstrip line resonator is proposed by Dr F. Ghanem [10], a Research Visitor at the University of Birmingham. A significant improvement from the original idea has been proposed. The original idea has a limited tuning range. A new idea has been developed to achieve a tuning capability within the whole band of operation resulting in a very wide tuning range. To give a narrow, tunable stop band action, the resonator is loaded with varactors. Three methods are presented: one with fixed band notching at 5.75 GHz; one with a single varactor to give a tunable band notch between 4.2 – 5.5 GHz; and another with 3 varactors and a shorting post to the ground, widening the stop band in the frequency range between 2 GHz and 7 GHz and giving a tuning ratio of 3.5:1. The proposed antennas have the capability of rejecting combinations of interfering signals (e.g. WLAN signals) within the operating bandwidth. The design principles of the proposed antenna are described. Section 6.2 discuss the design and the configuration of the band notch resonator within the Vivaldi space in order to control the Q factor and the notched frequency. In section 6.3, the simulations and experimental results are explained in detail for each method, namely fixed, narrow and very wide tuning ranges concepts. The fabricated antenna with electronic tuning is discussed in section 6.4, followed by a summary in section 6.5.

6.2 Band Notch Resonator Design

The proposed Vivaldi with band notch capability is illustrated in Figure 6.1. The basic Vivaldi antenna was based on [82] and is similar to those described in Chapters 3 and 4 but they have been scaled down in frequency by a factor of two. The Vivaldi radiator consists of a circular slot of 2.3 mm radius connected to an elliptical shaped tapered slot with horizontal and vertical radius of 20 mm and 40 mm respectively. The tapered slot ends with 15 mm radius circles. A 2.75 mm width microstrip feed line terminated with a semi circular disk shape of 5.1 mm radius is printed on the reverse side. A Taconic TLY-5 substrate with $\varepsilon_r = 2.2$ and thickness = 0.787 mm is used. The Vivaldi covers the frequency range from 2.0 to 7.0 GHz.
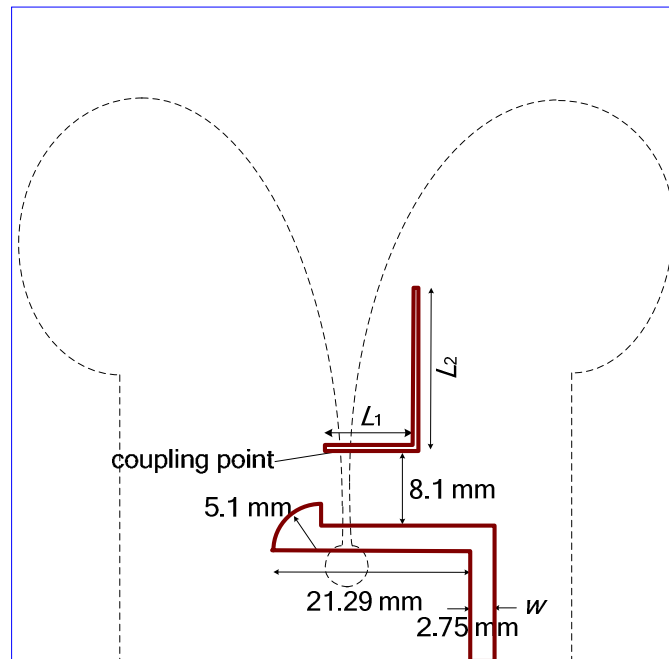
Figure 6.1 Vivaldi antenna with band notch resonator

To obtain a band notch property, a $\lambda/2$ open stub microstrip resonator is printed 8.1 mm above the feed line on the reverse side of the radiating element. The cut off band is formed when energy from the tapered slot on the opposite side is coupled to the line resonator,

stopping the propagation at which the line length is $\lambda/2$. To demonstrate the concepts, an L shaped resonator was designed and simulated.

6.2.1 Length and width of the resonator

The length of the resonator will determine the centre frequency of the notch band. The resonator can be in any appropriate shape, such as in an L shape, proposed in this design or in a straight line. Figure 6.2 shows the effect on S_{11} of the resonator in two different lengths. L_1 and the coupling point are unchanged. Clearly the centre frequency of the notch band is length dependent. It is also observed that the Q factor is low at high frequency indicating that the coupling factor is higher at higher frequencies. In the example shown here, the Q is 25.625 at the low and 8.49 at the high notch band. This happens because electrically, the centre of the coupling point is nearer to the middle point of the resonator for the short resonator where current distribution is high as opposed to the long resonator. Thus the coupling of the shorter resonator is higher, which produces a low Q. However, the Q factor can be increased or decreased if required by changing the horizontal position of the resonator as described in section 6.2.2.

The Q factor is also width dependent. Figure 6.3 shows the effect of the width, W. Generally, the narrower is the line, the higher is the Q factor. In the example shown here, the Q factor is 20.92, 25.32 and 29.76 for line width 1.0, 0.4 and 0.1 mm respectively. A relatively high Q for a thin line can be understood, as the energy is confined more and produces relatively less conductor loss. In the prototype version, a 0.4 mm width line is chosen to relax the tolerances required in the fabrication process.
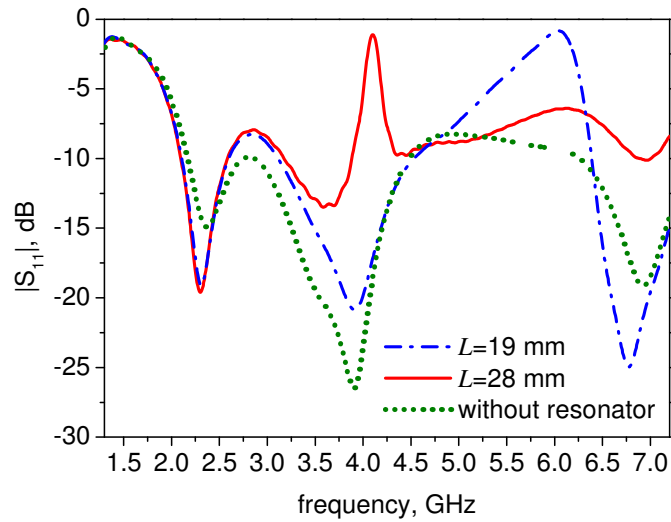
Figure 6.2 Simulated S_{11} of antenna of Figure 6.1 with different resonator length on band rejection centre frequency
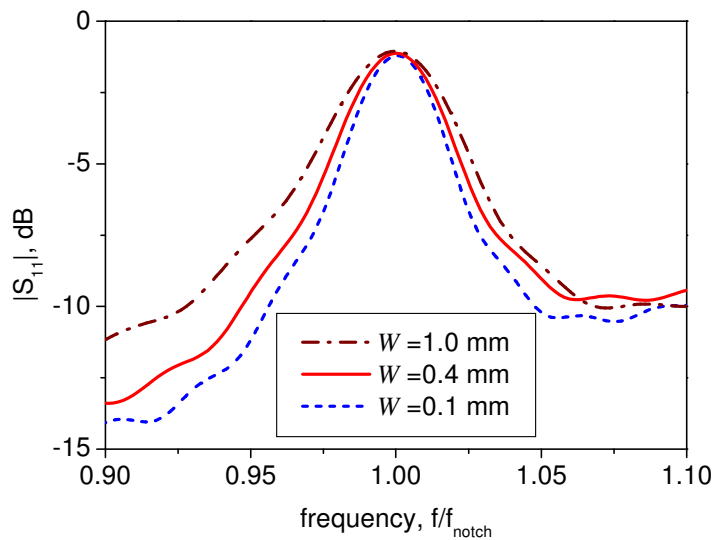
Figure 6.3 Simulated S_{11} of antenna of Figure 6.1 with different resonator width on quality factor

6.2.2 Resonator positions

The effects on S_{11} of the resonator position in the horizontal, *x*-, and vertical, *y*-directions are also studied. The *x*- and *y*- axes are shown in Figure 6.4. In Figure 6.5, it can be seen that, the rejection level in the S_{11} is increased as a function of *x*-direction. It is also

observed that the coupling factor becomes higher, as *x*-direction is greater and therefore the loaded Q is getting lower, as suggested by the equation $Q_{unloaded} = Q_{loaded} \cdot (1+k)$, by assuming the unloded Q is fixed. *k* is the coupling factor. This happens because electrically, the centre of the coupling point is nearer to the middle point of the resonator for the greater *x*-direction where current distribution is high. Thus the coupling of the resonator when positioned higher in the *x*-direction is higher, which produces a low Q. On the other hand, the vertical direction has pronounced effects on the Q factor as shown in Figure 6.6 where as higher in the *y*-direction, the resonator is coupled more into the slot line. It is observed that a low position, *y* = 9.6 mm, gave high Q, and also a good level of suppression. The position of the resonator is therefore chosen near to the narrow end part, the area where a reasonable Q factor can be obtained. The resonator is located 8.1 mm above the feed line or 12.6 mm in *y*-direction from the centre of the circular slot stub.
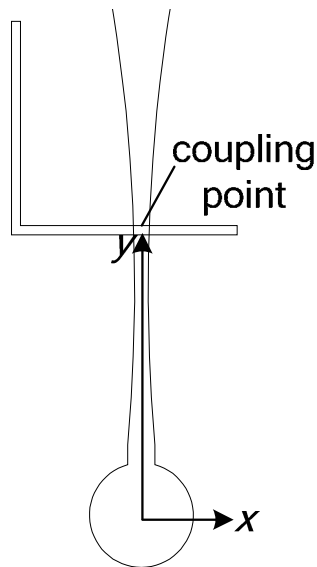
Figure 6.4 Stub position in *x* and *y*-direction
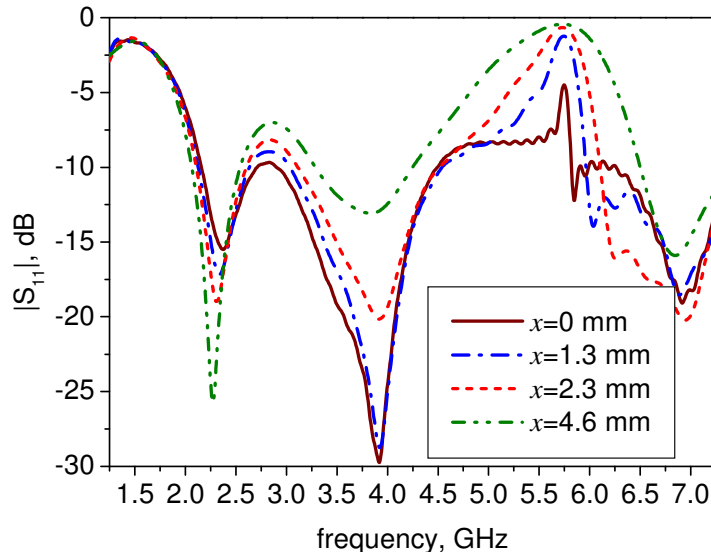
Figure 6.5 S_{11} vs frequency for different *x*-positions showing the change in Q factor
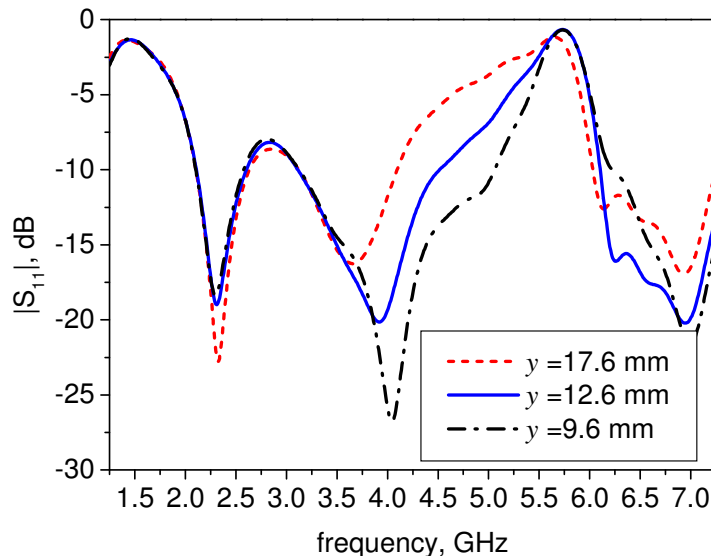
Figure 6.6 S_{11} vs frequency for different *y*-positions showing the change in Q factor

6.2.3 Varactor positions

To tune the centre frequency of the rejection band, it is appropriate to locate a varactor in the middle of the resonator. This is the optimum position for maximising the tuning range, because the maximum differential voltage can be established across the diode. Figure 6.7 shows current distributions on the resonator excited at the notch

frequency of 5.73 GHz. It is observed that the current is high in the middle of the line. Figure 6.8a shows the effect of varactor position in the line, showing that a tuning range of 680 MHz is achieved when the varactor is in the middle. Using the same values of the capacitances, the tuning range is slightly smaller at 364 MHz when it is ¼ of the line length away from the mid point of the resonator as shown in Figure 6.8b. It can be observed that the line gap is approximately short circuit when the varactor is set higher than 5.6 pF. The centre frequency of the notch band has a small effect on the capacitance above 5.6 pF as shown in Figure 6.9.
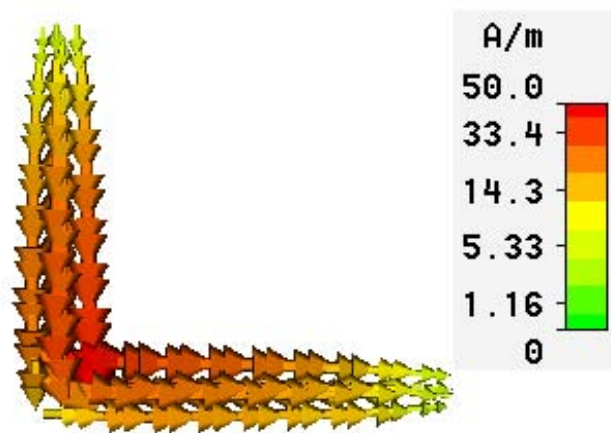
Figure 6.7 Current distribution in the resonator at notch frequency of 5.73 GHz

(a)

(b)
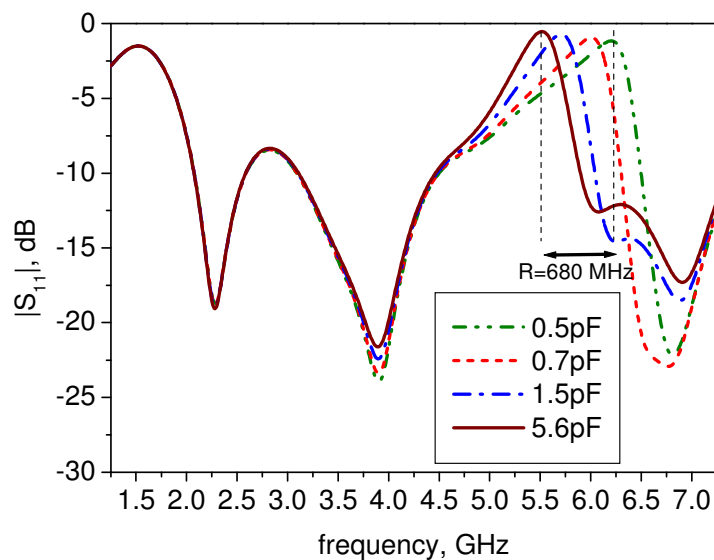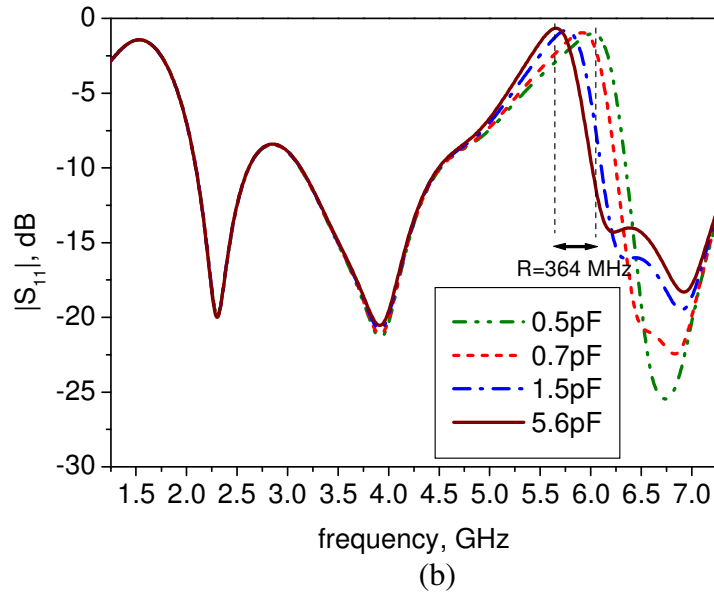
Figure 6.8 Simulated S_{11} of antenna of Figure 6.1 for different varactor position in the line, (a) Mid (b) ¼ of the line length away from the mid point of the resonator
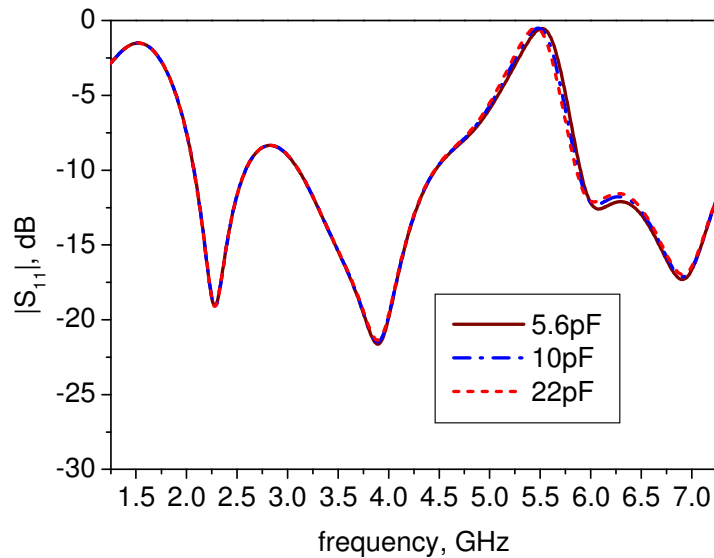
Figure 6.9 Simulated S_{11} of antenna of Figure 6.1 for capacitance more than 5.6 pF

The resonator transmission line equivalent circuit model is shown in Figure 6.10. The equivalent circuit shows a microstrip line open stub resonator is coupled through capacitors to a 2 port slot line terminated with its matched load. In this equivalent circuit, the coupling capacitor value (0.055 pF) is optimised, so that the centre frequency of the notch

band is approximately the same with the result obtained from full wave EM simulation. The objectives of this equivalent circuit are to show in general how changing the capacitance will change the centre of the resonant frequency and the Q factor. The equivalent circuit shown in Figure 6.10 approximately describes the resonator explained in section 6.3.2.
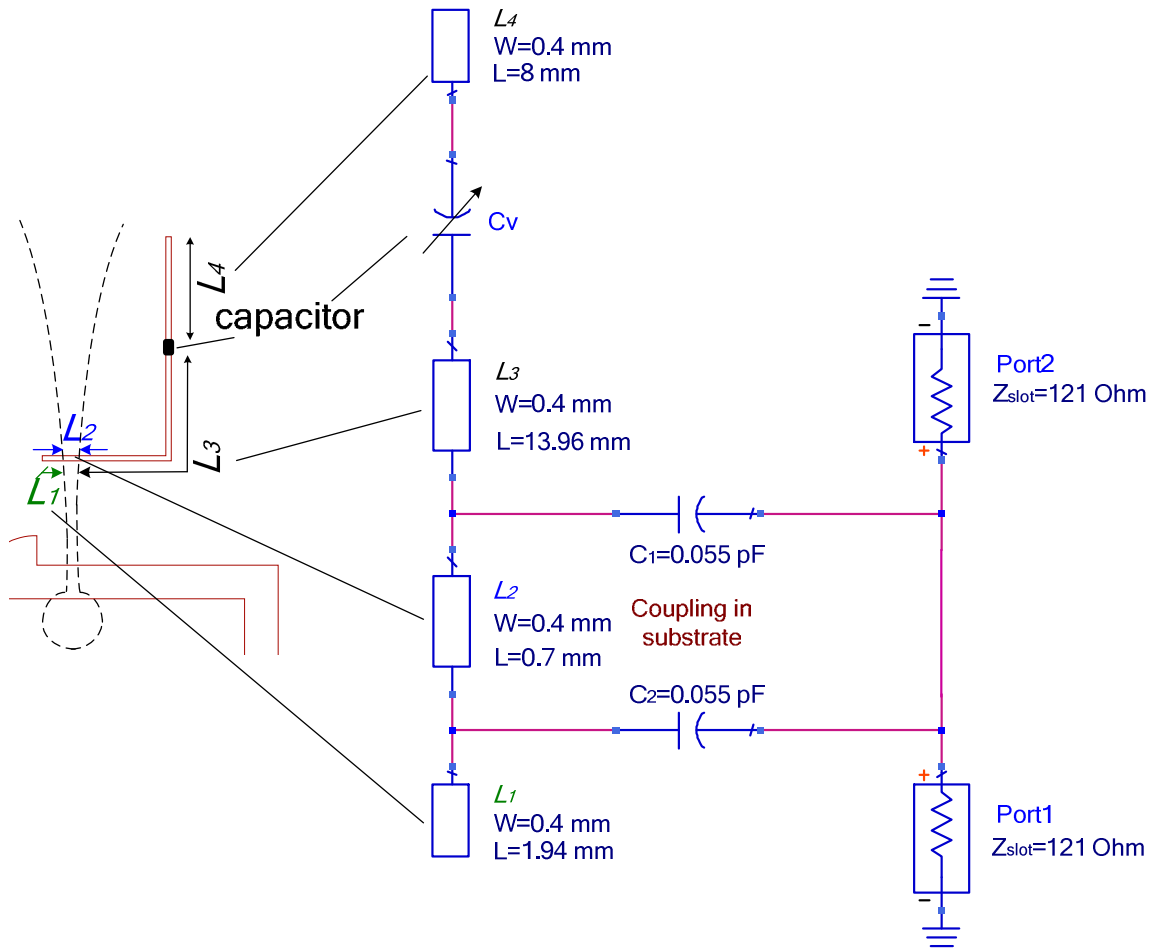
Figure 6.10 Resonator equivalent circuit

Figure 6.11a and Figure 6.11b show the s-parameters when the capacitor is set to 0.1 pF and 5.6 pF respectively. The corresponding VSWR is shown in Figure 6.12. When changing the capacitance values, the resonant frequency is also changed and the Q factor is increased at low frequency. This is presumably because, electrically the centre of the

resonator moves outward from the coupling point when the line is electrically longer and this therefore reduces the coupling. The coupling can also be observed through VSWR, where higher standing wave ratio shows high coupling.
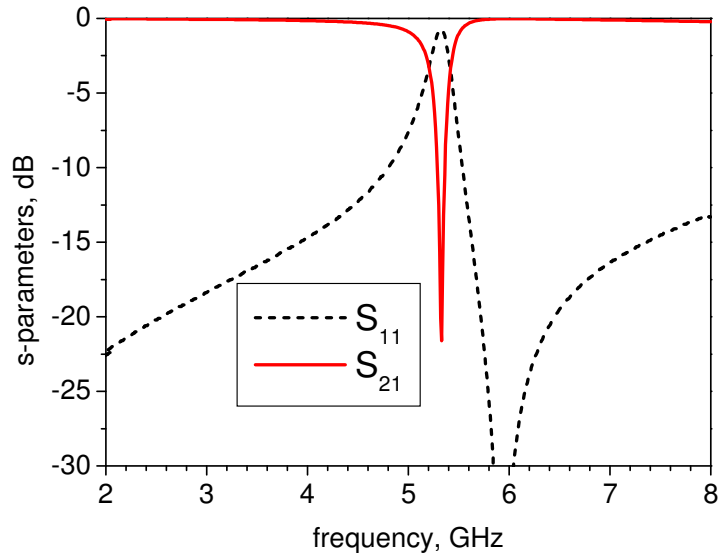
(a)
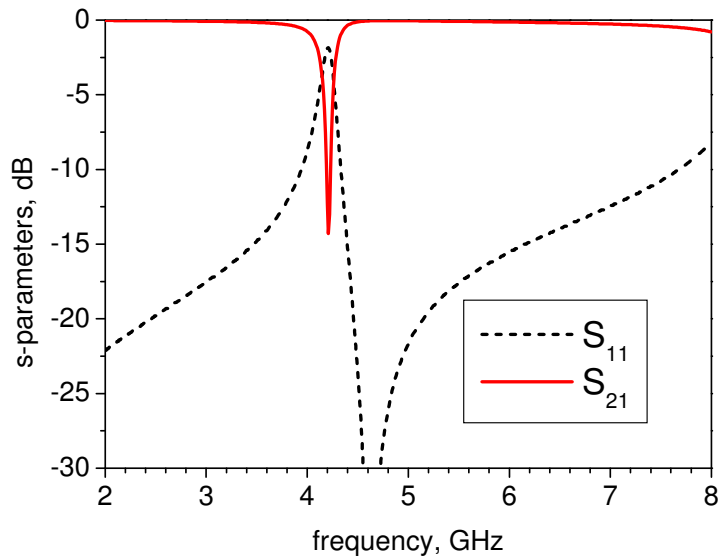
(b)

Figure 6.11 S-parameters of equivalent circuit of the resonator when capacitor is set to (a) 0.1 pF, (b) 5.6 pF
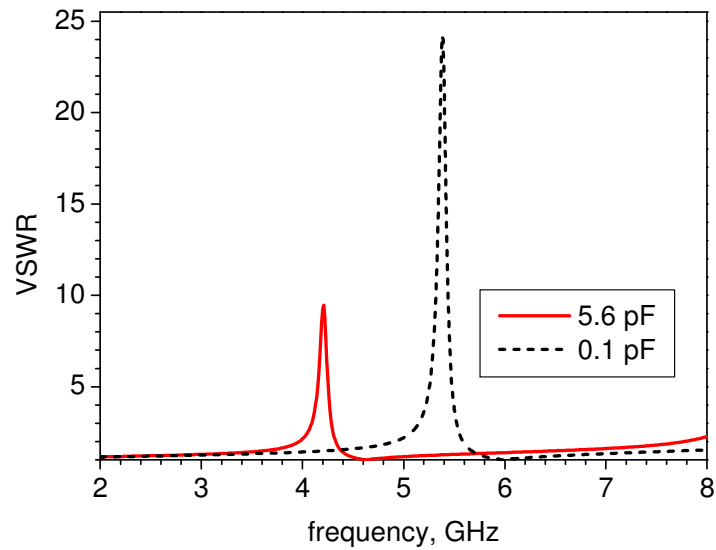
Figure 6.12 VSWR of equivalent circuit of the resonator when capacitor is set to 0.1 pF and 5.6 pF

6.3 Simulations and Experiments

Three types of design are presented. One with fixed band notching capability, one with a single varactor to give a tunable band notch between 4.2 – 5.5 GHz and another with 3 varactors and a shorting post to the ground to activate the stop band in the frequency range between 2 GHz and 7 GHz, giving a very wide tuning ratio, of 3.5:1

6.3.1 Fixed band notch

A 10 mm x 9 mm x 0.4 mm, *L* shaped resonator as shown in Figure 6.1 is designed, simulated and fabricated to give a fixed band notch at 5.75 GHz, ($L_1 = 10$ mm, $L_2 = 9$ mm). As a reference, the simulated and measured S_{11} of the Vivaldi without resonator is shown in Figure 6.13, showing wideband performance from 2 – 7 GHz. The measured and simulated S_{11} responses with the stop band resonator are shown in Figure 6.14. Good

agreement is obtained between measurement and simulation. The cut-off band occurs at 5.75 GHz, where the resonator length is half the guided wavelength. The level of the rejection in the S_{11} plot is -0.7 dB at the band notch frequency, giving good suppression of the corresponding frequency. Figure 6.15a and Figure 6.15b compares the measured S_{11} and gain between the reference and the band notch antenna respectively. It can be seen that the pass band response and gain at the maximum direction of the band notch antenna are similar to those of the reference antenna, showing that the inclusion of the resonator has a small effect on the overall pass-band performances. The gain at the rejection band is -12dBi, suppressed at about -16 dB. Figure 6.16 shows the simulated and measured H-plane radiation pattern excited in the pass bands at 4 and 6.5 GHz, and in the notch band at 5.75 GHz. Good agreement is observed between them, and the radiation at the notch frequency has been suppressed. The simulated total efficiency at those frequencies is shown in Table 6.1. The efficiency at the rejection band is only around 9.5% compared with the efficiency at the pass band, which is around 95%.
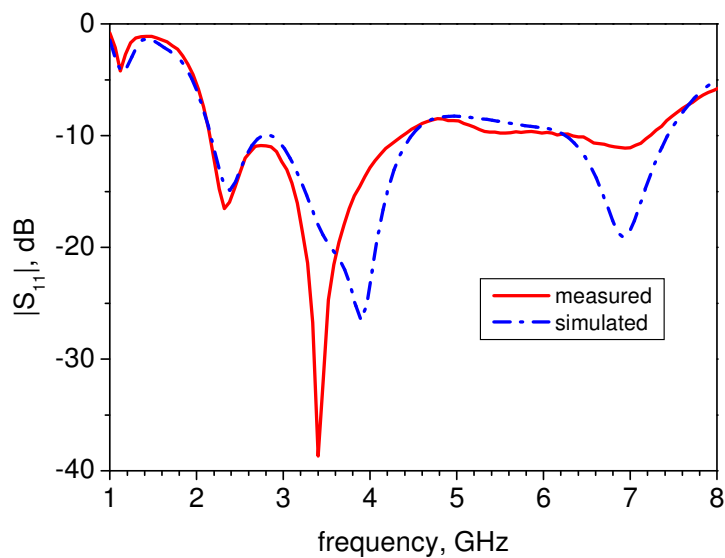
Figure 6.13 Frequency response (S_{11}), without the resonator
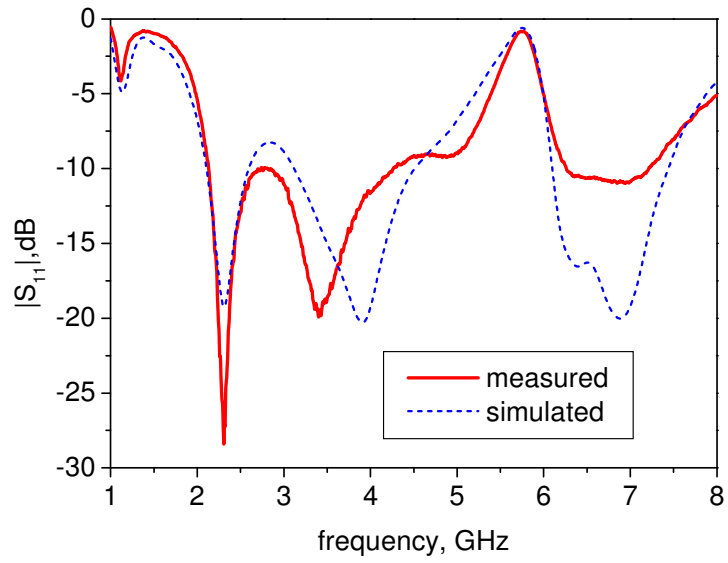
Figure 6.14 S_{11} characteristic of the antenna with stop-band resonator
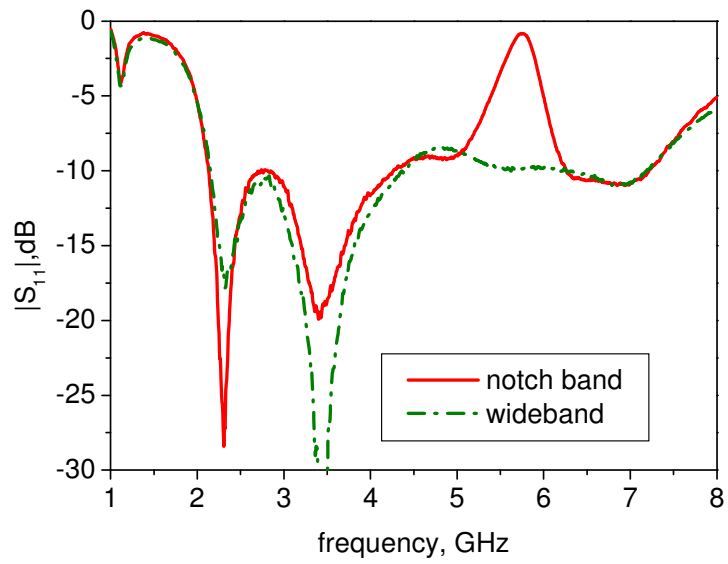
(a)
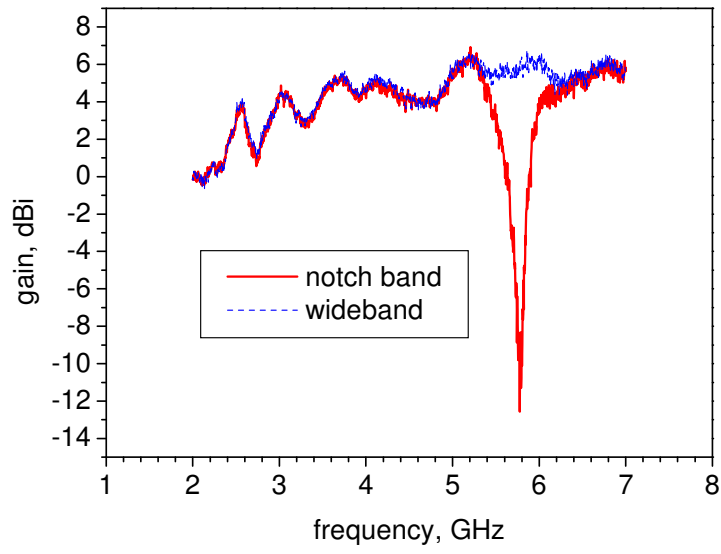
(b)

Figure 6.15 Band notch and reference antenna performances, (a) S$_{11}$, and (b) gain
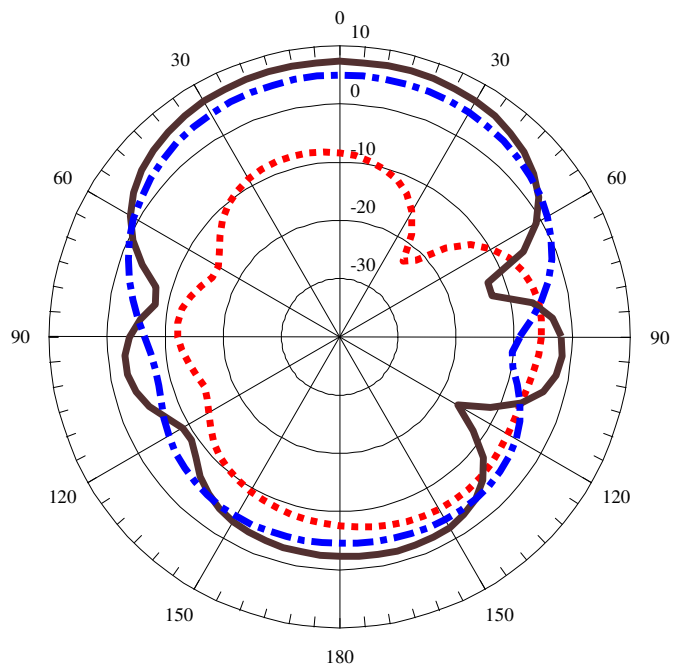
(a)
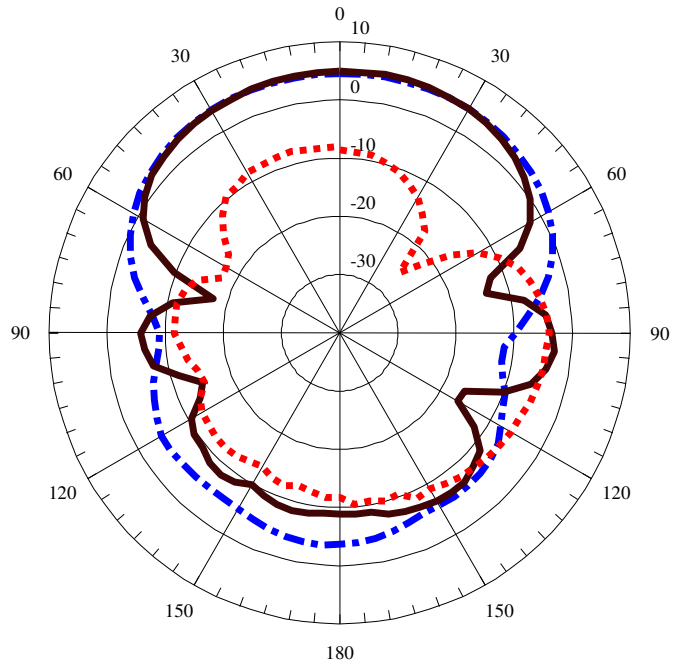
(b)

- · - 4 GHz
········ 5.75 GHz
——— 6.5 GHz

Figure 6.16 H-plane radiation pattern excited at pass band at 4 and 6.5 GHz, and notch band at 5.75 GHz, (a) simulated, and (b) measured

Table 6.1 Simulated total efficiency

Frequency (GHz)	4.0	6.5	5.75
Total efficiency (%)	97.35	95.53	9.57

6.3.2 Tunable Notch

The antenna concepts in this section is contributed by Dr F. Ghanem [10] and included to ensure continuity in the description of the new antenna. The simulation, measurement and the analysis of this section however are done by the author of this thesis.

A 10 mm (L_1) x 18 mm (L_2) x 0.4 mm L shaped resonator as shown in Figure 6.10 is designed and simulated. A 1 mm gap used to locate the capacitor is created 8 mm from the top of the microstrip resonator to give a tunable band notch between 4.2 – 5.5 GHz. Prototypes with different fixed capacitors are developed to verify the proposed concepts. Five capacitors with values from 5.6, 1.1, 0.5, 0.2, and 0.1 pF were used. The range of these capacitors can approximately be obtained from *Microsemi* varactor MV31013 (0.15 – 6.25 pF) or MV34001 (0.1 – 4.5 pF). The measured and simulated S_{11} responses with the stop-band are shown in Figure 6.17a and Figure 6.17b respectively. It is demonstrated that the stop-band at 4.2 to 5.5 GHz appears within the 2 – 7 GHz operating band. Figure 6.18 compares the measured and simulated S_{11} when capacitance of 0.1 pF is used. The corresponding gain is shown in Figure 6.19. A good agreement is observed, where the main features are well predicted. Measured gains at other stop-band are shown in Figure 6.20. The gain is suppressed significantly at about -11 to -14 dB in the stop band. On the whole, the lower and upper pass-band gains follows similar trends as compared with non-stop band version as shown in Figure 6.21. Figure 6.22 shows the simulated radiation pattern of the proposed antenna excited at pass band 4.5 GHz and 6 GHz, and notch band at 5.46 GHz. The radiated power has clearly dropped, by about -14 dB, in the notch band at 5.46 GHz compared to in the pass-band at 6 GHz and 4.5 GHz. The measured radiation pattern excited at pass-band 4.5 GHz and 6 GHz, and notch-band at 5.32 GHz is shown in Figure 6.23. Similar behaviour is observed.
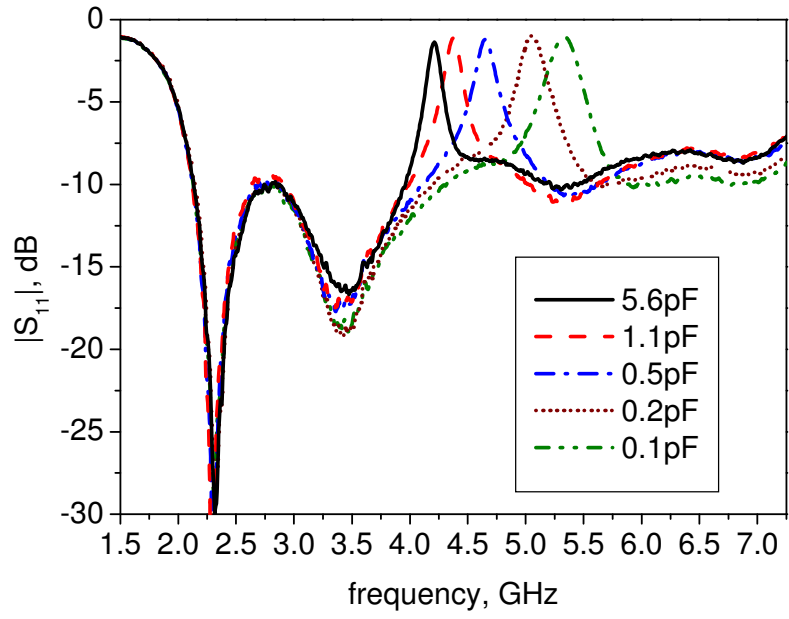
(a)
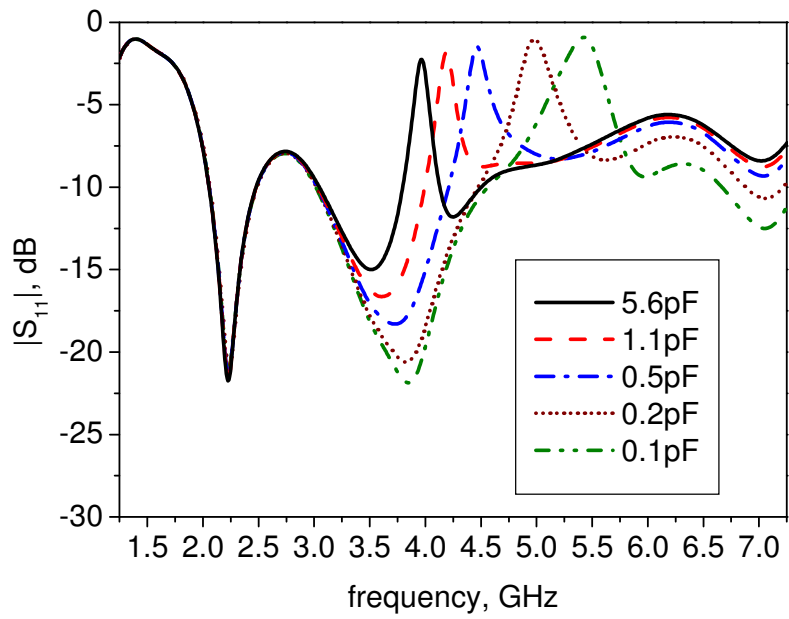
(b)

Figure 6.17 S$_{11}$ responses, (a) measured, (b) simulated
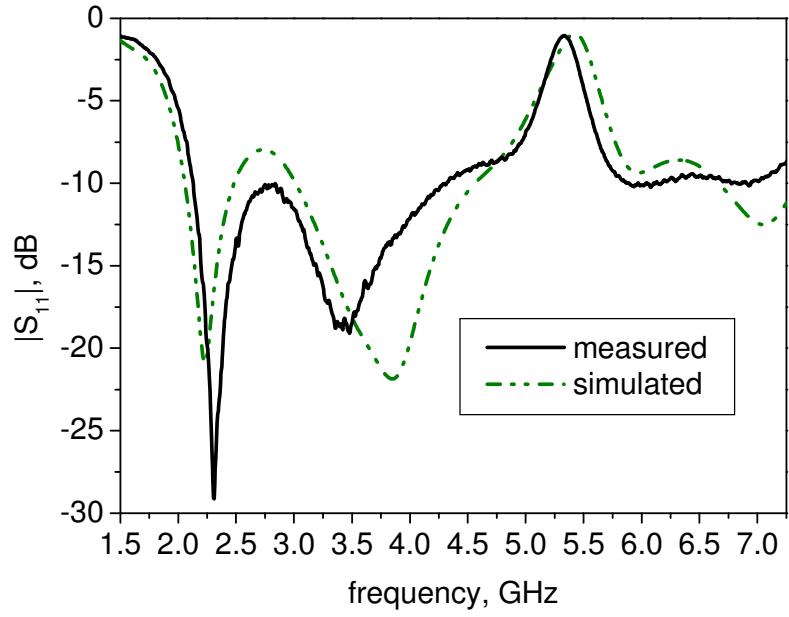
Figure 6.18 S$_{11}$ responses with 0.1 pF capacitance
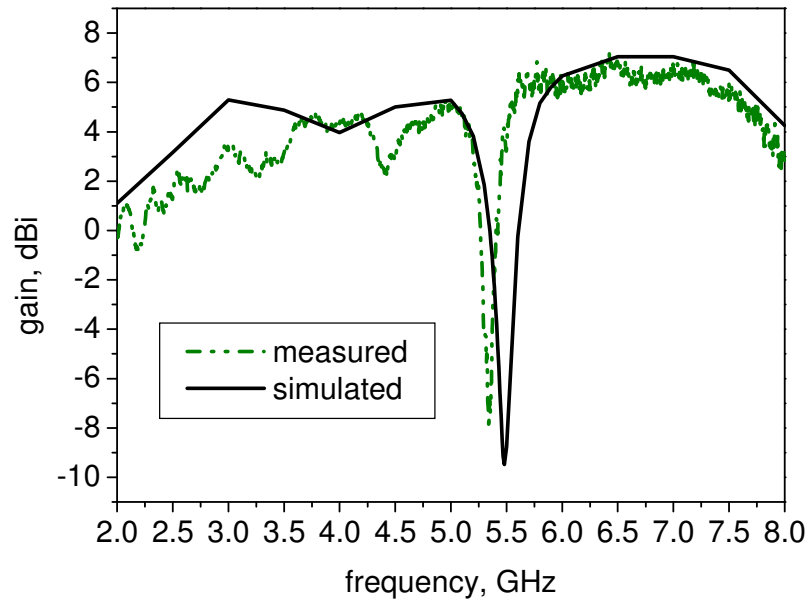
Figure 6.19 Gain with 0.1 pF capacitance
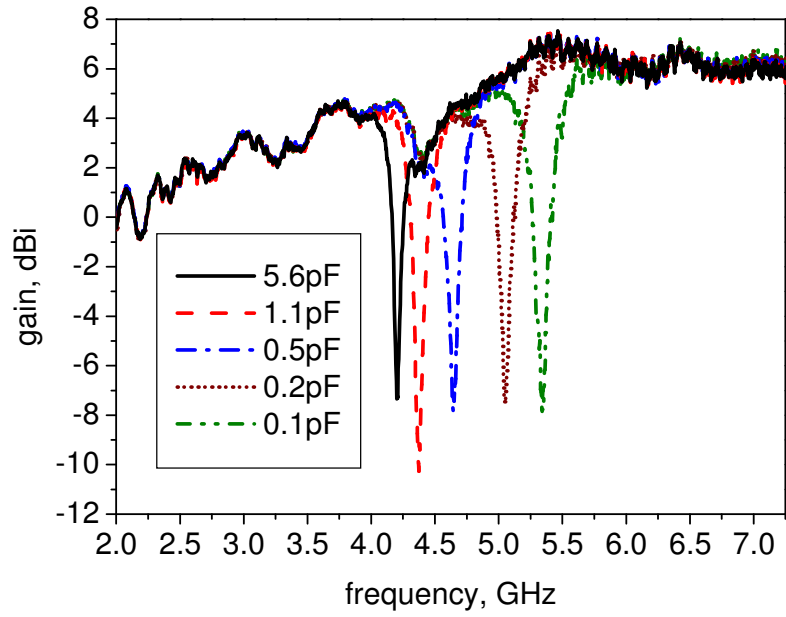
Figure 6.20 Measured gain of the proposed antenna with fixed capacitors
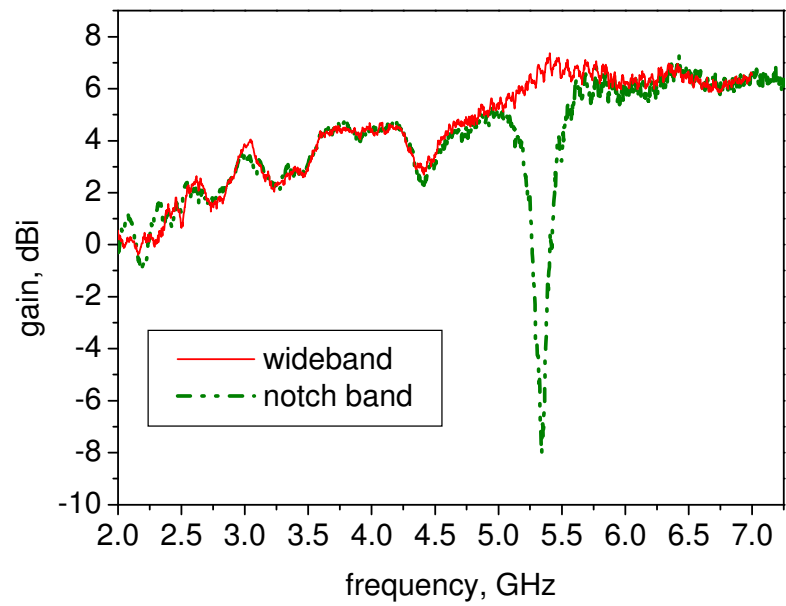
Figure 6.21 Antenna gain without resonator and with resonator using 0.1 pF
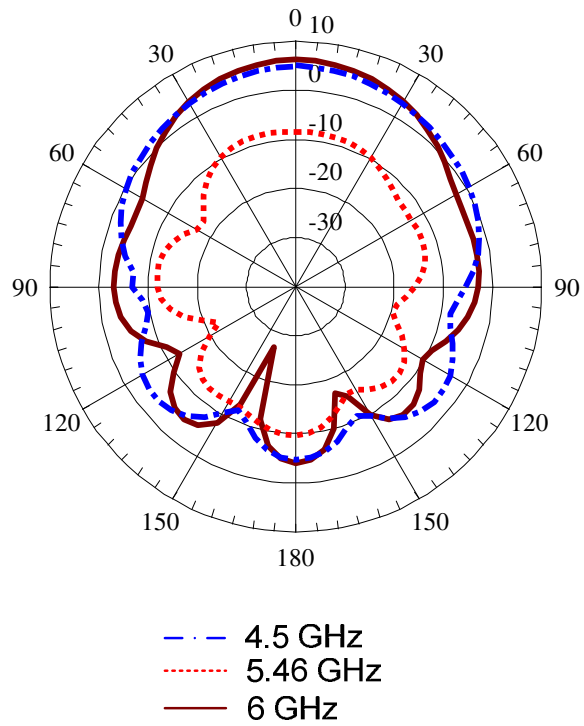
Figure 6.22 Simulated E-plane radiation pattern excited at pass band at 4.5 and 6 GHz, and notch band at 5.46 GHz
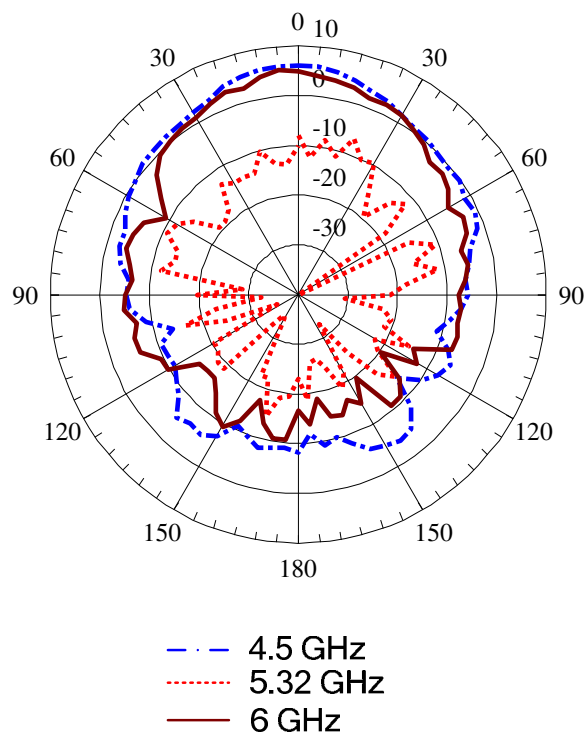
Figure 6.23 Measured E-plane radiation pattern excited at pass band at 4.5 and 6 GHz, and notch band at 5.32 GHz

This part ends the contribution of Dr F. Ghanem on this work.

6.3.3 Multiple Varactor for Wider Tuning Range

To achieve a very wide tuning range, the resonator has been divided into three sections using small gaps as shown in Figure 6.24. The stop band centre frequency will therefore be determined by the active total length. Three varactors are used. Two varactors, C_1 and C_2, are used to bridge the 1 mm gaps in the resonator. At the top end, a third varactor, C_3, is used to bridge the gap between the resonator and a shorting post to the ground. The varactors are used to vary the resonator impedance and hence effectively tune the stop band centre frequency. When the varactors are tuned to more than 5.6 pF or to their minimum capacitance of 0.1 pF, the gap in the line will approximate to a short or open circuit, respectively. Using a combination of shorts or opens at the gaps, three different sets of active resonator lengths, L_1, L_2 and $2L_2$, can be obtained.
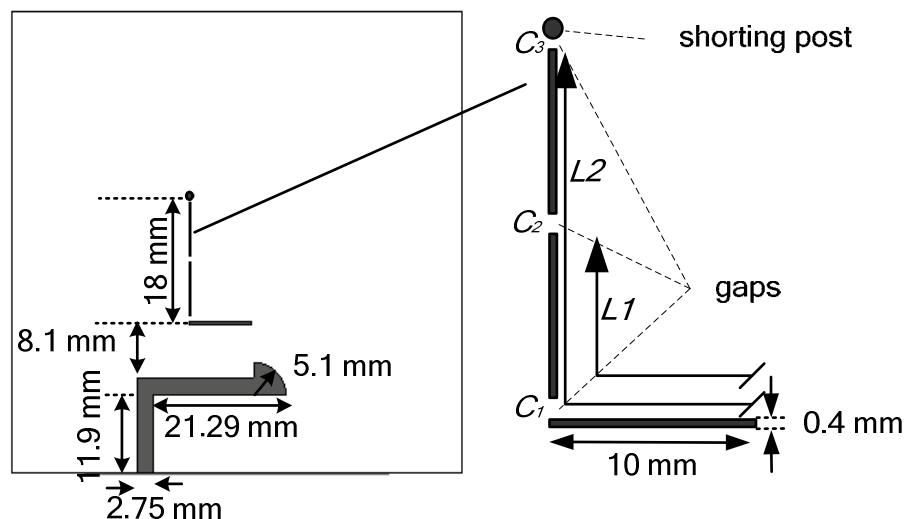
Figure 6.24 Proposed resonator with three gaps

The varactor settings for these are now described. To create the L_1 section, as the only active resonator, the three varactors, C_1, C_2 and C_3 are set to 5.6 pF, 0.1 pF and 0.1 pF respectively. Ideally, with $L_1 = 19$ mm, the length is approximately half a wavelength long at 5.75 GHz. However with the addition of the capacitors the actual electrical length of L_1 has been elongated so that the stop band now occurs at 4.9 GHz. The stop bands in the higher band between 4.9 to 6.8 GHz can be achieved when C_1 is tuned between 5.6 to 0.14 pF. On the other hand, to make the L_2 section, as the active resonator, the three varactors, C_1, C_2 and C_3 are set to 5.6 pF, 5.6 pF and 0.1 pF respectively. This makes the length of L_2 approximately half a wavelength at 3.5 GHz. Stop bands in the middle band between 3.5 to 4.8 GHz are obtained by varying C_2 between 5.6 to 0.15 pF. Finally, to obtain the L_2 section with a short circuit at the end, C_3 is set to 5.6 pF which effectively creates L_2 as a short circuit stub of length 90^0 at 1.8 GHz. Changing C_2 between 5.6 to 0.1 pF, the band stop centre frequency is tuned to a lower band between 2.1 and 4.2 GHz. Because the effective length is now longer, a third harmonic occurs at around 5.7 GHz. Nevertheless, the length is designed so that the band rejection at the third harmonic occurs at the WLAN frequency, around 5.7 GHz. Also, the varactor, C_2 has been positioned in the line where the current at the third harmonic frequency is zero as shown in Figure 6.25. Thus the 5.7 GHz stop band does not change with C_2.

Various fixed capacitors are used to represent varactors in the simulation and also in the fabricated antenna. The simulated S_{11} showing various tunable stop bands at different frequencies denoted as (*m1-m5*) when $2L_2$ is activated, (*m6-m10*) when L_2 is activated and (*m11-m17*) when L_1 is activated, are presented in Figure 6.26a, Figure 6.26b and Figure 6.26c respectively. Figure 6.27 shows all the notch bands. It is clearly seen that the stop band can be tuned between 2 – 7 GHz using the proposed concepts by activating three different resonator lengths. Table 6.2 give the capacitor values for these frequencies.
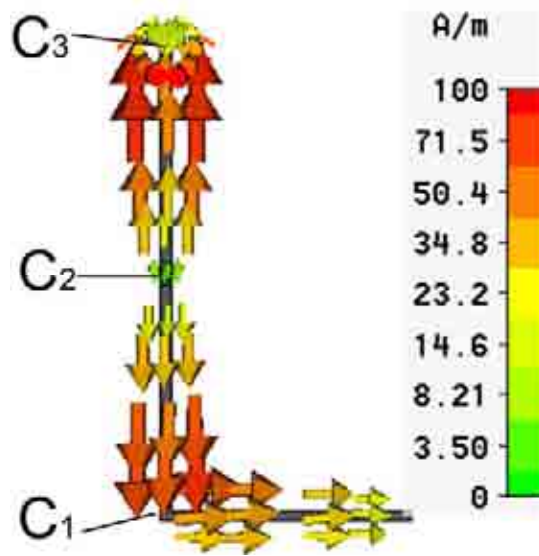
Figure 6.25 Current distribution at the third harmonic frequency showing current zero occurs at varactor C_2 position
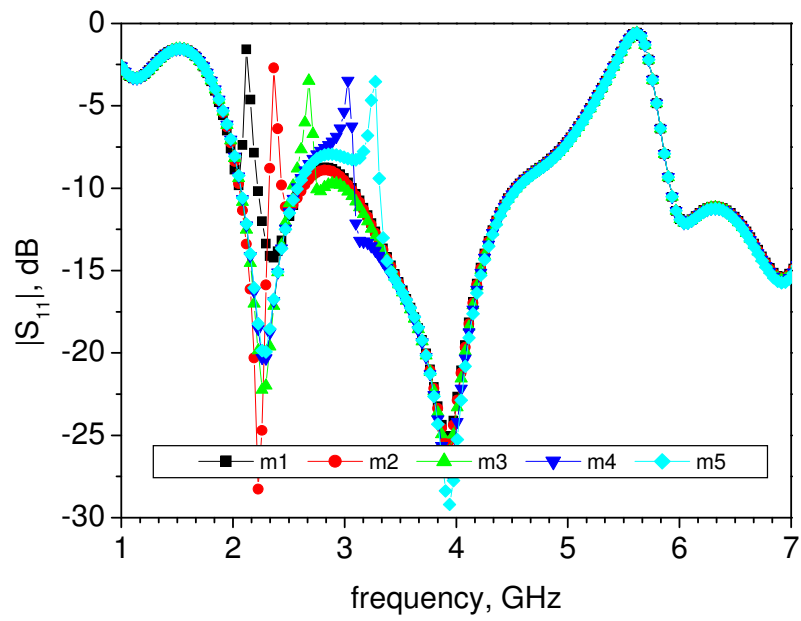
(a)
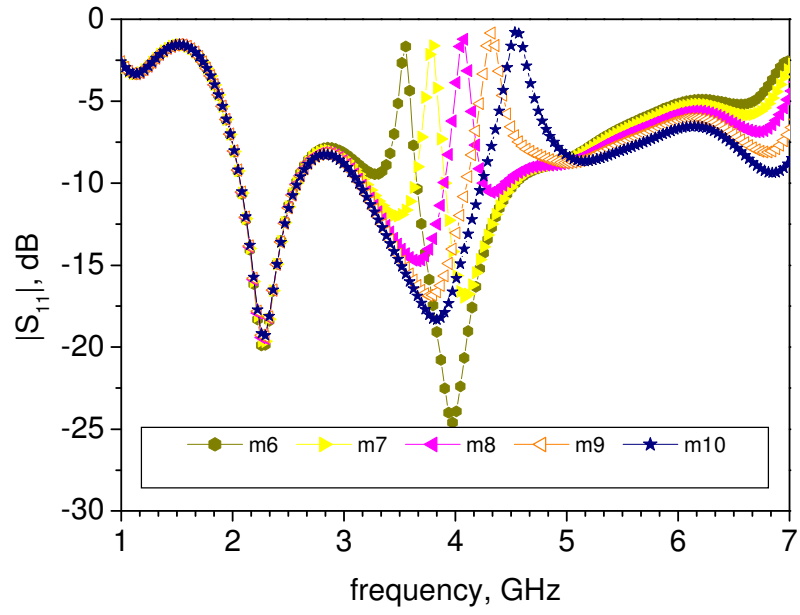
(b)
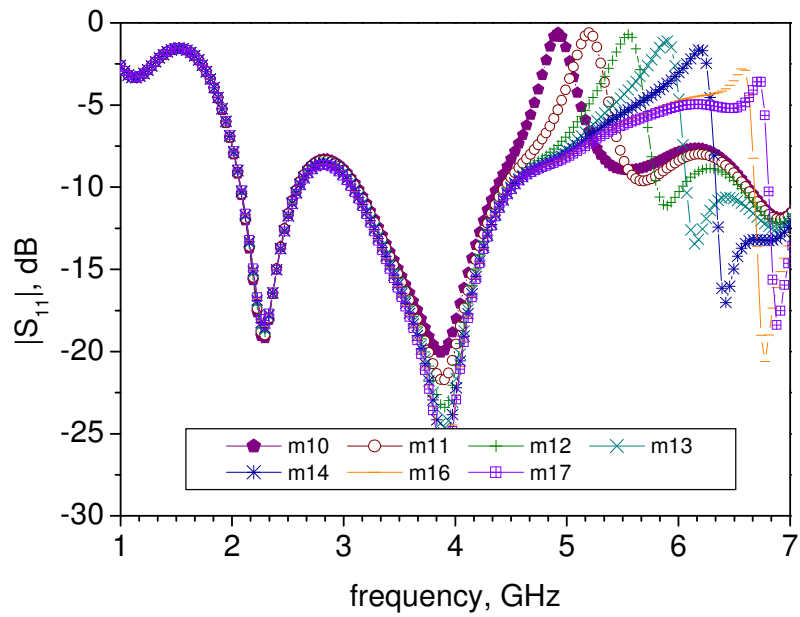
(c)

Figure 6.26 Simulated notch band frequency response (S₁₁), (a) 2*L₂*-(*m1-m5*), (b) *L₂*-(*m6-m10*), (c) *L₁*-(*m11-m17*) active
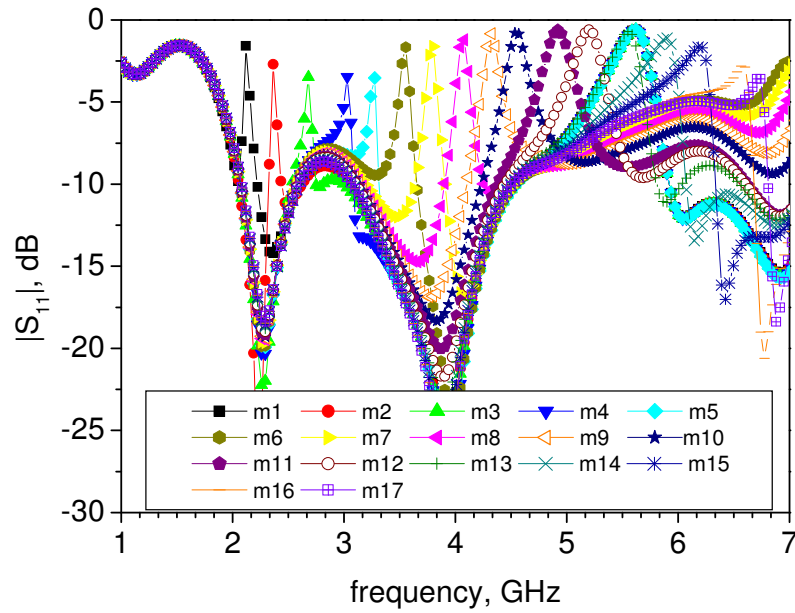
Figure 6.27 Simulated notch band frequency response (S$_{11}$)

Table 6.2 Varactor capacitance settings for various modes

Band notch	m1	m2	m3	m4	m5	m6	m7	m8	m9	m10
	resonator – $2L_2$					resonator – L_2				
C_1,(pF)	5.6	5.6	5.6	5.6	5.6	5.6	5.6	5.6	5.6	5.6
C_2,(pF)	5.6	1.5	0.7	0.4	0.3	5.6	1.1	0.5	0.3	0.15
C_3,(pF)	5.6	5.6	5.6	5.6	5.6	0.1	0.1	0.1	0.1	0.1

Band notch	m11	m12	m13	m14	m15	m16	m17
	resonator – L_1						
C_1,(pF)	5.6	1.1	0.5	0.3	0.2	0.14	0.1
C_2,(pF)	0.1	0.1	0.1	0.1	0.1	0.1	0.1
C_3,(pF)	0.1	0.1	0.1	0.1	0.1	0.1	0.1

Figure 6.28 shows the measured S$_{11}$ results showing examples of the band notch at *m1* (2.17 GHz), *m2* (2.39 GHz), *m6* (3.73 GHz), *m8* (4.30 GHz), *m11* (5.22 GHz), *m12* (5.53 GHz), *m14* (6.19 GHz) and *m15* (6.39 GHz). It is observed that a fixed band rejection occurs at 5.73 GHz in the *m1* and *m2* states which is due to the third harmonic.

181

This stop band is useful if the system needs a permanent band rejection at WLAN frequency. The third harmonic can be avoided up to the notch band at 3.5 GHz by using L_2 as the active resonator instead of $2L_2$. However the matching at the frequency above 6 GHz is slightly compromised. Figure 6.29 shows this.
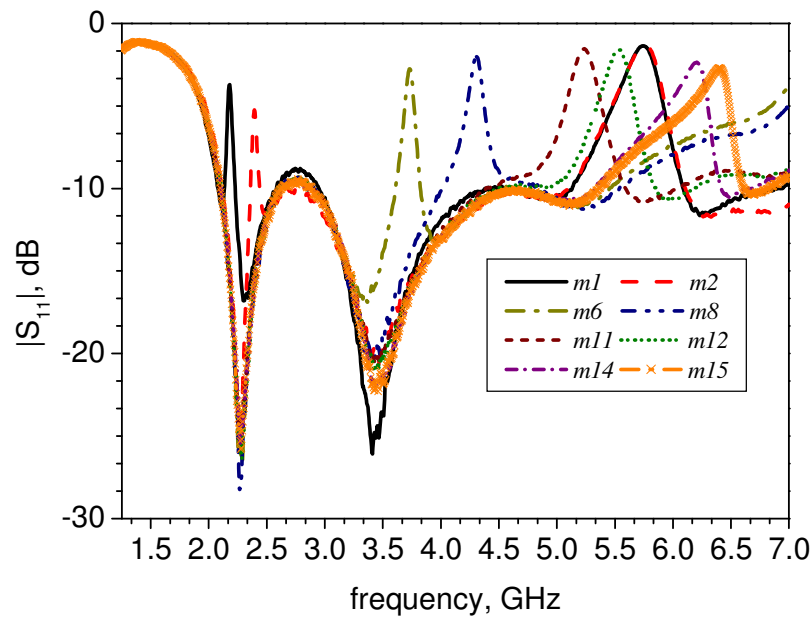
Figure 6.28 Measured notch band frequency response (S_{11})
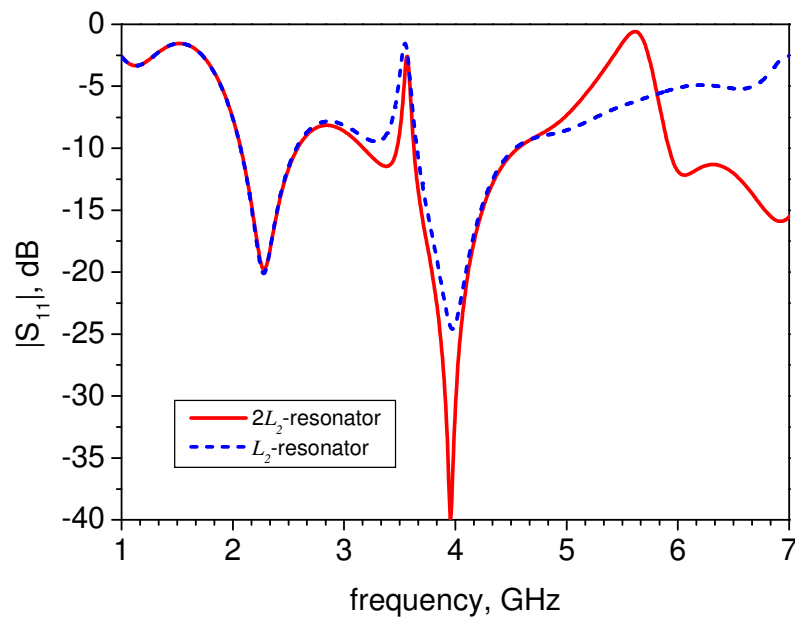
Figure 6.29 Notch band using L_2 and $2L_2$ active resonator

The measured gain for *m1*, *m2*, *m4*, *m6*, *m8, m11*, *m12*, *m14* and *m15* is shown in Figure 6.30. It is clearly seen that sharp gain reduction occurs in every stop band ranging between -7 and -16 dB. The measured E-plane radiation pattern excited at 2.18 GHz (*m1*) and 4.30 GHz (*m8*) before and after notching is shown in Figure 6.31. The gain is suppressed by about -10 dB in *m1* and -12 dB in *m8* operations. Figure 6.32 shows the measured radiation pattern of *m1* mode excited in the pass band at 4.3 and 6.18 GHz, and in the notch bands at 2.18 and 5.78 GHz. The radiated power is clearly seen to have dropped, by about -14 dB, in the notch band at 2.18 GHz and -18 dB at 5.78 GHz compared to in the pass band at 4.3 GHz and 6.18 GHz. The simulated radiation pattern excited in the pass band at 4.3 and 6.18 GHz, and in the notch bands at 2.18 and 5.78 GHz is shown in Figure 6.33. Similar behaviour is observed.
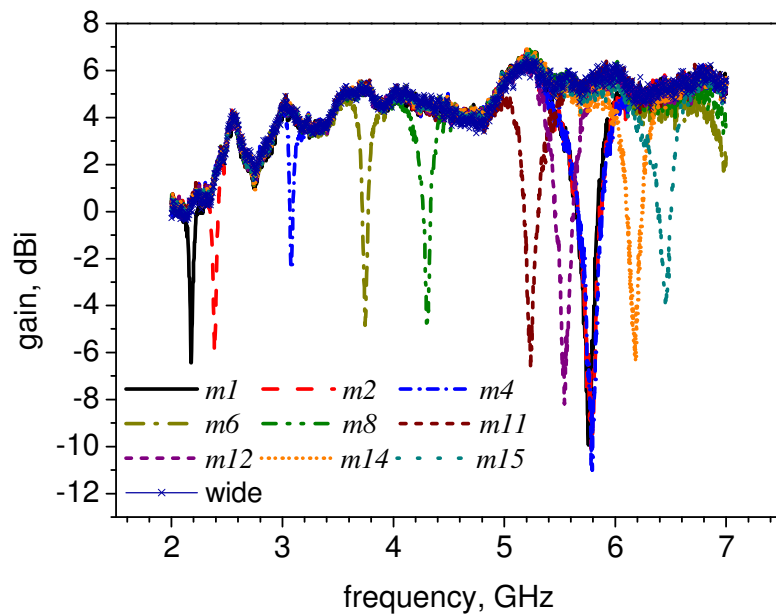
Figure 6.30 Measured gain
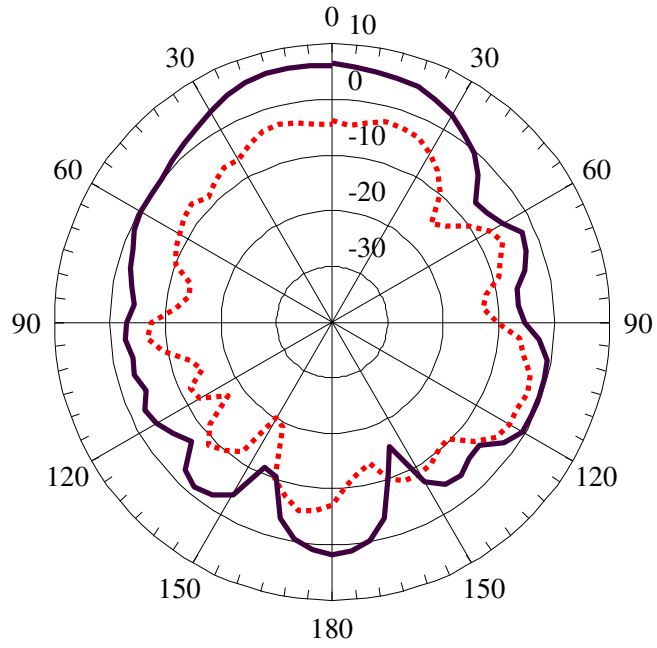
(a)
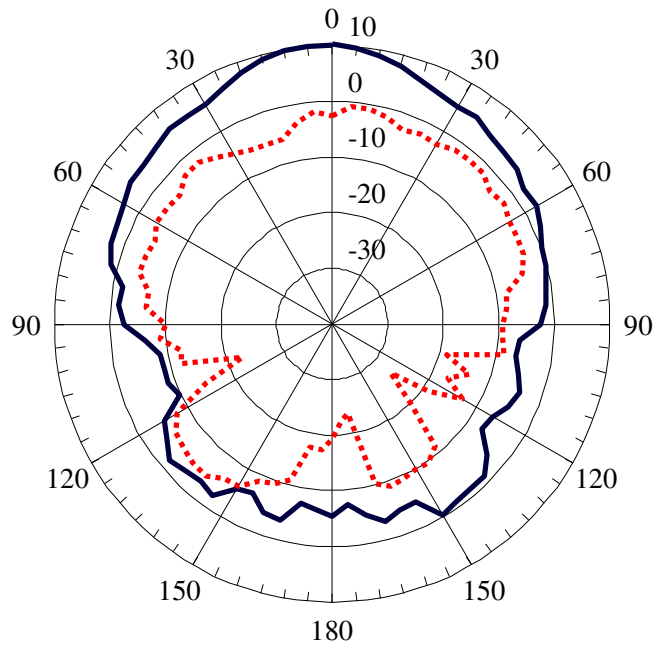
(b)

——— before; ------- after notching

Figure 6.31 Measured E-plane radiation pattern excited at (a) 2.18 GHz (*m1*), and (b) 4.30 GHz (*m8*), before and after notching
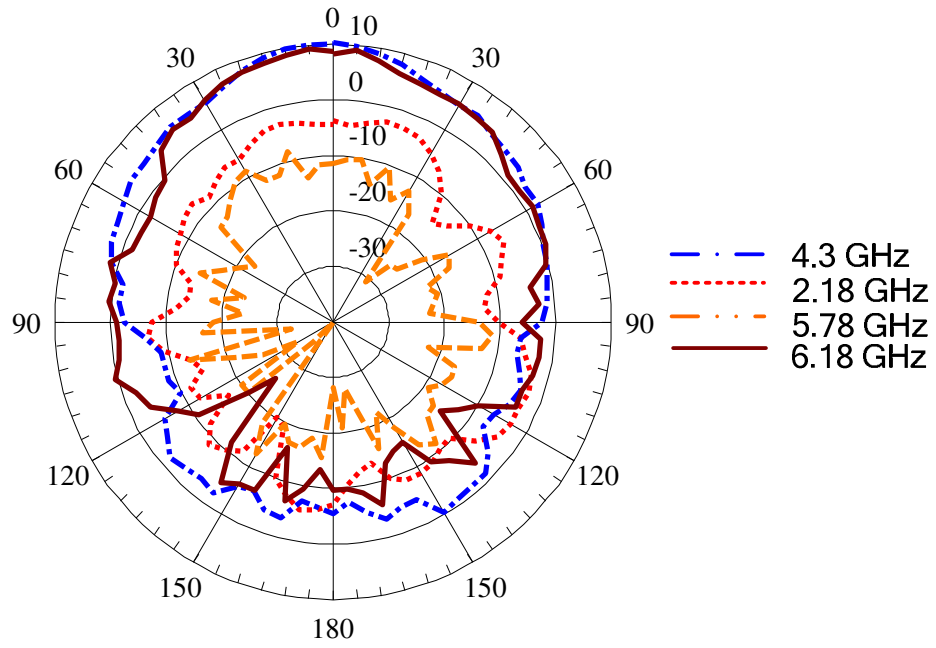
Figure 6.32 Measured E-plane radiation pattern in *m1* mode excited at pass band at 4.3 and 6.18 GHz, and notch band at 2.18 and 5.78 GHz
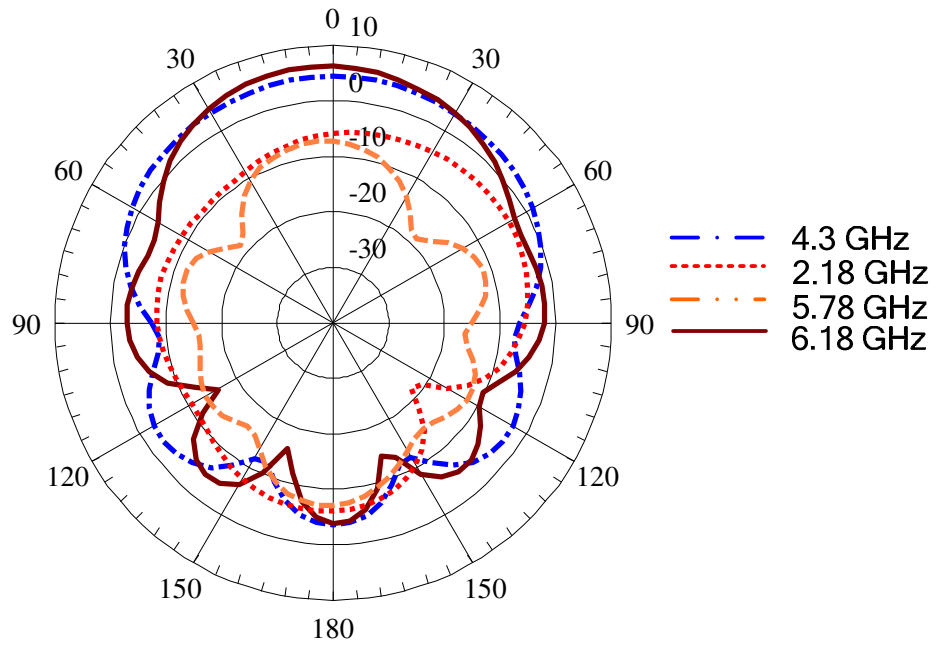
Figure 6.33 Simulated E-plane radiation pattern in *m1* mode excited at pass band at 4.3 and 6.18 GHz, and notch band at 2.2 and 5.89 GHz

185

6.4 Electronic tuning

Electronically tuned band notching is demonstrated here by using a varactor model MV31009 from Microsemi. The capacitance range is between 21.7 and 0.98 pF to give a tuning range between 4.0 – 4.45 GHz. The varactor is biased with bias line through 300kΩ RF choke as shown in Figure 6.34. Figure 6.35 shows the S_{11} response before and after the RF choke is inserted. It is observed the notch band shifted down in frequency from 6.4 GHz to 6 GHz. This can be explained by additional parasitic from the RF choke which elongates the effective electrical length of the resonator. The S_{11} response with varactor included is shown in Figure 6.36. Some degree of electronically band notch tuning is clearly seen. By comparing with the fixed capacitors version, as shown in Figure 6.37, the tuning range is approximately similar for the same capacitance values. The level of the rejection in the S_{11} plot is slightly lower and can be understood as an extra loss from the varactor and bias components. The measured gain is shown in Figure 6.38 where the suppression is ranging from -5 to – 8 dB. Figure 6.39 compares the gain of the varactor and fixed capacitor version with the similar notch band.
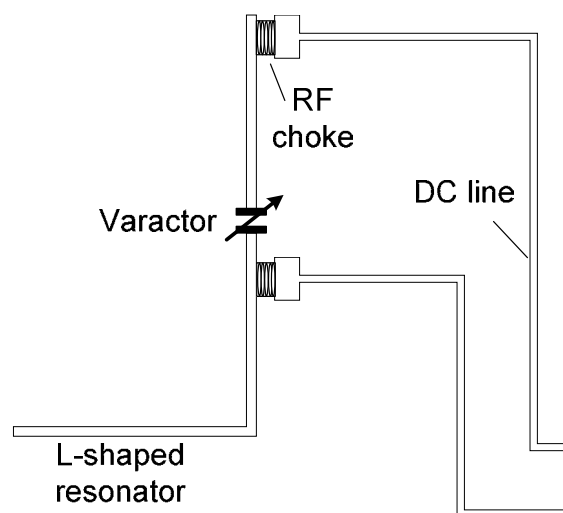
Figure 6.34 Dc bias configuration

186
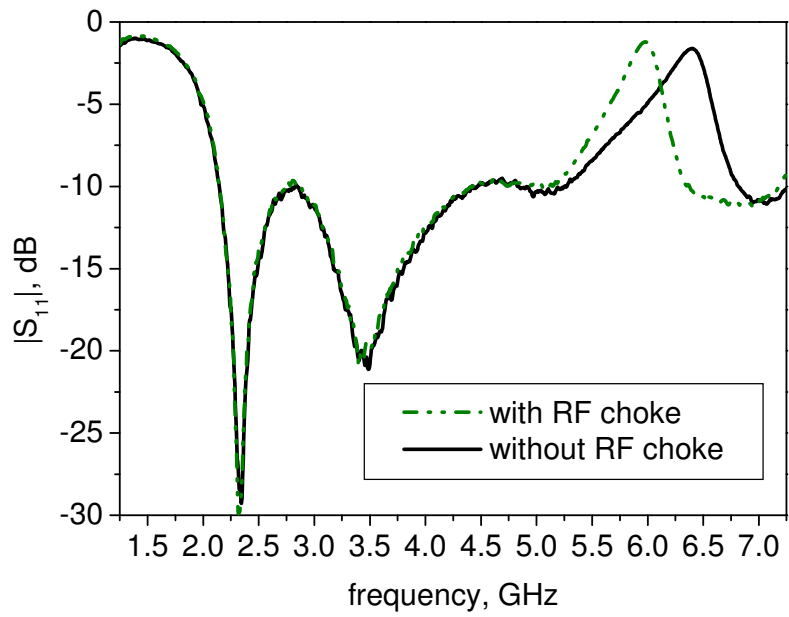
Figure 6.35 Simulated S₁₁ of the antenna with varactor controlled stop band resontor
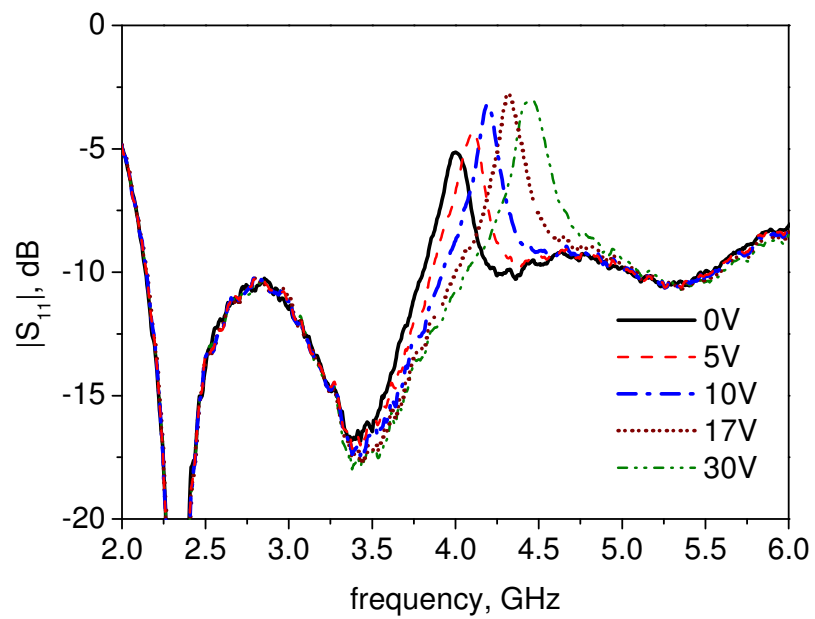
Figure 6.36 Tunable notch band using varactor
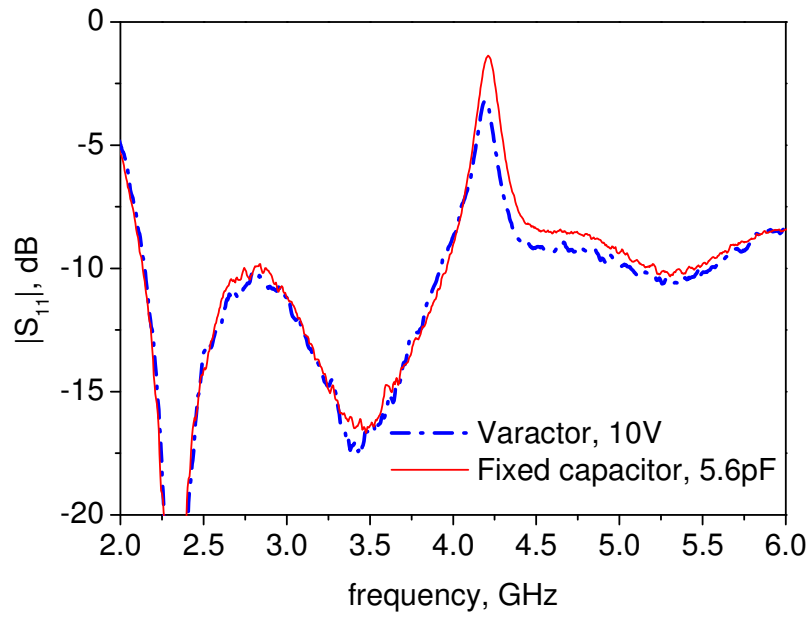
Figure 6.37 S_{11} plot with varactor and fixed capacitor
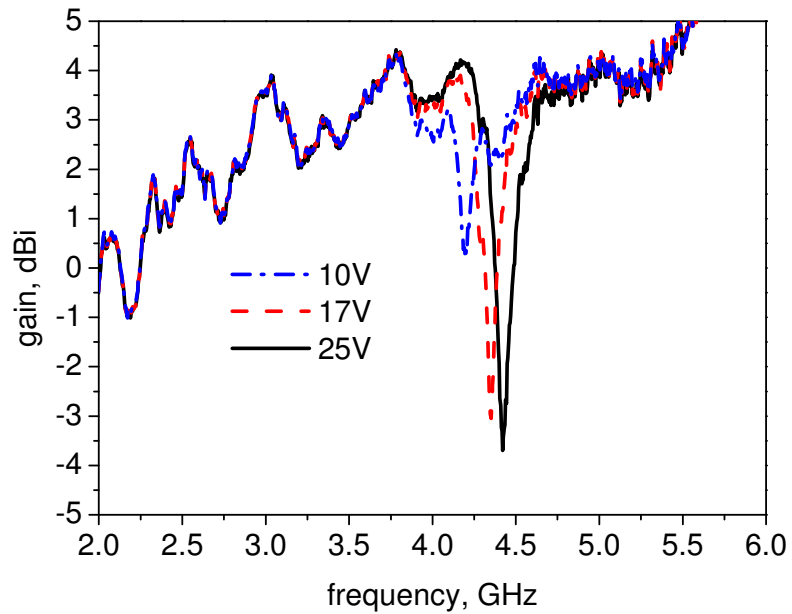
Figure 6.38 Measured gain of the proposed antenna with varactor

188
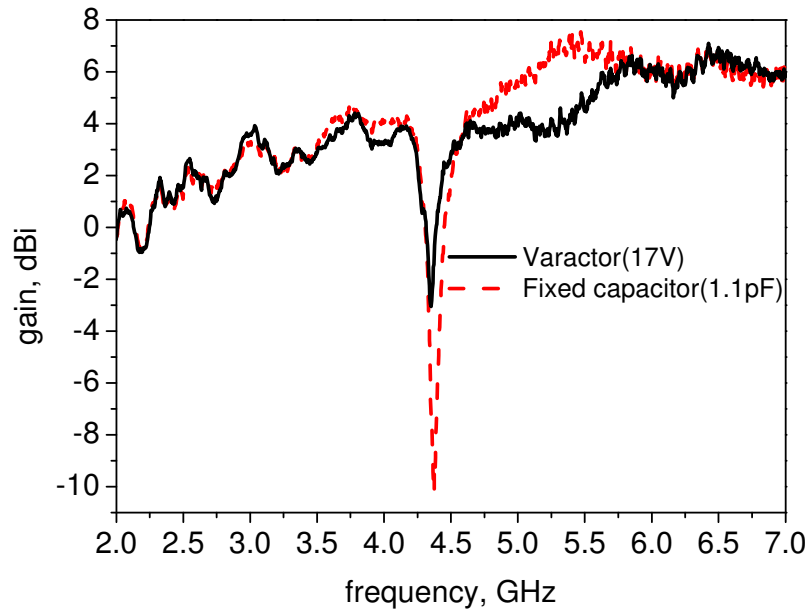
Figure 6.39 Varactor and fixed capacitor on gain

6.5 Summary

To realize a band notch capability in a Vivaldi antenna, a microstrip line resonator has been integrated to prevent the propagation of signals in the frequency notch band. Three methods have been demonstrated. In the first method, a 19 mm length resonator is used to stop the propagation at 5.75 GHz band. In the second method, some degree of tunable band notching is achieved, using a 28 mm length resonator and a single varactor. The third method shows a very high tuning range using the same length of the resonator and three varactors and a shorting post to the ground. The advantage of the proposed band rejection method here in which the resonator is integrated within the antenna space, is that it has a very minimal effect on the gain performances in the pass bands. The pass band response in gain and S_{11} is very similar to that reference antenna (i.e. without resonator). Furthermore the tuning range can be extended by elongating the electrical length of the

189

resonator. A tunable band notch antenna has been developed and tested. The performance shown verifies the proposed design concept. This work has been reported in [75, 88].

CHAPTER 7

COMBINED WIDE-NARROW-NOTCH BAND VIVALDI ANTENNA

7.1 Introduction

Multimode radio, UWB system and future cognitive radio pose considerable challenges for antenna designer. Many novel reconfigurable antennas and UWB antennas have appeared in the literature. In the three previous chapters two combined wideband-narrowband Vivaldi antennas and a wideband with tunable band notch have been described. Also most of the reconfigurable antennas reported so far have only a two mode capability, either reconfiguring from one narrowband to another narrowband [2], a wideband to a notch band [69] or a wideband to narrowband [7]. However, to the best of our knowledge, no attempt has yet been reported to combine three modes, namely wideband, notch, narrowband, in one single antenna. In this chapter we propose a novel multi-function Vivaldi antenna with the capability to switch between wideband, notch band

and narrowband mode by combining the concepts described in chapter 5 and 6 respectively. The antenna in a wideband mode is designed to have a bandwidth of 2 – 8 GHz. In the notch band mode, the antenna has tunable narrowband rejection between 5.2 GHz and 5.7 GHz. The Vivaldi can also operate in a narrow pass band modes centred on 3.6, 3.9, 4.8, 5.5 and 6.5 GHz. The notch band reconfiguration is realized by incorporating a microstrip line resonator across the tapered slot on the opposite side of the substrate. The resonator can be deactivated to obtain the wideband mode. The narrowband operation is realized by inserting a pair of ring slots into the radiating element. Measured and simulated results are presented. Details of the proposed design are described. Antenna design is explained in section 7.2. In section 7.3, the antenna operations and simulation and measurement results are discussed. Finally the conclusions are presented in section 7.4.

7.2 Antenna Design

A planar Vivaldi with a tapered slot profile shown in Figure 7.1 is designed on Taconic TLY-5 substrate with ε_r = 2.2. The size and geometry of the basic Vivaldi antenna are similar as described in Chapter 6.

Two types of resonators have been incorporated into the Vivaldi structure. First, a Z shaped 0.4 mm width microstrip line resonator is located on the reverse side of the slot in order to create a band rejection mode. The resonator is located 6.7 mm above the feed line as shown in Fig 1(b). The resonator is placed in the transmission line region in the lower throat. The microstrip line resonator ($L_1 + L_2$) acts as an open stub and has 22.3 mm length. It has a gap, bridged by a variable capacitor, placed at distance L_1 = 6 mm from the left end to obtain a tunable band notch mode. L_1 is chosen to be 6 mm so that the notch band will

be considerably weak (low coupling to L_2) when capacitance is set to 0.1 pF. A weak band

rejection is useful to deactivate the effect of the resonator which is described later.
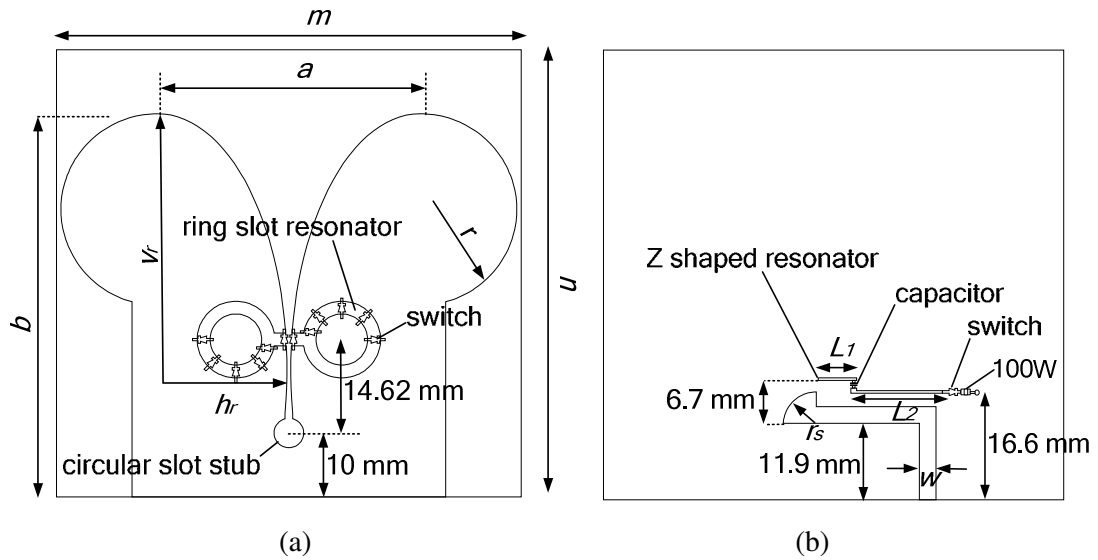
Figure 7.1 Antenna configuration (a) Front view, (b) Rear view

To obtain the wideband mode, the band notch element has to be deactivated. They

are sometimes effectively switched off by simply shifting them out of band. Due to the

wide bandwidth of this antenna, it has not been done here. Instead, the band notch is turned

off by connecting a resistor to the resonator.

To obtain the other function, a narrow pass band, a second resonator consisting of a

pair of ring slots is inserted into the radiating element. The centre of the ring slot is 14.62

mm above the center of circular slot stub. Similarly to the microstrip line resonator, the

ring slot is also placed at the lower throat of the tapered slot. The ring slot has an inner

radius of 4 mm and outer radius of 6 mm. Switches are positioned at specific locations.

Variation of the pass band response is achieved by setting up switch combinations as

shown in Figure 7.2. In the microstrip resonator, fixed capacitors are used to represent the

varactor. Metal pads of size 0.5 mm x 2 mm are used to represent the switches, such that

the presence and absence of the metal pad represents on and off states respectively. A prototype with ideal switches and fixed capacitors has been developed and tested. A prototype of the Vivaldi antenna with the ring slots and real switches but without the new notch tuning capability is described in detail in Chapter 5 and reported in [87].

Switch location and Pass band	
Band1 3.6 GHz	Band4 5.5 GHz
Band2 3.9 GHz	Band5 6.5 GHz
Band3 4.8 GHz	Wideband
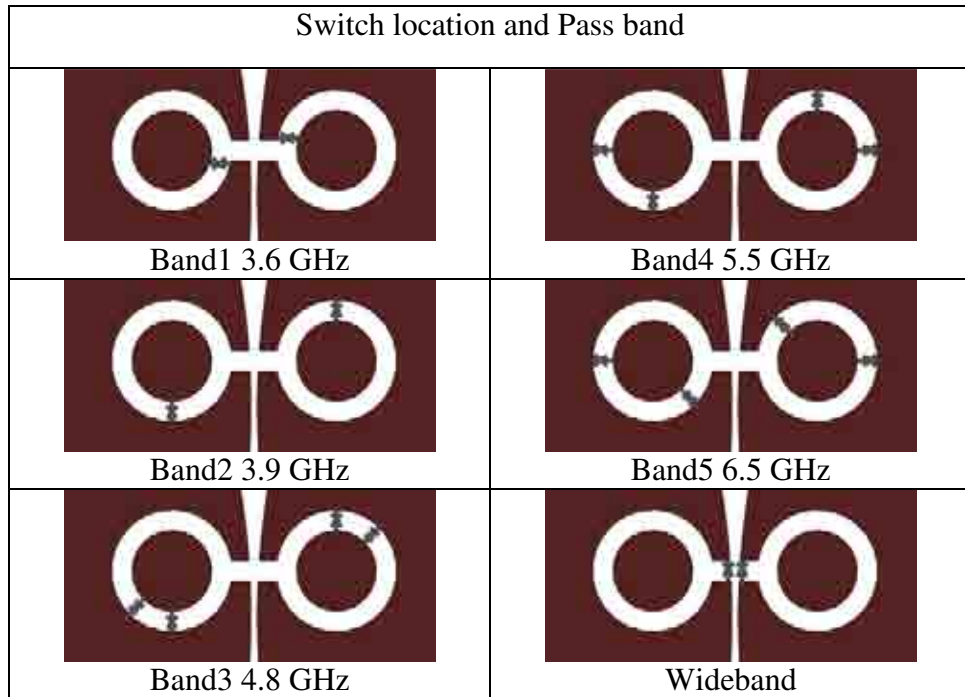
Figure 7.2 Pass band switch configuration

7.3 Antenna Operations and Results

A wideband mode is achieved after the ring slots are decoupled from the tapered slot by short circuiting the small gaps connecting them to the slot, whilst the capacitors on the microstrip line resonator are set to 0.1 pF and the resistive load is connected to switch off the notch. To deactivate the resonator, the capacitor is tuned to 0.1 pF, which electrically shortens the resonator and consequently reduces the coupling between L_1 and L_2. A low coupling between L_1 and L_2 reflects a weak notch. Figure 7.3 shows this, where a weak notch band is observed and the centre frequency of the band notch is approximately

corresponding to length L_2. With the weak notch, its effects can be easily removed by adding a resistive load at the other end via a PIN diode switch, which will change the standing wave at the coupling point. The resistor helps further to remove the notch band when the diode is in the on state. Because of the resistor location, only small current will flow through them. Figure 7.4 shows the effects of the notch band as a function of resistor value. By increasing the resistance, the unloaded Q is expected to be low and presumably the standing wave will also become low at the coupling point and this will probably reduce further the coupling factor. From parametric study, it was found that the notch band is removed completely when a 100 Ω resistor is used. A wide bandwidth of 2 – 8 GHz is achieved. Figure 7.5 shows the measured and simulated S_{11} in a wideband mode. Good agreement is observed. The measured S_{11} and the measured gain before and after the 100 Ω resistor is connected are shown in Figure 7.6 and Figure 7.7 respectively. Also compared in that Figure 7.7 is the reference antenna (without z-shaped and ring slot resonator). The notch effect from the gain suppression is removed after the resistive load is added and yet the gain is comparable with the reference gain.

To show how the resistive load helps in removing the notch effects, an equivalent circuit shown in Figure 7.8 (notes: given in previous chapter) is constructed. Figure 7.9 and Figure 7.10 compares the s-parameters and VSWR respectively, for a case when a 100 Ω resistor is connected or disconnected from the line. The capacitance is set to 0.1 pF. The stop band is reduced where the S_{11} is below -10 dB throughout the band. The VSWR is less than 2 for $R = 100$ Ω, indicating the coupling to the slot is very small, and therefore the resonator is effectively switched off hence killing the notch band and providing a wideband mode.
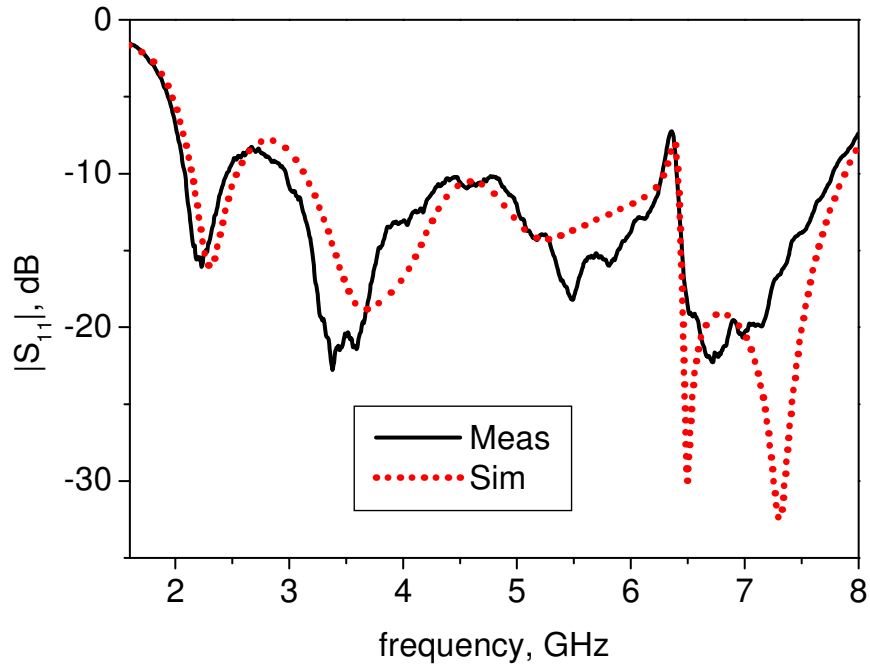
Figure 7.3 Frequency notch using 0.1 pF
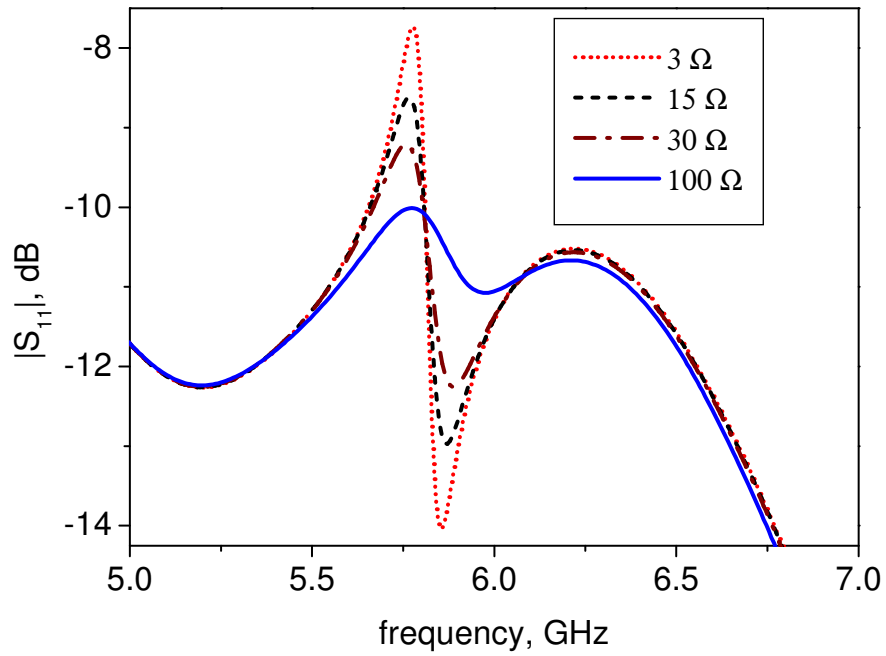
Figure 7.4 The effects of the notch band as a function of resistor value
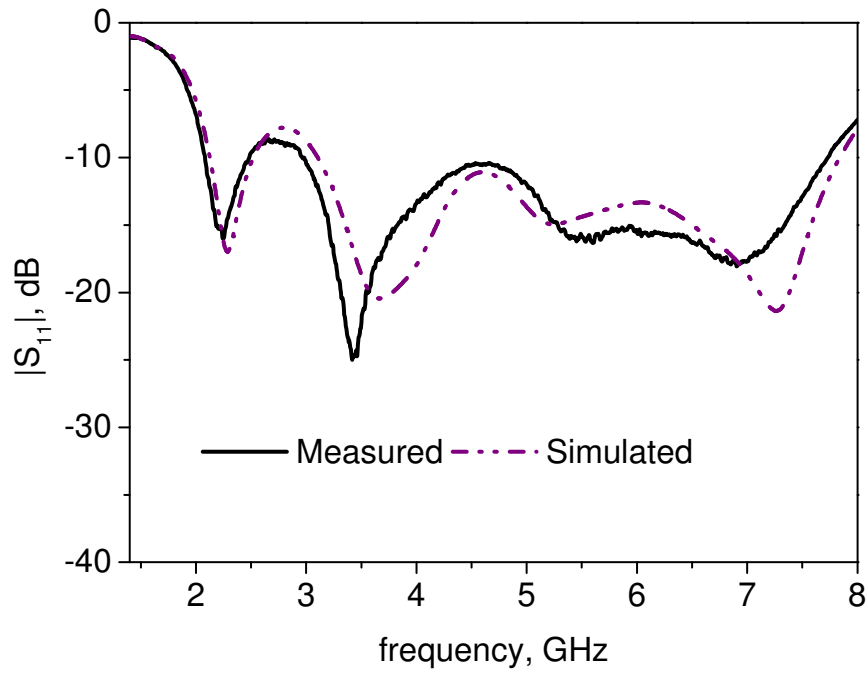
Figure 7.5 Wideband mode response
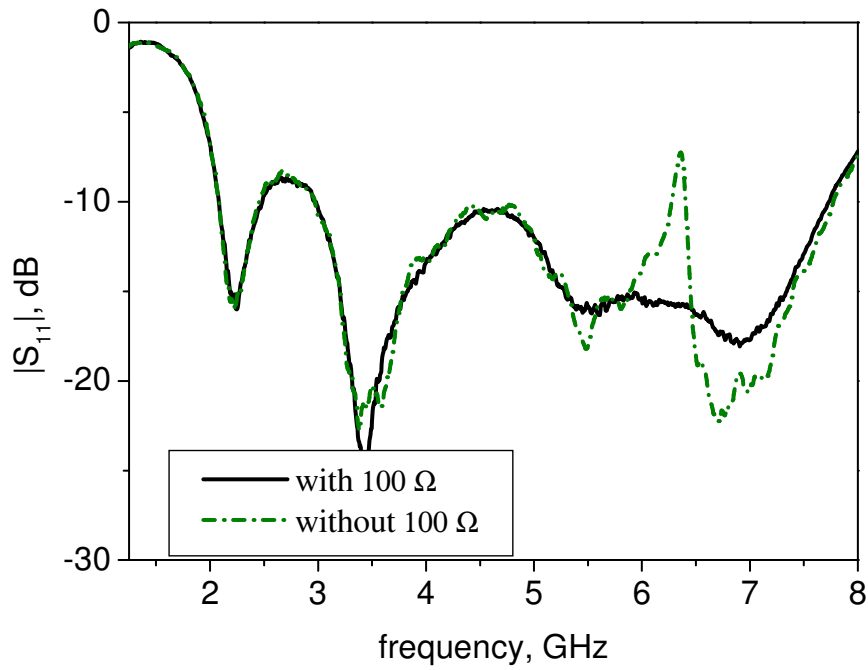
Figure 7.6 Measured S$_{11}$ with and without 100 Ω
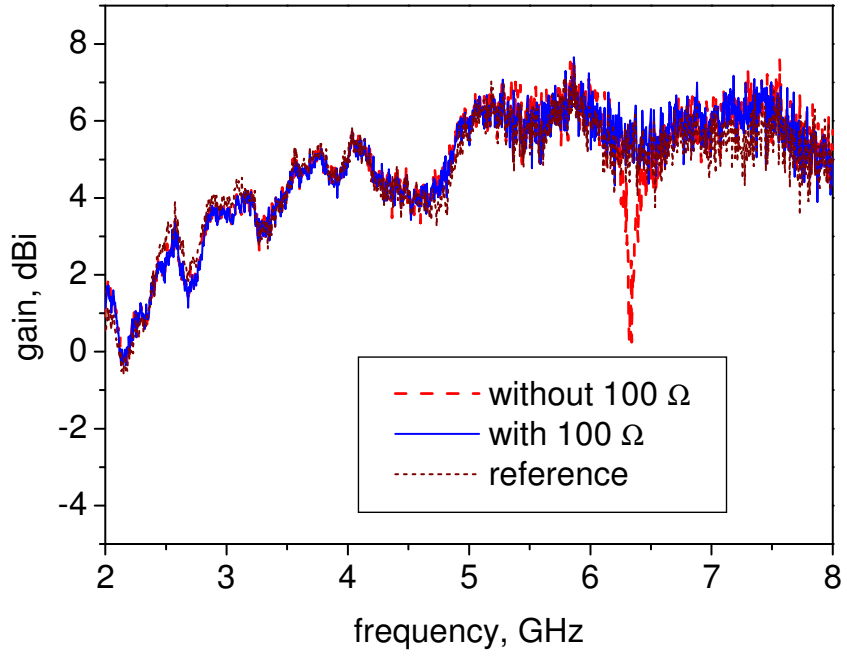
Figure 7.7 Resistor effects on gain
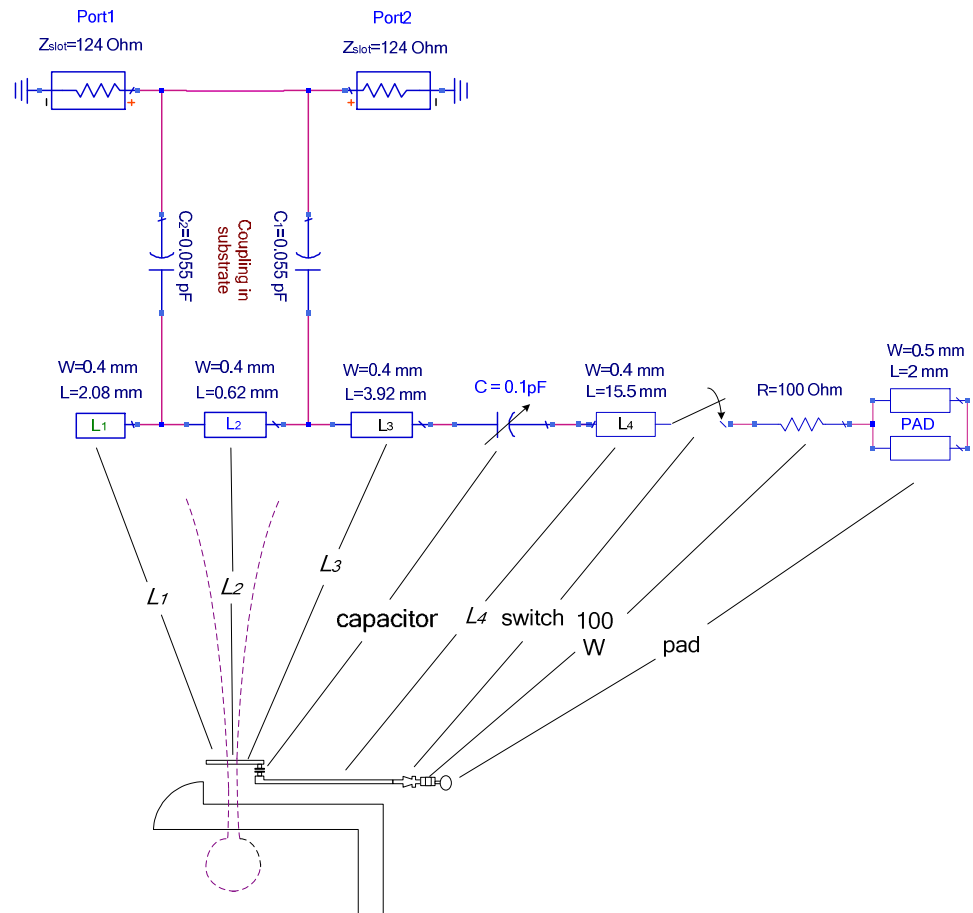
Figure 7.8 Equivalent circuit of the resonator where a single port is used to extract VSWR at the coupling point
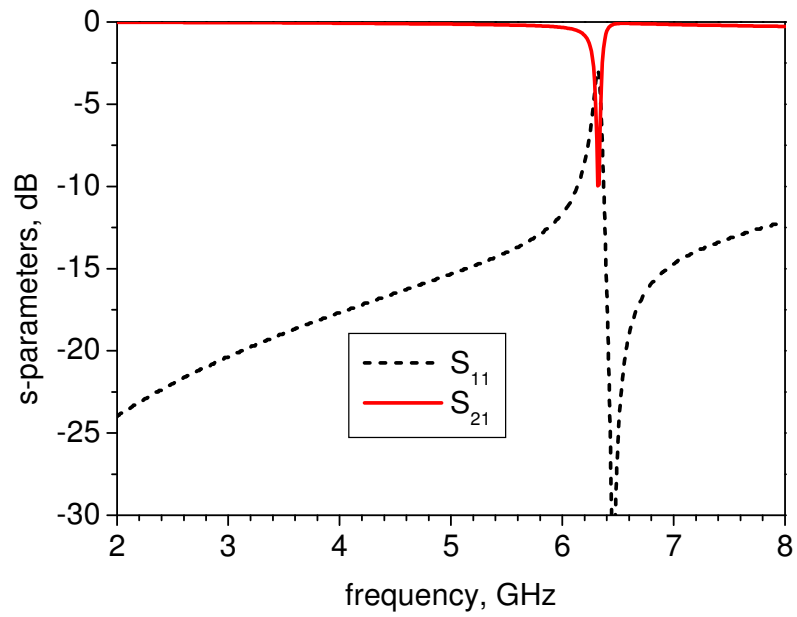
(a)
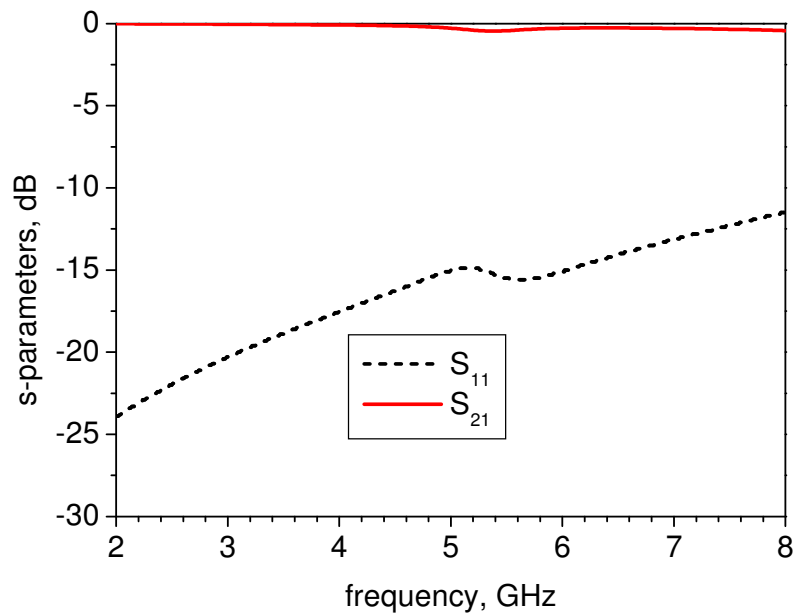
(b)

Figure 7.9 S-parameters of the resonator equivalent circuit when 100 Ω resistor is (a) disconnected, and (b) connected
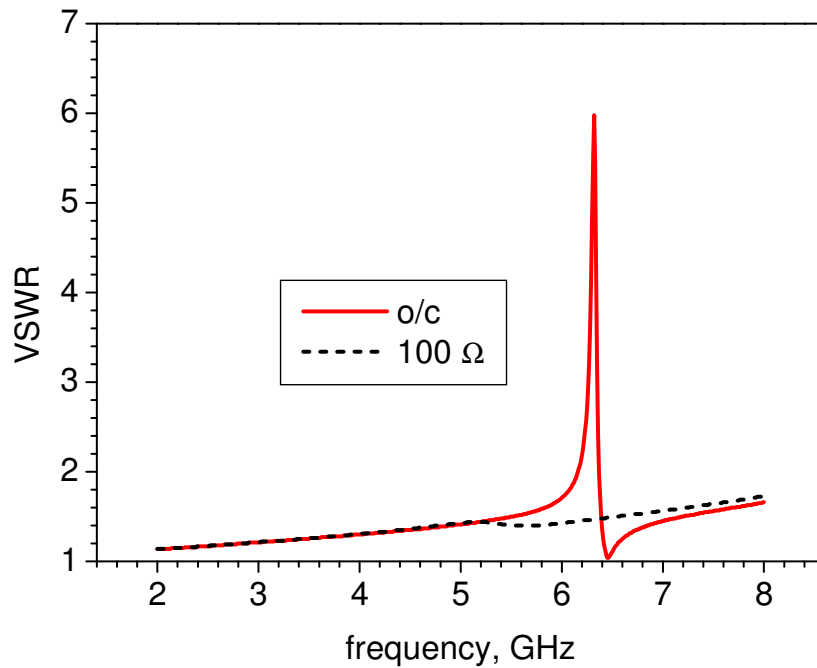
Figure 7.10 Resistor effects on VSWR, with and without R = 100 Ω

A tunable band rejection is obtained, when the resistive load in the resonator line is disconnected, whilst the capacitance is tuned from 5.6 pF to 0.3 pF. The band rejection centre frequency is varied from about 5.2 to 5.7 GHz respectively. Figure 7.11a and Figure 7.11b shows the simulated and measured S_{11} respectively in the notch band mode. On the whole good agreements are obtained. An example of the measured gain in the notch band mode is shown in Figure 7.12. A 10 to 15 dB gain reduction is observed.
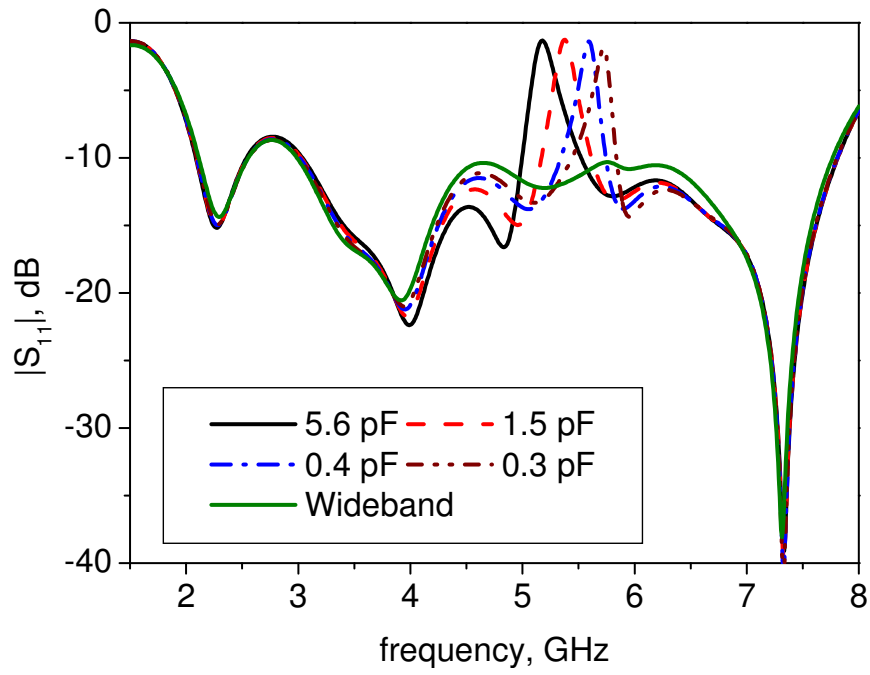
(a)
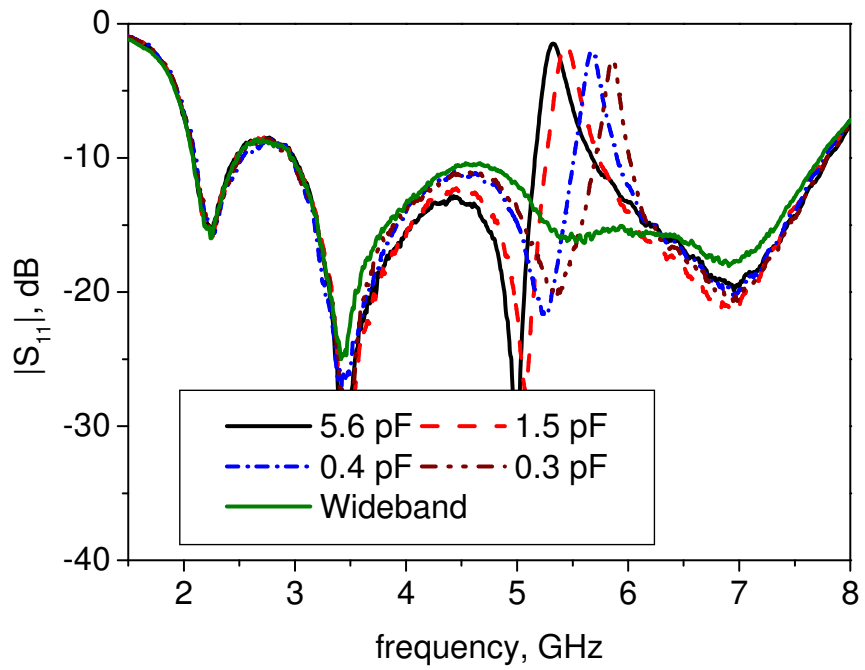
(b)

Figure 7.11 Notch band mode response, (a) Simulated, (b) Measured
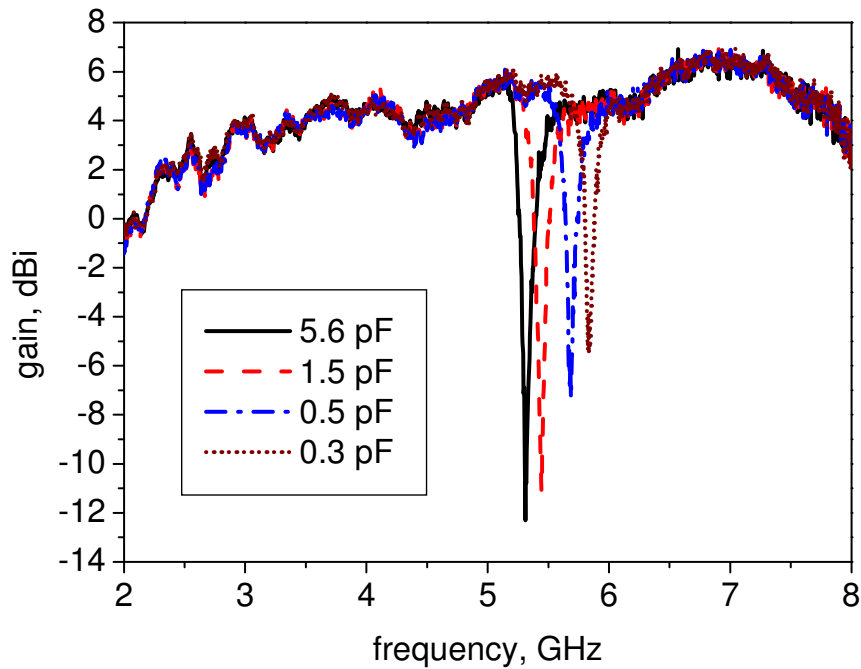
Figure 7.12 Measured gain in notch band mode

The narrow pass band mode is achieved when the ring slots are coupled to the tapered slot by open circuiting the small gaps, whilst the microstrip line resonator located below the ring slots is deactivated to avoid spurious. (If the position of the microstrip line resonator is after the ring slots the deactivation may not be needed). The capacitance is set to 0.1 pF. The ring slot is bridged as indicated in Figure 7.2 for the various frequencies. The narrow pass band mode is obtained either at 3.6 GHz, 3.9 GHz, 4.8 GHz, 5.5 GHz or 6.5 GHz. The simulated and measured S_{11} of the narrow band and wideband modes are shown in Figure 7.13. Figure 7.14 shows the simulated S_{11} of Band 1 when the microstrip line resonator is not deactivated. The spurious occurs at different frequencies corresponding to the effective electrical lengths arising from the capacitance values.

The measured and simulated gains are compared in Table 7.1. Table 7.2 compares how much loss the reconfiguration adds compared to the reference Vivaldi without any resonator inserted. The difference is observed in between 0.22 and 2.36 dB. The measured gain in wideband mode however is comparable with the reference Vivaldi as shown in Figure 7.15.

(a)

(b)
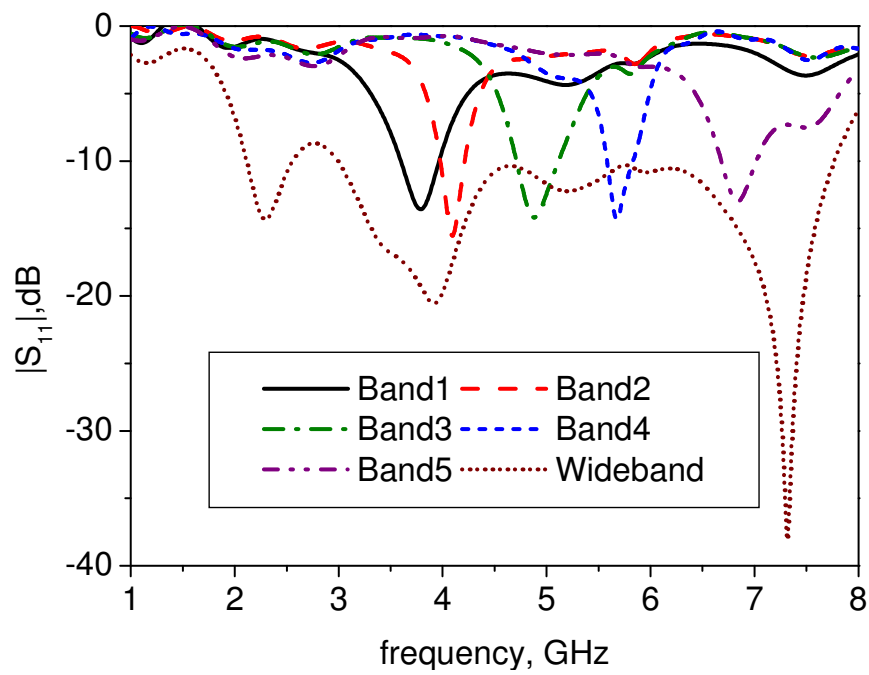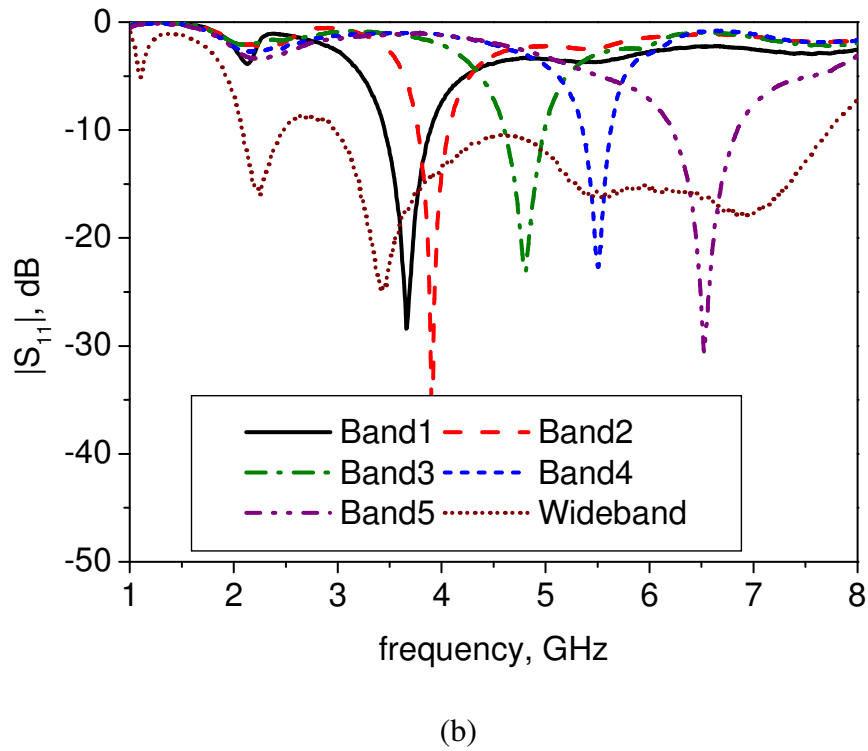
Figure 7.13 Frequency response (S₁₁) in narrow pass band and wideband modes (a) simulated, (b) measured
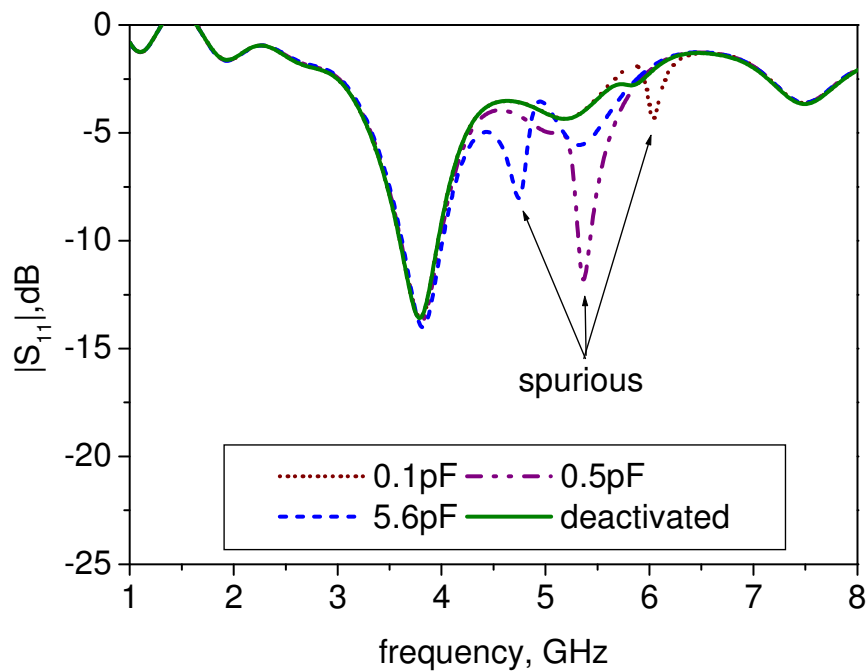
Figure 7.14 Simulated frequency response (S₁₁) in Band1 when microstrip line resonator is not deactivated

Table 7.1 Antenna gain in narrow pass band and wideband modes

Gain (dBi)	Band 1 (3.6GHz)	Band 2 (3.9GHz)	Band 3 (4.8GHz)	Band 4 (5.5GHz)	Band 5 (6.5GHz)	Wideband (5.5GHz)
Simulated	3.85	3.52	3.94	2.98	4.25	5.93
Measured	3.63	3.25	3.71	2.76	4.13	5.25

Table 7.2 Added losses to the antenna from the reconfiguration

Gain (dBi) (measured)	Band 1 (3.6GHz)	Band 2 (3.9GHz)	Band 3 (4.8GHz)	Band 4 (5.5GHz)	Band 5 (6.5GHz)
Proposed Vivaldi in narrowband mode	3.63	3.25	3.71	2.76	4.13
Reference Vivaldi without any reconfiguration	4.82	4.5	3.93	5.12	5.62
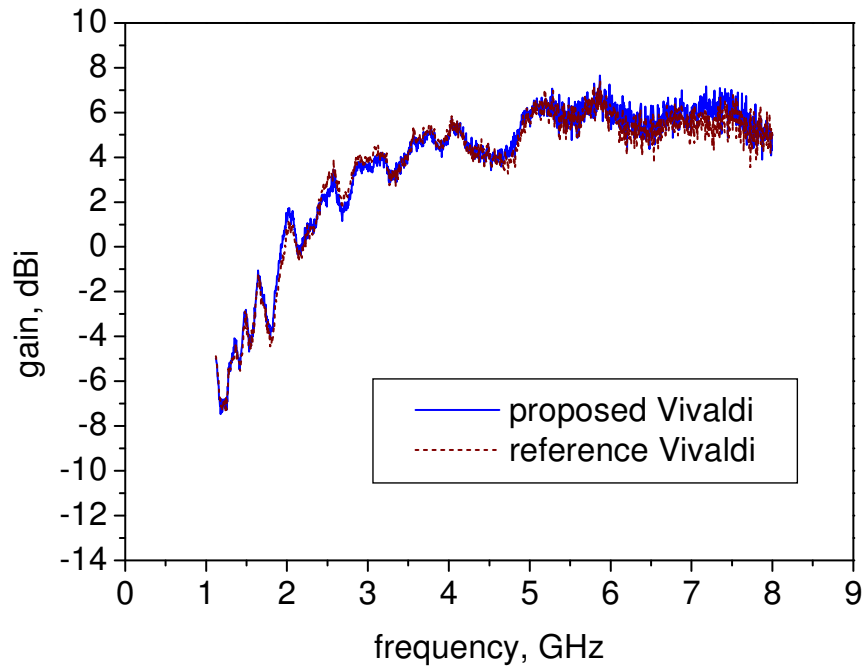
Figure 7.15 Measured gain of the proposed Vivaldi in wideband mode and reference Vivaldi without any reconfiguration

Example of radiation patterns for each mode, wide-, narrow-, and notch band excited at 5.5 GHz are shown in Figure 7.16. Well behaved patterns and good gain suppression at notch band are observed.

(a)

(b)
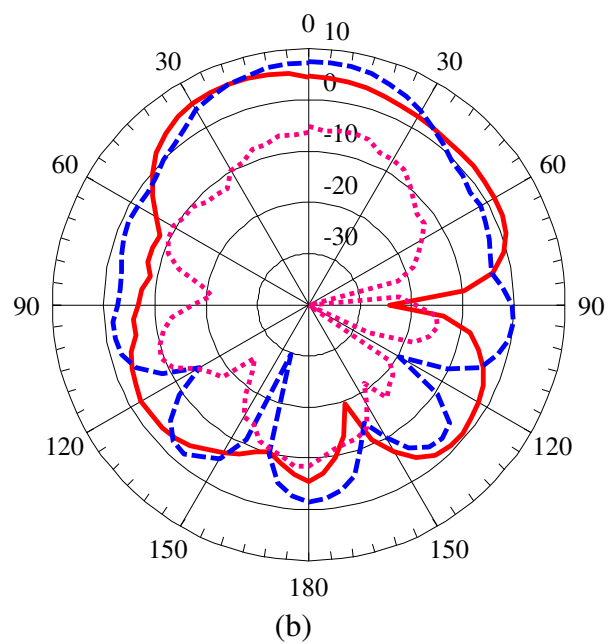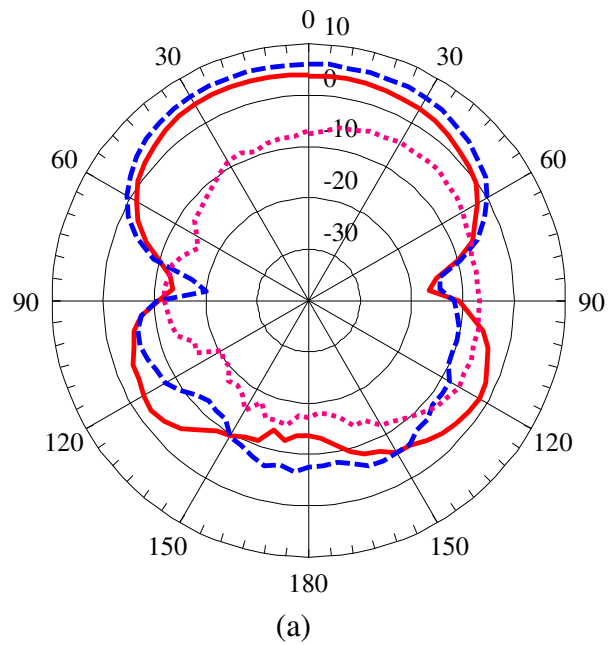
- - - wide
—— narrow
········ notch

Figure 7.16 Measured radiation pattern (a) H-plane (b) E-plane, excited at 5.5 GHz

7.4 Summary

A multi-function antenna has been developed and tested. Three main functions, namely wideband, notch band and narrow pass band, are achieved. A capability to switch from broad band operation to narrower band operations, and to include stop bands so that interference from other communications systems can be eliminated, has been introduced. The reconfiguration is realised by means of two types of resonant filter that can be switched in to interrupt the flow of currents in the edges of the slot transmission line. To obtain a narrow band mode, a simple band pass ring slot resonator has been introduced, whilst switching off the band notch effect is achieved by adding a resistor to the resonator. The antenna is believed advances the state of the art by introducing for the first time, a high degree of flexibility in a reconfigurable wideband antenna. The antenna can operate in 5 different sub bands whilst in wideband mode, and it can operate with or without band rejection. In addition, the band notch can be tuned between 5.2 and 5.7GHz. The performance shown verifies the proposed design concept. This work has been reported in [89].

CHAPTER 8

CONCLUSIONS AND FUTURE WORK

8.1 Conclusions

In this study two types of wideband antennas have been examined, to assess their suitability for frequency reconfiguration. One, the log periodic, as its name implies consists of many conventional antenna elements with size scaling, whilst the Vivaldi, represents the class of frequency independent antennas. The two types demonstrate different approaches to frequency band control. In the first, switching off the radiating elements can be performed whilst in the second it is necessary to introduce resonators.

8.1.1 Reconfigurable Log Periodic Patch Array [80, 81]

In this thesis, a log periodic antenna with added switched band functionality to operate in a wideband or narrowband mode has been presented [80, 81]. The antenna reconfiguration is realized by inserting switches into the slot aperture of the structure. A prototype with ideal switches has been developed. Measured results show good

performance of the proposed designs and good potential for a number of applications. However the antenna has some drawbacks. In particular the out of band rejection is relatively poor which is presumably due to poor feed line radiation screening. The roll off at the edge of the pass bands is also not fast enough (see Figure 3.32), when these parameters are compared to a well designed filter [90, 91]. In general terms though, filters are constructed with high Q elements, whose Qs are in the range of at least hundreds if not thousands. In addition fast roll off can be aided by design of individual resonator frequencies and coupling. This is hard to do in a log periodic antenna as the resonator frequencies are specified for the correct radiation properties. In addition the antenna needs low Q elements as each needs to radiate efficiently. Radiation loss thus reduces Q factors to less than 10 and sometimes less than 1. It is concluded that such reconfigurable antennas will only do a limited degree of pre-filtering before the front end. However the demands of future radio systems are so great, particularly in very wideband cognitive radio, that any pre-filtering from the antenna may be welcomed by systems designers.

8.1.2 Reconfigurable Vivaldi Antenna

In this thesis also, four different approaches to reconfigure the Vivaldi operating band have been shown. The first approach employed multiple slot rings in different positions [83-86]. The second approach employed a single set of slot rings with switchable length [87, 92]. Instead of using the slot, the third approach used a microstrip line resonator concept [75, 88]. The final approach used combined ring slots and a microstrip line resonator [89, 93]. The first two approaches show band pass reconfiguration, the third approach shows band notch reconfiguration and the final approach shows a high degree of flexibility in a reconfigurable Vivaldi.

8.1.2.1 Multiple position slot ring resonators [83-86]

In this first approach, it shows how coupling the slot ring to the tapered slot in different positions in the radiating region can reconfigure the operating band. In general the wider end of the Vivaldi structure is where the lowest band signals propagate and vice versa for the narrower end. Therefore by perturbing these areas it is possible to reject low and high frequency bands. The mid band operation is selected by positioning two ring slots in series which form a band pass filter.

8.1.2.2 Single position switchable length slot ring resonators [87, 92]

The second approach employed a single set of slot rings with switchable length. Instead of switching between different resonator positions, the second approach alters the operating frequency band by varying the electrical length of the resonators inserted into the tapered slot. This allows a better control of the operating bands but using only two slot ring resonators. The narrowband operation can be switched between six different frequency bands, which is double of what has been proposed in the multiple position ring resonators. The advance made in this work has been highlighted in 'In brief' section of the Electronics Letters volume 46, issue 7 which called 'Vivaldi's 7th'.

8.1.2.3 Microstrip line resonator [75, 88]

The third approach for altering the operating band of the Vivaldi antenna is by using microstrip line coupled resonators placed across the tapered slot in order to create band notches. The L shaped resonator is printed on the back of the substrate. To achieve a reconfigurable band notch, a varactor diode is integrated to the resonator. The resonant frequency then can be reconfigured by varying the capacitance value.

8.1.2.4 Combined ring and rectangular slot resonators [89, 93]

In the final approach, the second and the third approach are combined together. This antenna advances the state of the art by introducing for the first time, we believe, such a high degree of flexibility in a reconfigurable antenna. The antenna can operate in 5 different sub bands, whilst in wideband mode, it can operate with or without band rejection. In addition, the band notch can be tuned. This work has been selected as a feature article in Electronics Letters volume 46, issue 21 which called 'Vivaldi steps up a notch' [93].

Similar comments to those made about the reconfigurable log periodic patch array can also be made about the Vivaldi. The out of band rejection is relatively poor which is due to the substrate loss and the filter action. The roll off at the edge of the pass bands is also not fast enough. This can only be expected as the filtering or reconfiguration is achieved with a single resonator which has relatively low Q due to being mounted in an antenna. However unlike the log periodic patch array in which the filter elements were also the radiating elements, in the Vivaldi the resonators do not form part of the radiating structure. Thus there is some possible scope to increase their Q factor, such as use of higher dielectric constant substrate or the use of slot screening using additional ground planes above and below the slotted metallisations or even to introduce multiple resonator structures in the single switched ring configuration.

Examples have been demonstrated that changing the band over which the antenna operates is possible by switching off different patches group selection in log periodic array and by introducing ring slot or microstrip line within the Vivaldi. Some degree of reconfiguration is shown and verified. Nevertheless, there are rooms still can be improved as will described in the next section.

8.2 Future work

A novel reconfigurable log periodic patch array has been demonstrated by inserting ideal switches within the aperture slots. An array with real switches such as pin diodes could be implemented by following the described design guideline. However the off and on state model of the diode and decoupling components should be included in all calculations. In the demonstration described here, these were not included. In order to eliminate the structural stop band in the presence of the PIN diode, the off state model should be included to design a correct modulated impedance line. The same method is also applied when optimizing the low band performances. While using real switches, dc line and decoupling component must be included in the design. The biasing can be designed where each switch is controlled independently. This however requires a wider ground plane above the substrate to accommodate all the dc lines which is not available using the current shielding box. Therefore a new shielding box should be proposed. One potential design is shown in Figure 8.1. Instead of using a solid box, the new proposed design uses metal pins spaced apart by less than an eight wavelength at the cut off frequency of the waveguide, to approximate a solid box. This will then provide extra space for the dc lines. Figure 8.2 shows the simulated efficiency using a pin shielding box. A comparable out of band suppression with solid shielding box is shown. This however requires a complex fabrication process.

(a)

pin

(b)
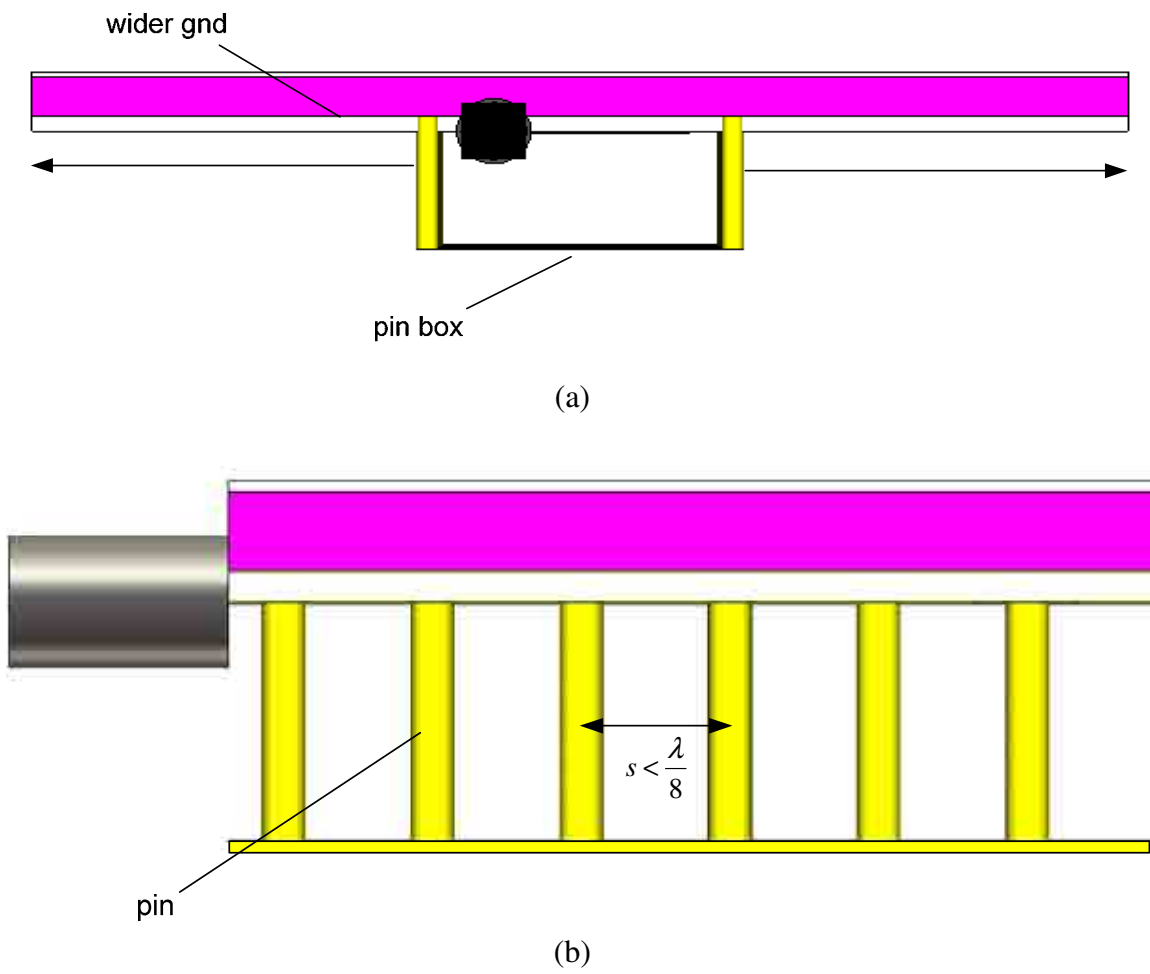
Figure 8.1 Proposed pins box (a) side view 1 (b) side view 2
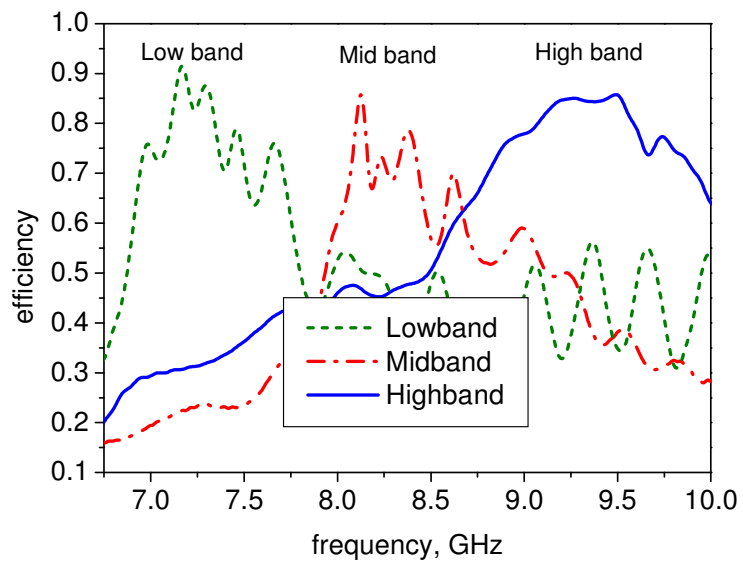
Figure 8.2 Simulated efficiency using pin box

Also, no attempts to suppress higher order modes in the patches have been made in the prototype described here. Higher order modes will give rise to patch excitation outside the desired band especially when a low band mode is selected. A method suggested in [94] by using a harmonic trap might be possible to used.

There is another different approach to frequency band control of log periodic arrays that can be investigated. Instead of switching off the radiating elements, selecting a different feed can also be performed. Figure 8.3 shows this. This method is also believed suitable to be implemented in log periodic electromagnetic coupled array types.
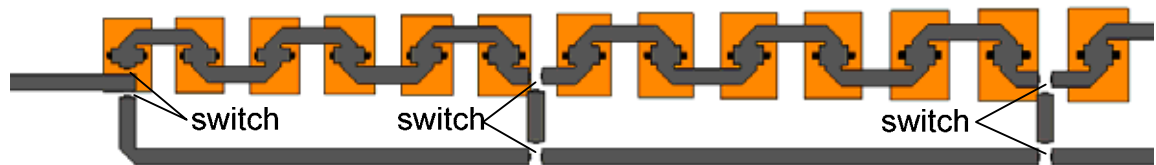
Figure 8.3 Selective feed method on LPA to frequency band control

In the Vivaldi reconfiguration, gaps of 4 mm are used to reduce spurious resonances at higher frequency due to parasitic capacitance across the gap sides. The width of the slot ring (4 mm) is also important to achieve a reasonably high quality factor of the narrowband modes. Therefore two diodes are used in series because a single diode having 1.2 mm length is unable to bridge the 4 mm gaps. However, this has double the series resistance and therefore double the loss in the on states. Further work might reveal alternative ways to design the gap that could be bridged by a single diode while avoiding spurious resonance problems as in the multiple ring configuration and maintaining the Q as in a single ring configuration.

Also, in the Vivaldi with a single pair of slot resonators, the switch arrangement style (asymmetric or symmetric) has an effect on the return loss and the radiation pattern. Generally, asymmetrical arrangements give a good match but the symmetry of the radiation pattern is slightly perturbed. Even though on the whole the radiation pattern is well behaved and it is hardly noticeable in the E-plane and H-plane polar plots, a symmetric radiation pattern is preferable. But in the symmetric switches configuration, a low match or high reflection will result. Further work might reveal better return loss in a symmetric arrangement. This might be achieved by positioning the ring slot section at the right position. The position of the ring slot section has an effect on the frequency response as described in Chapter 4 and reported in [85]. Alternatively, the symmetric switches configuration can be employed in an antipodal Vivaldi antenna arrangement. This will eliminate coupling between the feed line and the ring resonator and therefore, presumably, better return loss in a symmetric arrangement will result.

To further develop this work, it may be possible to use a varactor in a ring resonator, replacing all the switches. Instead of switched narrowband, a tunable narrowband is believed to be achievable.

In the Vivaldi with tunable band notch configuration, a third harmonic occurs when rejecting frequency at low band. Nevertheless, the length is designed so that the band rejection at the third harmonic occurs exactly at the WLAN frequency, 5.7 GHz. The tuning varactor, has been positioned in the line where the current at the third harmonic frequency is zero. Thus the 5.7 GHz stop band does not change with the varactor. Nevertheless it is interesting to have single notch at a time. Therefore further work on harmonic suppression is need to be done. Also, it is interesting to see the gain performances and the losses of the reconfiguration using real varactors.

Finally, even though real switches have been implemented in a single ring Vivaldi type [87], it is also interesting to see the performances of combined wide-narrow-notch reconfiguration using real switches and varactor. It is also interesting to see more antennas that can be reconfigured from wideband to single narrow band and also multiple narrow band, extending the previous work described in [95]. Also efficiency and linearity issues arising from real switches is suggested to be examined in the future work.

REFERENCES

[1] S. N. Yang, C. N. Zhang, H. K. Pan, A. E. Fathy, and V. K. Nair, "Frequency-Reconfigurable Antennas for Multiradio Wireless Platforms," *IEEE Microwave Magazine,* vol. 10, pp. 66-83, Feb 2009.

[2] J. Cho, C. W. Jung, and K. Kim, "Frequency-reconfigurable two-port antenna for mobile phone operating over multiple service bands," *Electronics Letters,* vol. 45, pp. 1009-1010, Sep 24 2009.

[3] T. Y. Han and C. T. Huang, "Reconfigurable monopolar patch antenna," *Electronics Letters,* vol. 46, pp. 199-U22, Feb 4 2010.

[4] S. L. S. Yang, A. A. Kishk, and K. F. Lee, "Frequency reconfigurable U-slot microstrip patch antenna," *IEEE Antennas and Wireless Propagation Letters,* vol. 7, pp. 127-129, 2008.

[5] A. F. Sheta and S. F. Mahmoud, "A widely tunable compact patch antenna," *IEEE Antennas and Wireless Propagation Letters,* vol. 7, pp. 40-42, 2008.

[6] T. Wu, R. L. Li, S. Y. Eom, S. S. Myoung, K. Lim, J. Laskar, S. I. Jeon, and M. M. Tentzeris, "Switchable Quad-Band Antennas for Cognitive Radio Base Station Applications," *IEEE Transactions on Antennas and Propagation,* vol. 58, pp. 1468-1476, May 2010.

[7] Y. Tawk and C. G. Christodoulou, "A New Reconfigurable Antenna Design for Cognitive Radio," *IEEE Antennas and Wireless Propagation Letters,* vol. 8, pp. 1378-1381, 2009.

[8] F. Ghanem, P. S. Hall, and J. R. Kelly, "Two port frequency reconfigurable antenna for cognitive radios," *Electronics Letters,* vol. 45, pp. 534-535, May 21 2009.

[9] P. S. Hall, P. Gardner, J. Kelly, E. Ebrahimi, M. R. Hamid, F. Ghanem, F. J. Herraiz-Martinez, and D. Segovia-Vargas, "Reconfigurable Antenna Challenges for Future Radio Systems," *2009 3rd European Conference on Antennas and Propagation, Vols 1-6,* pp. 902-908, 2009.

[10] P. S. Hall, M. R. Hamid, F. Ghanem, A. Mirkamali, and P. Gardner, "Reconfiguration of Vivaldi and log periodic antennas," in *Proc. Allerton Antenna Symposium* USA, 2009.

[11] C. Christodoulou, "Reconfigurable Antenna and the Military Applications," *IDGA 7th Military Antennas, http://www.militaryantennasevent.com*.

[12] C. Cordeiro, K. Challapali, D. Birru, and N. Sai Shankar, "IEEE 802.22: the first worldwide wireless standard based on cognitive radios," in *New Frontiers in Dynamic Spectrum Access Networks, 2005. DySPAN 2005. 2005 First IEEE International Symposium on*, 2005, pp. 328-337.

[13] J. Laskar, R. Mukhopadhyay, Y. Hur, C. H. Lee, and K. Lim, "Reconfigurable RFICs and modules for cognitive radio," in *Silicon Monolithic Integrated Circuits in RF Systems, 2006. Digest of Papers. 2006 Topical Meeting on*, 2006, p. 4 pp.

[14] H. Harada, "A Software Defined Cognitive Radio Prototype," in *Personal, Indoor and Mobile Radio Communications, 2007. PIMRC 2007. IEEE 18th International Symposium on*, 2007, pp. 1-5.

[15] B. A. Fette, *Cognitive Radio Technology*: Elsevier, Burlington, MA, 2009.

[16] V. H. Rumsey, *Frequency Independent Antennas*: Academic Press, New York and London, 1966.

[17]   D. Isbell, "Log periodic dipole arrays," *Antennas and Propagation, IRE Transactions on,* vol. 8, pp. 260-267, 1960.

[18]   A. Mirkamali and P. S. Hall, "Wideband frequency reconfiguration of a printed log periodic dipole array," *Microwave and Optical Technology Letters,* vol. 52, pp. 861-864, 2010.

[19]   P. B. Green and P. E. Mayes, "50-Ohm Log-Periodic Monopole Array with Modulated-Impedance Microstrip Feeder," *IEEE Transactions on Antennas and Propagation,* vol. Ap22, pp. 332-334, 1974.

[20]   C. A. Balanis, *Antenna Theory: Analysis and Design*, 3rd ed.: A John Wiley and Sons Inc Publication 2005.

[21]   P. S. Hall, "Multioctave bandwidth log-periodic microstrip antenna array," *Microwaves, Antennas and Propagation, IEE Proceedings H,* vol. 133, pp. 127-136, 1986.

[22]   H. Pues, J. Bogaers, R. Pieck, and A. van de Capelle, "Wideband quasi-log-periodic microstrip antenna," *Microwaves, Optics and Antennas, IEE Proceedings H,* vol. 128, pp. 159-163, 1981.

[23]   Emmanouil and Siakavara, "Design of a log-periodic aperture-fed microstrip antenna array," *Electrical Engineering (Archiv fur Elektrotechnik),* vol. 85, pp. 17-20, 2003.

[24]   A. Calmon, G. Pacheco, and M. Terada, "A novel reconfigurable UWB log-periodic antenna," in *Antennas and Propagation Society International Symposium 2006, IEEE*, 2006, pp. 213-216.

[25]   A. A. Gheethan and D. E. Anagnostou, "The design of reconfigurable planar log-periodic dipole array (LPDA) using switching elements," in *Antennas and Propagation Society International Symposium, 2009. APSURSI '09. IEEE*, 2009, pp. 1-4.

[26]   D. N. West and S. K. Sharma, "Frequency reconfigurable compact multiband quasi-log periodic dipole array (QLPDA) antenna for wireless communications," in *Antennas and Propagation Society International Symposium (APSURSI), 2010 IEEE*, 2010, pp. 1-4.

[27]   J. R. Mruk, W. N. Kefauver, and D. S. Filipovic, "Band Rejection Methods for Planar Log-Periodic Antennas," *Antennas and Propagation, IEEE Transactions on,* vol. 58, pp. 2288-2294, 2010.

[28]   C. Shih-Yuan, W. Po-Hsiang, and P. Hsu, "Uniplanar Log-Periodic Slot Antenna Fed by a CPW for UWB Applications," *Antennas and Wireless Propagation Letters, IEEE,* vol. 5, pp. 256-259, 2006.

[29]   G. Lin, H. Fengyi, W. Yan, and T. Xusheng, "A band-notched UWB log-periodic dipole antenna fed by strip line," in *Ultra-Wideband (ICUWB), 2010 IEEE International Conference on*, 2010, pp. 1-4.

[30]   P. J. Gibson, "The Vivaldi Aerial," in *Microwave Conference, 1979. 9th European*, 1979, pp. 101-105.

[31]   R. Janaswamy and D. H. Schaubert, "Analysis of the Tapered Slot Antenna," *IEEE Transactions on Antennas and Propagation,* vol. 35, pp. 1058-1065, Sep 1987.

[32]   R. Q. Lee and R. N. Simons, "Effect of curvature on tapered slot antennas," *IEEE Antennas and Propagation Society International Symposium - 1996 Digest, Vols 1-3,* pp. 188-191, 1996.

[33]   P. Knott and A. Bell, "Coaxially-fed tapered slot antenna," *Electronics Letters,* vol. 37, pp. 1103-1104, 2001.

[34] H. Kim and C. W. Jung, "Ultra-wideband endfire directional tapered slot antenna using CPW to wide-slot transition," *Electronics Letters,* vol. 46, pp. 1183-1185, 2010.

[35] E. Gazit, "Improved Design of the Vivaldi Antenna," *IEE Proceedings-H Microwaves Antennas and Propagation,* vol. 135, pp. 89-92, Apr 1988.

[36] J. D. S. Langley, P. S. Hall, and P. Newham, "Novel Ultrawide-Bandwidth Vivaldi Antenna with Low Cross-Polarization," *Electronics Letters,* vol. 29, pp. 2004-2005, Nov 11 1993.

[37] A. Z. Hood, T. Karacolak, and E. Topsakal, "A Small Antipodal Vivaldi Antenna for Ultrawide-Band Applications," *Antennas and Wireless Propagation Letters, IEEE,* vol. 7, pp. 656-660, 2008.

[38] I. J. Yoon, H. Kim, H. K. Yoon, Y. J. Yoon, and Y. H. Kim, "Ultra-wideband tapered slot antenna with band cutoff characteristic," *Electronics Letters,* vol. 41, pp. 629-630, May 26 2005.

[39] M. John, M. J. Ammann, and P. McEvoy, "UWB Vivaldi antenna based on a spline geometry with frequency band-notch," in *Antennas and Propagation Society International Symposium, 2008. AP-S 2008. IEEE*, 2008, pp. 1-4.

[40] Y. Yashchyshyn, "Reconfigurable antennas by RF switches technology," in *Perspective Technologies and Methods in MEMS Design, 2009. MEMSTECH 2009. 2009 5th International Conference on*, 2009, pp. 155-157.

[41] P. Gardner, M. R. Hamid, P. S. Hall, J. Kelly, F. Ghanem, and E. Ebrahimi, "Reconfigurable Antennas for Cognitive Radio: Requirements and Potential Design Approaches," in *Wideband, Multiband Antennas and Arrays for Defence or Civil Applications, 2008 Institution of Engineering and Technology Seminar on*, 2008, pp. 89-94.

[42] G. M. Rebeiz and J. B. Muldavin, "RF MEMS switches and switch circuits," *Microwave Magazine, IEEE,* vol. 2, pp. 59-71, 2001.

[43] N. Symeon, R. Bairavasubramanian, C. Lugo, Jr., I. Carrasquillo, D. C. Thompson, G. E. Ponchak, J. Papapolymerou, and M. M. Tentzeris, "Pattern and frequency reconfigurable annular slot antenna using PIN diodes," *Antennas and Propagation, IEEE Transactions on,* vol. 54, pp. 439-448, 2006.

[44] C. Medeiros, J. R. Costa, and C. A. Fernandes, "MEMS reconfigurable stacked antenna for WLAN applications," in *Antennas and Propagation Society International Symposium, 2008. AP-S 2008. IEEE*, 2008, pp. 1-4.

[45] N. Behdad and K. Sarabandi, "A varactor-tuned dual-band slot antenna," *Antennas and Propagation, IEEE Transactions on,* vol. 54, pp. 401-408, 2006.

[46] T. Kato, Y. Tanaka, H. Ueda, H. Kano, and M. Hashimoto, "L-band phase shifter with switching FET's for phased array antenna," in *Microwave Symposium Digest, 1992., IEEE MTT-S International*, 1992, pp. 1527-1530 vol.3.

[47] B. Z. Wang, S. Xiao, and J. Wang, "Reconfigurable patch-antenna design for wideband wireless communication systems," *IET Microwaves Antennas & Propagation,* vol. 1, pp. 414-419, Apr 2007.

[48] M. Ali, A. T. M. Sayem, and V. K. Kunda, "A reconfigurable stacked microstrip patch antenna for satellite and terrestrial links," *IEEE Transactions on Vehicular Technology,* vol. 56, pp. 426-435, Mar 2007.

[49] C. W. Jung, Y. J. Kim, Y. E. Kim, and F. De Flaviis, "Macro-micro frequency tuning antenna for reconfigurable wireless communication systems," *Electronics Letters,* vol. 43, pp. 201-202, Feb 15 2007.

[50] K. Sakamoto, E. Nishiyama, and M. Aikawa, "Active microstrip planar antenna for frequency switching," *Electronics and Communications in Japan Part I-Communications,* vol. 88, pp. 1-8, 2005.

[51] K. R. Boyle and P. G. Steeneken, "A five-band reconfigurable PIFA for mobile phones," *IEEE Transactions on Antennas and Propagation,* vol. 55, pp. 3300-3309, Nov 2007.

[52] A. C. K. Mak, C. R. Rowell, R. D. Murch, and C. L. Mak, "Reconfigurable multiband antenna designs for wireless communication devices," *IEEE Transactions on Antennas and Propagation,* vol. 55, pp. 1919-1928, Jul 2007.

[53] E. Ebrahimi and P. S. Hall, "Integrated wide–narrow band antenna for multiband applications," *Microwave and Optical Technology Letters,* vol. 52, pp. 425-430, 2010.

[54] J. R. Kelly, P. S. Hall, P. Gardner, and F. Ghanem, "Integrated narrow/band-notched UWB antenna," *Electronics Letters,* vol. 46, pp. 814-815, Jun 10 2010.

[55] F. J. Herraiz-Martinez, P. S. Hall, and D. Segovia-Vargas, "Application of the Left-Handed half-loop antenna with wideband tuning to a Cognitive Radio terminal," in *Antennas and Propagation (EuCAP), 2010 Proceedings of the Fourth European Conference on*, 2010, pp. 1-4.

[56] M. Al-Husseini, A. El-Hajj, Y. Tawk, K. Y. Kabalan, and C. G. Christodoulou, "A simple dual-port antenna system for cognitive radio applications," in *High Performance Computing and Simulation (HPCS), 2010 International Conference on*, 2010, pp. 549-552.

[57] Y. Tawk, M. Al-Husseini, S. Hemmady, A. R. Albrecht, G. Balakrishnan, and C. G. Christodoulou, "Implementation of a cognitive radio front-end using optically reconfigurable antennas," in *Electromagnetics in Advanced Applications (ICEAA), 2010 International Conference on*, 2010, pp. 294-297.

[58] J. R. Kelly, P. S. Hall, and P. Gardner, "Integrated wide-narrow band antenna for switched operation," in *Antennas and Propagation, 2009. EuCAP 2009. 3rd European Conference on*, 2009, pp. 3757-3760.

[59] J. R. Kelly and P. S. Hall, "Reconfigurable slot antenna for Cognitive Radio applications," in *Antennas and Propagation Society International Symposium, 2009. APSURSI '09. IEEE*, 2009, pp. 1-4.

[60] F. Ghanem, J. R. Kelly, and P. S. Hall, "Switched UWB to narrowband planar monopole antenna," in *Antennas and Propagation (EuCAP), 2010 Proceedings of the Fourth European Conference on*, 2010, pp. 1-3.

[61] Z. Zhou and K. L. Melde, "Frequency agility of broadband antennas integrated with a reconfigurable RF impedance tuner," *IEEE Antennas and Wireless Propagation Letters,* vol. 6, pp. 56-59, 2007.

[62] Z. D. Liu, K. Boyle, J. Krogerus, M. de Jongh, K. Reimann, R. Kaunisto, and J. Ollikainen, "MEMS-Switched, Frequency-Tunable Hybrid Slot/PIFA Antenna," *IEEE Antennas and Wireless Propagation Letters,* vol. 8, pp. 311-314, 2009.

[63] H. F. A. Tarboush, S. Khan, R. Nilavalan, H. S. Al-Raweshidy, and D. Budimir, "Reconfigurable wideband patch antenna for cognitive radio," in *Antennas & Propagation Conference, 2009. LAPC 2009. Loughborough*, 2009, pp. 141-144.

[64] W. Sung-Jung, K. Cheng-Hung, C. Keng-Hsien, and T. Jenn-Hwan, "Study of an Ultrawideband Monopole Antenna With a Band-Notched Open-Looped Resonator," *Antennas and Propagation, IEEE Transactions on,* vol. 58, pp. 1890-1897, 2010.

[65] W. S. Lee, D. Z. Kim, K. J. Kim, and J. W. Yu, "Wideband planar monopole antennas with dual band-notched characteristics," *IEEE Transactions on Microwave Theory and Techniques,* vol. 54, pp. 2800-2806, Jun 2006.

[66] K. S. Ryu and A. A. Kishk, "UWB Antenna With Single or Dual Band-Notches for Lower WLAN Band and Upper WLAN Band," *Antennas and Propagation, IEEE Transactions on,* vol. 57, pp. 3942-3950, 2009.

[67] Y. L. Zhao, Y. C. Jiao, G. Zhao, L. Zhang, Y. Song, and Z. B. Wong, "Compact planar monopole UWB antenna with band-notched characteristic," *Microwave and Optical Technology Letters,* vol. 50, pp. 2656-2658, Oct 2008.

[68] J. Perruisseau-Carrier, P. Pardo-Carrera, and P. Miskovsky, "Modeling, Design and Characterization of a Very Wideband Slot Antenna With Reconfigurable Band Rejection," *Antennas and Propagation, IEEE Transactions on,* vol. 58, pp. 2218-2226, 2010.

[69] S. Nikolaou, N. D. Kingsley, G. E. Ponchak, J. Papapolymerou, and M. M. Tentzeris, "UWB Elliptical Monopoles With a Reconfigurable Band Notch Using MEMS Switches Actuated Without Bias Lines," *IEEE Transactions on Antennas and Propagation,* vol. 57, pp. 2242-2251, Aug 2009.

[70] A. H. Khidre, H. A. El Sadek, and H. F. Ragai, "Reconfigurable UWB printed monopole antenna with band rejection covering IEEE 802.11a/h," in *Antennas and Propagation Society International Symposium, 2009. APSURSI '09. IEEE*, 2009, pp. 1-4.

[71] E. Antonino-Daviu, M. Cabedo-Fabres, M. Ferrando-Bataller, and A. Vila-Jimenez, "Active UWB antenna with tunable band-notched behaviour," *Electronics Letters,* vol. 43, pp. 959-960, 2007.

[72] J. Won-Seok, L. Sang-Yun, L. Won-Gyu, L. Ho, and Y. Jong-Won, "Tunable Band-notched Ultra Wideband (UWB) Planar Monopole Antennas Using Varactor," in *Microwave Conference, 2008. EuMC 2008. 38th European*, 2008, pp. 266-268.

[73] Z. H. Hu, P. S. Hall, J. R. Kelly, and P. Gardner, "UWB pyramidal monopole antenna with wide tunable band-notched behaviour," *Electronics Letters,* vol. 46, pp. 1588-1590, 2010.

[74] B. Rahmati and H. R. Hassani, "Wideband planar plate monopole antenna with dual tunable notch," *Electronics Letters,* vol. 46, pp. 480-481, Apr 5 2010.

[75] M. R. Hamid, P. Gardner, P. S. Hall, and F. Ghanem, "Vivaldi with Tunable Narrow band Rejection," *Microwave and Optical Technology Letters,vol 53, no 5 ,* 2011.

[76] G. Ruvio, M. J. Ammann, and C. Zhi Ning, "Wideband Reconfigurable Rolled Planar Monopole Antenna," *Antennas and Propagation, IEEE Transactions on,* vol. 55, pp. 1760-1767, 2007.

[77] K. W. Lam and E. K. N. Yung, "Series feed aperture-coupled leaky wave antenna," in *Antennas and Propagation Society International Symposium, 2000. IEEE*, 2000, pp. 706-709 vol.2.

[78] P. Ingerson and P. Mayes, "Log-periodic antennas with modulated impedance feeders," *Antennas and Propagation, IEEE Transactions on,* vol. 16, pp. 633-642, 1968.

[79] D. M. Pozar, *Microwave Engineering*, 2nd ed.: Wiley, New York Chichester, 1998.

[80] M. R. Hamid, P. S. Hall, and P. Gardner, "Frequency Reconfigurable Log Periodic Patch Array," *Electronics Letters,* vol. 46, pp. 1648-1650, Dec 9 2010.

[81]   M. R. Hamid, P. Gardner, and P. S. Hall, "Reconfigurable log periodic aperture fed microstrip antenna," in *Antennas & Propagation Conference, 2009. LAPC 2009. Loughborough*, 2009, pp. 237-239.

[82]   P. Li, J. Liang, and X. Chen, "UWB Tapered-Slot-Fed Antenna," in *Ultra Wideband Systems, Technologies and Applications, 2006. The Institution of Engineering and Technology Seminar on*, 2006, pp. 235-238.

[83]   M. R. Hamid, P. S. Hall, P. Gardner, and F. Ghanem, "Frequency reconfigurable Vivaldi antenna," in *Antennas and Propagation (EuCAP), 2010 Proceedings of the Fourth European Conference on*, 2010, pp. 1-4.

[84]   M. R. Hamid, P. Gardner, P. S. Hall, and F. Ghanem, "Reconfigurable Vivaldi Antenna," *Microwave and Optical Technology Letters,* vol. 52, pp. 785-787, Apr 2010.

[85]   M. R. Hamid, P. Gardner, P. S. Hall, and F. Ghanem, "Switched Band Vivaldi Antenna," *IEEE Transactions on Antennas and Propagation, vol 53, no 5*, 2011.

[86]   M. R. Hamid, P. Gardner, P. S. Hall, and F. Ghanem, "Switchable wideband-narrowband tapered slot antenna," in *Antennas & Propagation Conference, 2009. LAPC 2009. Loughborough*, 2009, pp. 241-244.

[87]   M. R. Hamid, P. S. Hall, P. Gardner, and F. Ghanem, "Switchable filtering in Vivaldi antenna," *Electronics Letters,* vol. 46, pp. 477-478, Apr 1 2010.

[88]   M. R. Hamid, P. Gardner, P. S. Hall, and F. Ghanem, "Reconfigurable Vivaldi Antenna with Tunable Stop Band," *IWAT 2011, Hong Kong, 7-9 March*, 2011.

[89]   M. R. Hamid, P. Gardner, P. S. Hall, and F. Ghanem, "Multimode Vivaldi antenna," *Electronics Letters,* vol. 46, pp. 1424-1425, Oct 14 2010.

[90]   W. Peng and I. Hunter, "Electronically Tunable Filters," *Microwave Magazine, IEEE,* vol. 10, pp. 46-54, 2009.

[91]   G. Rebeiz, K. Entesari, I. Reines, S. J. Park, M. El-tanani, A. Grichener, and A. Brown, "Tuning in to RF MEMS," *Microwave Magazine, IEEE,* vol. 10, pp. 55-72, 2009.

[92]   M. R. Hamid, P. Gardner, P. S. Hall, and F. Ghanem, "Vivaldi Antenna with Integrated Switchable Pass Band Resonator," *IEEE Transactions on Antennas and Propagation,* submitted, 2011.

[93]   "Vivaldi steps up a notch," *Electronics Letters,* vol. 46, pp. 1412-1412, 2010.

[94]   A. Mirkamali, P. S. Hall, and M. Soleimani, "Reconfigurable printed-dipole antenna with harmonic trap for wideband applications," *Microwave and Optical Technology Letters,* vol. 48, pp. 927-929, May 2006.

[95]   M. R. Hamid, P. S. Hall, P. Gardner, and F. Ghanem, "Switched WLAN-wideband tapered slot antenna," *Electronics Letters,* vol. 46, pp. 23-24, Jan 7 2010.

**Appendix A: Switched DC voltages**

Figure A1 shows the antenna described in chapter 4. Shown here is the example of two pin diode switches, biased with a DC voltage. The lumped element equivalent circuit in Figure A1 for bias purposes, is shown in Figure A2. In ON state, the forward current of the circuit is set to 100 mA. the maximum rating allowed is 100 mA in order to achieve the smallest forward resistance. The typical ON state resistance is 3 ohm. The diode forward voltage is in between 0.95 and 1.1 volt for 50 mA forward current. Details of diode parameters can be found from the diode datasheet in Appendix C. With the total of 90 ohm current limiter resistor, the supplied DC voltage will be approximately 11 volt to achieve 100 mA forward current. A photograph of the DC power supply is shown in Figure A3. The OFF state is obtained by leaving the PIN diode unbiased. Figure A4 shows the photograph of antenna in Figure A1. Figure A5 shows the antenna described in chapter 5, showing the example of two pin diode switches, biased with a DC voltage. Similar biasing methods are used.
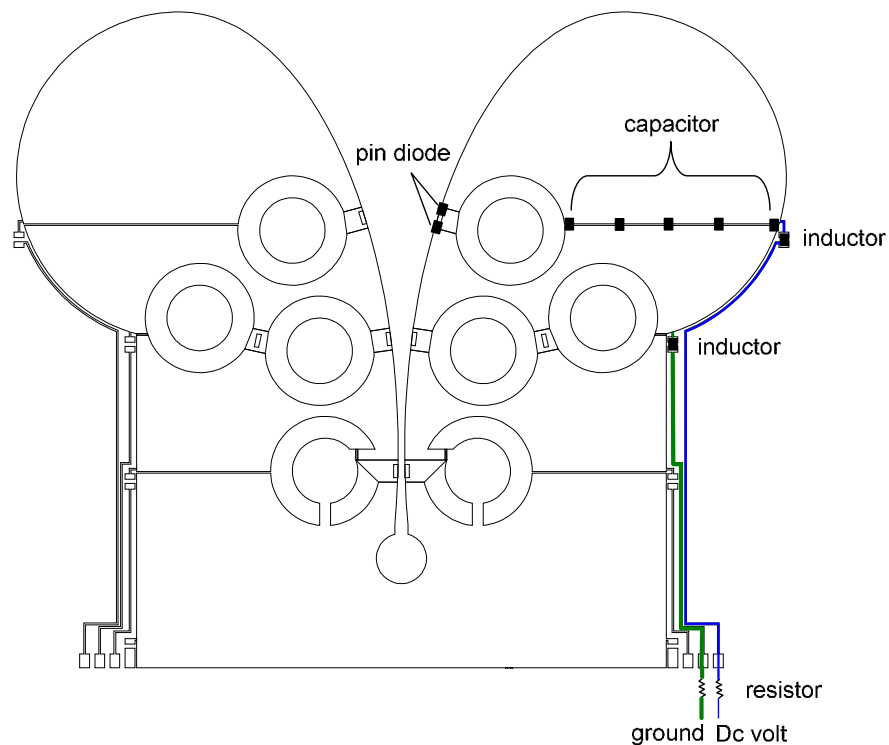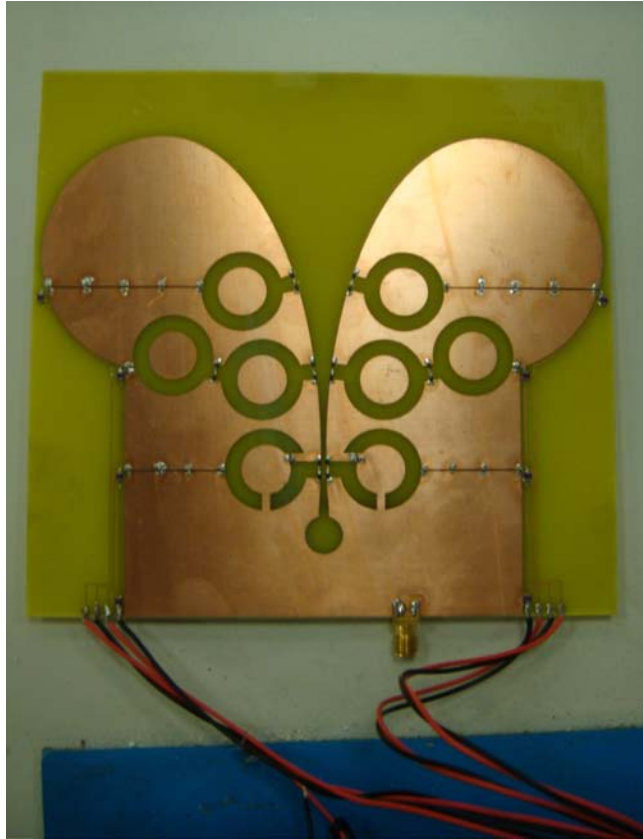

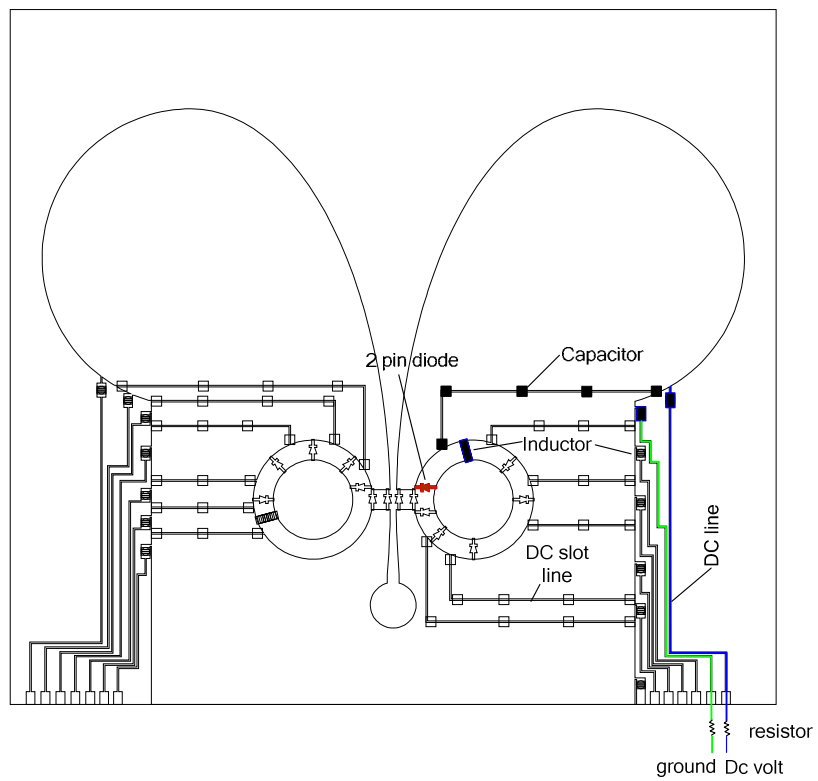**Figure A1: Multiple ring Vivaldi antenna with bias circuit**
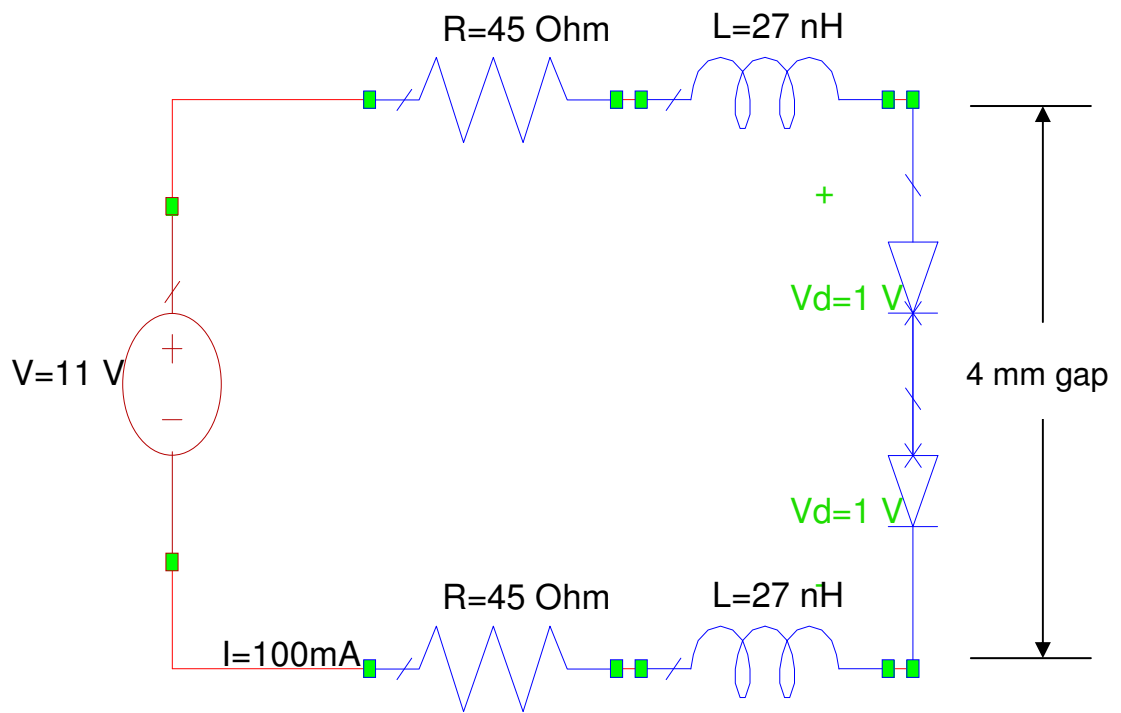
Figure A2: Lumped element bias circuit in Figure A1
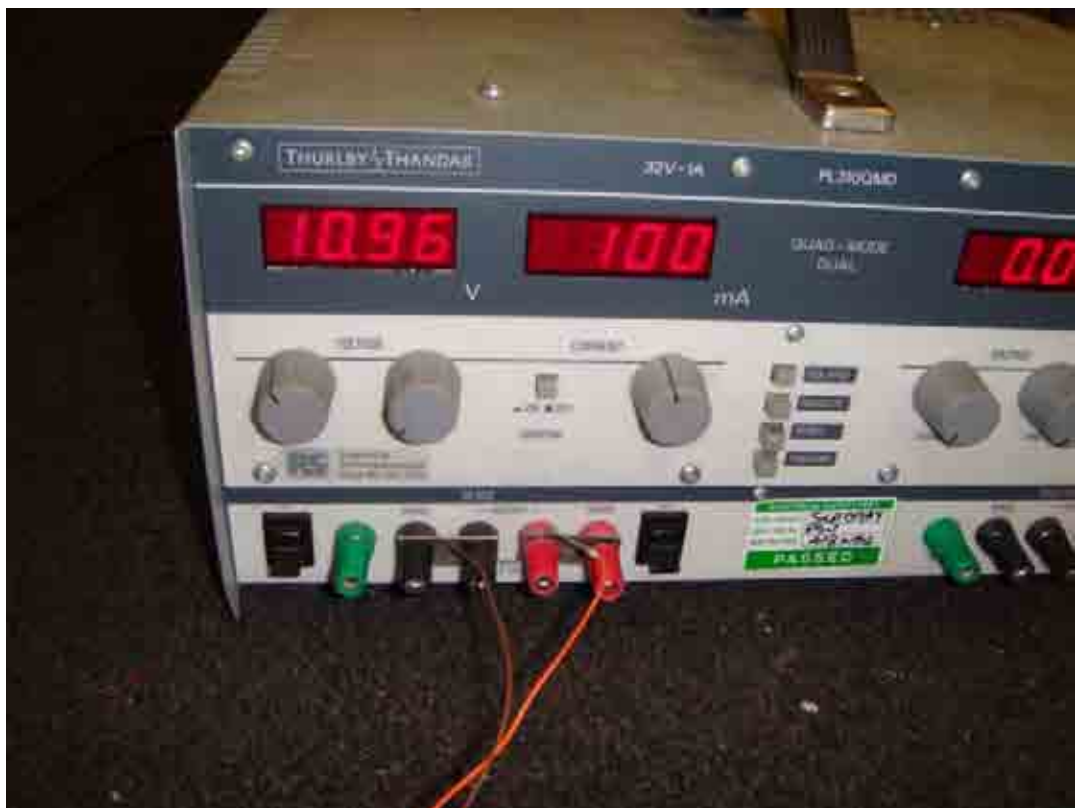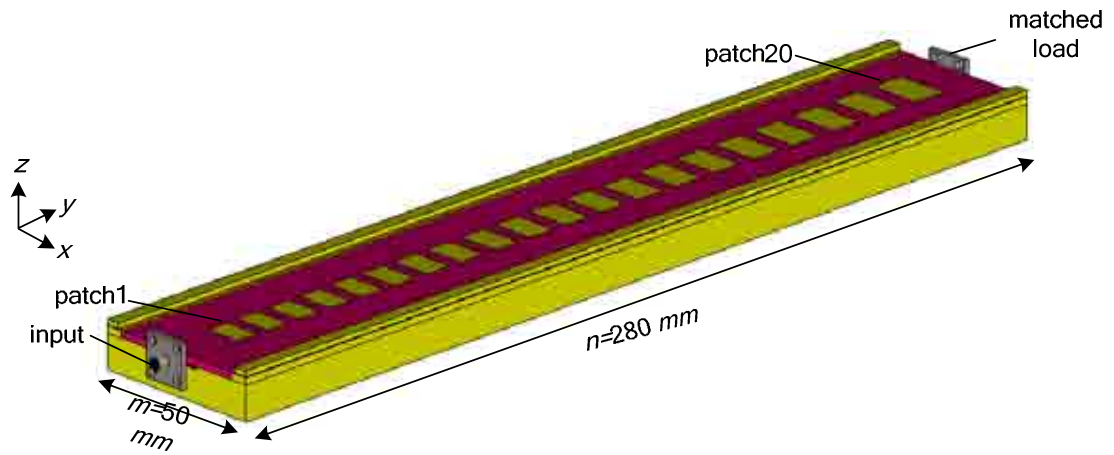

Figure A3: DC power supply

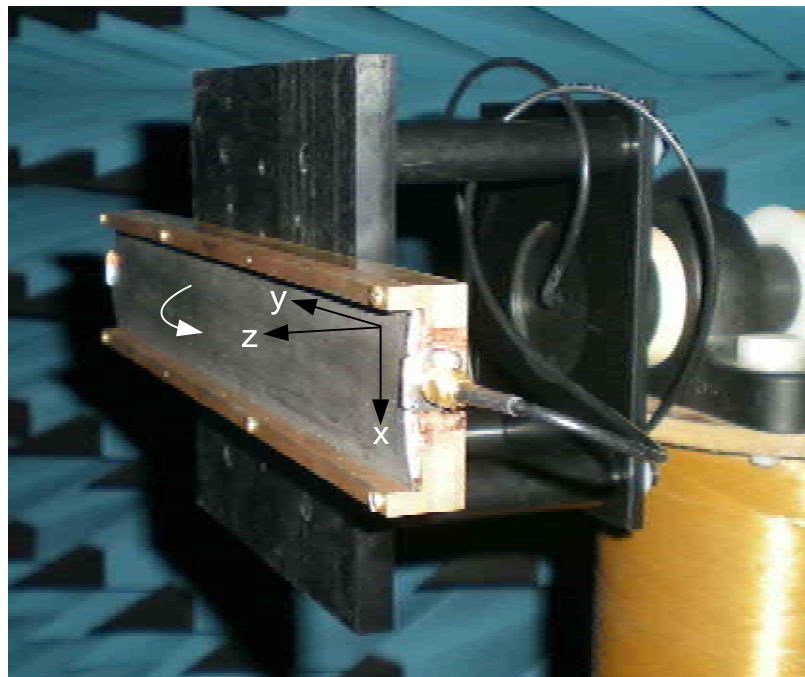**Figure A4: Photograph of multiple Vivaldi antenna**

Figure A5: Single ring Vivaldi antenna with bias circuit

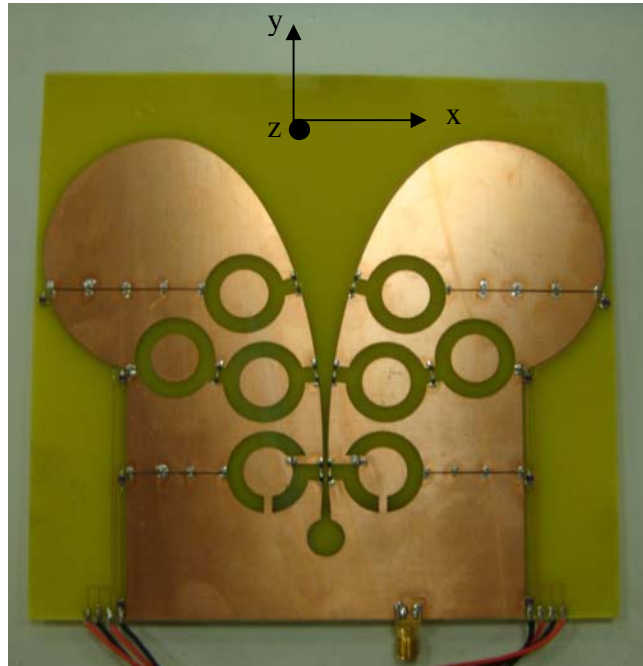**Appendix B: E-plane, H- plane and gain measurement coordinate**

Figure B1 Coordinate systems for log periodic array
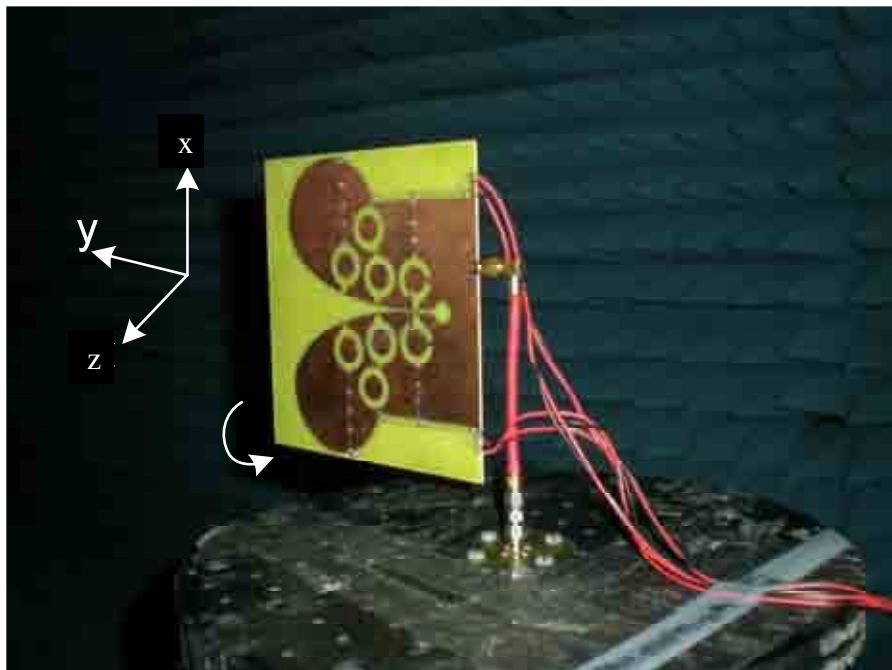**(E-plane = XY-plane, H-plane = YZ-plane)**

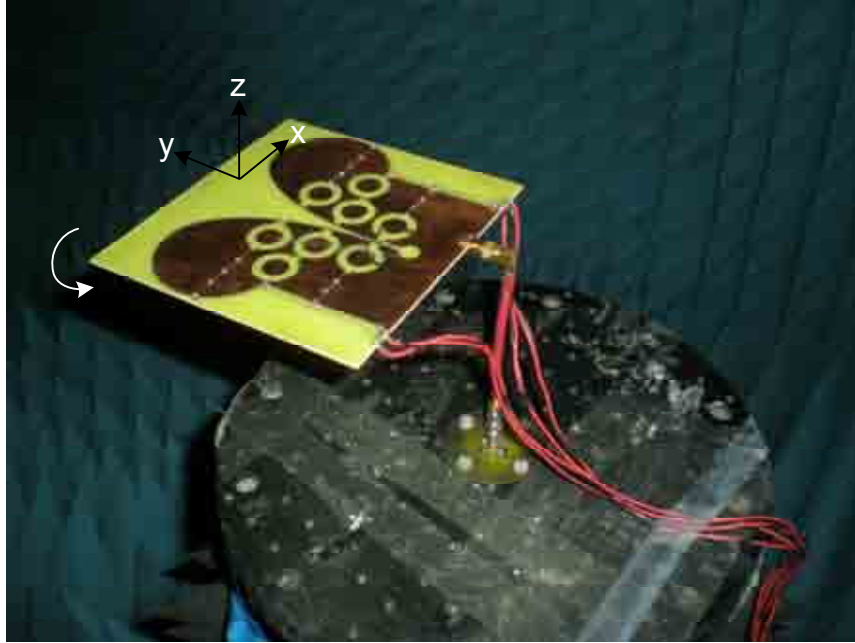**Figure B2 H-plane (YZ-plane) and gain measurement setup (coordinate) for log periodic array**

**Figure B3 Coordinate arrangement for Vivaldi antenna
(E-plane = XY-plane, H-plane = YZ-plane)**

**Figure B4 H-plane (YZ-plane) and gain measurement setup (coordinate) for Vivaldi
antenna**

Figure B5 E-plane (XY-plane) measurement setup (coordinate) for Vivaldi antenna

Appendix C: PIN Diode BAR50-02V Data Sheet

Silicon PIN Diodes

- Current-controlled RF resistor
  for switching and attenuating applications
- Frequency range above 10 MHz up to 6 GHz
- Especially useful as antenna switch
  in mobile communication
- Very low capacitance at zero volt reverse bias
  at freuencies above 1 GHz (typ. 0.15 pF)
- Low forward resistance
- Very low harmonics distortion
- Pb-free (RoHS compliant) package [1]
- Qualified according AEC Q101
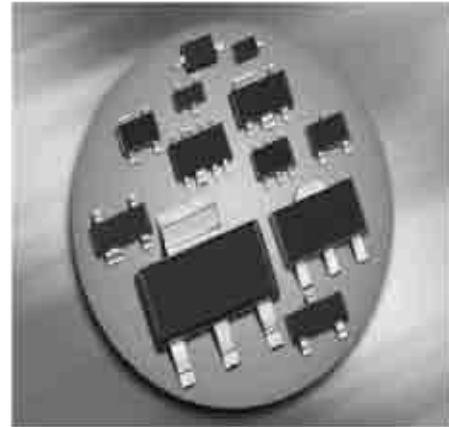
BAR50-02L
BAR50-02V
BAR50-03W
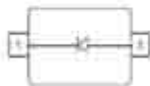
Type	Package	Configuration	L_S(nH)	Marking
BAR50-02L	TSLP-2-1	single,leadless	0.4	AB
BAR50-02V	SC79	single	0.6	a
BAR50-03W	SOD323	single	1.8	A

Maximum Ratings at T_A = 25°C, unless otherwise specified

Parameter	Symbol	Value	Unit
Diode reverse voltage	V_R	50	V
Forward current	I_F	100	mA
Total power dissipation	P_{tot}		mW
BAR50-02L, $T_S \leq 130°C$		250	
BAR50-02V, $T_S \leq 120°C$		250	
BAR50-03W, $T_S \leq 115°C$		250	
Junction temperature	T_j	150	°C
Operating temperature range	T_{op}	-55 ... 125	
Storage temperature	T_{stg}	-55 ... 150	

[1]Pb-containing package may be available upon special request

Thermal Resistance

Parameter	Symbol	Value	Unit
Junction - soldering point[1]	R_{thJS}		K/W
BAR50-02L		≤ 80	
BAR50-02V		≤ 120	
BAR50-03W		≤ 140	

Electrical Characteristics at T_A = 25°C, unless otherwise specified

Parameter	Symbol	Values			Unit
		min.	typ.	max.	
DC Characteristics					
Reverse current $V_R = 50$ V	I_R	-	-	50	nA
Forward voltage $I_F = 50$ mA	V_F	-	0.95	1.1	V

[1]For calculation of R_{thJA} please refer to Application Note Thermal Resistance

Electrical Characteristics at $T_A = 25°C$, unless otherwise specified

| Parameter	Symbol	Values			Unit
		min.	typ.	max.	
AC Characteristics					
Diode capacitance	C_T				pF
$V_R = 1$ V, $f = 1$ MHz		-	0.24	0.5	
$V_R = 5$ V, $f = 1$ MHz		-	0.2	0.4	
$V_R = 0$ V, $f = 100$ MHz		-	0.2	-	
$V_R = 0$ V, $f = 1...1.8$ GHz, BAR50-02L		-	0.1	-	
$V_R = 0$ V, $f = 1...1.8$ GHz, all other		-	0.15	-	
Reverse parallel resistance	R_P				kΩ
$V_R = 0$ V, $f = 100$ MHz		-	25	-	
$V_R = 0$ V, $f = 1$ GHz		-	6	-	
$V_R = 0$ V, $f = 1.8$ GHz		-	5	-	
Forward resistance	r_f				Ω
$I_F = 0.5$ mA, $f = 100$ MHz		-	25	40	
$I_F = 1$ mA, $f = 100$ MHz		-	16.5	25	
$I_F = 10$ mA, $f = 100$ MHz		-	3	4.5	
Charge carrier life time	τ_{rr}	-	1100	-	ns
$I_F = 10$ mA, $I_R = 6$ mA, measured at $I_R = 3$ mA, $R_L = 100$ Ω					
I-region width	W_I	-	56	-	µm
Insertion loss[1]	I_L				dB
$I_F = 3$ mA, $f = 1.8$ GHz		-	0.56	-	
$I_F = 5$ mA, $f = 1.8$ GHz		-	0.4	-	
$I_F = 10$ mA, $f = 1.8$ GHz		-	0.27	-	
Isolation[1]	I_{SO}				
$V_R = 0$ V, $f = 0.9$ GHz		-	24.5	-	
$V_R = 0$ V, $f = 1.8$ GHz		-	20	-	
$V_R = 0$ V, $f = 2.45$ GHz		-	18	-	
$V_R = 0$ V, $f = 5.6$ GHz		-	12	-	

[1]BAR50-02L in series configuration, $Z = 50$ Ω
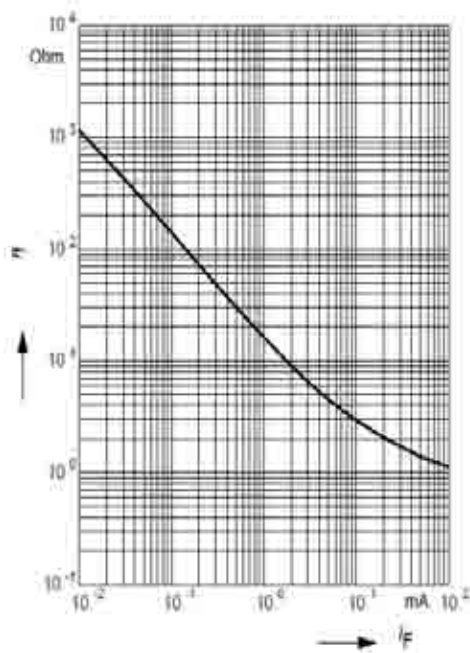
Diode capacitance $C_T = f(V_R)$
f = Parameter
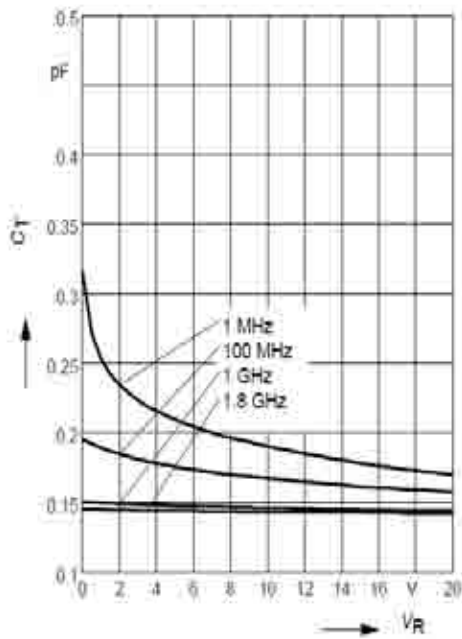
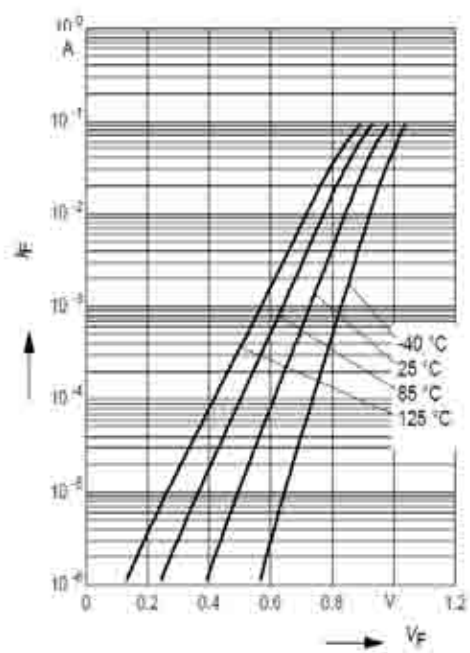**Reverse parallel resistance** $R_P = f(V_R)$
f = Parameter
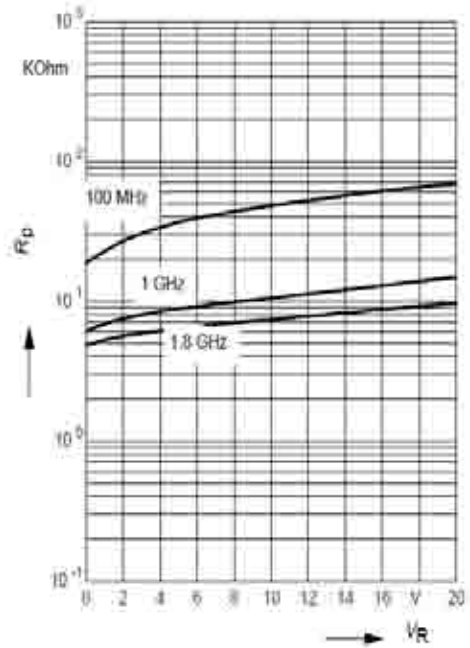
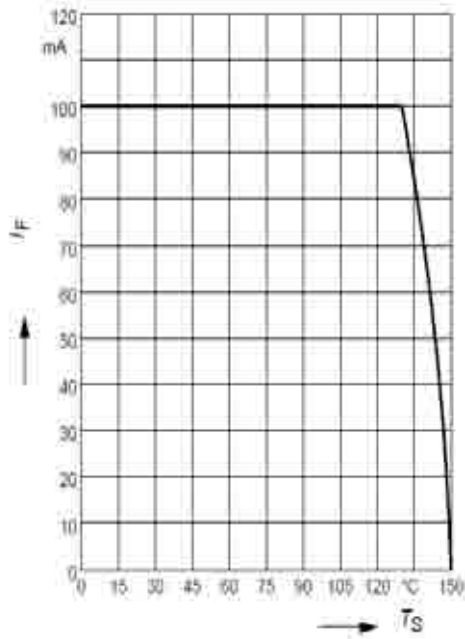

Forward resistance $r_f = f(I_F)$
f = 100 MHz

Forward current $I_F = f(V_F)$
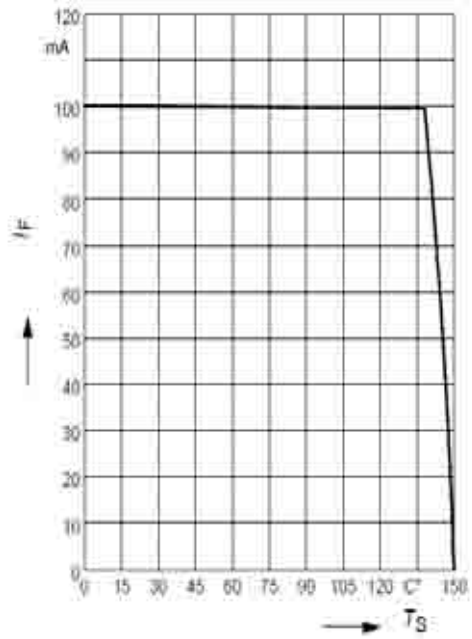T_A = Parameter

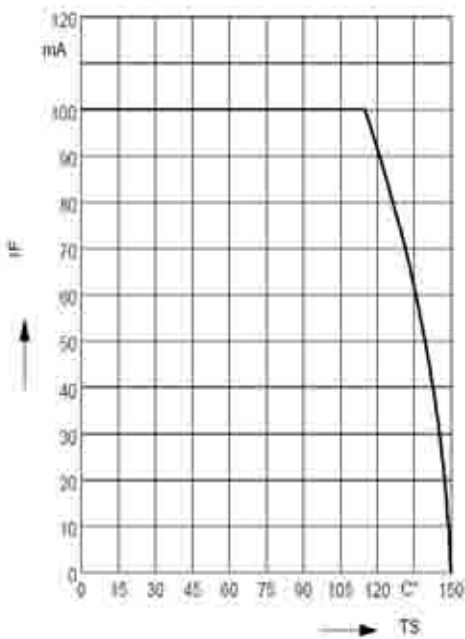Forward current $I_F = f(T_S)$
BAR50-02L
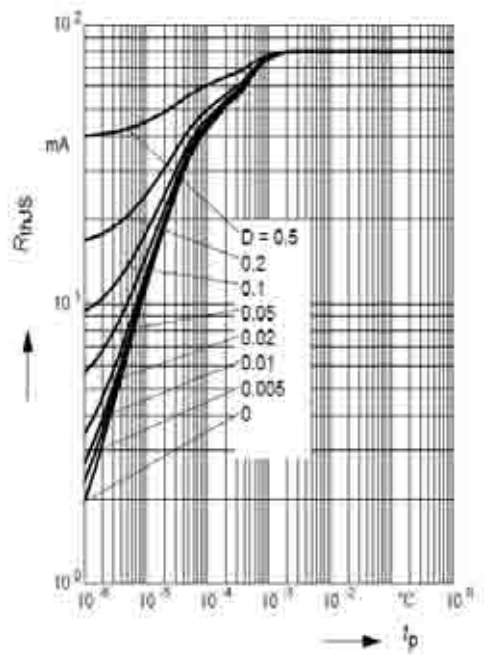

Forward current $I_F = f(T_S)$
BAR50-02V

Forward current $I_F = f(T_S)$
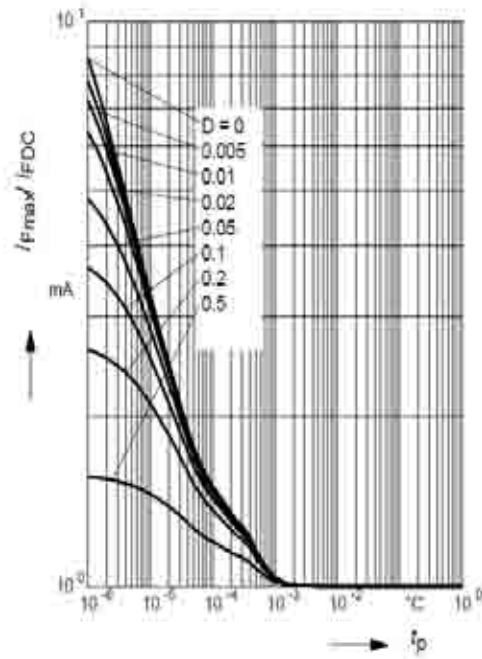BAR50-03W

Permissible Pulse Load $R_{thJS} = f(t_p)$
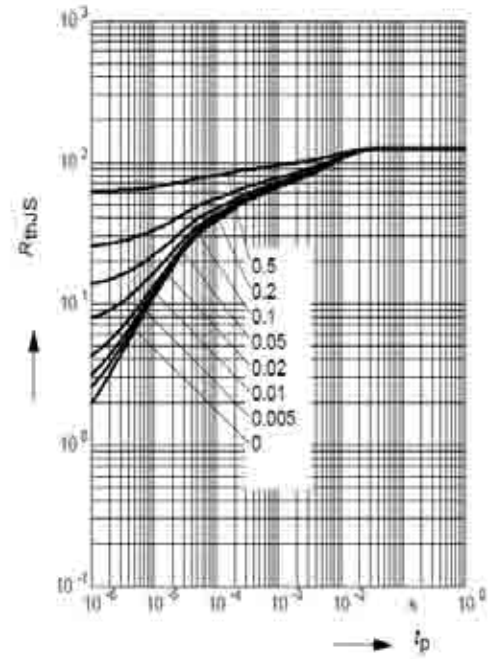BAR50-02L

233

Permissible Pulse Load

$I_{Fmax} / I_{FDC} = f(t_p)$

BAR50-02L

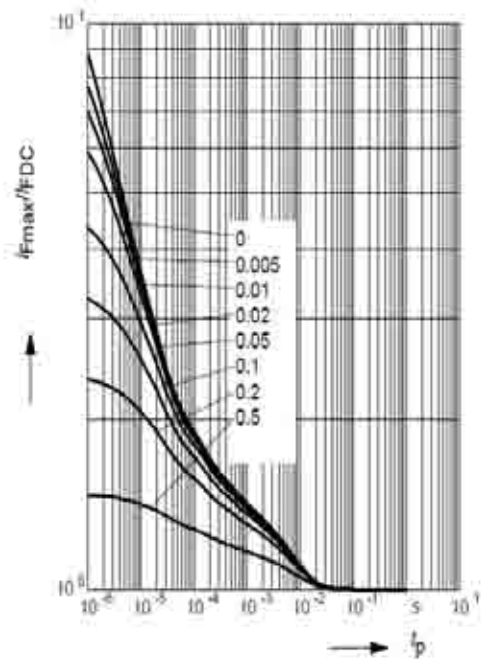**Permissible Pulse Load** $R_{thJS} = f(t_p)$
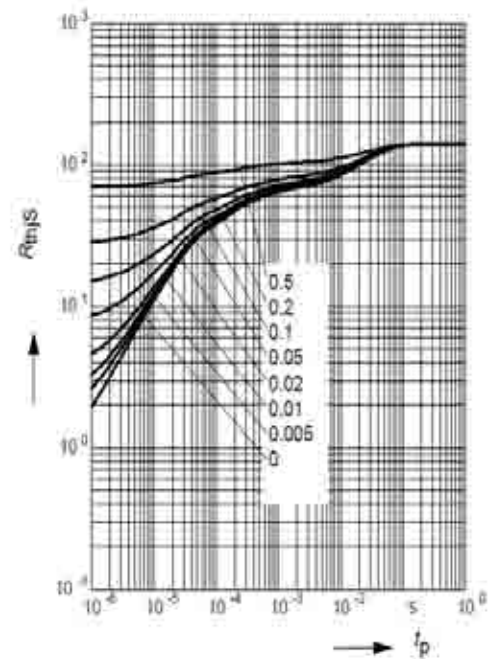
BAR50-02V

Permissible Pulse Load

$I_{Fmax} / I_{FDC} = f(t_p)$

BAR50-02V

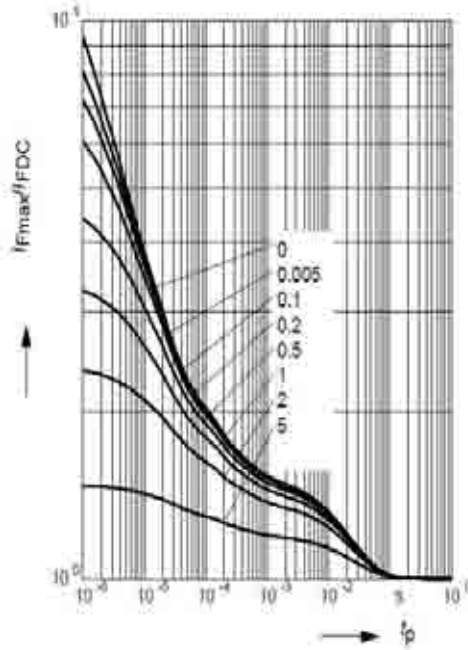

Permissible Pulse Load $R_{thJS} = f(t_p)$

BAR50-03W

234

Permissible Pulse Load
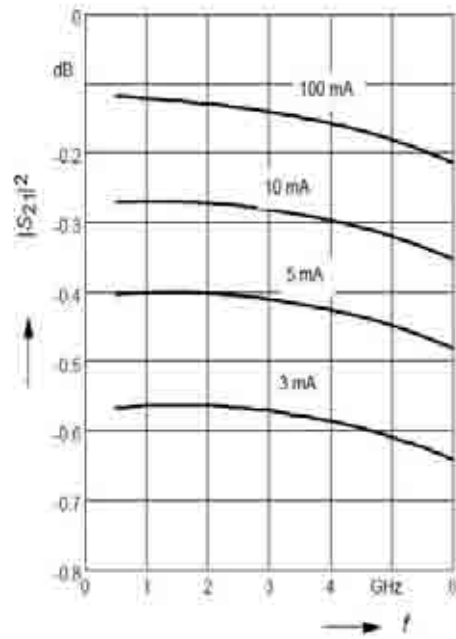
$I_{Fmax}/ I_{FDC} = f (t_p)$

BAR50-03W

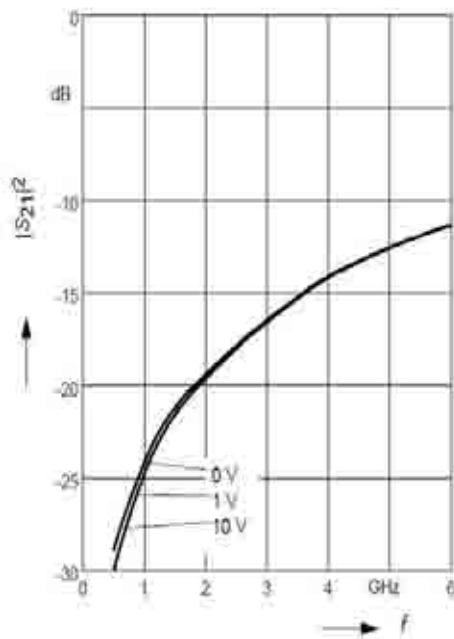## Insertion loss $I_L = -|S_{21}|^2 = f(f)$

I_F = Parameter

BAR50-02L in series configuration, $Z = 50\Omega$

Isolation $I_{SO} = -|S_{21}|^2 = f(f)$

V_R = Parameter

BAR50-02L in series configuration, $Z = 50\Omega$

Package Outline
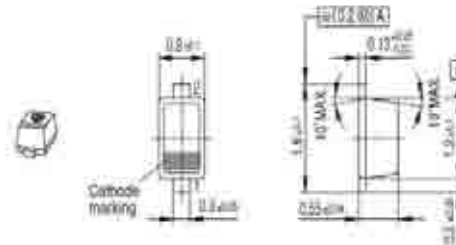
Foot Print

Marking Layout (Example)

2005, June
Date code

GF

BAR83-02V
Type code

Cathode marking
Laser marking
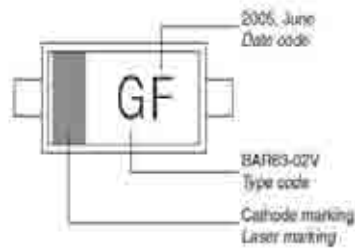
Standard Packing

Reel ø180 mm = 3.000 Pieces/Reel
Reel ø180 mm = 8.000 Pieces/Reel (2 mm Pitch)
Reel ø330 mm = 10.000 Pieces/Reel

Standard

Reel with 2 mm Pitch

Cathode
marking

Cathode
marking
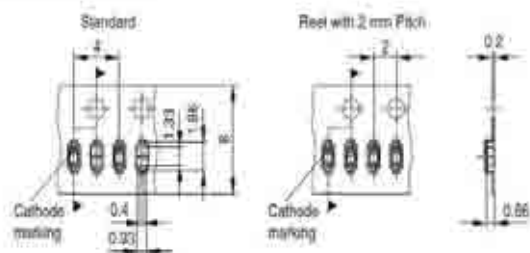
Date Code marking for discrete packages with
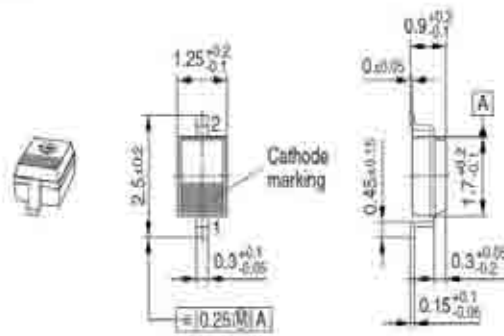one digit (SCD80, SC79, SC75[1]) CES-Code

Month	2003	2004	2005	2006	2007	2008	2009	2010	2011	2012	2013	2014
01	a	p	A	P	a	p	A	P	a	p	A	P
02	b	q	B	Q	b	q	B	Q	b	q	B	Q
03	c	r	C	R	c	r	C	R	c	r	C	R
04	d	s	D	S	d	s	D	S	d	s	D	S
05	e	t	E	T	e	t	E	T	e	t	E	T
06	f	u	F	U	f	u	F	U	f	u	F	U
07	g	v	G	V	g	v	G	V	g	v	G	V
08	h	x	H	X	h	x	H	X	h	x	H	X
09	j	y	J	Y	j	y	J	Y	j	y	J	Y
10	k	z	K	Z	k	z	K	Z	k	z	K	Z
11	l	2	L	4	l	2	L	4	l	2	L	4
12	n	3	N	5	n	3	N	5	n	3	N	5

1) New Marking Layout for SC75, implemented at October 2005.

237

Package Outline

Cathode marking

Foot Print

Marking Layout (Example)

GG

BAR63-03W
Type code

Cathode marking
Laser marking

Standard Packing

Reel ø180 mm = 3.000 Pieces/Reel
Reel ø330 mm = 10.000 Pieces/Reel

Cathode marking

Package Outline

Top view

Bottom view

0.4 +1)

0.05 MAX.

0.6 ±0.05

0.65 nom

0.5 ±0.05 1)

Cathode
marking

1) Dimension applies to plated terminal

Foot Print

For board assembly information please refer to Infineon website "Packages"

0.6

0.45 ø0.275

Copper   Solder mask   Stencil apertures

Marking Layout (Example)

BAS16-02L
Type code

A6

Cathode marking
Laser marking
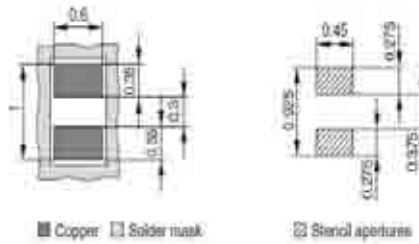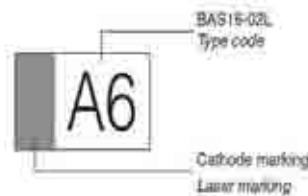
Standard Packing

Reel ø180 mm = 15.000 Pieces/Reel
Reel ø330 mm = 50.000 Pieces/Reel (optional)
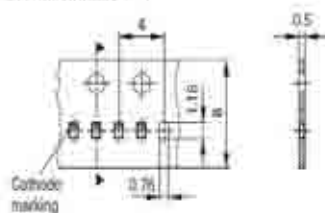
0.5

Cathode
marking

Attention please!

The information given in this dokument shall in no event be regarded as a guarantee of conditions or characteristics ("Beschaffenheitsgarantie"). With respect to any examples or hints given herein, any typical values stated herein and/or any information regarding the application of the device, Infineon Technologies hereby disclaims any and all warranties and liabilities of any kind, including without limitation warranties of non-infringement of intellectual property rights of any third party.

Information

For further information on technology, delivery terms and conditions and prices please contact your nearest Infineon Technologies Office (**www.Infineon.com**).

Warnings

Due to technical requirements components may contain dangerous substances. For information on the types in question please contact your nearest Infineon Technologies Office.
Infineon Technologies Components may only be used in life-support devices or systems with the express written approval of Infineon Technologies, if a failure of such components can reasonably be expected to cause the failure of that life-support device or system, or to affect the safety or effectiveness of that device or system.
Life support devices or systems are intended to be implanted in the human body, or to support and/or maintain and sustain and/or protect human life. If they fail, it is reasonable to assume that the health of the user or other persons may be endangered.

Appendix D: Varactor MV31009 Data Sheet

Microsemi

GaAs Varactor Diodes
Hyperabrupt

MV30011 – MV34010

Features

- High Q Values for Higher Frequency Performance
- Large Tuning Ratios
- Low Reverse Current
- Gamma Values to 1.5
- Available as Bondable Chips and as Packaged Diodes
- Available in Chip-on-Board Packaging
- Custom Designs Available

Applications

- VCOs
- Phase-Locked Oscillators
- High Q Tunable Filters
- Phase Shifters
- Pre-Selectors

Maximum Ratings

Reverse Voltage	Breakdown Voltage
Forward Current	50 mA @ 25°C
Incident Power	+20 dBm @ 25°C
Operating Temperature	-55°C to +175°C
Storage Temperature	-55°C to +200°C

Description

Microsemi's GaAs hyperabrupt junction varactor diodes are fabricated from epitaxial layers grown at Microsemi by the Chemical Vapor Deposition technique. The layers are processed at using proprietary techniques resulting in varactors with constant gamma, high Q factor and repeatable tuning curves. These varactors are available in a variety of microwave ceramic packages or bondable chips for operation from UHF to millimeter wave frequencies.

![Microsemi logo]

High Q Constant Gamma Tuning Varactors (Specifications @ 25°C)

Gamma = 0.75

Part Number	C_T @ 4 V ± 10% (pF)[1,3,4]	Typ. C_T@2V / C_T@20V[5]	Min. V_{BR} @ 10 µA (V)	Typ. Q @ -4 V[2]
MV32001	0.6	2.8	22	4000
MV32002	1.0	3.1	22	3000
MV32003	1.2	3.2	22	3000
MV32004	1.5	3.3	22	3000
MV32005	1.8	3.4	22	3000
MV32006	2.2	3.5	22	3000
MV32007	2.5	3.6	22	2500
MV32008	3.0	3.6	22	2500
MV32009	3.6	3.7	22	2000
MV32010	4.5	3.8	22	1500

Gamma = 1.00

Part Number	C_T @ 4 V ± 10% (pF)[1,3,4]	Typ. C_T@2V / C_T@12V[5]	Min. V_{BR} @ 10 µA (V)	Typ. Q @ -4 V[2]
MV30001	0.6	3.2	15	4000
MV30002	1.0	3.7	15	3000
MV30003	1.2	3.8	15	3000
MV30004	1.5	4.0	15	3000
MV30005	1.8	4.1	15	3000
MV30006	2.2	4.2	15	3000
MV30007	2.5	4.3	15	2500
MV30008	3.0	4.4	15	2500
MV30009	3.6	4.5	15	2000
MV30010	4.5	4.5	15	1500

Part Number	C_T @ 4 V ± 10% (pF)[1,3,4]	Typ. C_T@2V / C_T@20V[5]	Min. V_{BR} @ 10 µA (V)	Typ. Q @ -4 V[2]
MV30011	0.6	3.9	22	4000
MV30012	1.0	4.8	22	3000
MV30013	1.2	4.9	22	3000
MV30014	1.5	5.2	22	3000
MV30015	1.8	5.4	22	3000
MV30016	2.2	5.6	22	3000
MV30017	2.5	5.8	22	2500
MV30018	3.0	6.0	22	2500
MV30019	3.6	6.1	22	2000
MV30020	4.5	6.3	22	1500

Gamma = 1.25

Part Number	C_T @ 4 V ± 10% (pF)[1,3,4]	Typ. C_T@2V / C_T@12V[5]	Min. V_{BR} @ 10 µA (V)	Typ. Q @ -4 V[2]
MV31001	0.6	4.2	15	4000
MV31002	1.0	5.1	15	3000
MV31003	1.2	5.4	15	3000
MV31004	1.5	5.7	15	3000
MV31005	1.8	5.9	15	3000
MV31006	2.2	6.2	15	3000
MV31007	2.5	6.3	15	2000
MV31008	3.0	6.5	15	2000
MV31009	3.6	6.7	15	2000
MV31010	4.5	6.8	15	1500

Part Number	C_T @ 4 V ± 10% (pF)[1,3,4]	Typ. C_T@2V / C_T@20V[5]	Min. V_{BR} @ 10 µA (V)	Typ. Q @ -4 V[2]
MV31011	0.5	5.5	22	4000
MV31012	0.7	6.5	22	4000
MV31013	1.0	7.1	22	3000
MV31014	1.2	8.3	22	3000
MV31015	1.5	9.1	22	3000
MV31016	1.8	9.6	22	3000
MV31017	2.0	9.9	22	3000
MV31018	2.2	10.2	22	3000
MV31019	2.7	10.8	22	2000
MV31020	3.3	11.3	22	2000
MV31021	3.7	11.5	22	2000
MV31022	4.7	12.0	22	1500
MV31023	5.6	12.3	22	1500
MV31024	6.8	12.6	22	1500
MV31025	8.2	12.9	22	1500
MV31026	10.0	13.1	22	1500

[1] Capacitance is specified at 1 MHz
[2] Measured by DeLoach Technique and referenced to 50 MHz
[3] Tightened tolerances available upon request
[4] Package capacitance is 0.15 pF is included in the above specification
[5] The capacitance ratio is calculated using C_p = 0.15 pF Ratios will vary depending upon package selection

242

High Q Constant Gamma Tuning Varactors (Specifications @ 25°)

	Gamma = 1.50			
Part Number	C_T @ 4 V ± 10% (pF)[1,3,4]	Typ. C_T @ 2 V C_T @ 12V[4]	Min. V_{BR} @ 10 µA (V)	Typ. Q @ 4 V[2]
MV34001	0.5	4.5	15	3000
MV34002	1.0	5.9	15	2500
MV34003	1.8	7.1	15	2500
MV34004	2.8	7.3	15	2500
MV34005	2.2	7.4	15	1800
MV34006	2.5	7.6	15	1800
MV34007	3.0	7.9	15	1800
MV34008	3.8	8.1	15	1800
MV34009	4.5	8.3	15	1200
MV34010	10.0	8.9	15	1200

[1] Capacitance is specified at 1 MHz.
[2] Measured by DeLoach Technique and referenced to 50 MHz.
[3] Tightened tolerances available upon request.
[4] Package capacitance is 0.15 pF is included in the above specification.
[5] The capacitance ratio is calculated using $C_p = 0.15$ pF. Ratios will vary depending upon package selection.
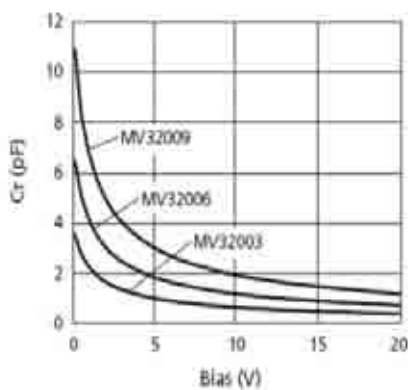
Typical Total Capacitance vs. Bias
Gamma = 0.75
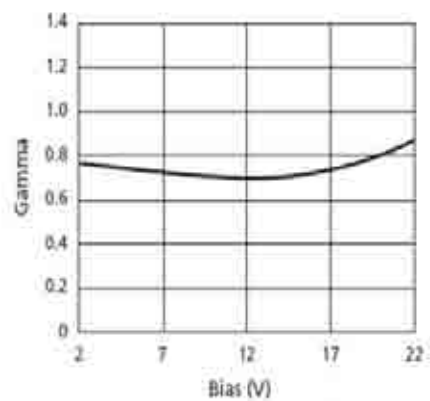
Typical Gamma vs. Bias
Gamma = 0.75

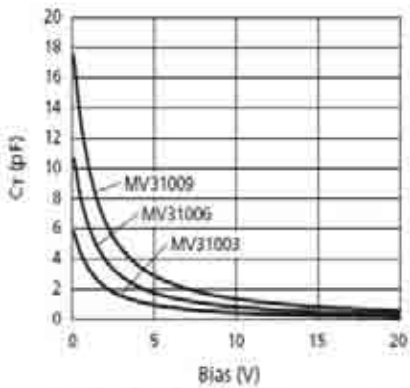## Typical Characteristics
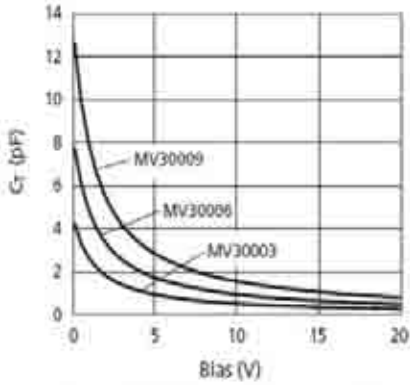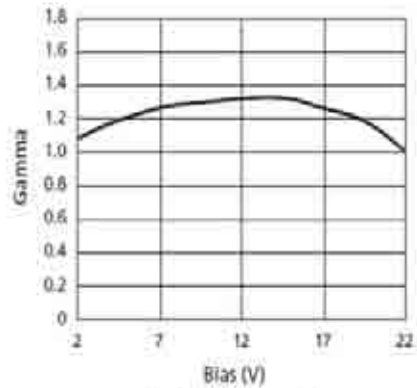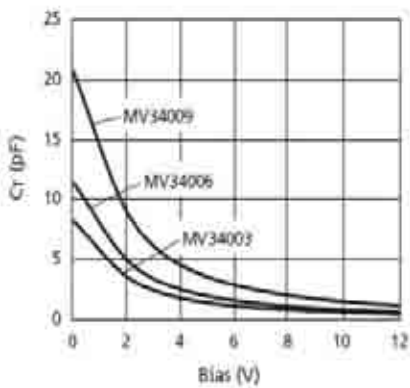

Typical Total Capacitance vs. Bias
Gamma = 1.00
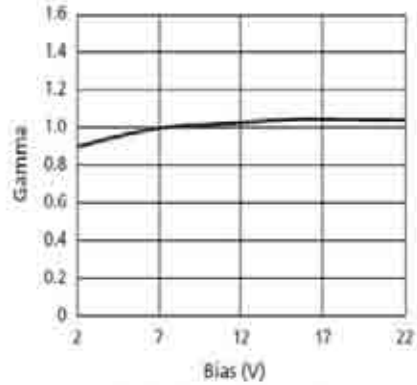
Typical Gamma vs. Bias
Gamma = 1.00
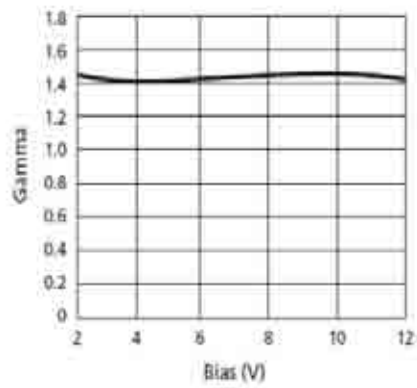

Typical Total Capacitance vs. Bias
Gamma = 1.25

Typical Gamma vs. Bias
Gamma = 1.25
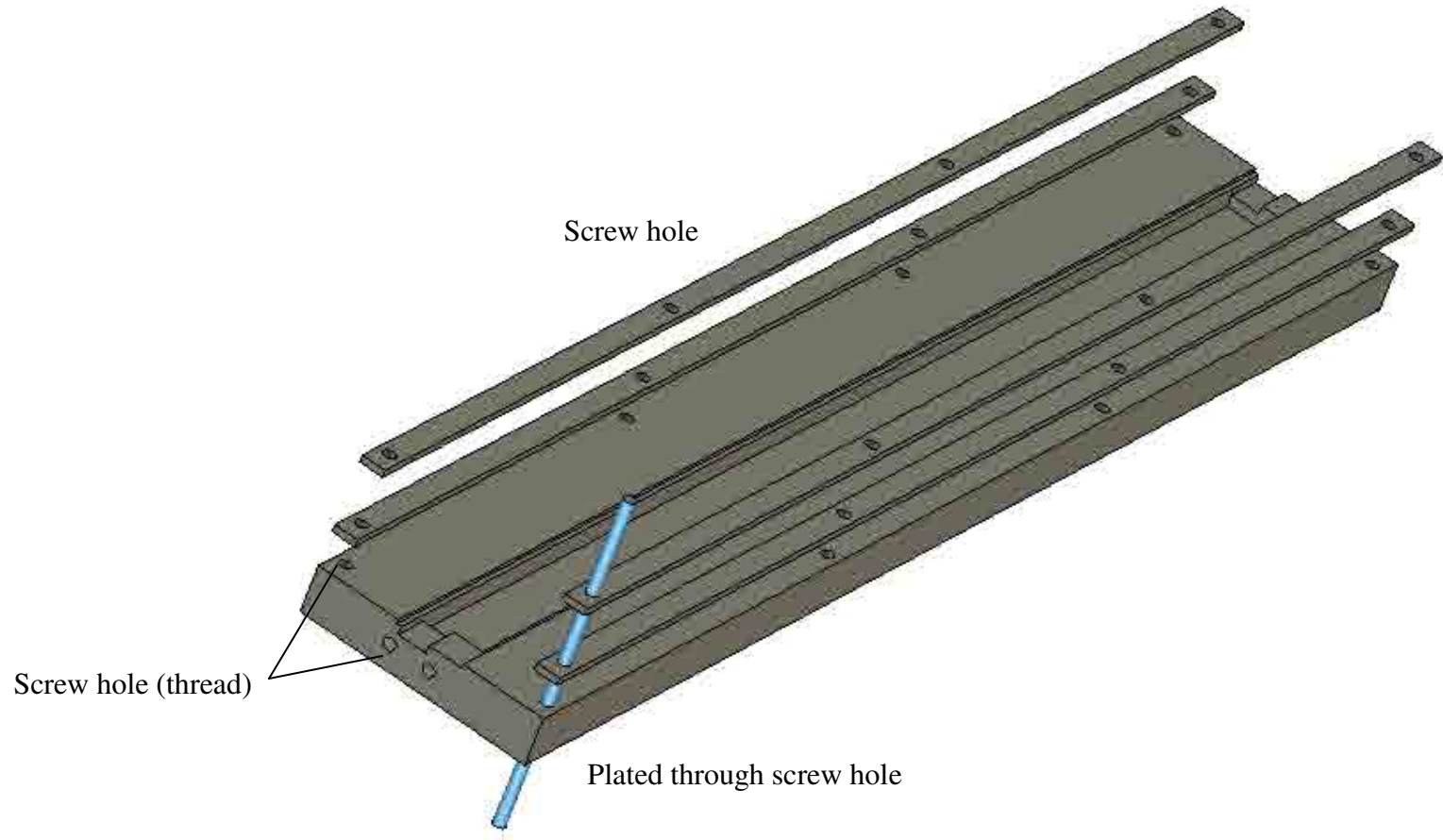

Typical Total Capacitance vs. Bias
Gamma = 1.50

Typical Gamma vs. Bias
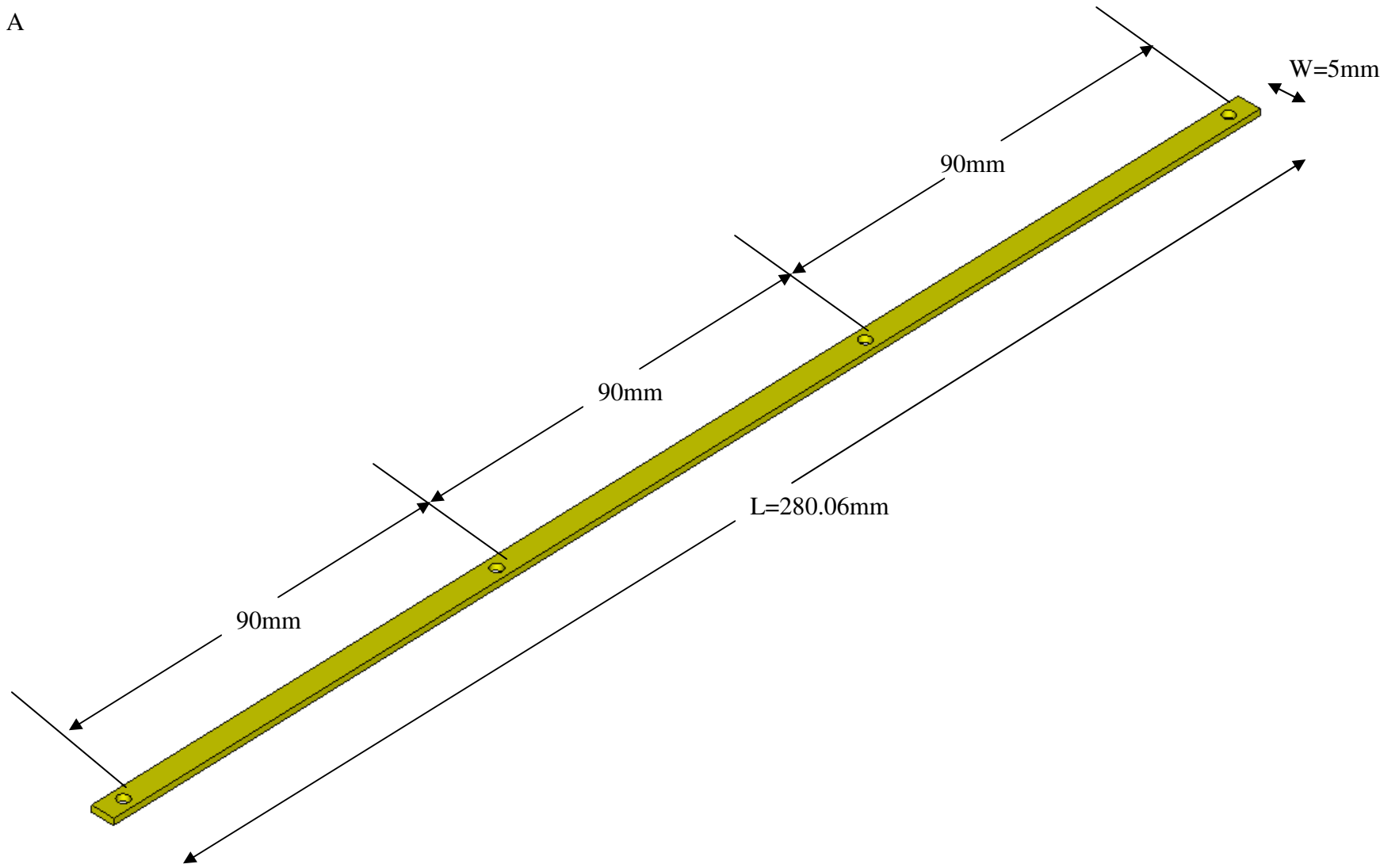Gamma = 1.50

244

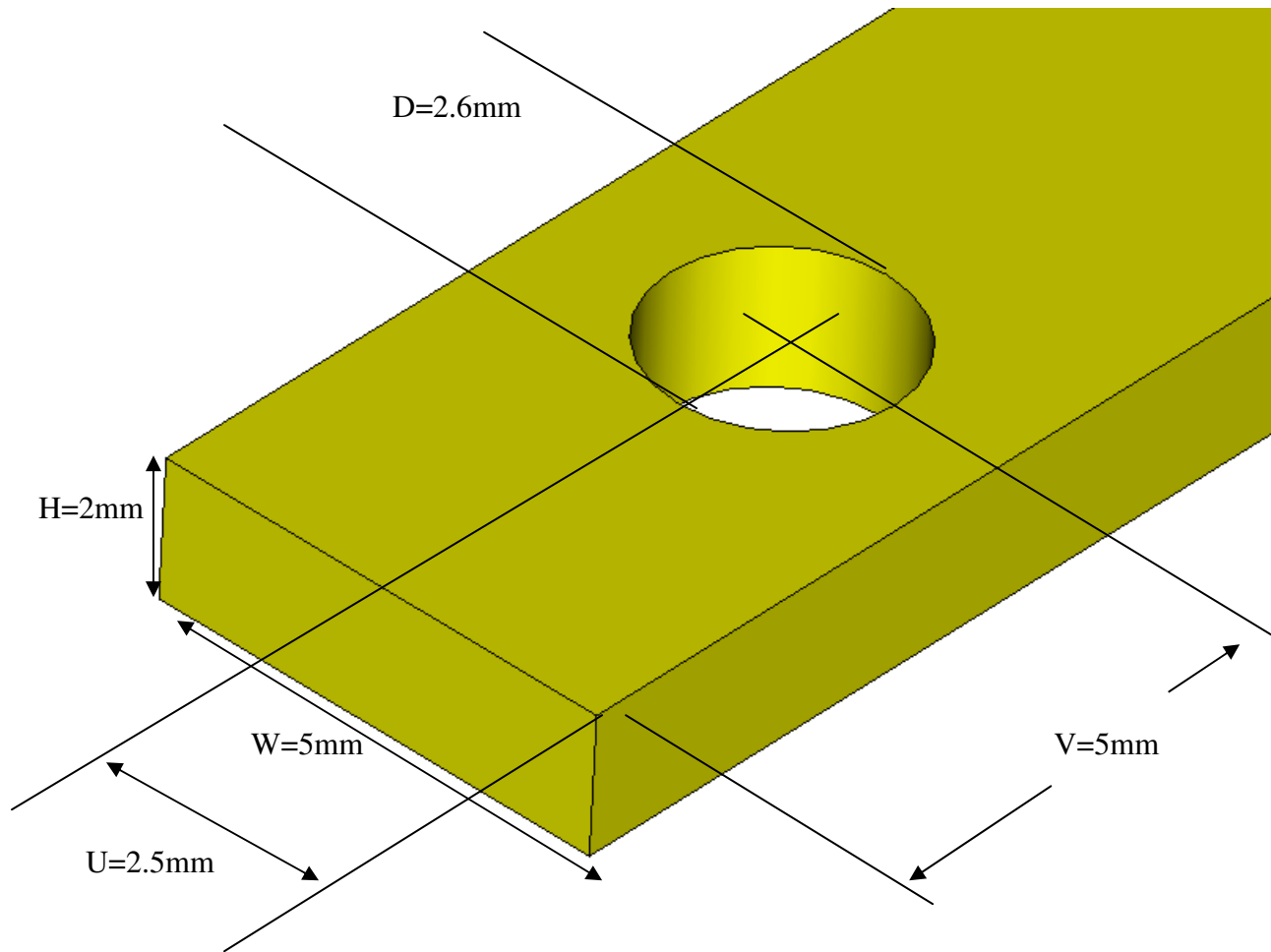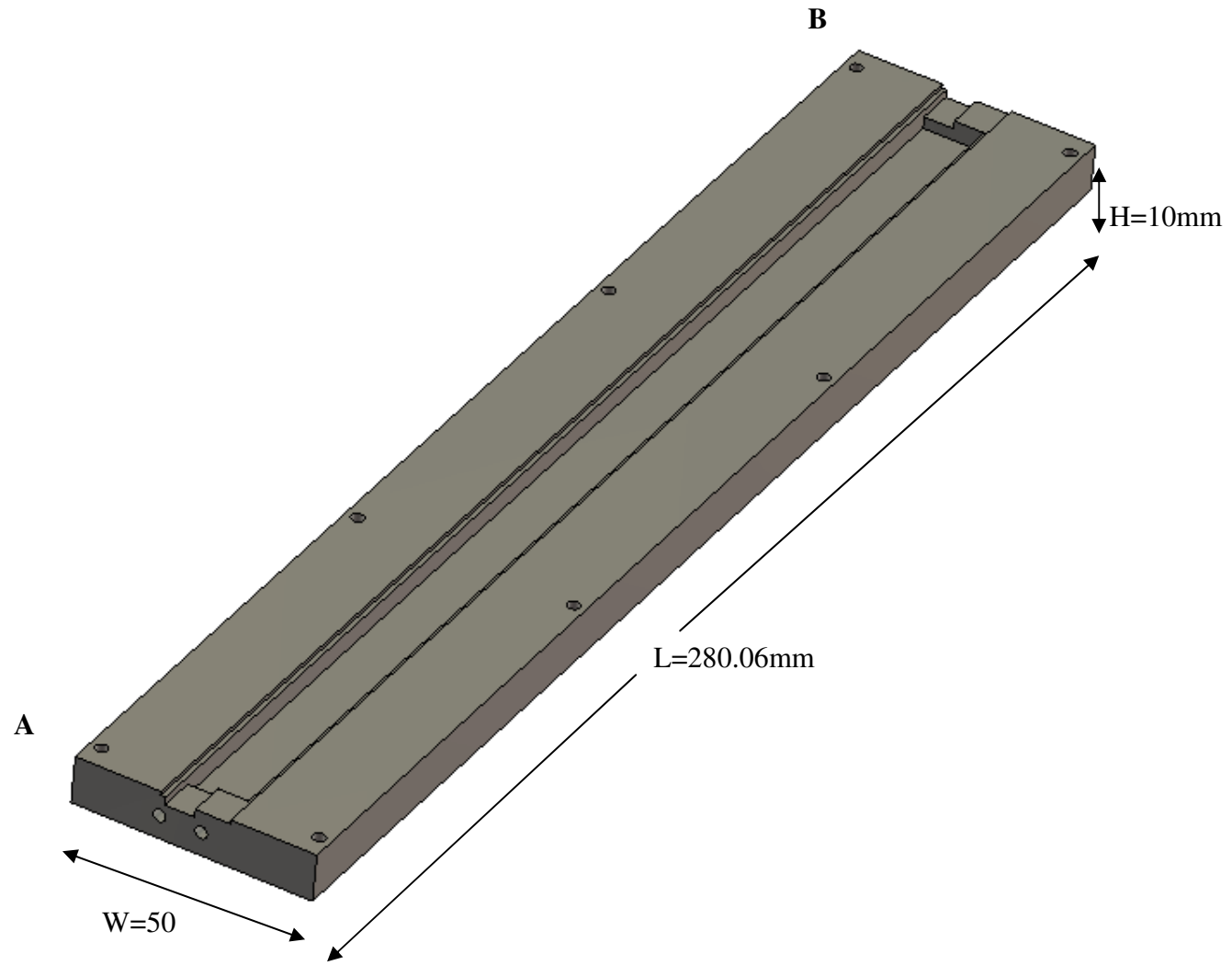Appendix E: Screening Box Layout and Plan

Screw hole

Screw hole (thread)

Plated through screw hole

Plan A

W=5mm

90mm

90mm

L=280.06mm

90mm

Plan A (Zoom)

D=2.6mm

H=2mm

W=5mm

V=5mm

U=2.5mm

Plan B

B

H=10mm

L=280.06mm

A

W=50

248
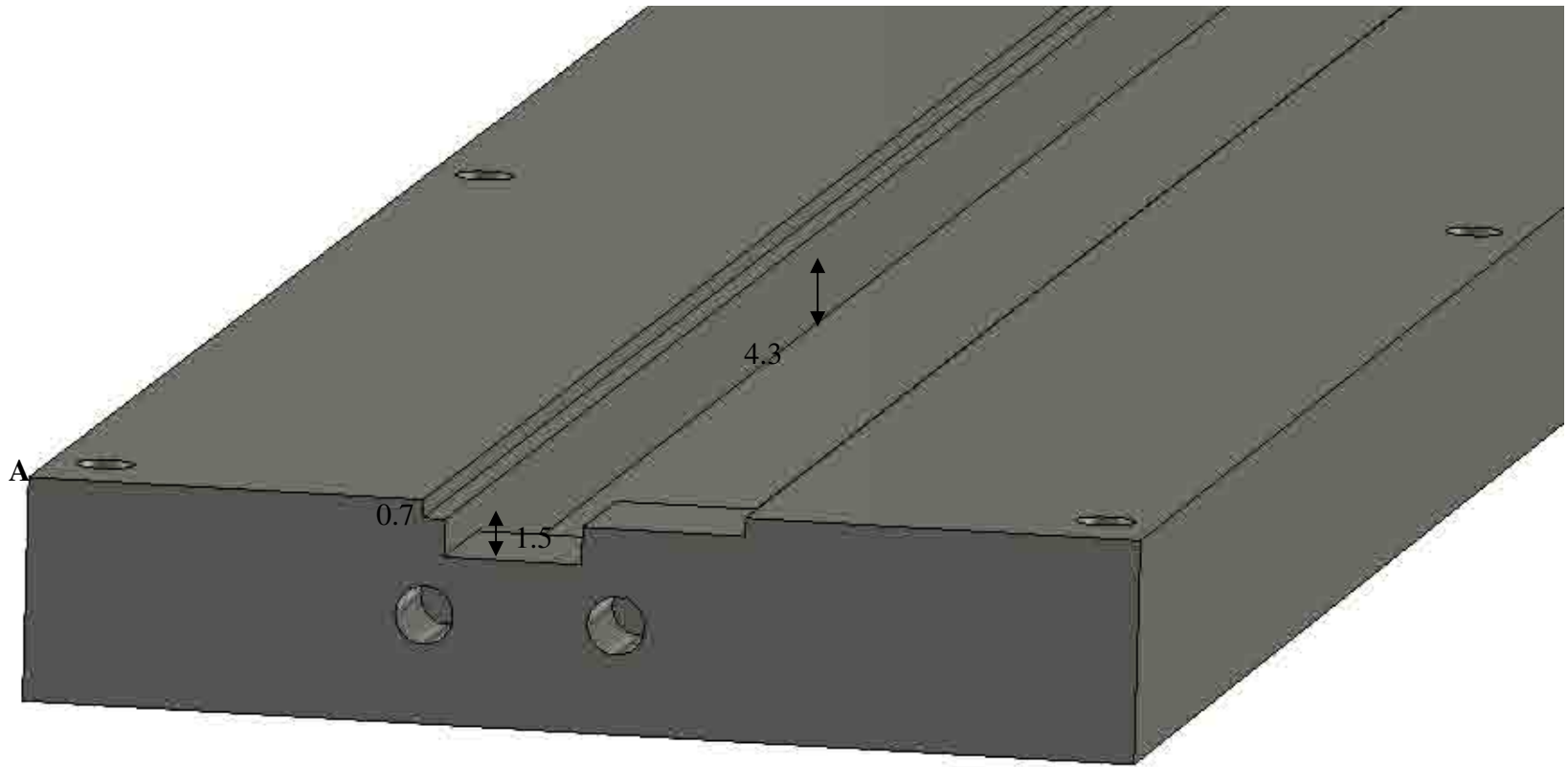
Plan B (Zoom @ **A**)

Plan B (Zoom @ **A**)

$W_7=1$

$W_6=12.5$

$h=8$

A

$W_1=17.75$

$W_3=6.2$ $W_4=7.3$ $W_5=17.75$

$W_2=1$

250

Plan B (Zoom @ **A**)

10.65   2.5

D=2.6

L=6

V=5

A   17.935   8.64

26.575

A

0.7

1.5

10

5.18

D=2.6

Plan B (Zoom @ **B**)

B

4.3

B

25.24

16.6

8.64

264.06

A

17.935

8.64

26.575